Aerodynamic Deorbit Experiment

Mission Plan v4

Purdue University

List of Acronyms

ABC	Aft Bulkhead Carrier
ADE	Aerodynamic Deorbit Experiment
ASU	Arizona State University
bps	Bits per second
C&DH	Command and Data Handling
C_d	Coefficient of Drag
CDR	Critical Design Review
CSV	Comma Separated Value
dB	Decibel
dBi	Decibel Isotropic
ECEF	Earth-Centered, Earth-Fixed
ECI	Earth-Centered Inertial
EPS	Electrical Power System
FMSC	Full Mission Success Criteria
FSK	Frequency Shift Keying
GEO	Geostationary Earth Orbit
GMAT	General Mission Analysis Tool
GTO	Geosynchronous Transfer Orbit
I&TRR	Integration and Testing Readiness Review
IMU	Inertial Measurement Unit
IPv4	Internet Protocol, version 4
JSPOC	Joint Space Operations Center
LNA	Low Noise Amplifier
MAVEN	Mars Atmosphere and Volatile Evolution
Mission MEO	Medium Earth Orbit
MGS	Mars Global Surveyor
MHz	Megahertz
MMSC	Minimum Mission Success Criteria
MOC	Mission Operations Center
MRO	Mars Reconnaissance Orbiter
PCB	Printed Circuit Board
PCM	Phase Change Memory
PDR	Preliminary Design Review
PIB	Payload Interface Board
P-POD	Poly Picosatellite Orbital Deployer
$[PS]^2$	Passively Stable Pyramid Sail
PTE	Periapsis Time Estimator
RAAN	Right Ascension of the Ascending Node

RMS	Root Mean Square
RVM	Requirements Verification Matrix
RX	Received
SHEARLESS	SHEAth-based Rollable LEnticular-Shaped and low-Stiction
SPI	Serial Peripheral Interface
SRP	Solar Radiation Pressure
STK	Systems Took Kit
TLE	Two Line Element
UDP	User Datagram Protocol
UHF	Ultra-High Frequency
ULA	United Launch Alliance

Table of Contents

List of Figures

List of Tables

1. Introduction

1.1 Purpose and Scope

The intent of this Mission Plan is to provide an overview of the Aerodynamic Deorbit Experiment (ADE) mission. It will define the mission's objectives and describe the main aspects of the mission, ranging from mission design, to the various subsystems, to testing procedures. This document shall be a reference that justifies design decisions and guides future work for the project.

1.2 Project Organization

The ADE Project is being implemented by undergraduate and graduate students across Purdue University and the California Polytechnic State University at San Luis Obispo, with previous participation from the Georgia Institute of Technology. Oversight is provided by faculty, and technical experts serve as advisors to the implementing organizations. As this is a university project, the specific students assigned to these tasks may no longer be up to date.

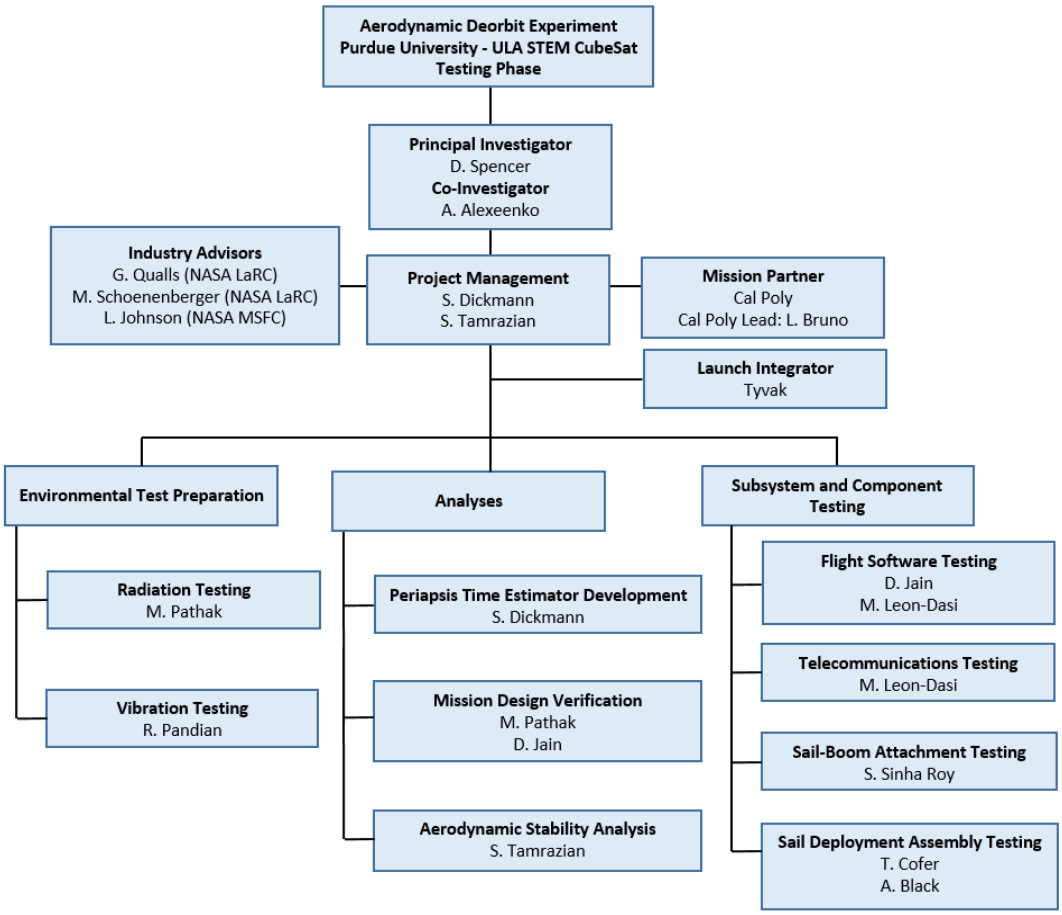

Figure 1.1: ADE Project Organization Chart

Principal Investigator Dr. David Spencer is an Associate Professor within the School of Aeronautical & Astronautical Engineering, and Director of the Space Flight Projects Laboratory at Purdue University. Co-Investigator Dr. Alina Alexeenko is a Professor in the School of Aeronautical & Astronautical Engineering at Purdue University, and a resident faculty member at the Birck Nanotechnology Center. For the ADE project, Dr. Alexeenko will be responsible for overseeing aerothermodynamic modeling, the analysis of the IMU data from flight operations, and evaluation of the aerodynamic characteristics of the deployable drag device. Three external advisors to the ADE project include Mr. Les Johnson, Technical Assistant for the Advanced Concepts Office at NASA Marshall Space Flight Center and Solar Sail PI for Near Earth Asteroid Scout Project. Mr. Johnson will advise the project on the deployable drag sail design and implementation. Mr. Garry Qualls leads LarkWorks at NASA Langley Research Center, a MakerSpace facility used to prototype, innovate, and collaborate with researchers both inside and outside of NASA. LarkWorks will assist the ADE team as they prototype and test small satellite deployment mechanisms and mechatronic systems. Mr. Mark Schoenenberger, a senior aerospace engineer at NASA LaRC, will advise the team regarding the geometry and performance characterization of the drag device.

1.3 Project Schedule

ADE was selected by the United Launch Alliance (ULA) for participation in the CubeSat rideshare initiative in the fall of 2016. In the spring of 2017, students began preliminary design work on project, and completed the Preliminary Design Review in April 2017. Fall of 2017 was devoted to the detailed design, and saw successful completion of the Critical Design Review in October of 2017. In winter of 2017, the project was refocused for incremental progress through small specialized task teams to minimize down time during transitional periods from semester to semester. Tasks were focused on developing and performing tests and specific analyses. As of early summer 2019, the project has recently completed a test readiness review in April of 2019, culminating with the completion of test procedures for several environmental, subsystem, and component tests. Following completion of the flight software and component/subsystem testing, system level testing will ensure that the CubeSat can function as a whole under flight like conditions. Launch is estimated for summer of 2020, preceded by a 45 day period for launch integration. After launch, ADE is expected to deorbit within three months.

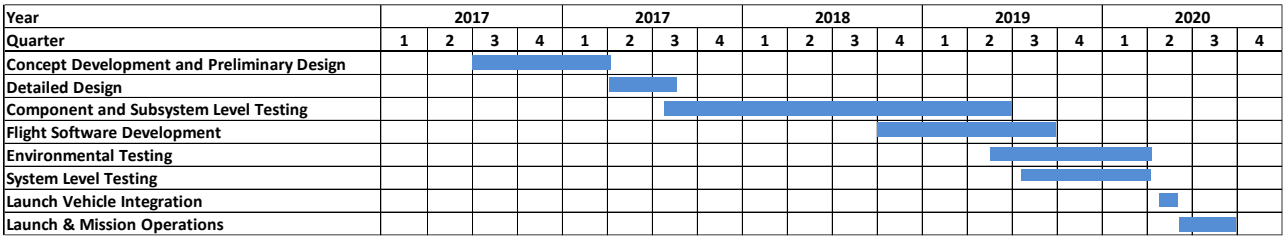

Figure 1.2: ADE Project Schedule

2 Mission Overview

2.1 Mission Summary

ADE is a 1U CubeSat that will be deployed from the Centaur upper stage on a future United Launch Alliance launch. The baselined orbit for ADE is a geosynchronous transfer orbit (GTO), with perigee/apogee orbit altitudes of 185 km/35,786 km and an inclination of 27.0 deg. The ADE mission will provide flight qualification and characterize the performance of a deployable drag device to accelerate the deorbit of small satellites. The demonstration of a passive aerodynamically-stable deployable drag device will give satellite operators an efficient option to deorbit craft after mission completion, in order to avoid the creation of additional space debris.

2.1.1 Mission Success Criteria

In order to determine whether ADE has achieved mission success, mission success criteria have been established, and have been grouped into a set of minimum mission success criteria (MMSC), and full mission success criteria (FMSC):

Minimum Mission Success Criteria

1. ADE shall be a 1U CubeSat launched as a secondary payload and deployed via a P-POD into a geosynchronous transfer orbit
2. ADE shall deploy a drag sail providing increased drag area to accelerate the deorbit timeline
3. The passive aerodynamic stability provided by the drag sail shall be assessed

Full Mission Success Criteria

1. ADE shall downlink IMU data for at least 5 perigee passes
2. A radiation sensor shall characterize the radiation environment in GTO for 3 orbits
3. ADE shall take and return one image of the deployed sail

The MMSC have been designed to ensure that the drag sail effectiveness at accelerating deorbit can be assessed without reliance on on-board instrumentation. The FMSC provide additional data with which to back out performance, and supplemental data of interest that ADE is uniquely suited to obtain, being the first CubeSat mission launched into GTO.

2.2 Concept of Operations

ADE will be deployed from the P-POD following a ULA launch out of Kennedy Space Center. ADE will be electrically inhibited while in the P-POD. Following deployment, ADE will

power on and begin battery charging in safe mode. The flight processor will power on, and the UHF dipole antenna will be deployed via burn wire no sooner than 45 minutes after deployment from the P-POD. RF transmission of the telemetry beacon will begin 1 minute later, and will continually transmit every 5.5 seconds thereafter.

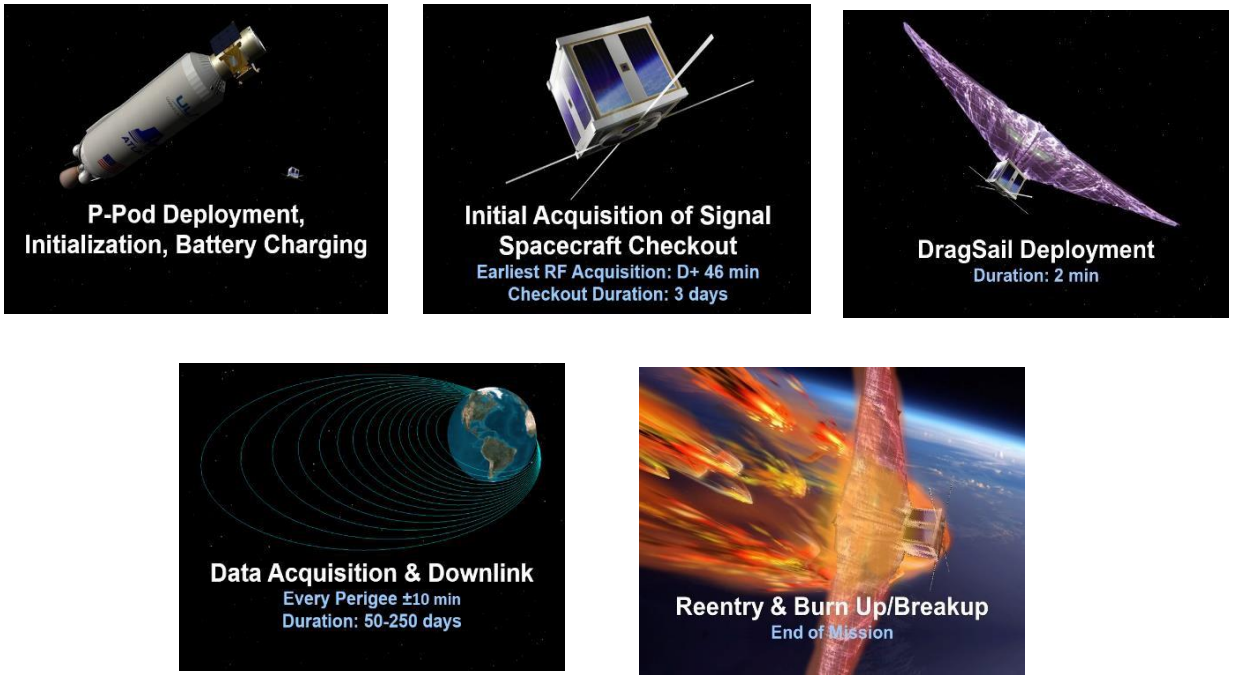

Figure 2.1: ADE Concept of Operations, Graphical Representation

After initial signal acquisition, the spacecraft checkout will begin, where the payload instrumentation and supporting systems will be tested and confirmed to be operating nominally. When it is understood that the spacecraft is within acceptable functionality, the drag sail will be deployed via ground command. Confirmation will come from the regular telemetry and instrumentation. If it is impossible to deploy the sail via ground command, an on-board timer is set to deploy the sail autonomously.

Following deployment of the drag sail, the on-board instrumentation will collect Inertial Measurement Unit (IMU) data, photos, and radiation data at a regular cadence, outlined in further detail in following sections. Any anomalous activity will revert the spacecraft to safe mode, and will generally be addressed with ground-in-the-loop recovery measures.

2.3 Sequence of Events

There are four mission phases that form the sequence of events for ADE. They are as follows: Launch and Initial Acquisition, Checkout, Deployment, and Science. The mission begins with the ADE CubeSat deployment from the P-POD. The initial phase of the sequence of events comprises of startup events (such as turning on the components of the CubeSat) and the earliest signal acquisition. The checkout phase is composed of checking and verifying all the components (systems and IMU) onboard the CubeSat to ensure proper functionality. The deployment phase of

the mission starts approximately 7 days after the CubeSat deploys from the P-POD. It involves the deployment of the drag sail device and setting the CubeSat to experiment mode. Finally, the science phase consists of all the core data collection and storage for the mission as well as the downlinking of data until deorbit occurs. The sequence of events timeline is provided in Table 2.1. The same copy can also be found in the shared OneDrive under Mission Design.

Table 2.1: Sequence of Events Timeline

Procedure Step	Mission Elapsed Time (dd/hh:mm:ss)	Participants	Event	Event Description	Commands	Notes	Contingency Plans
1	-01:00:00	All	Voice Checks	On-console voice checks: PI, S/C Systems, Power, Telecom, ACS, Thermal, Ground Systems (Cal Poly, ASU, Purdue, GT)		Voice checks led by Mission Manager (Mission). MET measured from P-POD deployment time.	
2	0:00:00		P-POD Deployment	P-POD deployment		Autonomously initiated by L/V. ADE will turn on and initiate battery charging.	
3	0:05:00		Antenna Deployment	Antenna deployment via burnwire	ANT-DEPLOY-NOW	Autonomous via startup sequence	
4	0:45:00		Beacon On	Beacon transmission begins; 1 beacon packet every 15 sec	BEACON-ON		
5	02:00:00 (TBD)	Ground Systems	AOS	Acquisition of Signal (AOS): Announced by Ground Systems when RF signal is detected			
6	02:05:00 (TBD)	Ground Systems	Telemetry Available	Ground Systems announces when telemetry packets are available on downlink server			
7	02:10:00 (TBD)	All	AOS + 5 min Poll	AOS + 5 min Health & Status poll		All subsystems provide initial health & status summary to Mission Manager	Power Anomaly, Telecommunications Anomaly, Component Incorrect On/Off State
8	02:15:00 (TBD)	Mission/PI	AOS + 5 min Summary	Mission Manager to PI: AOS + 5 min Health & Status summary			
9	08:00:00 (second tracking pass)	Ground Systems	Update Clock	Send command to update spacecraft clock	SCLOCK_SET	Initial command to s/c. Command counter should increment. (Command does not currently exist in command dictionary, but CaPoly said they will create it. Make sure to update once command exists-MP)	Loss of Time Reference
10	18:00:00	ACS	IMU Checkout	Command IMU data acquisition for 5 min.	IMU-START	Should be structured as a CMD sequence, such that IMU turnoff is automated.	
11	01/06:00:00	Ground Systems	IMU Checkout	Command downlink of IMU checkout data	IMU-GET-ALL	All raw data and compressed data for gyros, accels, magentometers	
12	01/18:00:00	Payloads	Payload Checkout	Command image acquisition from -Z and side panel cameras	CAM-RAPID-CAPTURE	Will use same image sequence as planned for sail deployment	
13	01/18:02:00	Payloads	Rad Checkout	Downlink radiation detector data	RAD-GET		
14	01/18:04:00	Thermal	Thermal Checkout	Downlink stored temp sensor data	SYS-TEMP	Will report detailed temperature telemetry data	
15	01/18:05:00	Ground Systems	Command a Reboot	Command a reboot	SYS-REBOOT		Commanded Reboot
16	03/00:00:00	Ground Systems	Update Onboard TLE	Uplink TLE to spacecraft	SET-TLE		Orbit Model Inaccurate
17	03/00:02:00	Ground Systems	Perigee Time Table	Uplink perigee time tiable	PERIGEE-PUT		Perigee Time Estimation errors
18	03/00:04:00	Ground Systems	IMU Data Acquisition Turn-on	Initiate IMU data acquisition, 20 minutes centered about each perigee	IMU_ON		
19	04/00:00:00	All	Sail Deploymnt Go/No-Go	Mission Manager conducts sail deployment go/no-go poll: S/C Systems, Power, telecom, ACS, Thermal, Payloads, Ground Systems (Cal Poly, ASU, Purdue, GT), PI		Go/no-go led by Mission Manager. Do we want to command a reboot prior to sail deployment activity?	
20	04/01:00:00	Ground Systems	Arm Sail Deployment		ARM-SAIL		
21	04/01:00:10	Ground Systems	Fire Sail Deployment	Initiates sail deployment sequence: IMU data acquisition, camera image acquisition sequence, door open burnwire initiation.	DEPLOY-SAIL		
22	04/08:00:00	ACS, Ground Systems	IMU Data Downlink	Downlink IMU data from sail deployment	IMU-GET-ALL		
23	04/08:01:00	Payload	Side Camera Downlink	Downlink side camera images from sail deployment	CAM-RAPID-CAPTURE		
24	04/08:03:00	Ground Systems	Perigee Time Table	Uplink perigee time table	PERIGEE-PUT	Updated with drag sail deployed	repeat every x number of 20min cycles
25	04/16:00:00	Ground Systems	Update Onboard TLE	Uplink TLE to spacecraft	SET-TLE		
REPEAT 18, 22, 24, 25 AS NEEDED							

2.4 Requirements Flowdown

The Minimum Mission Success Criteria and the Full Mission Success Criteria serve as high-level sources from which a flow-down of the requirements is performed. Requirements for the ADE mission shall be traceable to these sources, which allows each requirement to serve a specific purpose in achieving the overall mission success. This helps to avoid unnecessary requirements which would complicate the mission design. To see the full list of requirements see Appendix A.

Additional high-level sources from which requirements are derived are:

- CubeSat Design Specifications [1]
- Application for STEM CubeSat Launch Opportunity [2]
- Initial Proposal [3]
- ULA Do-no-harm requirements [4]

These high-level sources are the root for a hierarchical structure of all requirements. This structure is shown in Figure 2.2. The requirements for the branches 'Mission Design', 'Flight System', 'Mission Operations', 'Payload', and 'STEM/Outreach' originate and can be traced back to the three high-level sources 'MMSC', 'FMSC', and 'External Sources'. This hierarchical structure ensures that all requirements in the individual sub-branches contribute to the overall mission success.

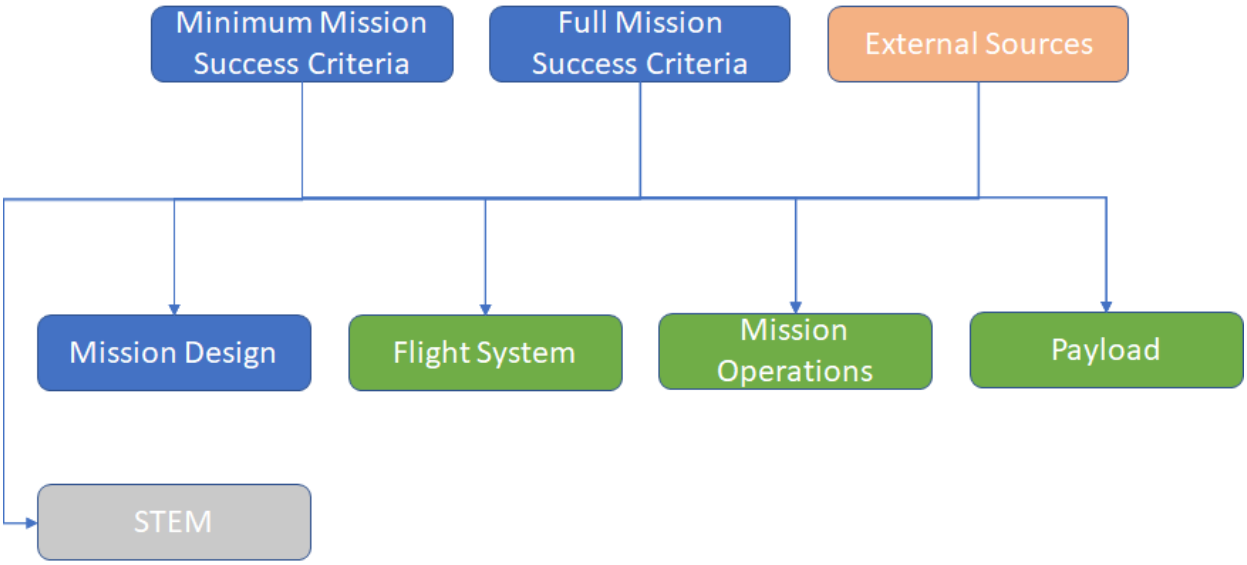

Figure 2.2: Hierarchical Requirements Flowdown

The requirements that are derived are compiled in the Requirements Verification Matrix (RVM). In this matrix, all sub-systems are represented and further branched out. When requirements in a sub-branch need to be further refined, sub-requirements are created in the following fashion:

- MD-1
    - MD-1.1
    - MD-1.2
    - …

Each of those sub-requirements inherits from the main requirement.

Each requirement needs to be clear and verifiable. This means, that requirements shall use quantifiable benchmarks whenever possible and are phrased unambiguous. The verification method (‘Analysis’, ‘Inspection’, or ‘Testing’) is specified for each requirement in the RVM. These verification methods are later mapped to the test plan for validation and verification.

Requirements for ‘Mission Design’ are concerned with the mission architecture of ADE, orbit requirements and the sequence of events. They detail the way the mission success criteria are met on a mission design level and can subsequently serve as higher level sources for other subsystems as well. This is necessary because detailed requirements for the mission are stated here that need to be met by other subsystems and are not specified in the mission success criteria.

The branch ‘Flight Systems’ is further divided into the subsystems relevant for the ADE mission: ‘Thermal’, ‘Attitude’, ‘Structure’, ‘Electrical Power System’, ‘Telecom’, and ‘Command & Data Handling’. Flight system requirements are derived from MMSC-1, FMSC-1, and FMSC-3, that the CubeSat shall be launched as a secondary payload into GTO and establish two-way communications with Earth to downlink data. In the ‘Flight System’ branch of the RVM, the constraints on the spacecrafts design and construction are specified and thermal and structural limits are set. Most requirements in ‘Structures’, ‘Thermal’ and ‘EPS’ fall into the previous description and dictate ADE’s CubeSat design, the number of solar panels and batteries and the operational thermal limits among others. Requirements in the Subsystems ‘Attitude’, ‘Telecom’, and ‘Command & Data Handling’ for example are concerned with the data acquisition by the IMU, the processing of this data, and finally downlinking those data packages that are critical for achieving FMSC-1, the downlink of IMU data for five perigee passes.

The branch ‘Mission Operations’ is subdivided into ‘Ground Data System’ and ‘Tracking Stations’. In this sub-branch, operational requirements are defined. This includes capabilities on the ground, specifications for the ground data system and tracking stations as well as soft- and hardware constraints in the ground data system.

The branch ‘Payload’ is divided into the categories ‘Drag Sail’, ‘Cameras’, and ‘Radiation Detectors’. ‘Drag Sail’ is covered by MMSC-2 and MMSC-3, to deploy a drag sail and verify the orbital decay rate. The geometry, material and thermal constraints of the drag sail, which is the center of the ADE mission, are defined here. The ‘Cameras’ requirements inherit directly from FMSC-3, to take a photo of the drag sail. FMSC-2, to characterize the radiation environment in GTO for three orbits, is ensured by the requirements in the ‘Radiation Detectors’ section.

The final branch of the requirements flow-down is the 'STEM/Outreach' branch which formulates requirements to cooperate with high schools, public relations and in general to increase the visibility of the ADE mission.

2.5 Verification and Validation

Verification and validation are two key ingredients for confirming that a product is ready for a successful launch. In validation, the set of requirements for ADE are certified to meet the purpose of the project. In verification, the purpose is to ensure that the set of requirements are met. As discussed in 2.4, the RVM lists the set of requirements that must be verified for inspection and analysis, or testing operations.

For the project thus far, the main focus has been the verification phase. This incorporates the list of requirements in the RVM and breaks each set of requirements into a designated method of verification. For this project there are 3 types of verification methods, inspection, analysis, and testing. The inspection and analysis was completed by each sub-team for their appropriate set of components. The testing phase is the more hands-on activity that will occur in the spring of 2018.

The requirements that depend on the testing verification method will have gone through an official closeout document, which is signed by several systems sub-team members in order to ensure accuracy of the document. The closeout document provides proof that the all requirements have been verified for a particular component or system. There are 3 levels of testing that will be completed after the I&TRR, component-level testing, subsystem-level testing, and system-level testing. Table 2.2 below shows the different tests to be completed throughout the next semester.

Table 2.2: Testing Levels for I&T

Testing Level	Description
Component	Integral parts of the final product. Includes power-on tests, data flow, radiation testing, budget, operating modes, etc.
Subsystem	Combined testing of several components. Includes subsystem operability, command & data handling, flight-like harnessing, etc.
System	Routine tests of connected subsystems. Includes function spacecraft for testing, lifecycle charging, command execution, telecom tests, thermal vacuum testing, vibration and radiation testing, etc.

The goal of the I&TRR is to ensure that all of the requirements are ready to be verified, along with a concise schedule for the testing phase to begin and end. These testing levels cover a range of rigorous tests that challenge the robustness of ADE on several different levels. Only then will the team be fully confident in the success of ADE in the mission. The mission itself is described in greater detail in the next section.

3 Orbit Analysis

3.1 Initial Orbit

ADE will be delivered into a geosynchronous transfer orbit, and will be subject to launch insertion errors as specified by the United Launch Alliance. The nominal parameters for the initial orbit are summarized along with the current best estimates for the spacecraft parameters in Table 3.1 and Table 3.2. The initial Right Ascension of the Ascending Node (RAAN) is not listed because there is currently too much uncertainty for this parameter, which is dependent on the time of launch. For the spacecraft parameters, it should be noted that due to tumbling, the drag coefficient will keep changing based on the spacecraft orientation. However, near perigee due to restoring torque we have linearly estimated the variation of Cd. More about this is explained in this chapter. Also, the drag sail for this deorbit sail is made of a transparent material, CP1, so only the CubeSat body must be considered for solar radiation pressure (SRP). The SRP area would also change because of tumbling and change in the CubeSat's orientation relative to Sun but we are neglecting the change in SRP area in this analysis. We are neglecting this because it is extremely difficult to know how the orientation of ADE will change relative to Sun

Table 3.1: Nominal Initial Orbital Parameters

Parameter	Value	Units
Semi-major axis (a)	24364	km
Perigee Altitude (r_p)	185	km
Apogee Altitude (r_a)	35786	km
Eccentricity (e)	.7306	dimensionless
Period	10.51	hours
Inclination	27	degrees
Argument of Periapsis	180	degrees

Table 3.2: Spacecraft Parameters

Parameter	Value	Units
Dry Mass	2	kg
Drag Area	0.7-2	m^2
Drag Coefficient (C_D)	Varied 0.7 - 2	dimensionless
Coefficient of Reflectivity (C_R)	1	dimensionless
CubeSat SRP Area	.015	m^2

The following images display the initial orbit, which is expected to experience changes due to perturbations until the drag sail is deployed.

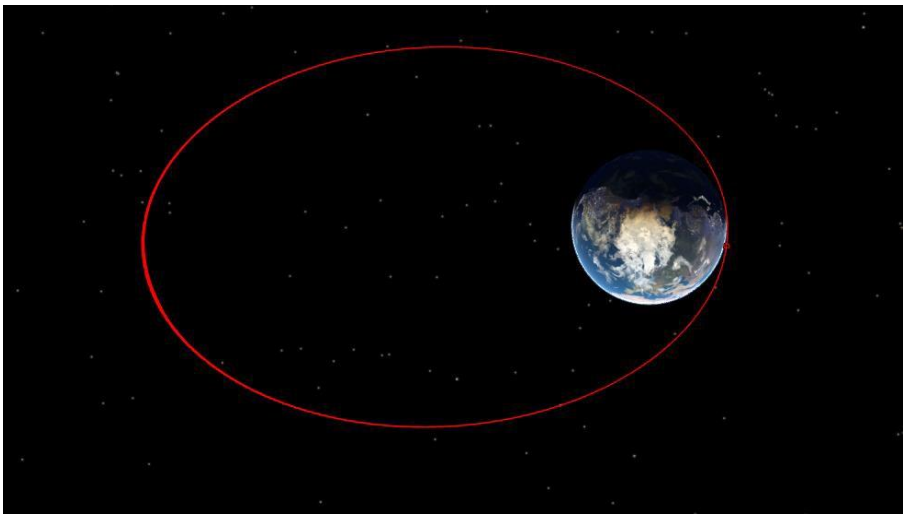

Figure 3.1: View of Initial Orbit In-Plane

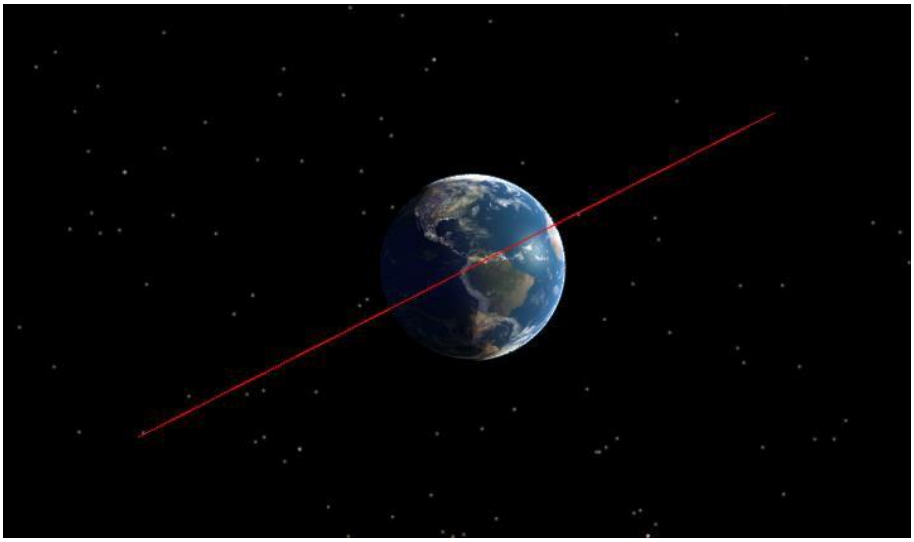

Figure 3.2: View of Initial Orbit Looking Down Line of Nodes

This orbit has a relatively high eccentricity and low perigee. Due to this, the dominating perturbing force changes throughout the course of the orbit, and these will be further analyzed in the following sections.

3.2 Orbital Perturbations

Within the spacecraft orbit, there are multiple regions that the spacecraft enters, changing the dominating perturbing force. The perturbing forces experienced during the lifetime of the spacecraft include drag, third body gravitational models, Earth (J2 till 15^{th} term), and solar radiation pressure. No significant changes will occur to the initial orbit before sail deployment as the time before sail deployment to deorbit duration is negligible.

Once the sail is deployed, the atmospheric drag perturbation is the primary perturbing force during the spacecraft lifetime and has the most significant effect on orbit changes. As the satellite reaches apogee, the third body gravitational effects become the dominating perturbing force. Since the initial orbit has a large eccentricity, the satellite will spend a large percentage of the orbit time near apogee during the beginning of the mission. Isolating this perturbing force shows that the third body gravitational model can cause significant changes to the periapsis altitude and is dependent on the relative position of the Earth, Sun, Moon, and satellite and is most noticeable when the satellite has not yet experienced much orbital decay.

The next perturbing force experienced is the orbital perturbation due to Earth's oblateness, and this force is noticeable throughout the course of the mission. However, as the spacecraft decays, this force has increasing effects because it begins to feel the uneven distribution of Earth's mass more and the point mass attracting body assumption begins to break down. The last perturbing force experienced is solar radiation pressure due to the sun and albedo. However, the sail material for the ADE mission is transparent, and therefor does not count towards the overall area that the solar radiation pressure acts over. This leaves just the spacecraft area, with an assumed coefficient of reflectivity of 1. However, because this area is small, analysis has shown that this perturbing force is negligible for this mission.

3.2.1 Deorbit Profile - GMAT

Figure 3.3 and Figure 3.4 show the combined effects of all the perturbing forces in the simulation discussed in the previous section. These plots were made in GMAT. The simulation starts after sail deployment and the key features to note in both figures include the decreasing apogee and precession of the orbit. The effects on the perigee due to third body gravitational cannot be easily seen in these visualizations but should not be overlooked and will be discussed in further depth in upcoming sections.

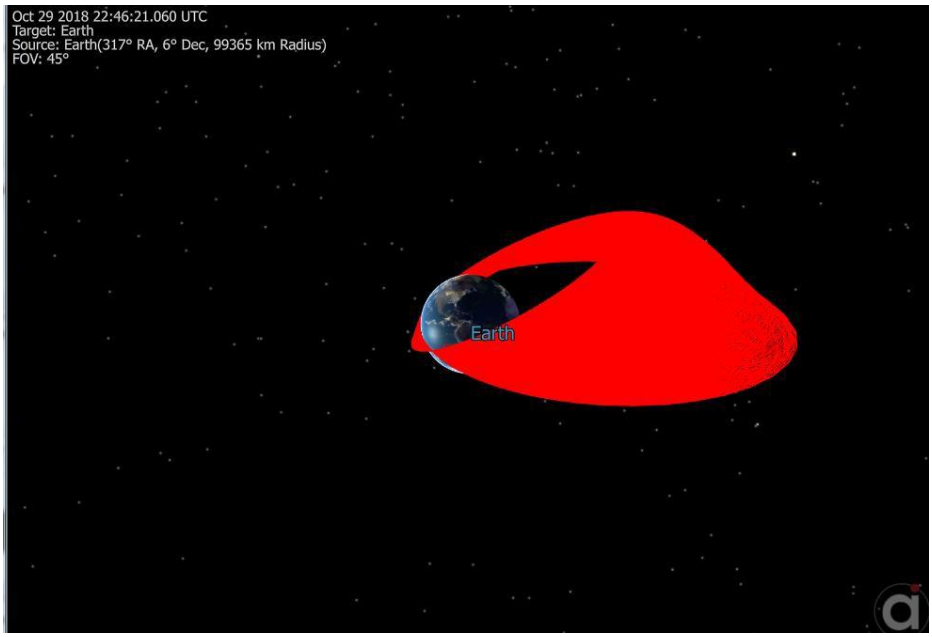

Figure 3.3: View of Deorbit Profile

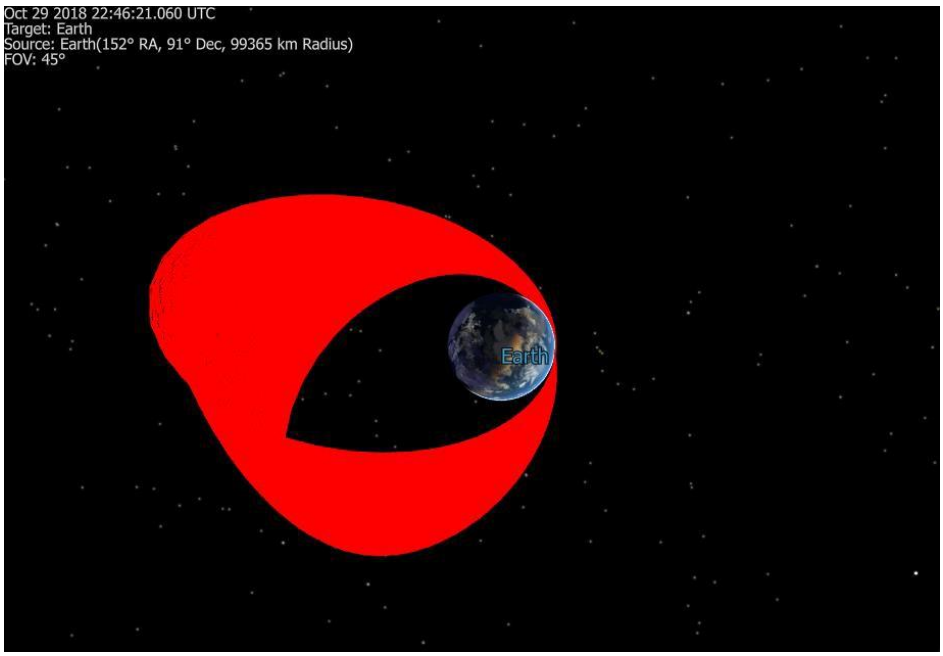

Figure 3.4: In-Plane View of Deorbit Profile

3.2.2 Third Body Gravitational Effects

Previous analysis of this orbit displayed the deorbit time's dependency on initial RAAN value of the orbit. The initial RAAN has a large amount of uncertainty because it is highly sensitive to the launch date and time and therefore cannot accurately be estimated. Therefore, RAAN is evaluated for all possible values. Looking at a further in-depth analysis of the RAAN dependency

shows that the results vary depending on the gravitational force models used. Figure 3.5 shows variation of deorbit times due to initial RAAN dependent on the gravitation force models used including just the isolated two-body Earth and satellite model and combinations of perturbing third body forces summarized in the figure's legend. The main effects noted are that a simple two body model shows a significantly smaller variation in deorbit times compared to inclusion of the third body gravitational models. The Moon and Sun model has the largest variations in deorbit times and when compared to just the Sun third body gravitational model deorbit times, it is seen that the sun has the dominant effect on varying the deorbit times. The figure summarizes the significant impact that the initial RAAN has on the deorbit times due to these third body gravitational forces experienced.

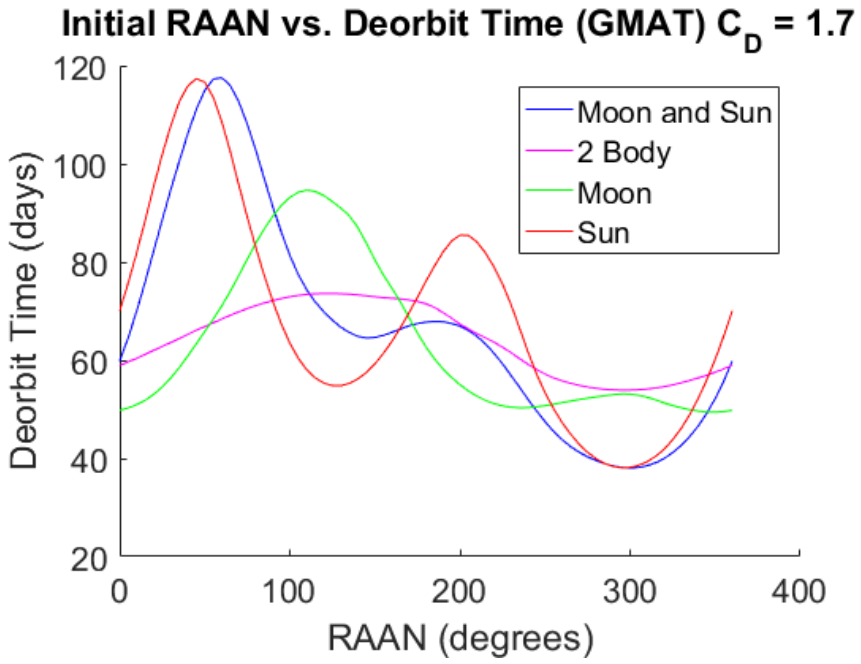

Figure 3.5: Dependency of Deorbit Time on Initial RAAN - GMAT Analsis

3.2.3 Atmospheric Model

The atmospheric model chosen for analysis follows is MSIS-2000. This atmospheric model defines more accurate than the previously considered Jacchia Roberts Atmospheric Model value for atmospheric temperature, pressure, and density for altitudes ranging from 90 – 1000 km (30). The MSIS-2000 atmospheric model includes latitudinal, seasonal, geomagnetic, and solar effects and generally models the upper limit of the atmosphere to a statistical accuracy of 15 percent. The most significant assumption of the Jacchia-Roberts atmospheric model is that the atmosphere rotates with the Earth as a rigid body. In terms of STK, the easiest way to implement the models was to use a blended density model, in which Jacchia-Roberts was used for altitudes above 1,000km, and MSIS-2000 was used for the aforementioned altitude range. While this resulted in a longer computation time and took around 6 days for all simulations to run, it provided more accurate estimates of the deorbit profile.

3.1 Orbit Lifetime

3.1.1 Monte Carlo RAAN Analysis

For this mission, there are still large amounts of uncertainty that will affect the orbit lifetime. In order to understand the possible deorbit times, a Monte-Carlo analysis was performed that varied the significant uncertain parameters within minimum and maximum expected values. The variations are summarized in Table 3.3 with the values and distributions included the simulation. The initial date for the simulation is assumed to be June, 1st 2020 at 00:00:00 and has an impact on the simulation results. The analysis is performed for different initial date, different RAAN value for each initial date and the Cd is varied as explained later in the chapter.

Table 3.3: Varied Parameters for Monte Carlo Analysis

Parameter	Expected	Min	Max	Distribution
RAAN (degrees)	N/A	0	360	Uniform, in increments of 3
Mass (kg)	1.8	1	1.9	Uniform
Projected Area (m2)	1.13	1	1.2	Uniform
Perigee altitude (km)	185	-	-	Normal
CD	1.7	0.7	2	Constant at 0.7 for above 500 km then varied linearly every 50 km till 200 km to reach 2

The results for 500 cases with the previously listed varied parameters are summarized in Table 3.4. Assuming that the probabilities for each parameter's distribution are accurate, results show that there is an 80% likelihood that deorbit will occur within approximately 80 days.

Table 3.4: Results from 500 Cases in Monte Carlo Simulation - GMAT

Deorbit Case	Deorbit Time (days)
Average	80.81
Median	71.36
Max	320.45
Min	29.52

Plotting each of the deorbits, as apogee altitude as a function of time is seen in Figure 3.6 shows the deorbit envelope with maximum and minimum cases. This displays the deorbit profile for each of the cases that was run in the Monte Carlo analysis and yields the maximum and minimum profiles for the deorbit.

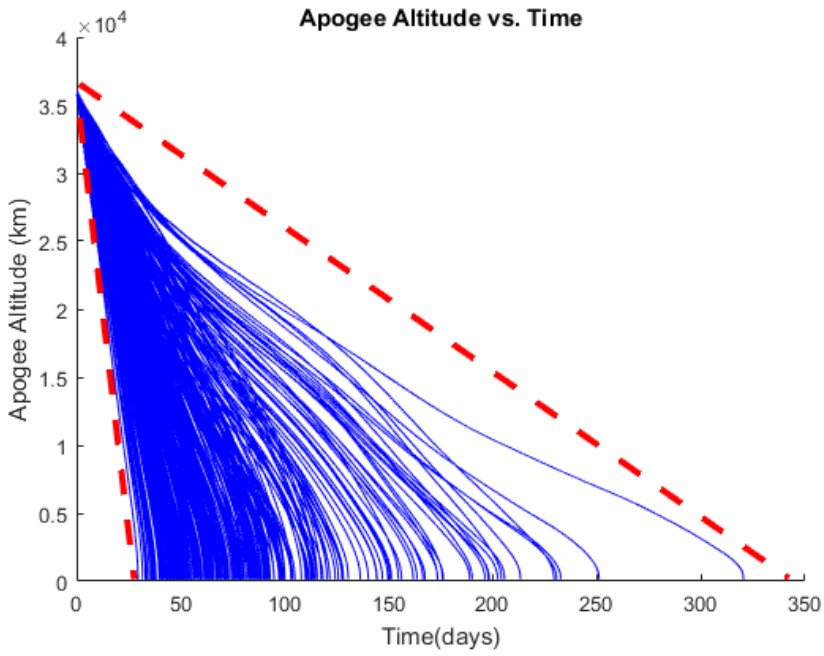

Figure 3.6: Monte Carlo Deorbit Envelope

Looking at this wide range of deorbit profiles, each of the individual parameters were investigated against deorbit time to better understand which uncertainties yield the largest impacts on deorbit times. The initial RAAN had the largest effect on determining the deorbit times followed by the uncertainty of the drag coefficient. The plots for each of these are shown in Figure 3.7 and Figure 3.8 respectively. These results are not initially intuitive and warranted a deeper investigation of the behavior of the orbit for various RAAN cases.

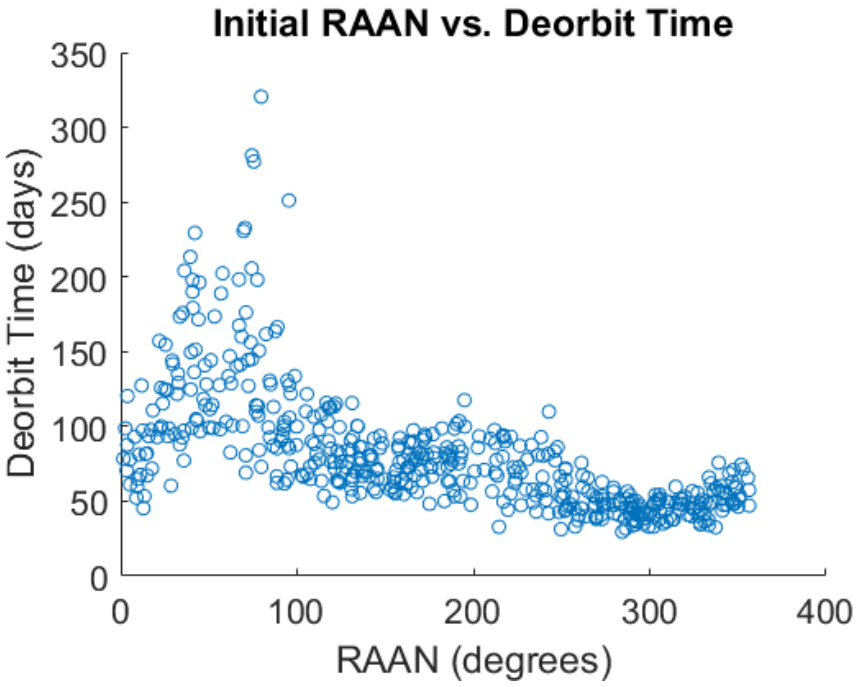

Figure 3.7: Deorbit Time vs. Initial RAAN for varied Monte Carlo Parameters

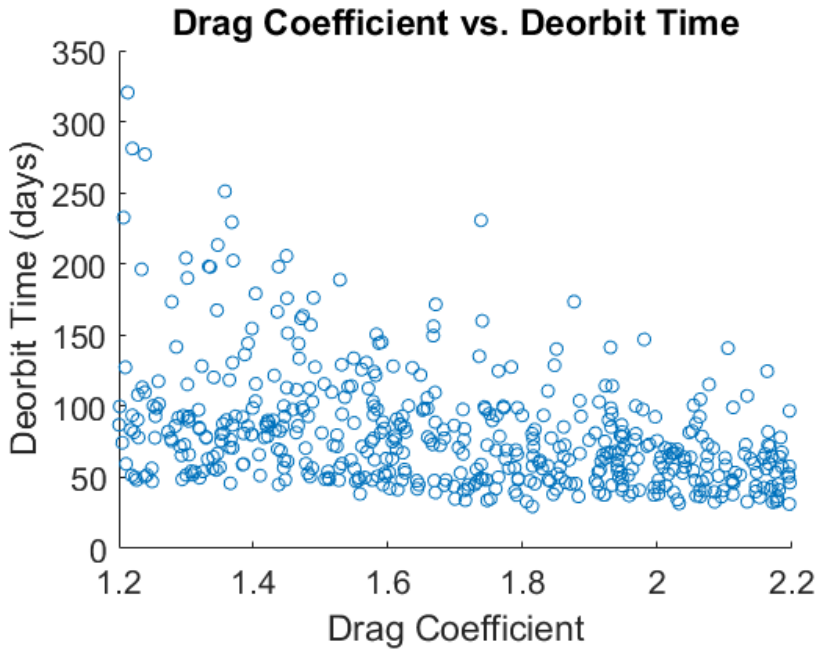

Figure 3.8: Deorbit Time vs. Drag Coefficient for varied Monte Carlo Parameters

Evaluating the plots knowing that the new best estimate for the drag coefficient is about 2.09, this should tighten the uncertainty ranges. The new ranges would likely yield deorbit times between 30 – 150 days, with an average around 70 days and median around 60 days, but these cases should be rerun for better precision in the Monte Carlo code.

3.3.2 *Effects of Initial RAAN*

Evaluating the results from of the extreme cases for varied initial RAAN for the Monte Carlo analysis yielded a clear trend as the deorbit time increased. Plotting the perigee altitude as a function of time, seen in Figure 3.9 shows that for the long deorbit times, the perigee actually displays an initial rise in perigee altitude on the order of approximately 30 kilometers. In the minimum cases, the opposite occurs, and the initial perigee is actually lowered by about the same order before deorbit occurs. For the average case, the perigee displays a nearly constant behavior. These results were consistent with each of the deorbit profiles in the Monte Carlo analysis. The apogee versus time plots in Figure 3.10 show that the deorbit rates are nearly linear as the apogee decays for each of the cases.

Returning to the effects of orbital perturbations, it was noted that the third body perturbations cause long term changes in perigee. The third body perturbations are a function of the initial RAAN value, which was also displayed in previous sections because of the relative positioning of the Earth, Sun, Moon, and Spacecraft. Gathering all of this insight, it is determined that the initial RAAN affects the relative positioning for third body gravitational forces, which can cause the perigee to change. An initial rise in perigee decreases the drag force due to a thinner atmosphere, while an initial drop in perigee increases the drag force due to a thicker atmosphere. This affects the force exerted on the drag sail and leads to significant variations in deorbit time. It should also be noted that the relative locations of the gravitation models depend on the epoch date for the mission. Therefore, a different launch date and deployment date could lead to significant changes in deorbit evaluation. If the launch date changes, a new analysis should be performed to capture these changing effects.

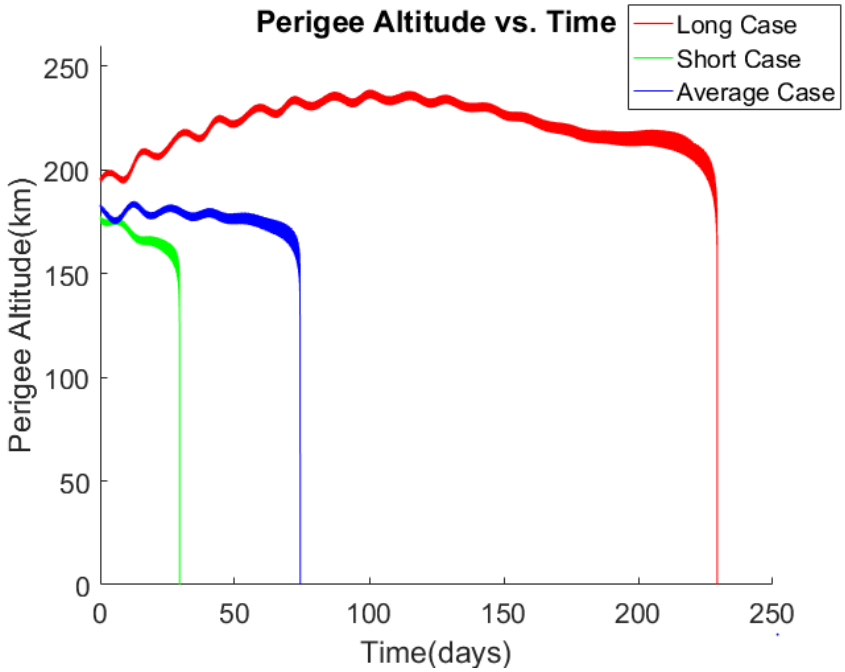

Figure 3.9: Perigee as a function of time for various deorbit cases

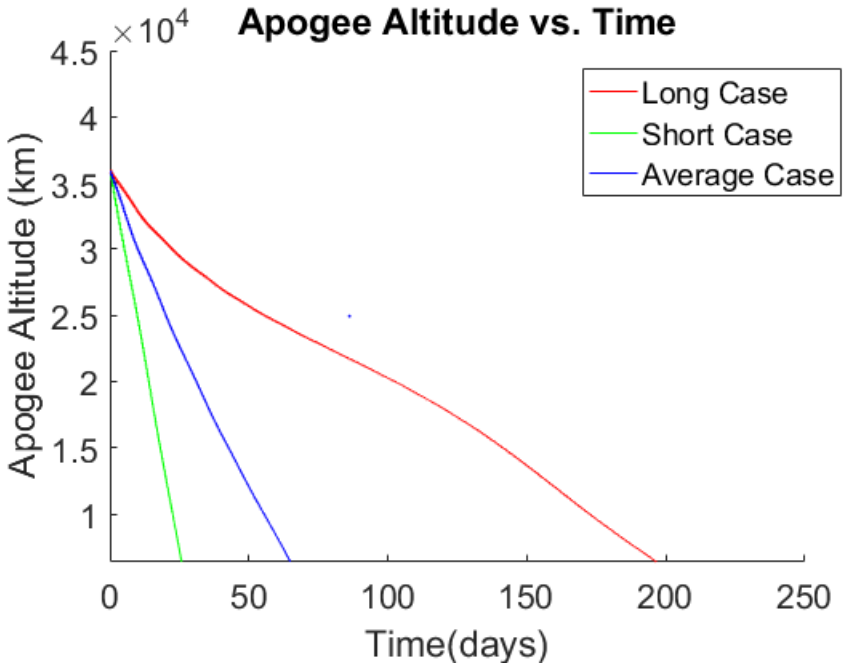

Figure 3.10: Apogee Altitude for various deorbit cases

During the Spring 2019 semester, quite a few modifications were made in terms of simulating the orbit of the cube satellite. Two different software were used, STK and FreeFlyer. Data from each of the software was compared and was found to be reasonably similar, with an average deorbit duration difference of about 6 days. This suggests that both the softwares are extremely reliable and useful for performing Monte Carlo simulations. When designing the simulations, it was critical that each parameter was as similar as possible between both software. Therefore, input parameters and initial state data was checked before each simulation was ran. This ensured accurate simulations between the two software, hence, resulting in a small difference of only 6 days. While running these simulations, the MSIS 2000 atmospheric model was used for analysis. This was mostly because it is more accurate at altitudes below 1,000 km. With STK, Jacchia Roberts was used for analysis at altitudes above 1,000 km, and a blended atmospheric model was utilized to ensure accurate deorbit duration of the mission. It is important to note that FreeFlyer predicted negligible difference between the blended model and the MSIS 2000 model, and MSIS 2000 was used for the entire deorbit duration of the mission.
The major Monet Carlo analysis that was performed was with 16 epochs, varying the RAAN and the Cd value as described above. It was found that the general deorbit duration of the cube satellite decreased as the epoch was increased. The following table lists all the epochs that were tested:

Epochs Simulated
June 1st, 2020 00:00:00
June 1st, 2020 12:00:00
June 8th, 2020 00:00:00
June 8th, 2020 12:00:00
June 15st, 2020 00:00:00

June 15st, 2020 12:00:00
June 22nd, 2020 00:00:00
June 22nd, 2020 12:00:00
June 29th, 2020 00:00:00
June 29th, 2020 12:00:00
July 6th, 2020 00:00:00
July 6th, 2020 12:00:00
July 13th, 2020 00:00:00
July 13th, 2020 12:00:00
July 20th, 2020 00:00:00
July 20th, 2020 12:00:00

Deorbit Duration, Access Times, RAAN, Cd, access start times and stope times, for all these epochs were outputted to files. All the data is available in the shared drive. It is not possible to include all this data in this document, as it will result in extreme inconvenience for the reader. However, to highlight the deorbit duration for the June 1st, 2020 epoch, the following table gives the data obtained from both STK and FreeFlyer, and the graph on the right shows how Cd was varied with altitude:

Software	Minimum (days)	Maximum (days)	Average (days)
STK (based on changing atmospheric model)	28.65	84.97	45.05
Freeflyer(Only MSIS-2000 as the values of changing atmospheric model is comparable with MSIS as shown in earlier update)	29.01	97.9	51.43

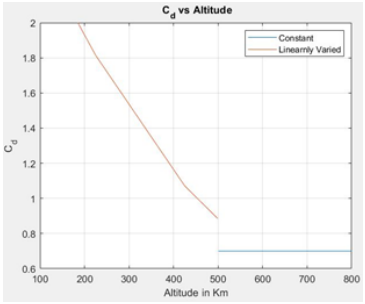

It is clear that the deorbit duration has decreased significantly in the simulations ran this semester. It is equally important to note that these simulations were not simulating the attitude of the cube satellite, and only considered the cube satellite as a rigid body. Therefore, it is likely that the actual deorbit times will vary a little bit than the results presented above. Overall, the orbits of the cube-sat were modeled as accurate as possible based on the data that was provided. While it took an extremely long time to run 1,920 Monte Carlo simulations with STK and FreeFlyer, we are confident that the code that was developed during this semester as well as the data acquired on the simulations will be helpful in understanding the orbit of the mission better. The one thing in the future that could be implemented is simulating the attitude of the cube satellite. This was not possible this semester, as it would have taken quite some time to learn the spacecraft attitude dynamics. All the code is available in the shared drive, and if we want to run any of the simulations again, we could vary any of the parameters mentioned above in the code itself.

3.4 Deorbit Rates of Previous Missions

Considering similar missions related to passive deorbiting for satellites, our simulation model fidelity was evaluated. Three different missions were investigated specifically, with the following parameters input into our simulation model. The parameters and results from our

simulations compared to each of the missions are summarized in Table 3.5. The results initially showed that our simulation had a much faster deorbit time when compared to the expectations and results from the other missions. The primary reason for this is that the total drag area was used for initial simulations. In the drag area, it assumes that the sail will be perpendicular the velocity vector, so the full area experiences the drag force.

However, in the other simulations, the attitude changes may have been considered for the propagations meaning a much smaller area experienced the drag force. Therefore, the effective drag area is greatly reduced so the data we had was retrofitted to match the deorbit data. This resulted in an effective drag area of approximately one quarter of the entire drag sail area. Also, comparing the orbits from the previous missions to ADE, the periapsis for each case is much higher and the orbits are much more circular. This also changes the dominant perturbing forces throughout the course of the orbit. For the ADE table drag area data, it is assumed that the drag sail will provide attitude stability during its drag passes.

Table 3.5: Previous Similar Missions Parameters and Results Compared to Simulation

Parameter	ADE	LightSail [5]	NanoSail-D [6]	CanX-7 [7]
Sail Deploy Date	June 1st, 2018	May 20th, 2015	January 21st, 2011	May 11th, 2017
Perigee Alt (km)	185	350	800	800
Apogee (km)	35786	700	650	800
Inclination (deg)	27	55	72	80
Drag Area	1.12	32	10	5
Mass (kg)	1.8	5	4	3.6
C_D	2.09	1.05	1.05	1.05
Sail Material	CP1	Aluminized Kapton	CP1 (front) Aluminum (back)	Aluminized Kapton
SRP Area (m^2)	.015	32	10	5
C_R	1	1	1	1
Expected Deorbit Time	30-300 days	3-10 days	70-120 days	2-3 years
Actual Deorbit Time	-	7 days	240 days	In Progress
ADE GMAT Sim Deorbit Time	30-300 days	1.88 days	94.11 days	1.687 years

3.5 Attitude Stability

One of the primary objectives of the ADE mission is to evaluate the potential stability of the spacecraft during deorbit. Given the GTO orbit parameters, the spacecraft will pass through apogee of the orbit with a minimum altitude of 185 km. Since the effect of earth atmosphere is nearly negligible at a much higher altitude, it can be justified to focus the analysis of aerodynamic stability in the window in which the spacecraft is in the part of orbit that the altitude is below 800km. Under this assumption, multiple cases of deorbit are simulated with focus on different factors that governs the deorbit process. Aerodynamic stability provided by the drag sail, assuming the sail is fully deployed at the point of injection, has minimal effect on the spacecraft without an environment with dense enough atmosphere.

Previously it was determined that specific orbit parameters, namely RAAN and true anomaly, can't be yet determined due to uncertainty about the launch provider. Without specific injection data, the analysis looked at a range of different injection conditions and evaluated the stability of the spacecraft for each. The analysis then experimented with different atmospheric models to account for their uncertainties. The conclusion we can draw from this analysis is that the drag sail is capable of stabilizing the spacecraft within approximately 200 seconds of perigee.

3.5.1 Methodology

In this analysis, both GMAT from NASA and the SixDOF.m code developed by Purdue students are utilized to simulate the deorbit process. GMAT is mainly used for the analysis of the full timeline that gives us quantitative results in a straightforward fashion and relative short time. However, GMAT is constrained by lacking the ability to predict the aerodynamic influence and stability due to its structure of input. The program is limited in considering the shape of the spacecraft, and thus its coefficient of drag. To serve as a complementary method, SixDOF.m is used to generate a more accurate result that considers the environmental perturbing force and torques which then generate aerodynamic influences.

Using these tools, an analysis on the influence of injection parameters is done to compare the total angle of attack close to perigee. By varying the RAAN input into SixDOF.m, the code simulates the first 300,000 seconds of deorbit. A customized MATLAB script then takes the program outputs of total angle of attack (tAOA) history and plot graphs of tAOA under 600km of altitude. Basic statistical analysis is also performed to support the study.

The analysis of the various atmospheric models is done in GMAT. Similar to the approach of the previous analysis, the input of orbit parameters and spacecraft specifications are held the same while changing the atmospheric model.

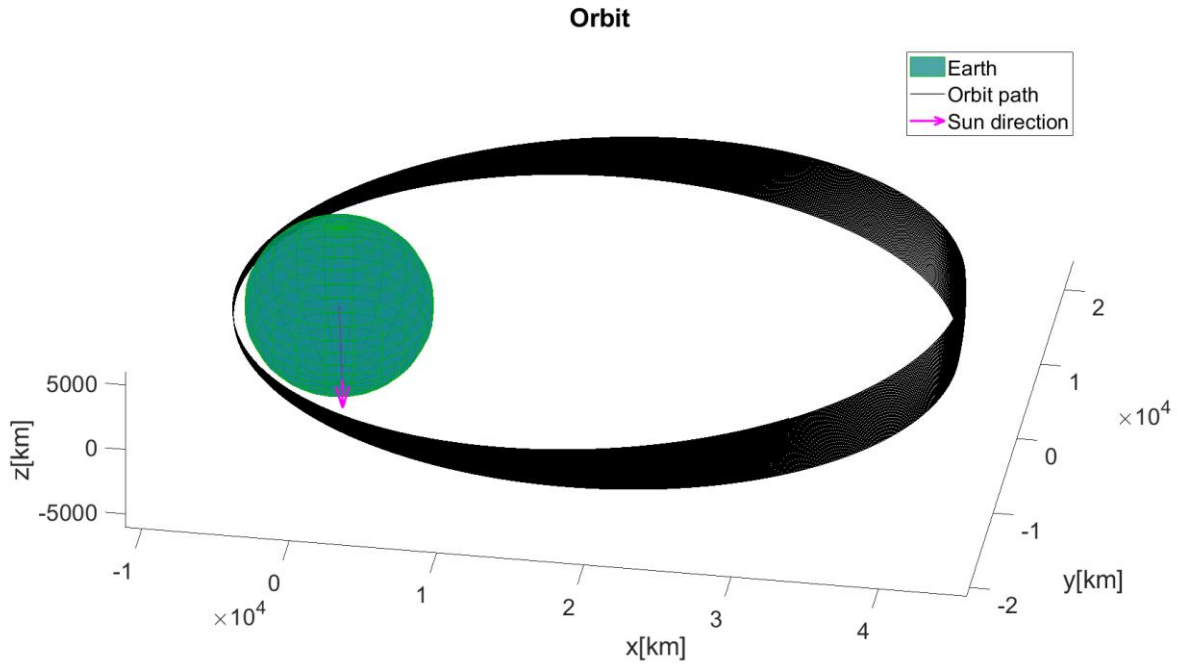

Figure 3.12 SixDOF.m generated orbit view

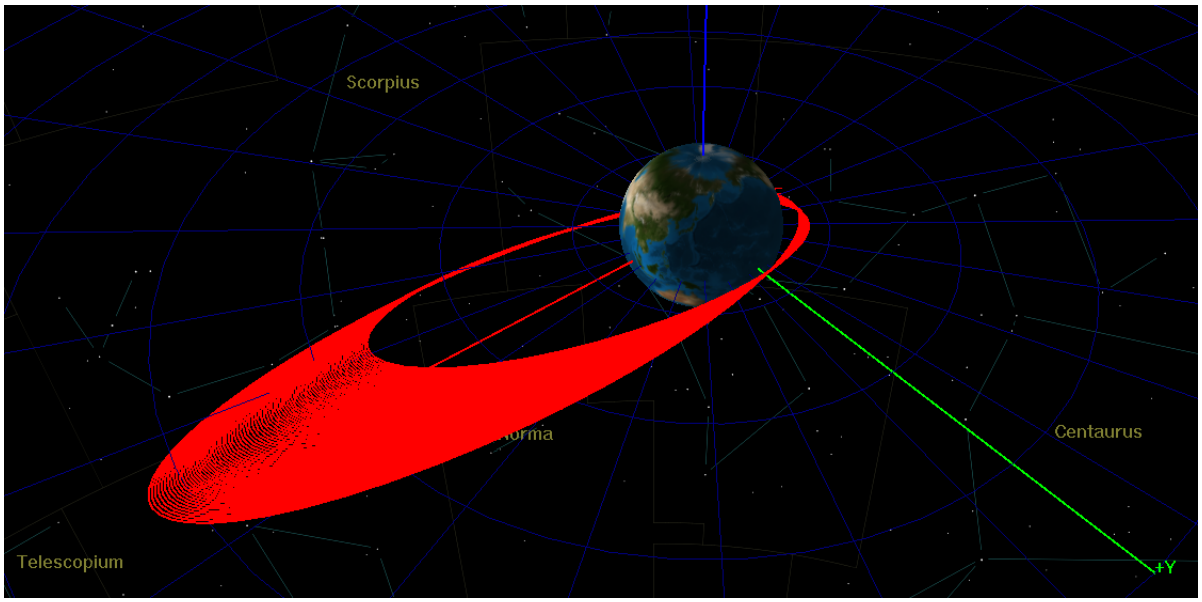

Figure 3.13 GMAT generated orbit view

3.5.2 *Effect of Injection Point*

As mentioned above, RAAN has a large effect on the deorbit duration, so this would be one of the first influencing factors we would analyze. Using SixDOF.m code, the following scenarios are simulated:

RAAN (deg)
0
30
60
90
120
150
180

The results from the analysis all show a decrease of tAOA up to 300 sec from perigee. For example, in figure 3.13, the orbit is configured with 0 degree RAAN, the curve decrease to about 25 degree at 300 seconds and remains under 30 degrees before reaching 300 seconds pass perigee. This indicates the increase of stability results from the drag sail around perigee. And when we look into the range of tAOA for each orbit, it is to point out that the increase in number of orbits in general sees an increase in the magnitude of tAOA. When the spacecraft leaves the perigee, the total angle of attack increases.

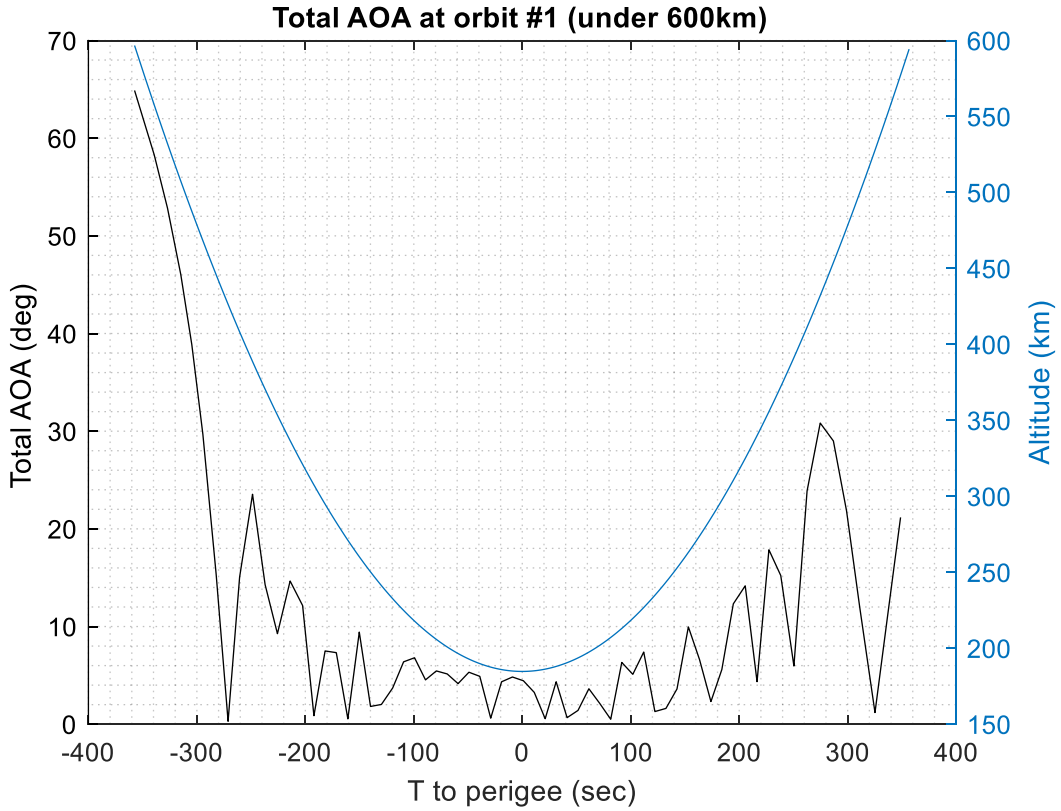

Figure 3.14 tAOA and altitude vs orbit time for 0 degree RAAN under 600 km

Now when changing the RAAN value, the spacecraft still gain the stability at lower altitude. Combining the average tAOA for each orbit at different RAAN, we can generate a plot as below. The cases all have the average tAOA under 60 degrees, which could be considered to be stable for the amount of time simulated. For stability of further time especially those that display a tendency of increasing over the number of orbit could require further simulation and analysis.

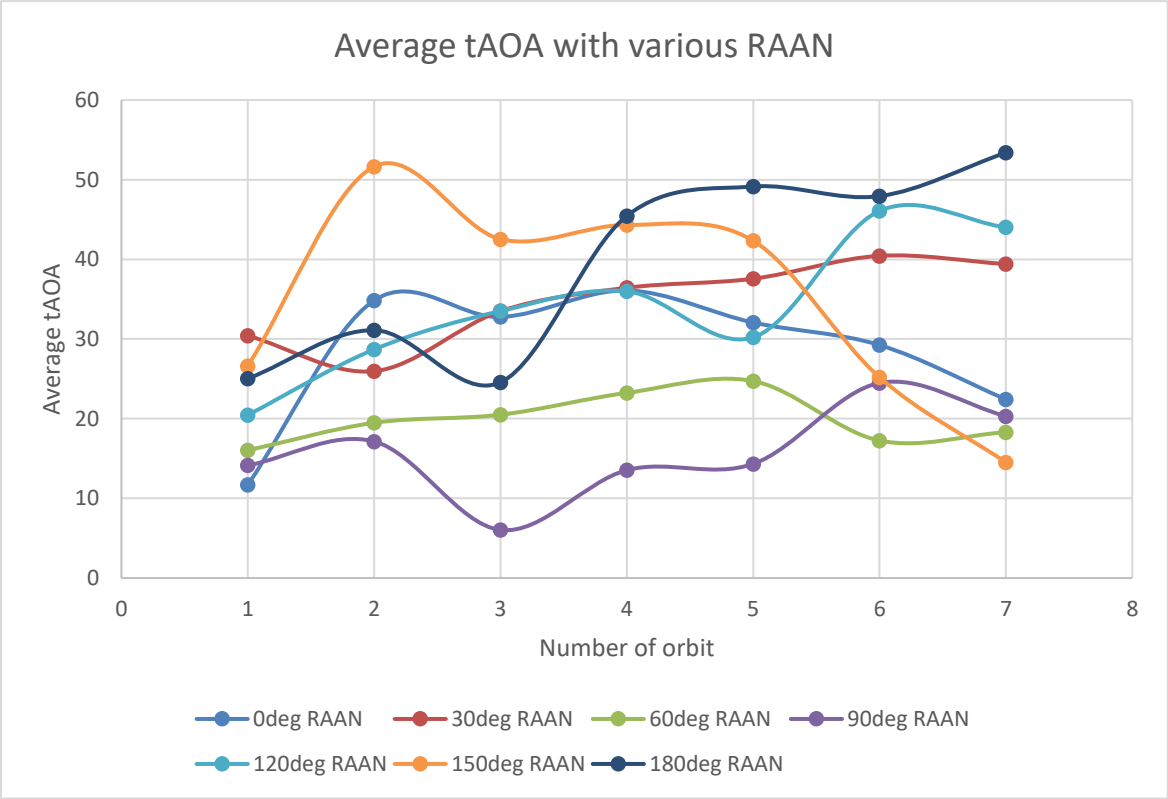

Figure 3.15 Average tAOA over number of orbit for different RAAN values

3.5.3 Effect of Initial Attitude

Initial condition also plays an important role in the dynamics of attitude. The initial attitude in this study, this effect was only studied briefly for an initial idea of the influence of initial condition. But from the results, we can see that although the average tAOA of the cases simulated are all under 60 degrees which could be consider as stable, but some cases surely are more stable than others. In figure 3.16, we can see the total angle of attack is under 30 degrees from -300 seconds to 300 seconds, indicating a stable state. In figure 3.17, the situations simulated are plotted, except for 20 degrees, other cases are all inside the 20 to 40 degree range. This doesn't seem to comply with what we would predict and could be further studied with more analysis.

The MATLAB code for this analysis can be found in Appendix B.

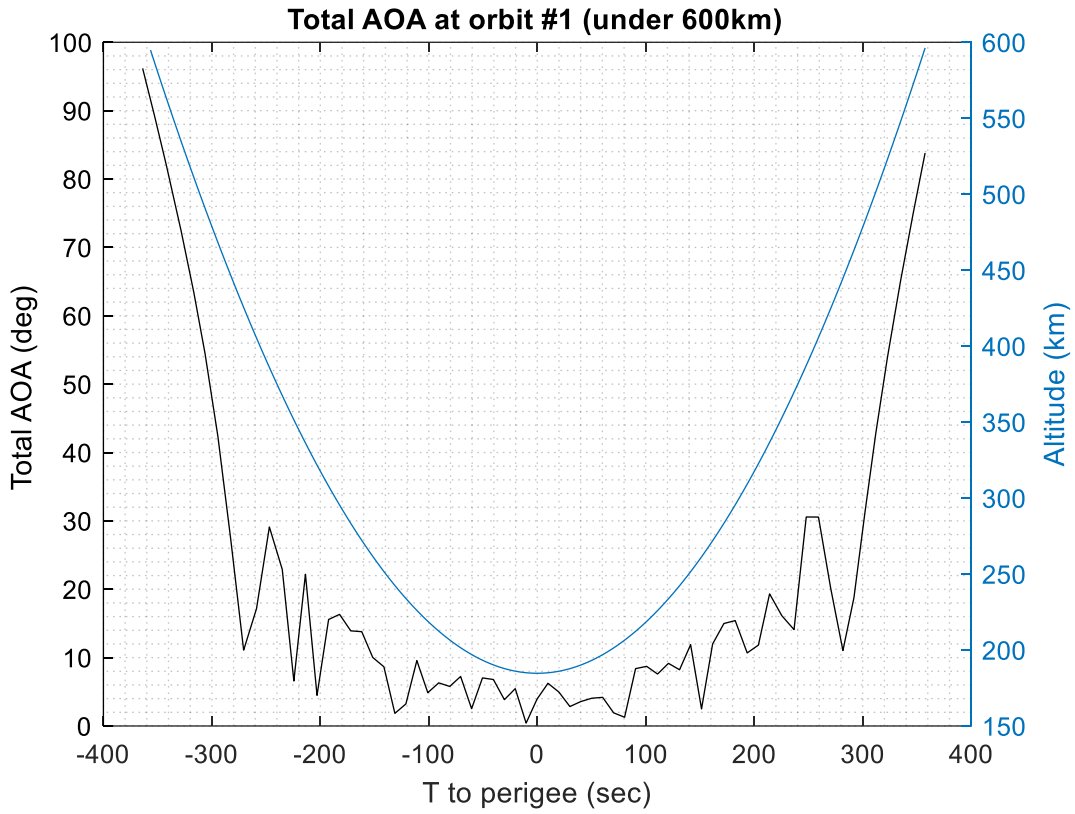

Figure 3.16 tAOA and altitude vs orbit time for 0 degree RAAN and 40 degree yaw under 600 km

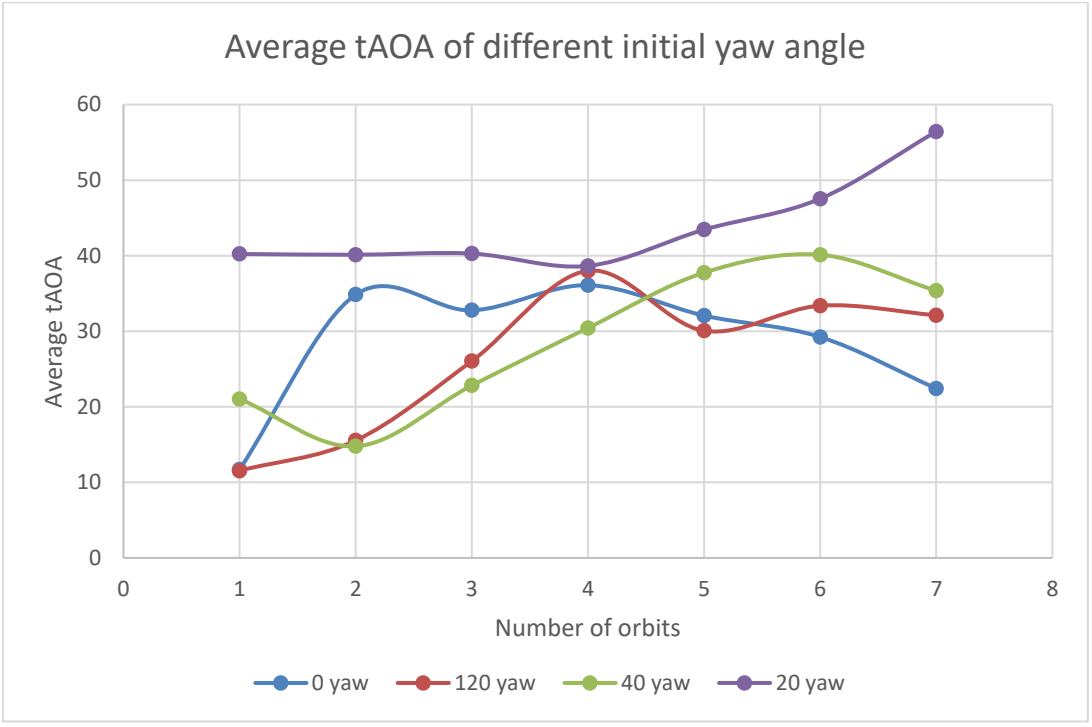

Figure 3.17 Average tAOA of different initial yaw angle

4 Coordinate Systems

4.1 P-POD Coordinate System

As can be seen in Figure 4.1, the P-POD coordinate system is defined in a way such that the +Z axis is defined along the height of the P-POD, towards the exit, the +Y axis directed along the length of the P-POD, and the +X axis directed along the width of the P-POD.

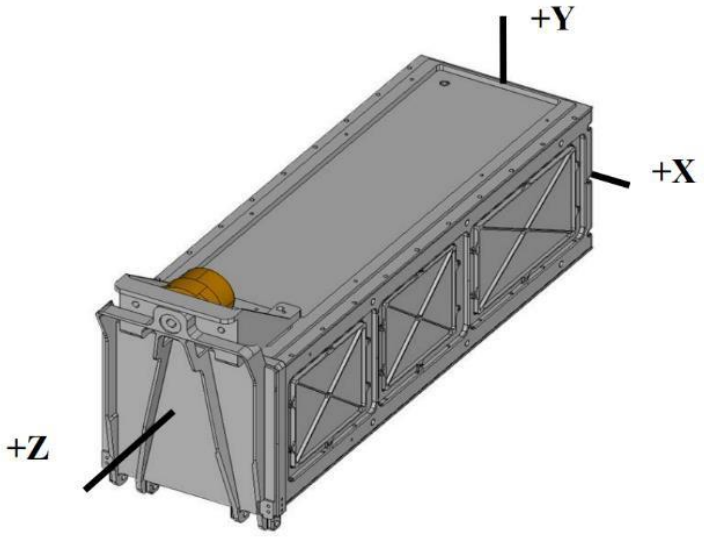

Figure 4.1: P-POD Coordinate System

4.2 Spacecraft Coordinate System

As defined in Cal Poly's CubeSat Design Specification document [3], the spacecraft's coordinate system is aligned with that of the P-POD when it is stowed in the P-POD prior to deployment. This is done for simplification, as it prevents confusion between the CubeSat and P-POD. The origin of this system is the center of gravity of the satellite, and as can be seen in Figure 4.2, this definition means that the drag sail will be deployed in the +Z direction. In addition, solar panels will cover the satellite's body on the ±X and ±Y sides.

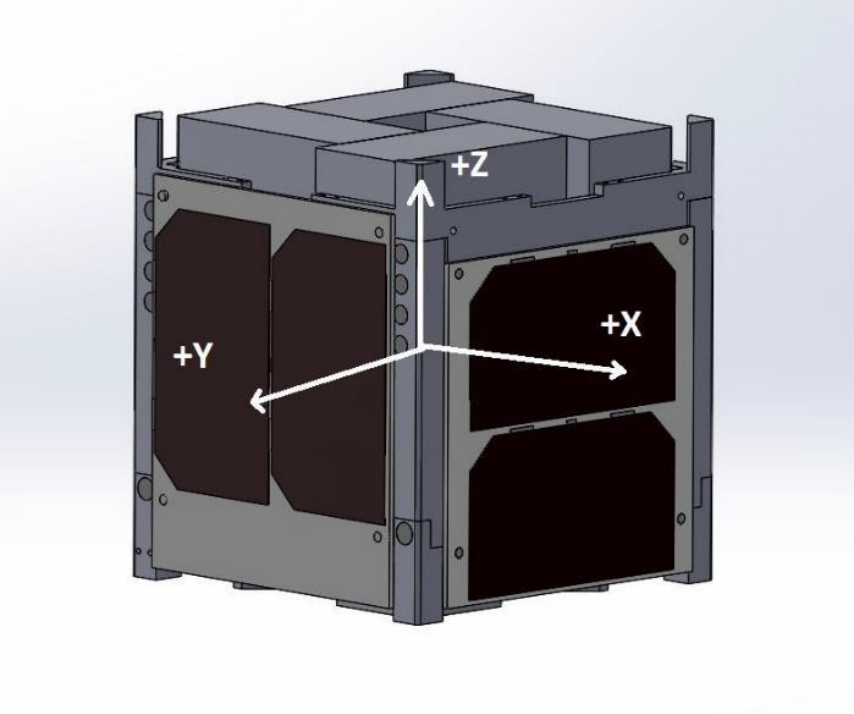

Figure 4.2: ADE Coordinate System

4.3 Earth-Centered Inertial J2000 Frame

An Earth Centered Inertial coordinate system is a Cartesian coordinate system that uses the center of the Earth as its origin. Since the frame is inertial, it is fixed in its original orientation and does not rotate with the rotation of the Earth. In this system, an object's position relative to the center is defined by its distance from the center in all three coordinate axes. As can be seen in Figure 4.3 [8], the +Z-axis is defined along the Earth's rotational axis pointing North, the +X-axis is defined in the direction of the Vernal Equinox, and the +Y-axis is defined as perpendicular to both the +X-axis and the +Z-axis.

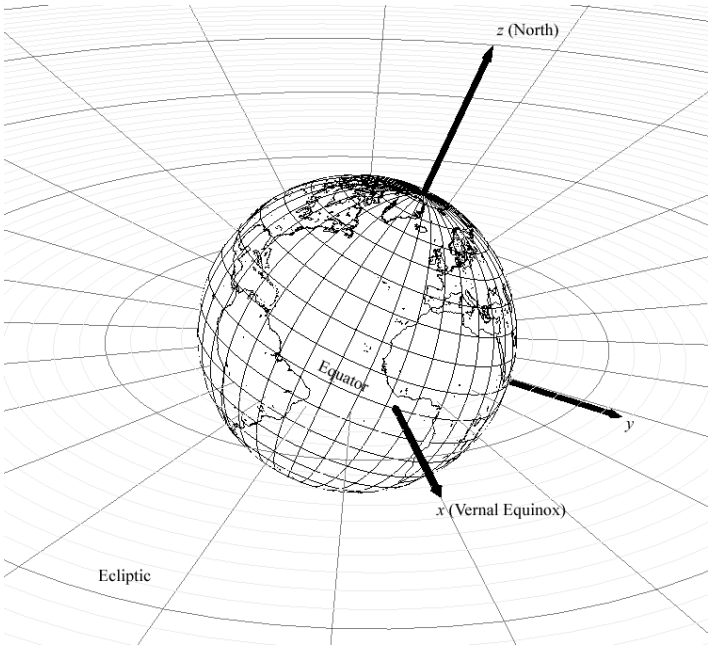

Figure 4.3: Earth-Centered Inertial Coordinate System

Th ECI J2000 coordinate frame is defined by Earth's Mean Equator and Equinox at 12:00 Terrestrial Time on January 1, 2000. The inertial +X-axis is aligned with the mean equinox, the +Z-axis is aligned with the Earth's axis of rotation, and the +Y-axis is rotated by 90 degrees East about the equator. An image defining the ECI J2000 frame is provided in Figure 4.4 [9].

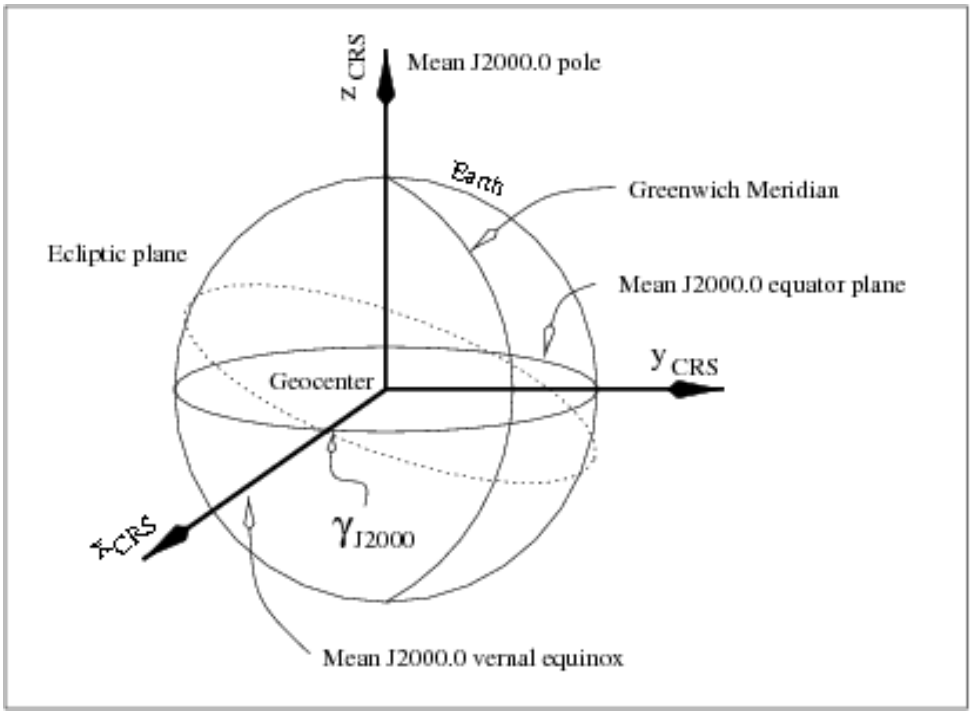

Figure 4.4: ECI J2000 Coordinate System

4.4 Earth-Centered, Earth-Fixed

The ECEF coordinate system also uses the center of the Earth as the origin. Unlike the ECI coordinate system, the ECEF coordinate system rotates with the rotation of the Earth. This property of the coordinate system makes it especially beneficial to Global Positioning System satellites, as the coordinates of a position can be easily interpreted from the origin. The axes are defined with the +X axis passing through the intersection of the Equator and the Prime Meridian, the +Z axis passing through the North Pole, and the +Y axis orthogonal to both +X and +Z. This definition can be seen in Figure 4.5 [10].

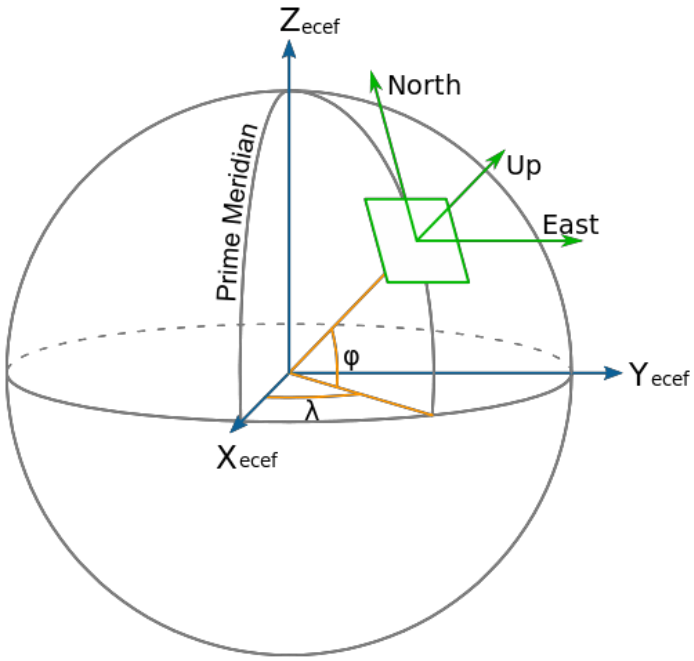

Figure 4.5: ECEF Coordinate System

5 Flight System Description

The ADE spacecraft contains a multitude of systems for orchestrating mission events and gathering valuable data. Each aspect of spacecraft operations is handled either by a specialized board such as the Radio Board, -Z board, or Deployer Board, or is handled by the main flight processor and System Board.

5.1 Flight System Overview

The various components making up the Flight Systems are shown in Figure 5.1.

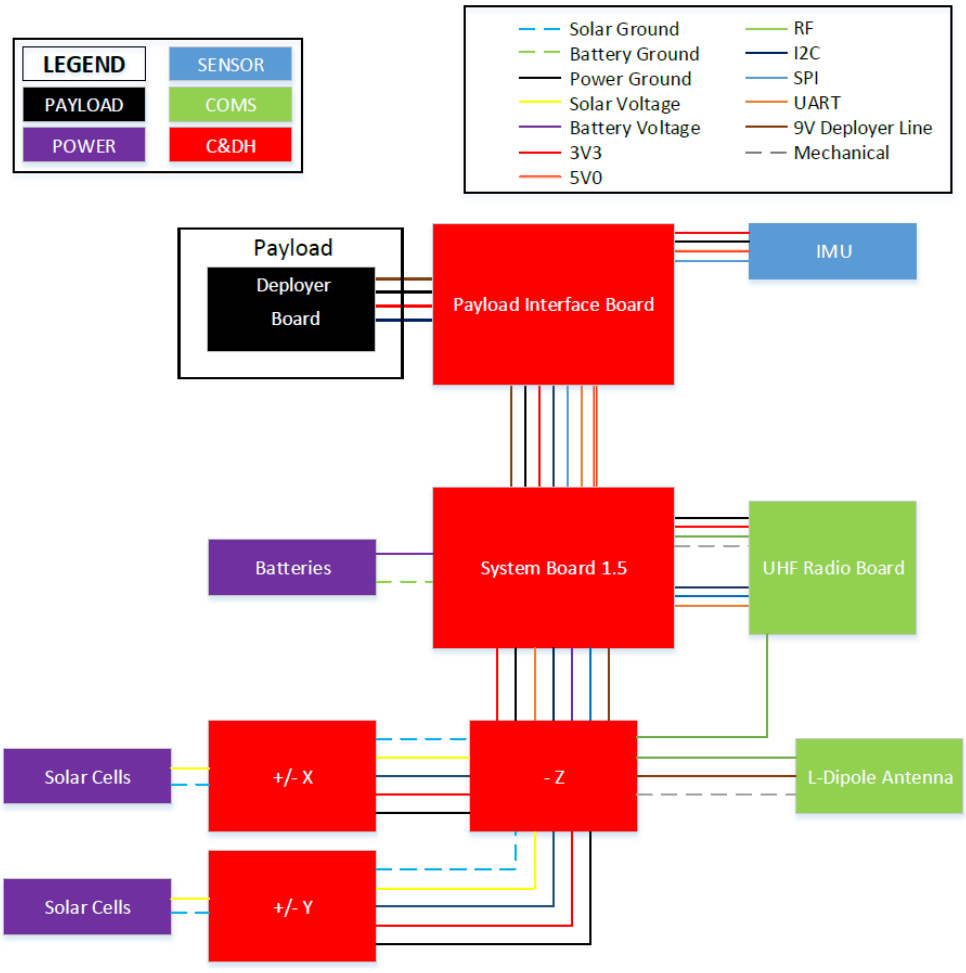

Figure 5.1: Flight System Block Diagram

5.2 Structures & Mechanisms

5.2.1 Structures

Figure 5.2 and Figure 5.3 show a completed and a final CAD model of the ADE. The coordinate system is inscribed into the very left of Figure 5.2. The order in which the internal components will be discussed will go from top to bottom, (from positive Z to negative Z, in the spacecraft coordinate system). The antenna assembly houses the dipole antenna that will be used to transmit and receive messages to and from the ground stations on Earth. The antenna assembly is attached to the external face of the positive Z panel. The positive Z panel also has one of the two cameras as shown in Fig 1. The system board sits beneath the positive Z panel closer to the center of the cube. It is responsible for proper functioning of the cube sat as long as programming is considered. The UHF Radio works directly with the antenna assembly and sits atop the payload interface board which is directly beneath the UHF Radio. The IMU is attached to the payload interface board in the negative Z direction. The batteries, which provide power to all the CubeSat subsystems, lie beneath the IMU. Beneath the batteries is the payload volume, this payload volume will be the heart of the ADE as it will contain the drag sail and necessary deployment mechanisms important to the payload. The entire external surface area consists of 8 solar panels on the four sides that provide charge for the batteries.

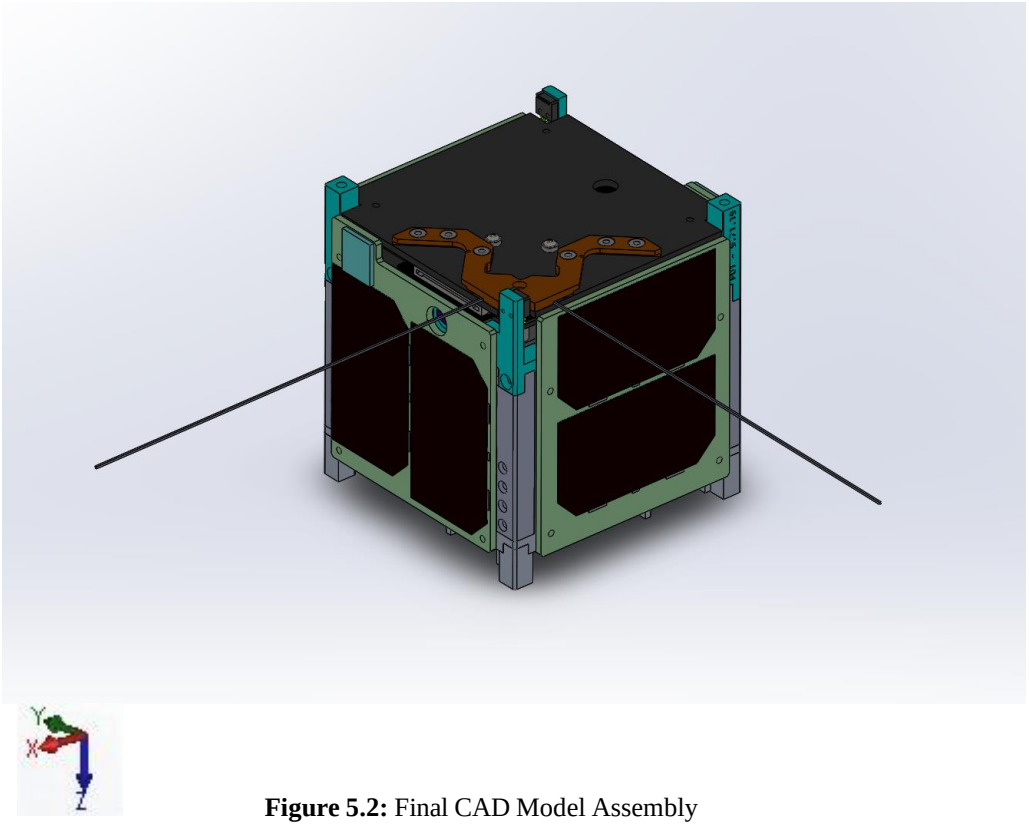

Figure 5.2: Final CAD Model Assembly

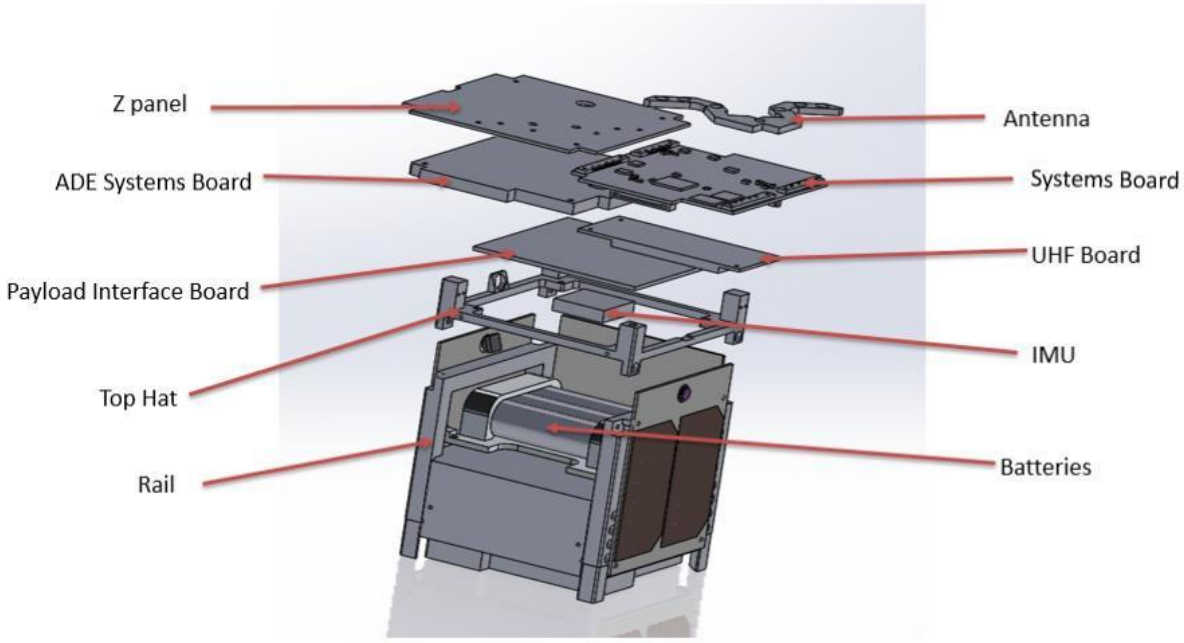

Figure 5.3: Exploded View of the CAD Model

5.2.2 Quasi-Static Analysis

To verify the structural design of the ADE, a finite element analysis was performed on the different components of the CubeSat to ensure that the launch environment does not compromise the mission. Data on the launch environment was obtained from the ULA's ABC Auxiliary Payload User's Guide [11] and can be seen in Table 5.2

Table 5.2: Acceleration Limit Load Factors of the ABC during Launch

Acceleration Limit Load Factors (*g*)	
X_{AP}	5.0
Y_{AP}	5.0
Z_{AP}	7.0

A quasi-static finite element analysis that uses these g-forces was completed using CATIA V5. The results of this analysis can be found in Table 5.3. It is a worst-case scenario of the stresses seen due to launch g-forces, in addition to being on the bottom of the P-POD, with two 1.33 kg CubeSats stacked above the ADE. The results of this structural analysis validate the basic design of the CubeSat and show that it can handle the expected launch loads

while maintaining ample margin.

Table 5.3: Launch Load Limits and Margins of Safety

Component	Failure Limit (MPa)	Maximum Stress (MPa)	Margin of Safety
Solar Panels	242	1.73	68.94
Chassis	276	15.50	7.90
System Board	242	5.63	20.49
Drag Sail Assembly	276	3.07	43.95
UHF Radio Board	242	28.1	3.3
IMU & Payload Interface Board	242	10.7	10.30

The failure criterion of each component was determined by taking the failure stress of the material associated with the component or given by the manufacturer of the component [12]. The maximum stress is the maximum Von Mises stress that the given component undergoes throughout the launch. Finally, the margin of safety is a comparison between the maximum stress the component experiences and the failure limit of that component.

These analyses include a factor of safety of two for all calculations to account for any discrepancies in this analysis.

The following figures are visual representations of the deformations and stresses that the spacecraft may experience during launch. Analyzing the top hat of the CubeSat, Figure 5.8 is an exaggerated visualization of the Von Mises stress contour and deformation associated with the maximum g-force case outlined in Table 5.2. Likewise, Figure 5.9 is an exaggerated visualization of the Von Mises stress contour and deformation for ADE's UHF Board.

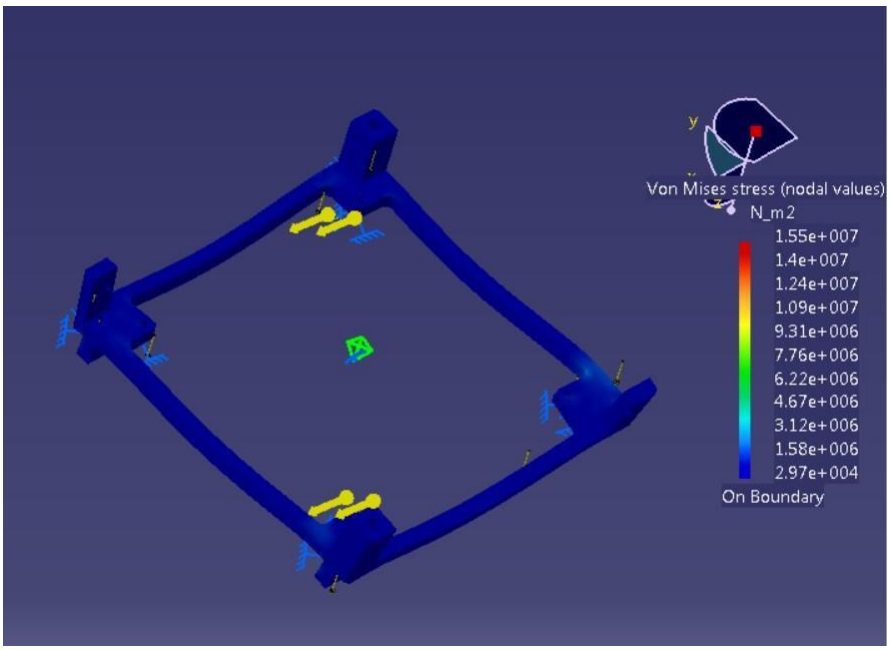

Figure 5.8: Von Mises Stress of Top Hat for Max G-Force Case

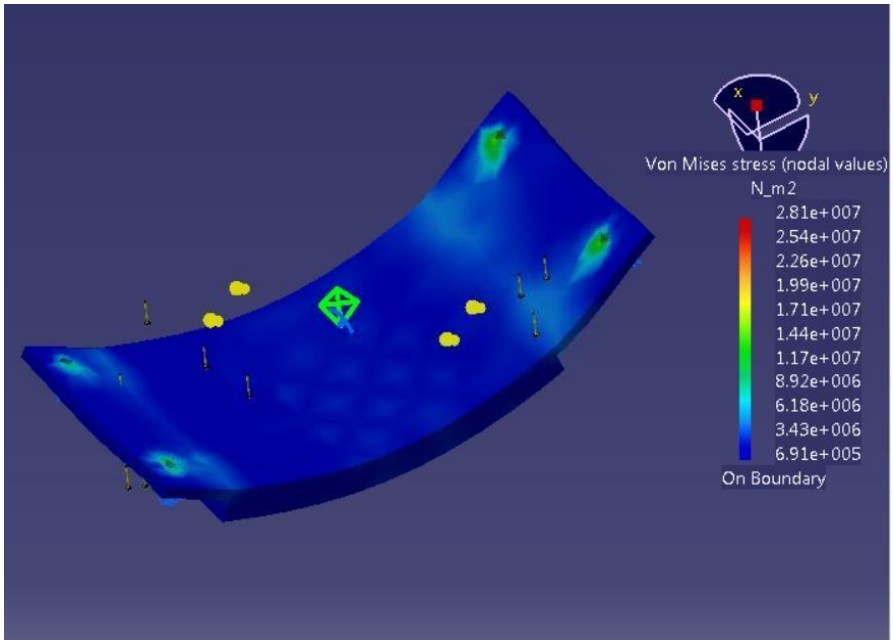

Figure 5.9: Von Mises Stress of UHF Board for Max G-Force Case

5.3.1 Vibrational Analysis

The ULA ABC Auxiliary Payload User's Guide [11] also specifies a random vibration environment as detailed in Table 5.4 and Figure 5.10. Figure 5.10 shows the envelope beneath which all random vibration will occur. As such, analyses of the stresses in the satellite at the specified frequencies and accelerations at the boundary of the envelope, and across the frequency range at the G_{rms} acceleration provides verification of the model.

Table 5.4: Specified Vibration Intensity at the Boundary of the Random Vibration Envelope.

Frequency (Hz)	Random Vibration (G^2/Hz)	Acceleration (m/s^2)
20	0.03	7.599
40	0.125	21.936
240	0.125	53.732
2000	0.003	24.029
Overall	7.6 G_{rms}	74.556
Duration	60 sec/axis	

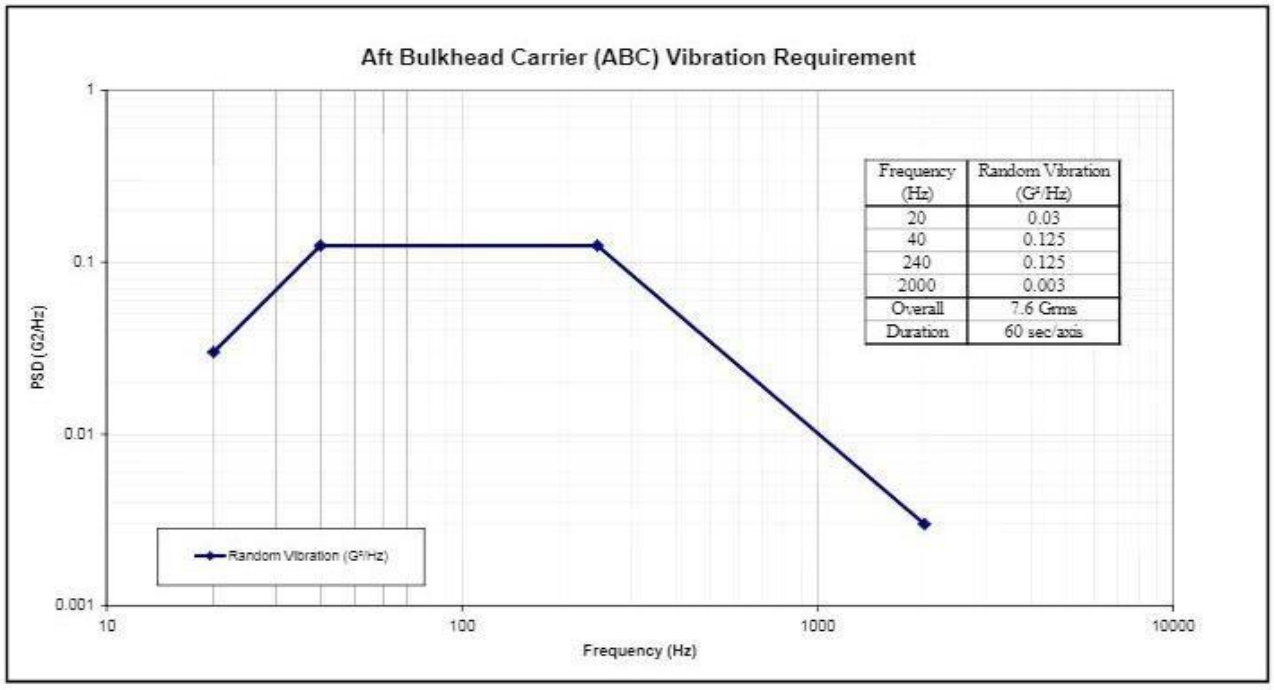

Figure 5.10: Plot of the Upper Bound of the Vibration Environment.

The accelerations in Table 5.4 were calculated by multiplying the random vibration G^2/Hz value by the corresponding frequency and square rooting it to get the acceleration in

G's, then multiplying by 1G ($9.81 m/s^2$).

Modal and harmonic response analyses were conducted using *Ansys* to evaluate the performance of the design when subjected to the vibration environment. 15 Modes were extracted across a range of frequencies from 0 to 3500Hz (larger than the specified range to ensure all significant modes were captured) and are shown in

Table 5.5: Vibrational Modes

Mode	Frequency (Hz)	Mode (continued)	Frequency (Hz)
1	292.2	9	1814.2
2	407.18	10	1839.9
3	893.99	11	1870.8
4	986.8	12	1913.2
5	1029.9	13	1936.3
6	1399.1	14	2186.3
7	1437.6	15	2368.4
8	1477.7		

The fundamental frequency (mode 1) is above 30 Hz [13] and none are close to the specified bounds of the vibration environment as in Table 5.4 therefore resonance should not be a problem for this mission.

We ran the harmonic response tool for each acceleration and frequency as in Table 5.4 and also for the G_{rms} acceleration over a range of frequencies from 0 to 2500 Hz. The Von-Mises stress through the satellite was output for the cases in Table 5.4. The maximum stresses are shown in Table 5.6 after being multiplied by a safety factor of 1.4 as per the NASA standard for metallic flight structures [14]. The lowest tensile strength material is the F-4 glass/epoxy phenolic [15] used for the PCB's, having a strength of 262MPa (Al 6061 T6 is 310MPa [16]). As such it can be seen that the satellite will not fail due to random vibration as all the maximum stresses are well below this value.

Table 5.6: Maximum Von-Mises Stress in ADE for Each Random Vibration Case.

Frequency (Hz)	Max Stress x1.4 (MPa)
20	0.959
40	2.800
240	16.384
2000	3.094

Figure 5.11 is the harmonic response spectrum, for G_{rms} in the +Z direction, showing the maximum stress in the aluminum components of the satellite at each frequency. The data collection was clustered around the modes found previously as these are the critical frequencies where the stress peaks. As can be seen, the maximum stress is only 72MPa which is well below the strength of Al 6061 as stated earlier. Similar graphs were created for the G_{rms} acceleration in all directions (and for each material group) to check for the worst case. This is presented in Figure 5.11.

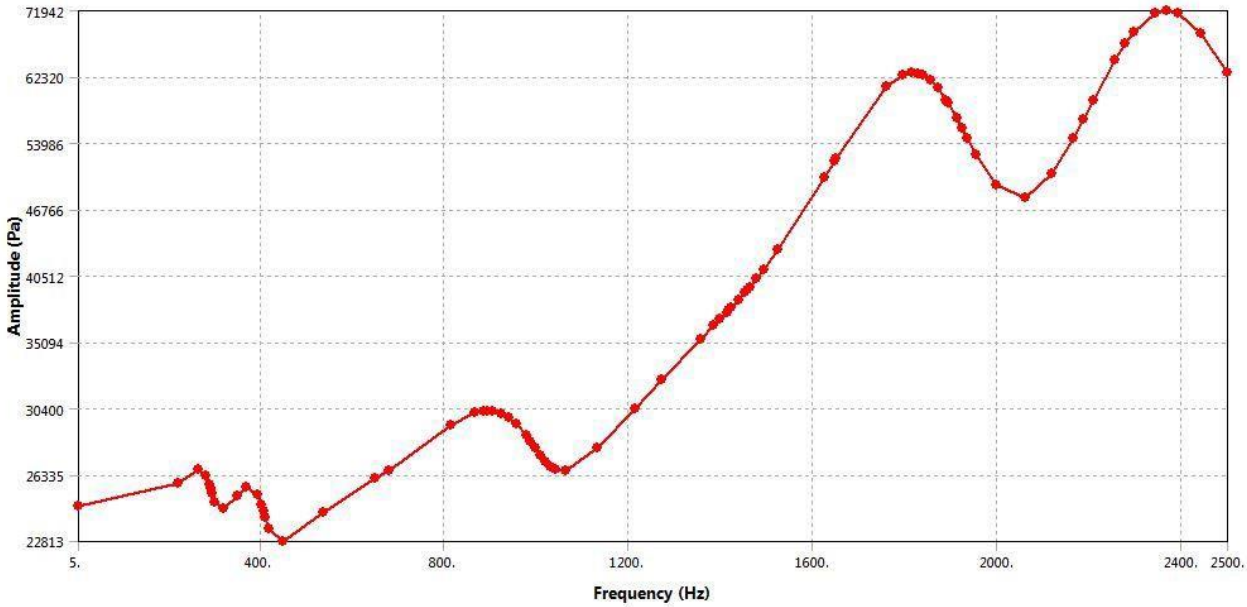

Figure 5.11: Harmonic Response Spectrum for the G_{rms} Acceleration in the +Z Direction

5.3 Electrical Power Subsystem

The Electrical Power Subsystem provides the necessary regulated energy for all the ADE CubeSat system components and processes. The system consists of power generation, storage and regulation components.

5.3.1 EPS Control Board

The Intrepid Pico-Class CubeSat System Board R5 is provided by Cal Poly and provides regulated 3.3V and 5.0V nominal outputs for the CubeSat. The bus voltage of the system is 3.7V. The system board will be in control of power distribution from these sources to all necessary connected devices. The power distribution of the System Board is specifically designed for CubeSat missions.

Figure 5.12: Intrepid Pico-Class CubeSat Systems Board R5

5.3.2 Batteries

The batteries are Tenergy 30011-02. This battery is a lithium ion, single cell battery. The nominal capacity of the battery is 2600 mAh and has a nominal voltage of 3.7V. The Tenergy battery has been used by Cal Poly in previous spacecraft mission and has a reliable flight record. The ADE CubeSat contains three units with a maximum total energy storage capacity of 28.8Wh. The three units are wired in parallel. The Tenergy battery is pre-packaged with cell protection circuitry. This circuitry helps mitigate overcharging and undercharging. The ADE CubeSat will not have heating hardware for the batteries but will have a temperature senor on each of the three battery units.

Figure 5.13: Tenergy 30011-02 Battery

5.3.3 Solar Panels

Four of the six sides of the ADE CubeSat will have solar panels. Each side will have two solar panels built into the side structure, wired in series. The solar panel used is the UTJ Spectrolab Solar Panel. The UTJ solar panel is specifically designed for CubeSat missions and provides the necessary recharging capabilities for ADE's mission. Each panel set will produce 1.9W power when fully exposed to perpendicular sunlight. Average power generation is closer to 1.5W per

side from Cal Poly flight heritage data and Purdue Monte Carlo analysis. Additionally, Cal Poly has observed that the maximum angle of incidence of sunlight for power generation is 47 degrees from perpendicular.

Figure 5.14: NeXt Triple Junction (XTJ) Solar Cell

5.4 Telecommunications

The driving requirement of the telecommunication subsystem is to establish uplink and downlink communication between the ADE CubeSat and the ground stations. The CubeSat will deploy a dipole antenna that will be able to uplink and downlink commands utilizing Ultra-High Frequency, at 437.5 Mhz. Using this, the telecom system shall be capable of downlinking stored telemetry, IMU data, and images at a data rate of 9600 bps or greater. It also shall be capable of receiving uplinked commands at a data rate of 1100 bps. It is required that the telecom subsystem shall maintain a link margin of at least 3 dB for uplink/downlink communications except for the case when antenna null is aligned toward Earth.

Because ADE is a secondary payload in the launch vehicle, there are requirements during launch and initial separation that must be abided by. The telecom subsystem cannot deploy the dipole antenna and cannot be able to make transmissions until 45 minutes after P-POD deployment. The telecom subsystem will consist of the Tyvak UHF Radio board that will contain the transmitter, filters, amplifiers, and receiver. The antenna itself will require brackets and burn wire resistors for the deployment system. The total system mass will be 20 grams.

The antenna will deploy 45 minutes after being deployed from the P-POD. The antenna deployment system involves fishing wire as the antenna which is curled around a bracket and uses burn wire resistors to release the stored energy and extend the antenna. Two brackets are placed on opposite corners of the top plate and used to wound the antenna around so that it extends out in opposite directions when deployed. Two burn wire resistors are used on each line to ensure that

the wire will be severed and deployed without a failure. Once activated, the system should take less than 15 seconds to deploy the antenna. The parameters of the hardware are tabulated below.

Table 5.7: Tyvak Communications Board Specifications

Parameter	Value
Operating Voltage	3.3 Volts
Encoding	AX.25
Data Interface	SPI
Operating Frequencies	400-470Mhz, 800 to 930Mhz
Data Rates	1.2 - 250kbps
Mass	20 grams
Volume	70 x 30 x 7 mm

To fulfill all of the Telecommunications requirements for the mission, the parameters of the final system on the CubeSat are tabulated below.

Table 5.8: Actual flight specifications of Communications system for ADE

Parameter	Value
Transmitter Power	1 W
Antenna Type	Omnidirectional Dipole
Beam Width	156.2°
Antenna Gain	2.2 dBi
Polarization	Right-Hand Circular Polarization
Modulation Method	Non-Coherent FSK
Operating Frequency	437.5 Mhz
Data Downlink Rate	9600 bps
Data Uplink Rate	1100 bps

The modulation method chosen for the communication system is Non-Coherent Frequency Shift Keying, due to the low bit error rate for a relatively low power requirement per transmitted bit. This gives us a more reliable data connection, without having to increase the power draw for the transmitter.

The encoding method which the Tyvak hardware operates on is the AX.25 protocol, which is a data-link layer protocol. The maximum information field size in the AX.25 is 256 bytes, meaning each packet can contain up to 256 bytes of data. The higher level protocols used along with the AX.25 are IPv4 (Network layer) and UDP (Transport layer), which allow for more efficiency in data transmission, since they do not require handshakes or bidirectional connection establishment before being able to transmit data. The headers associated with all the protocols add up to 8 bytes, with compression, meaning that data is the primary component of transmitted bits, rather than protocol-based structures of bits.

5.5 Thermal Control

ADE will have temperature sensors on the Avionics Board, UHF Board, Batteries and one on both the inner and outer face of each panel. This results in a total number of seventeen temperature sensors and the specific location of each will be determined at a later date at Cal Poly's discretion. These temperature sensors will operate on a duty cycle that mirrors the beacon (30 second intervals).

Numerical simulations were conducted using various thermal analysis software to procure the worst-case temperature estimates for each component on the spacecraft. While we encountered numerous issues in our analysis that prevented us from having confidence in our results, the methodology of our analysis can be found in Section 12.2.4.

The purpose of these temperature sensors is primarily for experimental purposes. Since there are no battery heaters or other form of active thermal control, there is no course of action if one of the spacecraft component temperatures falls outside of its operational range. The data obtained from the temperature sensors will be useful for future CubeSat missions of this nature as they will indicate components that need either additional or less thermal protection. Table 5.9 shows both the operating temperature range and ultimate temperature range for each major component on the spacecraft.

Table 5.9: ADE Component Temperature Limits

Component	Operating Range [°C]	Do Not Exceed Range [°C]
Frame – 6061/7075 Aluminum	< +160	< +582
Batteries	+20 to +45	0 to +60
IMU	-40 to +85	-40 to +120
Flight Board	-40 to +85	-45 to +90
CP1 Sail	-185 to +260	< +263

5.6 Command & Data Handling

The Command and Data Handling (C&DH) subsystem covers the flight system board, the flight software and use of on-board processing, the interfaces between subsystems and the board, as well as the management of data produced and transmitted during the spacecraft's mission. It is the system board which issues commands to the various subsystems. The data collection in order to achieve mission success is also a critical function of C&DH.

5.6.1 Flight System Board

The ADE spacecraft will use the Intrepid Pico-Class CubeSat System Board R5 from Tyvak. This is the board identified by CalPoly, a mission partner. The board is acquitted to support a variety of communication protocols and interfaces, including I2C, UART, SPI, USB 2.0, and CMOS Image Sensor—useful capabilities with the different interfaces required by the ADE subsystems. Additionally, it runs a full Linux operating system and can support 16-32 MB of storage through one or two SDCards. Intrepid was designed specifically for CubeSats with low power, low volume, and high performance capabilities [17].

5.6.2 Subsystem Interfaces

The Intrepid board will continuously interact with and command the ADE subsystems, and various communication protocols are utilized to do so. The IMU will use SPI [18], which will be standard with Intrepid. Multiple radiation sensors will be located in ADE, but the expected interface is not defined. Several payload elements will communicate through the payload interface board, which is currently under development. An additional camera will be routed directly to the Intrepid board. It is noted that the cameras operate with an MIPI control interface and a SCCB slave interface. Additionally, on-board processing may be done with the information or data obtained from a sensor, for example IMU data discretization to reduce the data volume to be downlinked by a quarter, and compression will be applied to all data packages in order to maximize transmissions.

5.6.3 Checkout Period Data

In the beginning of the mission, the spacecraft will undergo a Checkout period during which the board will power up itself and then power up and initialize the respective subsystems in turn, possibly drawing sample, checkout data, e.g. from the IMU and cameras. The Checkout sequence is described in more detail in Section 8.2 as part of mission phases and systems engineering; however, C&DH considers the flags and variables which need to be recorded during this time and therefore the total data volume which will be produced during checkout. Luckily, much of the definition of the data log produced during checkout will be defined very similarly to the beacon. In addition, one minute of running the IMU, one thumbnail from each camera, and one minute of collection from the radiation sensors will be recorded.

Table 5.10 provides a summary of the checkout return for immediate transmission to the ground. The values in the "Data Production (bits/pull)" column represents data produced by the subsystem at given frequency, prior to encoding or compression. Except for the cameras, one "data pull" is representative of 1 second. Various options for Checkout Duration were explored for the IMU, and one minute was deemed sufficient. Camera draw for checkout is defined by the downlink of zero full size images and one thumbnail, per camera. The total data volume identified here, 0.231 Mb, will be compressed, encoded, and in the case of the IMU, further compressed through discretization (see Section 12.2.5, Data Return Analysis), resulting in a package for transmission of merely 0.0383 Mb. Due to the very low total volume and using the 9600 bps downlink rate, the Checkout Return is expected to be completed in only 4.0 s.

Table 5.10. Checkout Return Summary

Subsystem	Data Production (bits/pull)	Checkout Duration (mins)	Checkout Data Volume (bits)	Percent of Total Checkout Volume (%)
IMU	3520	1	**0.211×10^6**	**91.3**
		5	*1.056×10^6*	*N/A*
		10	*2.112×10^6*	*N/A*
Cameras (2)	8.0×10^3	N/A	**0.016×10^6**	**6.9**
Cameras (2), *incl. 1 full size photo*	*7.208×10^6*	*N/A*	*14.416×10^6*	*N/A*
Radiation Sensors (8)	4	1	**1920**	**0.8**
System Status/ Beacon Variables	6	N/A	**2048**	**0.9**
Total	–	–	**0.2310×10^6**	**100**
Total, Processed	–	–	**0.0383×10^6**	***16.6***

5.6.4 FMSC Data

Full Mission Success Criteria include five full orbits of IMU data, 3 full orbits of radiation sensor measurements, and one full size photo. It will be critical to analyze the spacecraft's capability to downlink these measurements and images as readily as possible. Table 5.11 provides a summary of the total FMSC data to be transmitted. As in Table 5.10, "Data Production (bits/pull)" values represent data produced by the subsystem at given frequency, prior to encoding or compression. Except for the cameras, one "data pull" is representative of 1 second. Considering both compression and encoding factors (see Section 12.2.5, Data Return Analysis), the FMSC summary when processed becomes 12.39 Mb. Based on a downlink rate of 9600 bps, the total downlink time for FMSC will be 1291 s, or 21.5 mins. It is important to note that this duration of

downlink will neither be continuous, based on contact capability with the ground, nor the first cumulative 21.5 minutes of downlink, since FMSC is defined over the course of up to five orbits.

Table 5.11. FMSC Return Summary

Subsystem	Data Production (bits/pull)	FMSC Data Volume (bits)	Percent of Total FMSC Volume (%)
IMU	3520	21.120×10^6	74.1
Cameras (2)	7.20×10^6	7.20×10^6	25.3
Radiation Sensors (8)	4	0.176×10^6	0.6
Telemetry	6	N/A	N/A
Total	**--**	**28.50×10^6**	**100**
Total, Processed	**--**	**12.39×10^6**	***43.5***

5.7 Flight Software

The flight software is responsible for accomplishing all on-board processes effectively and within any defined time constraints. CalPoly will deliver much of the flight software for ADE that is standard for CubeSats. This includes the watchdog processes and use of long-duration timers. Purdue will collaborate with CalPoly to develop specific pieces of software for ADE, including deployment of the drag sail, on-board processing of IMU data, and beacon definition.

5.7.1 Radiation Protection

The Intrepid system board will be exposed in the environment of space to two types of risks: radiation which disrupts or damages the board and processes, and radiation which affects the data and measurements. The board is therefore equipped to handle these radiation risks in two different ways. Watchdog processes and timers are used to monitor and possibly reset the system, and these will be further defined in Section 5.7.2. Phase Change Memory (PCM) is used by the Intrepid board to prohibit ionizing radiation from affecting ADE's stored data, so bit flips cannot occur. PCM memory works by storing each bit as a resistance, rather than a floating charge, and it is tolerant up to 30 Mrad.

5.7.2 Watchdog Processes

There is one watchdog built into the Intrepid board which operates under two function areas, Software Watchdog and External and Internal Hardware Watchdog. The Software Watchdog monitors all internal processes and taps the timer on the Hardware Watchdog. If there is an "unhealthy" process, it will first easily reinitialize the process, called a Process Reset. The

Hardware Watchdog times out on the order of 60 s, and initializes a Soft Reset in the case that there are several failed Process Resets or certain detected radiation effects to the processor. Finally, this system utilizes a Long-Duration Hardware Reset Timer. This timer will be manually configured before launch on the order of one week, and it may be reconfigurable and accessible by ground commands. Unless tapped by the watchdog, the timer will trigger a Hard Reboot of the system. During hard and soft reboots, it will be assured that the other timers, such as for antenna or sail deployment, remain independent and unaffected. These checks and timers are meant to monitor the spacecraft to ensure that everything is operating smoothly and without error or radiation damage.

5.7.3 Software Development for ADE

CalPoly will deliver much of the standard Flight Software and they have delivered the flight system board, but Purdue has taken the lead to define and develop certain pieces of software specific to ADE.

The first software element is the discretization of the IMU data, critical for reducing the IMU data volume significantly to deal with limited downlink capability. For the 20-minute IMU pulls, the data can actually be converted from 32-bit floats to only 8-bit bytes, dividing the total volume by four with compression not only possible but extremely efficient on top of that. This process is managed by defining the minimum value in the data set, and a step size between discrete levels. An individual value has the minimum subtracted away to normalize it and it then is divided by the step size to get an approximation to which out of 255 discrete levels the value falls closest to. This converted data gets stored in a new file with additional header information that stores the discovered minimum values and step sizes for each data axis. This process has already been tested using experimental data produced by ground tests of the IMU.

The third software element that is developed by Purdue is an interface in C called ‘UM7.c’ using ‘adcs.c’ code provided by CalPoly. This code extracts IMU data from the configuration files which are under development at Cal Poly. The code accesses the data read from IMU, converts the data into TCIP/IP format compatible with the Flight Software and saves the data in structures initialized in the code. Those structures can be accessed to downlink or to be processed onboard. The key for onboard processing are um7-util.c, and um7.cmd.cfg. To downlink the data telemetry.c and datalogger should be used. These files are included in the drive.

Below is a high level flowchart depicting the data flow using ‘UM7.c’

Figure 5.15: Data Flow using ‘UM7.c’

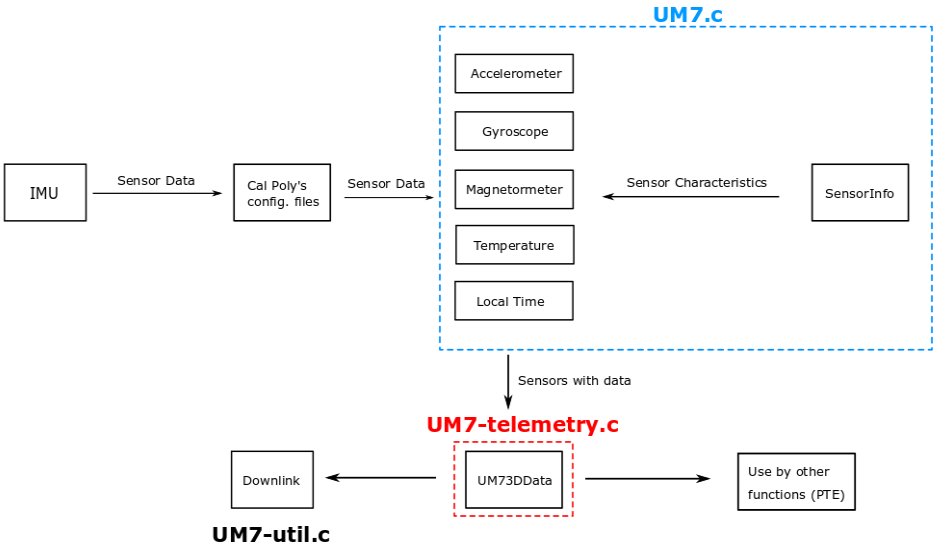

Finally, ADE will additionally have a customized beacon. The beacon is defined in detail in Section 9.2. The status of the subsystems and their processes will be reported by the beacon, but C&DH has also defined extra variables which record the “time since last reset” and “time since last soft/ hard reboot” which will give Mission Operations insight into the system health.

6 Payloads

6.1 Deployable Drag Device

The deployable drag device is a small-scale version of the Passively Stable Pyramid Sail or $[PS]^2$. As the name implies, this is a drag sail that has a square pyramid shape instead of the traditional flat shape to take advantage of aerodynamic stability. Figure 6.1 defines the dimensions that determine the sail. The two most important ones are the boom length, L, and the apex half-angle, Φ. The length of the boom is 1 m based on volume constraints while a nominal apex half-angle of 70° or 80° has been determined to be ideal for simultaneous stability and drag optimization [19] and to allow the sail to be deployed out of the bottom face rather than all four sides. Rollable booms, characterized by thin walls and a flexible structure, may be flattened and rolled around a hub. There are two boom geometries under evaluation for the supporting structure of the sail: SHEAth-based Rollable LEnticular-Shaped and low-Stiction (SHEARLESS) booms, and Triangular Rollable and Collapsible (TRAC) booms. The SHEARLESS boom, shown in Figure 6.2, consists of two convex tape springs enclosed within a polymer sleeve, rather than coupled through bonding. This gives the booms a mostly closed cross section for strength while allowing the tape springs to shear along each other when stowed, allowing for a smaller coiling diameter. The TRAC boom is a beam-like structure with a tape spring geometry bonded together at the base, as shown in Figure 6.3. Carbon fiber SHEARLESS booms provided by NASA Langley Research Center, and elgiloy TRAC booms provided by ROCCOR are being considered, as well as carbon fiber TRAC booms developed in-house at Purdue.

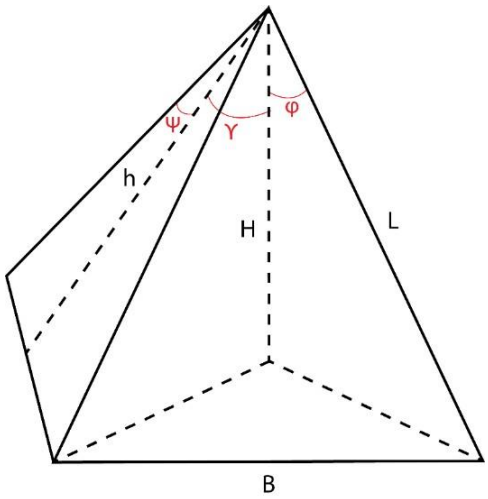

Figure 6.1: Drag Sail Diagram

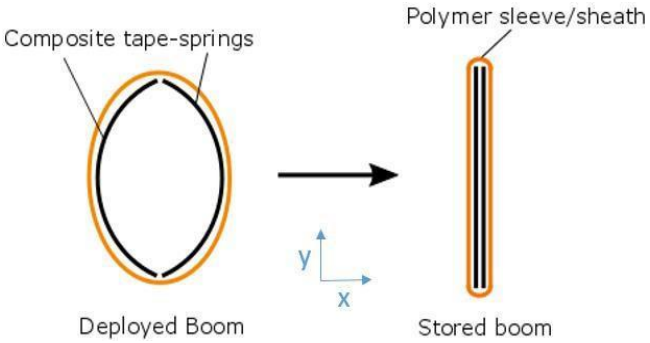

Figure 6.2: SHEARLESS Boom

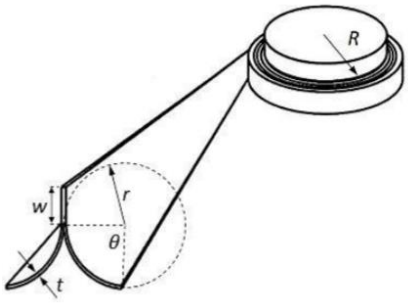

Figure 6.3: TRAC Boom

Table 6.1 Boom Options

Manufacturer	Boom Type	Material
NASA Langley	SHEARLESS	Carbon Fiber
ROCCOR	TRAC	Elgiloy
Purdue	TRAC	Carbon Fiber

The deployable drag device will be housed in a contained unit shown in Figure 6.5. The assembly for the casing of this unit is shown in Figure 6.4. This will decrease the complexity of integration with the rest of the spacecraft and provide a simple way to contain the sails and booms before deployment. The pyramidal shape requires each boom to be stowed in its own deployer assembly, and the sails will be folded up and stored between a boom deployer and the inner face of the top part of the housing, shown in Figure 6.6. The feet required by P-POD standards are designed into the top part of the assembly to ensure continuity of the load path.

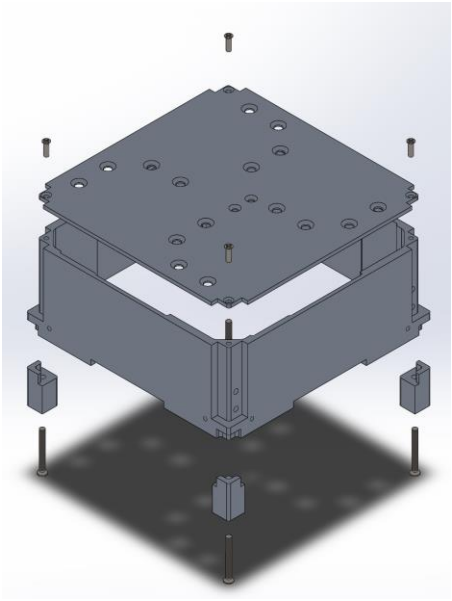

Figure 6.4: Mounting Hat Assembly Exploded View

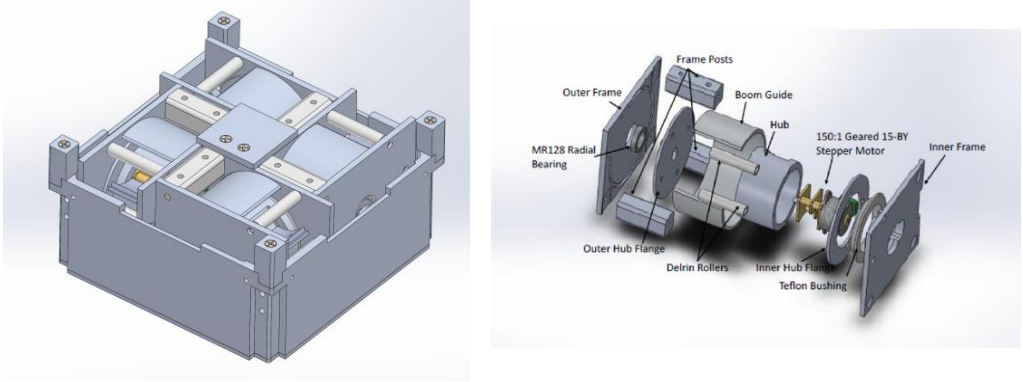

Figure 6.5: Deployer Device Subsystem and Exploded Assembly View of a Single Deployer

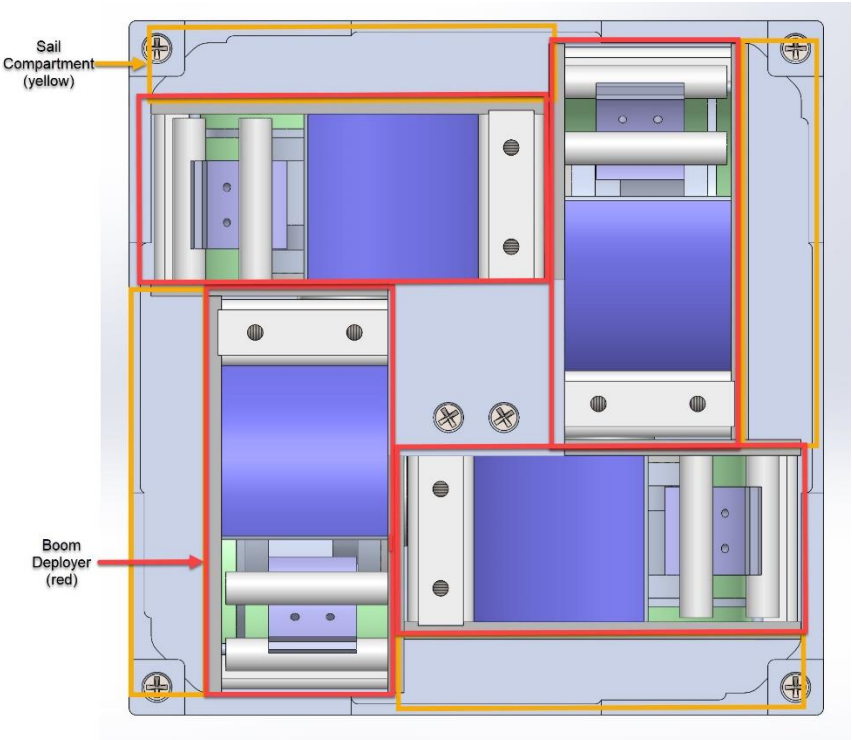

Figure 6.6: Assembly Bottom View

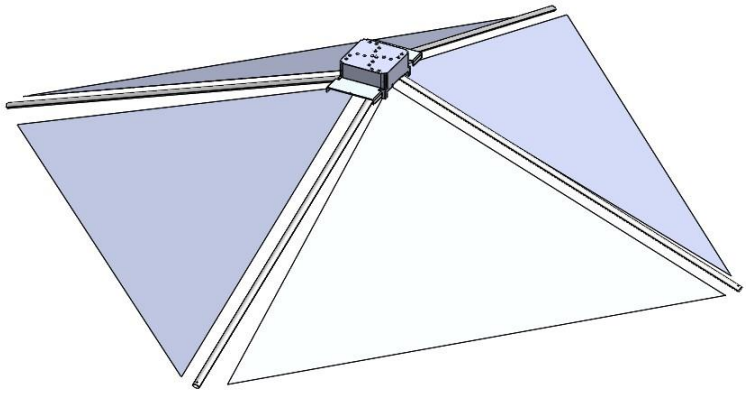

Figure 6.7: Fully Deployed Drag Device

6.1.1 Boom Deployer Design

As shown above in Figure 6.4, one main deployer component is the center hub, to which the boom is mounted then wrapped around to be stowed. The center hub freely rotates during the deployment to allow the boom to unroll in a single direction. That direction is controlled by two Delrin guide rollers that are placed at the exit of the boom deployer to enforce the apex half-angle of the sail. The center hub assembly contains two hub flanges that separate the boom roll from the outer frame. One of these flanges is in the shape of a gear to allow the boom deployer to be rotated when mounted inside the sail assembly. The next component is the anti-blossoming assembly, which provides a normal force to the outside of the boom roll that is continuous through the deployment to ensure that the center wraps of the boom do not separate from the central hub and jam the boom in the deployer. This phenomenon is called blossoming. The force is applied by torsion springs that are part of the anti-blossoming assembly. The final component is the outer structure. It consists of

two parts that sandwich all the components between them. It can be seen in the side view of Figure 6.6 that the structure covers part of the top and bottom of the boom deployer, this provides a surface through which the boom deployers can be mounted to the upper housing on top, and an interface plate on the bottom, shown in Figure 6.4 as a green cross.

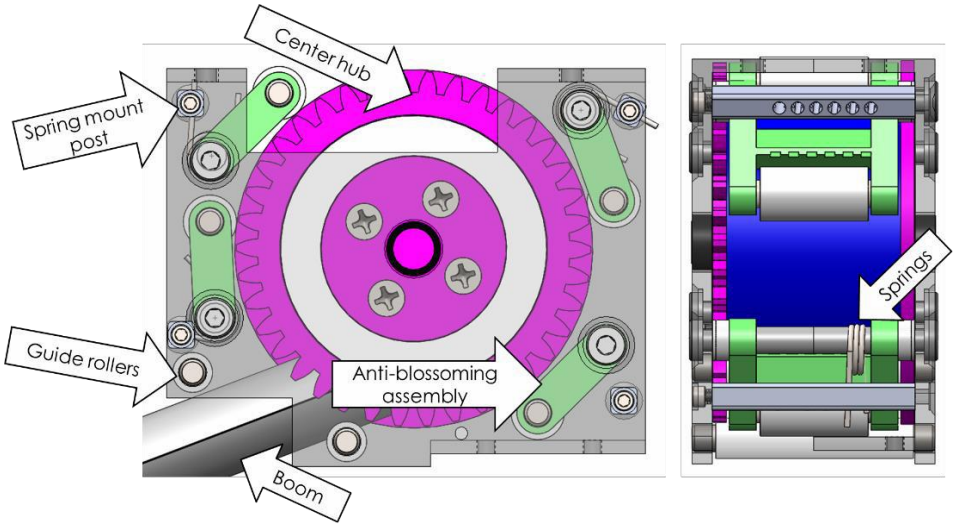

Figure 6.6: Boom Deployer Front View (Transparent Structure) and Side View

6.1.2 Sail Membrane Design and Fabrication

There will be four triangular sails made of uncoated CP1, five microns thick. Each sail will have each of the outer corners mounted to the tip of a boom with an extension spring and wire. The booms will pull out the sails as they deploy, and the springs will allow the tension to stay relatively constant in the sail as it expands and contracts due to thermal changes. Each sail corner has a metal grommet to create a reinforced hole in the CP1. Orbital debris and micrometeorites can rip through the thin material of the sail membrane. The tension in the membrane allows the tear to propagate through the sail, destroying the drag area it provides. This is mitigated by dividing the sail into four quadrants, so no more than ¼ of the drag area can be destroyed by a single piece of debris. The sail quadrants are further protected by adding ripstops. These are created by making a grid of Kapton tape on the surface of the membrane. A tear is only able to propagate to the nearest line of Kapton, assuming the initial hole is smaller than the grid sections. There is a design trade-off for the grid spacing because smaller grid sections reduce vulnerability to debris impacts, but locally increases the thickness of the membrane. It is also important that the ripstop lines are not perpendicular to the folds or else they will stack on top of each other. With that in mind, the ripstop pattern shown in Figure 6.7 was designed. The ripstop lines are parallel to the hypotenuse edges and evenly spaced. If one of the squares is completely destroyed, only 12% of the quadrant area and 3% of the total membrane area will be lost. The prototype of the sail can be seen in Figure 6.8. The edge reinforcements and the ripstops were taped using 12.7 mm wide Kapton tape.

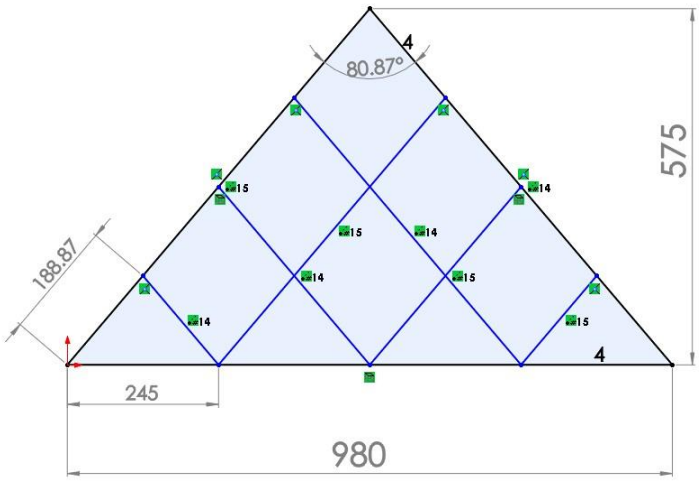

Figure 6.7: Sail quadrant ripstop pattern, dimensions in mm.

Figure 6.8: CP1 sail prototype with Kapton ripstops.

The sails will be folded per the "Frog Legs" scheme proposed by Dalla Vedova et al. in 2011 [20], and shown in Figure 6.9. It consists of taking the triangular sails and z-folding them so that they become a strip, then z-folding the ends into the middle. This allows the triangle to be deployed by pulling on the two ends. Eight people were used to fold a sail quadrant at the beginning to hold all of the folds down as a new one was being made, as shown in Figure 6.10. A teflon coated wire was used to create each fold by holding it tightly on top of the membrane while the unfolded membrane was passed over it. The wire was then pulled out of the fold and laid down on the other side. The green Teflon wire can be seen in the bottom right corner of Figure 6.10 as it is being held under tension.

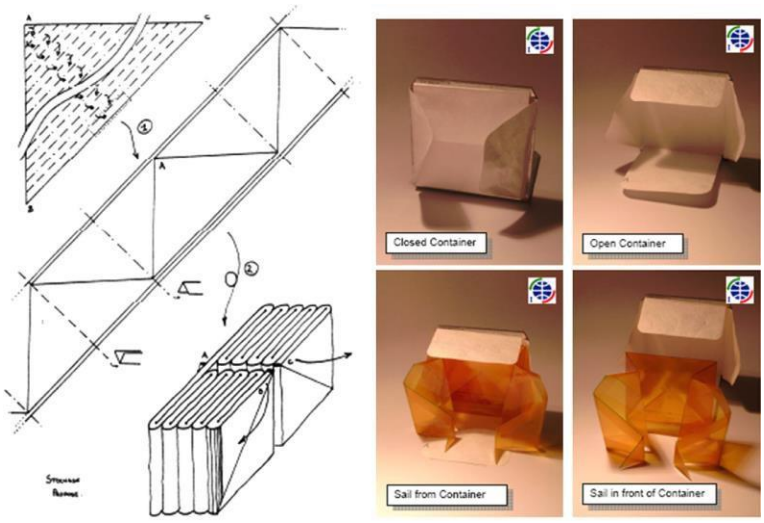

Figure 6.9: Frog Legs Folding Scheme Diagram [20]

Figure 6.10: Folding process. Note the green Teflon wire used to define the folds.

As more of the membrane was folded, new layers were not being added to the ends, so they were covered with thicker Mylar, and secured with binder clips. The sail after the first phase of folding is shown in Figure 6.11. Note that the rip stops did not stack on top of each other, reducing the thickness of the folded sail. The next phase was to fold both sides of the sail into the center.

Figure 6.11: CP1 prototype after initial folding phase.

In order to test if the folded sail will fit in the assigned volume, the outer casing and a few more deployer outer structures were printed out of ABS plastic on an Afinias machine. Figure 6.12 shows the fully folded sail in the allocated volume of the 3D printed structure, proving that the volume requirements will be met.

Figure 6.12: Fully folded CP1 sail quadrant in the allocated volume of a 3D printed prototype

6.1.3 Sail – Boom attachment method

The attachment between the sail and boom is critical to mission success. The corners of the drag sail must be attached to the supporting booms for proper deployment of the sails. The most important requirements for attachment are reliability and compactness. During deployment, the attachment point would face an outward tensional force as the boom pulls out the drag sail, causing it to unfold. Additionally, a drag force acts on the sail, which is supported by the attachment point. Therefore, for successful completion of the mission, it is important to ensure robustness of the attachment. However, due to limited stowage space, the attachment must be small enough to fit inside the payload casing.

The attachment assembly consists of the sail attachment point, the boom attachment point, and the connecting element between them.

Sail Attachment Point

Several options were considered for the sail attachment point, which include grommets or eyelets, D-rings and miniature clamps.

1. Grommet/Eyelet
    - Grommets shall be fixed onto the sail for facilitating its attachment to the boom. Reinforcement around the grommet hole shall be provided using Kapton tape. This type of attachment has been used for similar applications, including LightSail.
    - Pros: Simple, reliable, commonly used.
    - Cons: Potential weak point at the attachment location due to the punched hole, vulnerable to damage due to sudden tensile force during unfolding.

Fig. 6.1.3.1 Grommet. Digital Image. Airplanes and Rockets, http://www.airplanesandrockets.com/boats/victoria-sail-attachment.htm

2. D-ring
    - The sail can be attached to the booms using a D-ring. The edge of the sail material shall be folded into the D-ring and then reinforced with Kapton tape. Thus, the need for piercing holes can be eliminated and the chances of damage can be reduced.
    - Pros: No damage to sail material.
    - Cons: Not tested in a space-based application. It will require in-house testing to prove its feasibility.

Fig. 6.1.3.2 D-ring. Digital Image. Backyard City, http://www.backyardcity.com/Shade-Sails/Shade-Sails-Installation.htm

3. Clamp
    - Tiny clamps can also be used for the attachment of the sail to the boom. This avoids damage to the CP1 by eliminating the need to punch holes.
    - Pros: No damage to sail material.
    - Cons: Clamps small enough to fit inside the stowage space are extremely difficult to acquire. For this reason, clamps were dropped out of considerations in the test plan.

Boom Attachment Point

Several types of booms are being considered for the CubeSat at this point, including Roccor metallic (Elgiloy) TRAC booms, carbon fiber TRAC booms (manufactured in-house by Ariel Black and Anthony Cofer), and NASA's SHEARLESS booms. The advantage of using metallic booms is that a hole can be punched directly without damaging the boom.

However, in case of carbon fiber, punching holes can compromise boom strength by damaging the fibers. This can cause the boom the start breaking at the hole location. To avoid this, a few alternatives can be tested.

- Option 1: Metal or epoxy cap with a ring to hold the connector. Commercially available special adhesives can be used to glue them to carbon fiber boom. In case of the SHEARLESS booms, grommets can be used on the plastic sheath for attachment purposes.
- Option 2: Hole for sail attachment present in the mold (for in-house booms).

Some of the connectors considered are spring, fabric loop (e.g. shoe lace), mini-carabiner. The type of spring selected was extension spring with loop ends, similar to the ones used in LightSail. These would require additional split rings on both the loop ends for attachment to the sail and the boom.

The following table shows an intuitive evaluation of the possible attachment points.

Table 6.1.3.1 Morphological matrix of attachment point options

Component	Requirement	Option 1	Option 2	Option 3
Attachment Point on Drag Sail	Sail Material Robustness	Grommet: Small holes, careful reinforcement using Kapton tape.	D-ring: Use adhesives to stick folded corner, avoid sewing. Reinforcement in an octothorpe (#) orientation.	Clamp: Tight enough to hold the sail but not too tight. (Sail material may start tearing under pressure.)
	Probability of meeting size requirement	Grommet: High	D-ring: Mid	Clamp: Low
	Reliability	Grommet: High	D-ring: High	Clamp: Mid
Attachment Point on Boom	Boom Material Robustness	Metal Cap: "Tight fitted" at the outer end of boom, no holes drilled.	Ring w/ epoxy: Metal ring attached to boom using epoxy-based adhesives.	CF fabric loop: Attached to boom using epoxy-based adhesives.
	Probability of meeting size requirement	Metal Cap: Low	Ring w/ epoxy: High	CF fabric loop: High
	Reliability	Metal Cap: Mid	Ring w/ epoxy: Mid	CF fabric loop: Mid
Connector	Connector Feasibility	Carabiner clip: Easy and secure attachment.	Spring: Can keep the sail taut at all times.	CF fabric strip: Occupies the least space.
	Probability of meeting size requirement	Carabiner clip: Mid	Spring: High	CF fabric strip: High
	Reliability	Carabiner clip: High	Spring: High	CF fabric strip: Mid

Base Attachment Point

The base of the sail must be attached to a point on the CubeSat. A possible way of attachment is to bolt (or weld) a small U-hook to the base of the stowage section and use it for attaching the sail. A schematic diagram of the concept is shown below.

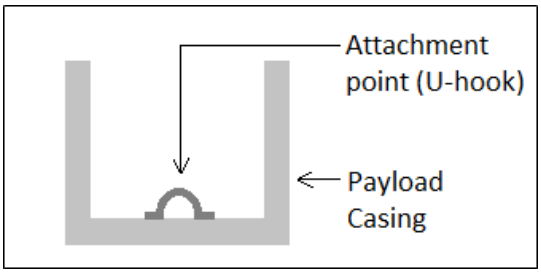

Fig. 6.1.3.3 Base attachment point

6.2 Inertial Measurement Unit

The Inertial Measurement Unit selected for ADE is the UM7, made by Redshift Labs. This IMU has many outputs but for the purposes of ADE it will measure the three-axis acceleration, angular rate, and magnetometer data. In addition to this data that will be used to confirm the stability of the drag sail, the IMU will measure the temperature data of the sensor. Table 6.1 shows the specification for the UM7 obtained from the data sheet found by redshift labs [21].

Table 6.1: UM7 Specifications

Parameter	Value
Weight	11 g
Dimensions	27 mm x 26 mm x 6.5 mm
Max Gyro Range	±2000 deg/s
Gyro Precision	5e-4 deg/s
Max Acceleration Range	±8 g
Acceleration precision	4e-5 g
Magnetometer Dynamic Range	±1200 uT
Temperature Range	-40C to +85C
Power Consumption	0.25 W

The IMU will collect data for 20 minutes at 10 Hz and this data will be stored onboard until it can be downlinked with any of the ground stations available.

6.2.1 Calibration

Since the IMU UM7 from Redshift Labs is factory calibrated, the calibration of the accelerometers, gyroscopes, and magnetometers is checked and completed as follows.

First, download the CHR Serial Interface from http://www.chrobotics.com/shop/um7-orientation-sensor. This is a free software provided by the UM7 vendor that allows the user to configure the IMU and to collect and plot data in real-time. Next, following the ESD Sensitive Component Handling Procedures, connect the IMU to the computer using the adapter. Use the free software to view the accelerometer and gyroscope data in real time and check the calibration. The magnetometer requires extra calibration depending on which environment it is placed in. This calibration is done using the software and by rotating the IMU in the environment it will be tested

in. An in-depth tutorial of the magnetometer calibration is listed at the same website above.

The results of the first calibration check validated the sensor noise sensitivity listed in the UM7 Datasheet [22]. The noise calculations were performed on acceleration data collected while the IMU was resting statically on a table.

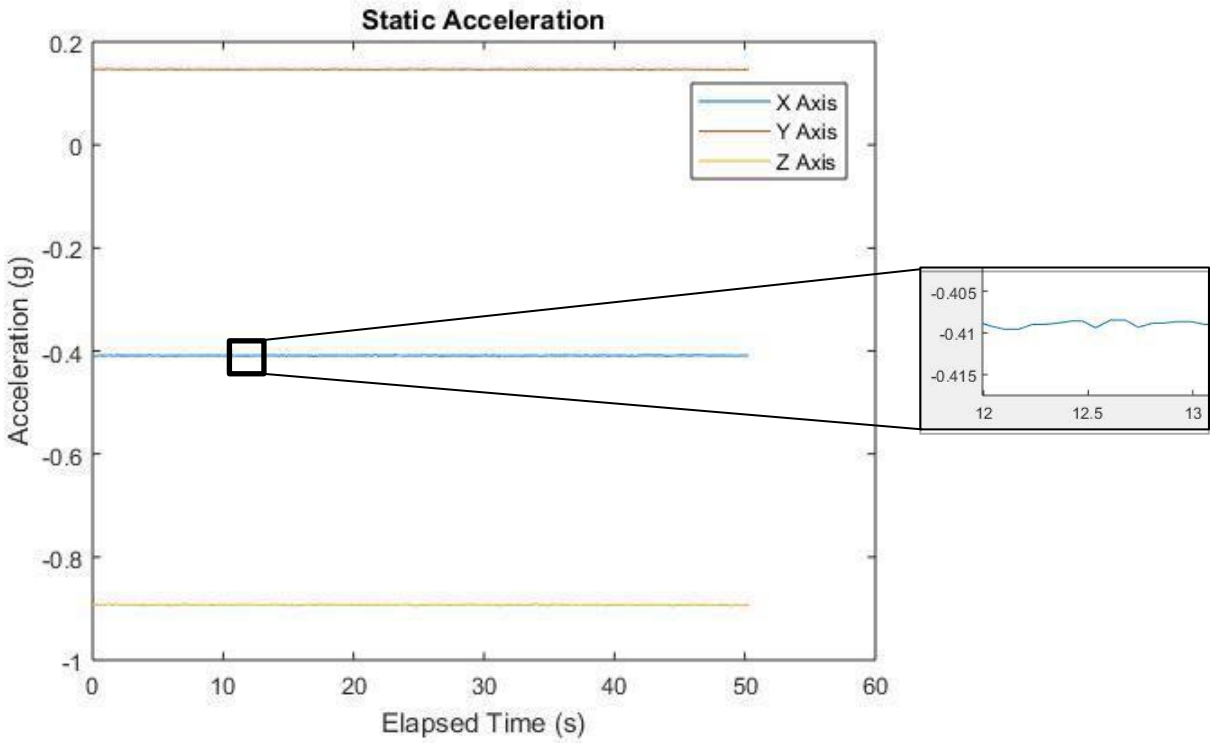

Figure 6.16: Static Acceleration Data

From this data, the rate noise density can be calculated using the equation below.

$$Rate\ Noise\ Density = \frac{RMS}{\sqrt{Hz}}$$

The results determined that at 10 Hz, the noise of the accelerometer is 0.00561 m/s^2. This noise is a measurement of the precision of the accelerometer readings. The precision can be increased by collecting data at lower frequencies.

6.2.2 Data Production

For each perigee pass the IMU will collect 20 minutes of data at a rate of 10 Hz. The total number of data points collected per perigee pass will be 132000. To achieve full mission success, IMU data for 5 perigee passes totaling of 660000 data points will need to be collected.

At each data pull of the IMU, data will be collected and stored for the 3 axes of the accelerometer, 3 axes of the gyroscope, 3 axes of the magnetometer, time, and temperature. Data is pulled and stored from the IMU as 4-byte floating points. Each data pull will retrieve data from 10 sensors, and time totaling 44 bytes. At a data collection rate of 10 Hz this sums up to 528000

bytes per perigee pass and 2.64 MB for 5 perigee passes.

To achieve full mission success, IMU data must be downlinked for 5 perigee passes. This would require 2.64 megabytes of IMU data to be downlinked. To reduce the data volume that needs to be downlinked, a data discretization algorithm was developed. The discretization method takes the minimum value and range of each sensor's data over each perigee pass. The range of each sensor is divided by 255 so that each floating-point sensor value can be mapped to an unsigned 8-bit integer. Knowing the minimum value of each sensor and the step size that each integer represents, the data can be reconstructed. The discretization of data significantly reduces the data volume to be downlinked and still provides accurate data following reconstruction after downlinking. Data volume following discretization reduces from 4 bytes per sensor reading to 1 byte. Discretized data volume for full mission success reduces to 0.66 MB. The minimum sensor readings and step size between each integer value need to be downlinked as well for data reconstruction. This information will be provided in a file header which will be downlinked twice for redundancy. The header will contain 11 minimum sensor values, and 11 sensor step values as 4-byte floating points and a header will be needed for each perigee pass. The total discretized data volume needed for full mission success is .66088 MB. The breakdowns of raw data volume and discretized data volumes are shown in Table 6.2 and Table 6.3.

Table 6.2: Raw Data Volume

Measurement	Data Type	Bytes per Draw	Bytes per Second	Bytes per Pass	Bytes per 5 Passes	MB per 5 Passes
Accelerometer X	Float	4	40	48000	240000	.24
Accelerometer Y	Float	4	40	48000	240000	.24
Accelerometer Z	Float	4	40	48000	240000	.24
Gyroscope X	Float	4	40	48000	240000	.24
Gyroscope Y	Float	4	40	48000	240000	.24
Gyroscope Z	Float	4	40	48000	240000	.24
Magnetometer X	Float	4	40	48000	240000	.24
Magnetometer Y	Float	4	40	48000	240000	.24
Magnetometer Z	Float	4	40	48000	240000	.24
Time	Float	4	40	48000	240000	.24
Temperature	Float	4	40	48000	240000	.24
Total		**44**	**440**	**528000**	**2640000**	**2.64**

Table 6.3: Discretized Data Volume

Measurement	Data Type	Bytes per Draw	Bytes per Second	Bytes per Pass	Bytes per 5 Passes	MB per 5 Passes
Accelerometer X	unsigned 8-bit integer	1	10	12000	60000	.06
Accelerometer Y	unsigned 8-bit integer	1	10	12000	60000	.06
Accelerometer Z	unsigned 8-bit integer	1	10	12000	60000	.06
Gyroscope X	unsigned 8-bit integer	1	10	12000	60000	.06
Gyroscope Y	unsigned 8-bit integer	1	10	12000	60000	.06
Gyroscope Z	unsigned 8-bit integer	1	10	12000	60000	.06
Magnetometer X	unsigned 8-bit integer	1	10	12000	60000	.06
Magnetometer Y	unsigned 8-bit integer	1	10	12000	60000	.06
Magnetometer Z	unsigned 8-bit integer	1	10	12000	60000	.06
Time	unsigned 8-bit integer	1	10	12000	60000	.06
Temperature	unsigned 8-bit integer	1	10	12000	60000	.06
Header Minimum Values	Float	0	0	88	440	.00044
Header Step Values	Float	0	0	88	440	.00044
Total		**11**	**110**	**132176**	**660880**	**.66088**

6.2.3 Data Reconstruction

The main function of the IMU is to analyze the stability of the drag sail assembly after it is deployed. A stable configuration being defined as the drag sail trimming to the maximum drag area, or with the z axis facing the flow. A stable orientation for this case will result in all of the angular rotation to be about the body z axis and little to no angular rotation about the body x and y axes.

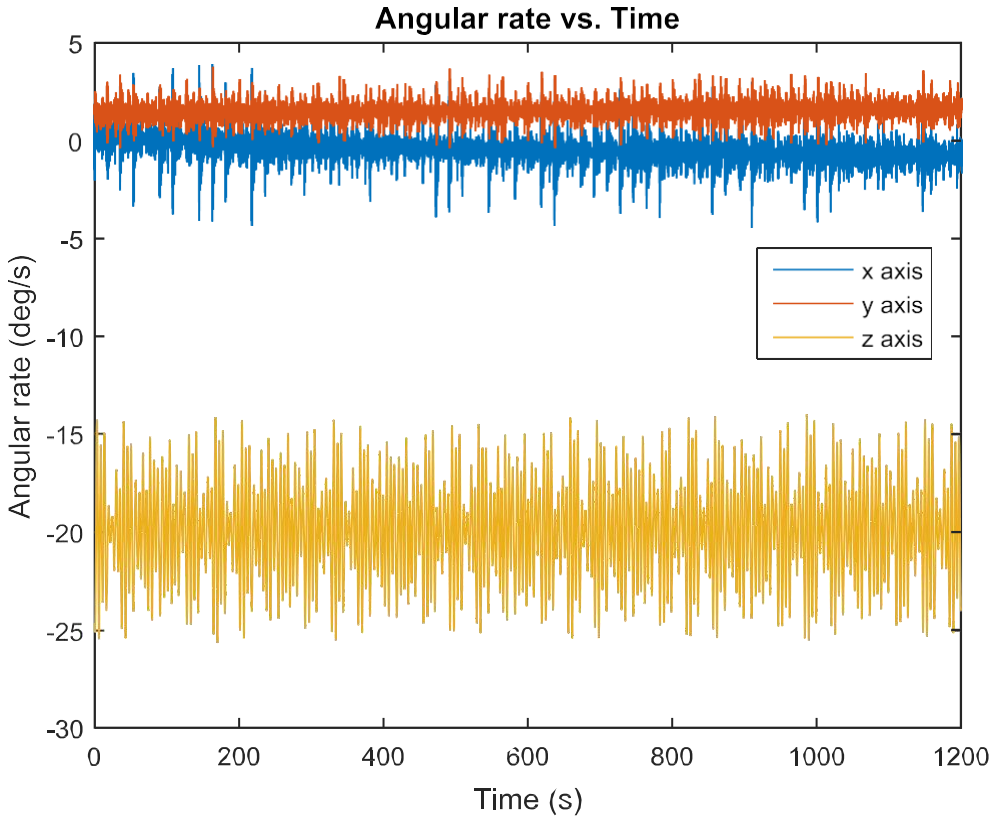

Figure 6.17: Sample Angular Rate Data for the Drag Sail in a Stable Configuration

Simply plotting the angular rate data as seen in the above figure may be enough to make inferences on the stability. This data, however, may accumulate biases as the mission progresses. It then becomes necessary to look elsewhere for inferences into stability. This too, can be seen in Figure 6.17 as the x and y angular rates begin to separate from each other at the end of the 20 minute data set.

The magnetometer provides a 3 axes representation of the earth's magnetic field. Operating under the same assumption that a stable orientation of the drag sail is characterized by rotation about only the z axis, the magnetometer data should remain relatively constant in the z axis and change dramatically in the x and y axes. The magnetic field that the spacecraft experiences will also be changing and will need to be corrected for. Provided the orbit of the spacecraft is known, the magnetic at each point along that orbit is also known and this correction can be made. The angular change in orientation can be computed by numerically differentiating the components of the corrected magnetic field vectors.

The acceleration data will act in the same way. A stable orientation would lead to a near constant acceleration in the z direction as the spacecraft undergoes the effects of the drag sail. Given a stable configuration, the magnitude of the acceleration in the z direction will shed light on the drag produced by the sail.

6.3 Radiation Detectors

ADE will have a total of eight radiation sensors onboard. There will be two sensors on each of the four panels, where one is located within the radiation shielding and the other located outside the radiation shielding. Each sensor is 14.5 mm x 16.5 mm, so the size of the sensors is not a concern. Additionally, each sensor will draw the minimum of 4 μW. Therefore, the radiation sensors do not put a large strain on the total system power.

The purpose of these sensors will be both scientific and observatory in nature. The outer radiation sensors will seek to characterize the environment around the spacecraft, while the inner radiation sensors will alert the ground team if harmful levels of radiation are penetrating the radiation shielding and present a danger to the system electronics. Part of the full mission success criteria is that the radiation sensors will characterize the environment in MEO and GEO for at least 3 full orbits.

It is important to note that the radiation sensors will not provide values of radiation dosage. Instead, they act as a diode, where the baseline status is "0" or "false". When a sensor detects a threshold energy of 5 keV, it records a value of "1" or "true". Therefore, more hits per time indicates higher levels of radiation. Additionally, the sensors are particularly sensitive to gamma radiation. Because the Van Allen Belts, another area of interest, do not contain large amounts of gamma radiation, one should see a significant drop in hits as the spacecraft passes through these zones.

Lastly, the cadence of the radiation sensors will be defined. It was determined that a continuous draw of 1/60 Hz was sufficient to meet the full mission success criteria and gather a reasonable amount of data. When each sensor draws once per minute, each draw takes 32 bits. A simple conversion results in 0.24 MB per sensor per hour. Assuming a 75 day deorbit period, this amounts to 3.46 GB of total radiation data from all eight sensors.

6.4 Cameras

ADE will carry three visual cameras to capture images of the drag sail and of Earth from near apogee. One of these cameras will be placed on the -Z panel along with the antenna, and the other two will be placed on perpendicular side panels. Each of the cameras has a 40x50 degree field of view, and the side panel cameras will be tilted in the +Z direction to look towards the sail to confirm deployment. Demonstrations of the viewing angles of the –Z camera and a side panel camera are included in Figures 6.18 and 6.19.

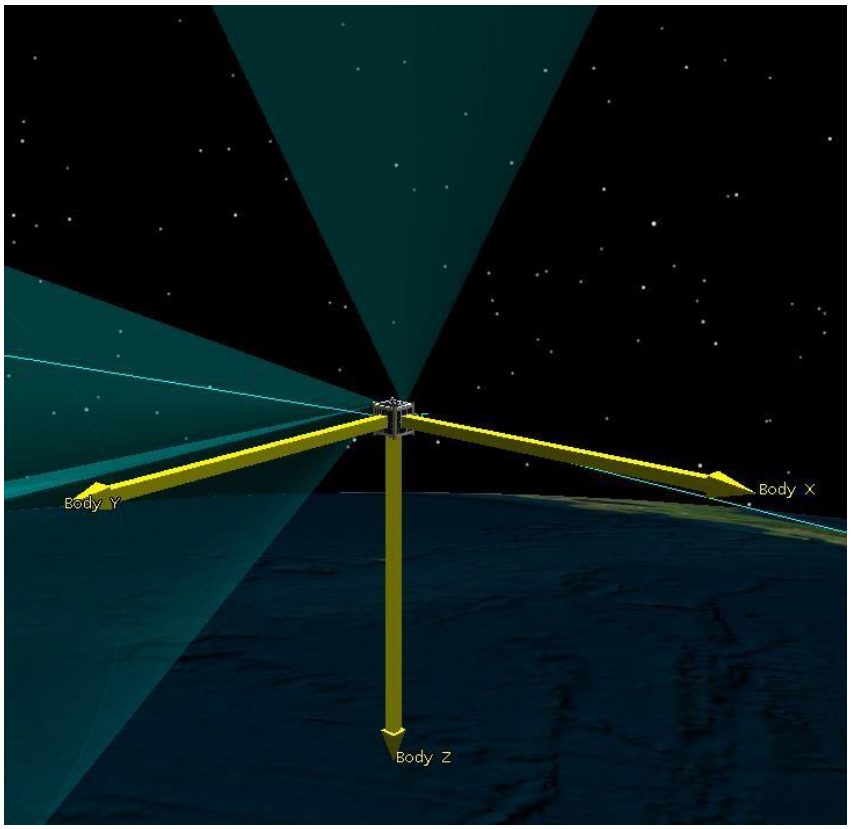

Figure 6.18: STK Model of each Camera's Field of View

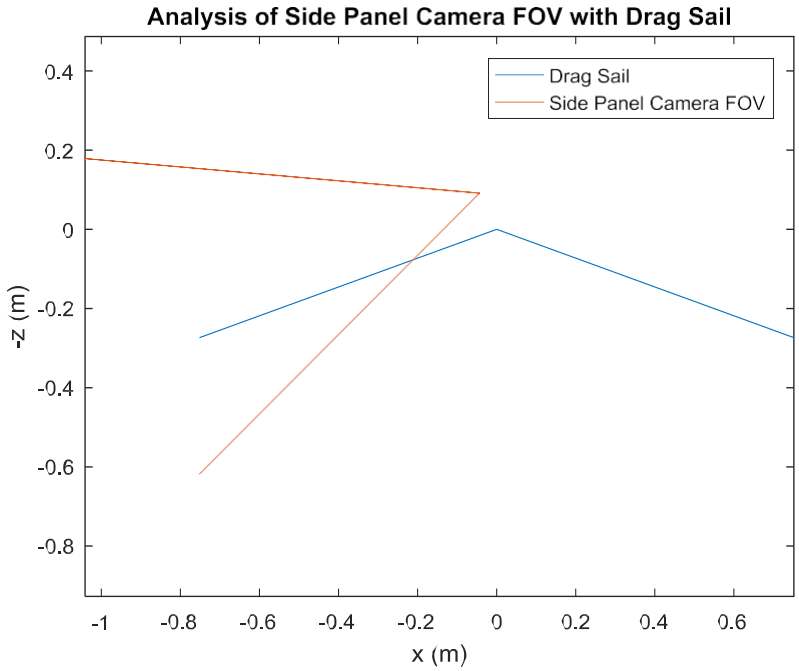

Figure 6.19: Visualization of the Deployed Drag Sail and the FOV of the Side Panel Camera

The three cameras will be built by OmniVision Technologies, and are a model OV3642. This model is a 3-megapixel camera that has a built-in microcontroller to adjust the imaging settings [23]. Each of our chosen camera systems comes mounted on a chip. This model has been previously flown on CalPoly-built CubeSat missions, and the software and commands for controlling them have been previously used.

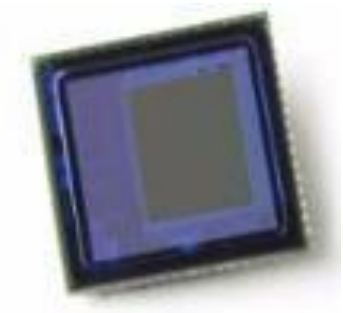

Figure 6.20: OmniVision OV3642 Camera Mounted on a Chip

For normal operations, each camera will take 1 image per hour. It's not expected that all taken images can or will be downlinked, but taking a larger number of photos than we can downlink is a good way to ensure at least one of them will contain the Earth from near apogee.

To provide a preliminary filter for the photos that will have thumbnails downlinked for review, we can simply ignore the images with the smallest file size. The cameras have a built-in JPEG compression engine, which dramatically reduces the size of "homogeneous" images. Meaning that if an image does not contain Earth, the Moon, or some other body, the image will be nearly entirely black, and the JPEG compression will make the file size significantly smaller than another image that may contain Earth. This is a crude filter, but has been used with success on previous CalPoly CubeSat missions, and does not require onboard processing such as a blob detection algorithm.

7 Radiation Environment

Given that ADE will go well beyond LEO, the effects of radiation become significant to understanding the expected lifetime of the spacecraft. Also, it will aid in anticipating how often the system may experience a fault.

7.1 Radiation Environment

Spring 2019 Semester Radiation Summary

The past analysis shown above discusses the NASA OLTARIS radiation tool. This semester, the AE9/AP9/SPM software was used to perform the radiation analysis. Initially, the orbit parameters were analyzed, and the initial orbit of the cube satellite was modeled. After the orbit simulations were completed, the orbit data was then used to generate a total of 12 radiation models, each with a different RAAN value that corresponded to the minimum, average, and maximum deorbit duration cases. The following table shows all the RAAN values, in degrees, that the radiation models were generated for.

RAAN Values Tested For Radiation Modeling

Minimum (days)	Average (days)	Maximum (days)
271	93	38
280	153	42
288	214	46
293	352	49

The total dose accumulation graphs that are outputted by AE9/AP9 are severely inaccurate, as they show a total accumulated dosage of about 140 k-rads. However, the dose rate graphs are more accurate. Therefore, the total accumulated dosage was calculated by integrating the dose rate over a period of 1 month to compare with the previous analysis performed using OLTARIS. Initially, aluminum shielding was used to perform the analysis because that is the only material permitted by AE9/AP9 software. The copper shielding values were computed by comparing the density values of the two materials. The density of copper is approximately 8.96 g/cm^3, while the density for aluminum is approximately 2.70 g/cm^3. Therefore, the ratio of the density of copper to the density of aluminum is about 3.32. The range of values used for the shielding were from 0.1 mm to 1.4 mm, computed in increments of 0.1 mm. At a shielding value of 1 mm, the total accumulated dose in one month was found to be about 20 k-rads with aluminum. This was computed using the fact that the dose rate graphs outputted a value of approximately 0.0076 rads/sec. This value was then multiplied by 2,628,000 seconds to get the total value of about 20 k-rads for the first month. It is important to note that this value is for aluminum shielding. As mentioned previously, copper is about 3 times as dense as aluminum. Therefore, if we divide 20 by 3.32, then we should expect to accumulate a total dosage of about 6.02 k-rad in the first month. Based on a paper by JPL that outlined some radiation tests performed by NASA, general 16-bit flight processors should be able withstand unbiased radiation dosage of 20 k-rad (31). However, “most biased devices were not functional at the 10 k-rad or 20 k-rad point”. All of the devices tested were functional up to 5 k-rad of total radiation. It is important to note that these devices were all 16-bit microprocessors. The AtTiny 1616 chip is an 8-bit micro-processor used for the motor driver board to deploy the booms. The maximum radiation dosage that the 8-bit chip can withstand

will only be found after performing the radiation test. Radiation data on this specific chip is not available online. The values for the 16-bit processors give us a general idea of what the radiation dosage we can expect similar board to handle. 8-bit micro-processors should be expected to be at least within the same order of magnitude to what the 16-bit micro-processors can withstand. It is no doubt that the shielding material used will have to be copper, due to its high density. The board shall be able to able to withstand a maximum radiation dosage of about 6-krads, and as referenced by the JPL paper, it seems likely that the board should survive the radiation conditions expected during the flight.

7.2 Shielding Considerations

Further discussions with CalPoly produced a shielding plan that coincided with the current architecture of the spacecraft. Instead of utilizing aluminum shielding as stated in the OLTARIS analysis, it was decided that extra copper substrate would be introduced into the construction of the side panels.

The bottom layer of the PCB of the side panels will have at least 1 mm thick layer of copper in order to provide shielding. This layer is a change from the standard side panel design flown by CalPoly on previous missions, but it should not affect the functionality of the spacecraft. Additional shielding will be applied according to the remaining available mass shown by the mass budget. It has also been considered to add additional shielding to the z-panel board that contains the antenna, but this decision is still under consideration. Given that the drag sail assembly itself is more than 1mm thick of aluminum, we can expect that the assembly will provide ample shielding in that axis by itself. This is because the minimum amount of shielding needed to protect the board is 1 mm of copper. Therefore, if we have additional shielding by the aluminum drag sail assembly, then we can be certain that the cube satellite will be able to withstand the 6-krads of radiation dosage as predicted by AE9/AP9 radiation models.

Based on AE9/AP9 radiation environment and results, we would need a shielding thickness of 1 mm of copper to withstand the expected radiation dosage of 6 krads, as outputted from the AE9/AP9 radiation models. All the graphs and the radiation models can be found in the shared drive and are not included here due to the size of the files. However, it is important to note that given the radiation dosage of 0.0076 rads/sec, the board should withstand an accumulated dosage of 20 k-rads with the aluminum 6 k-rads with copper shielding, at a shielding depth of 1 mm.

A shielding plate was added to the drag sail deployer sub assembly that covers the control board for the deployers. This is a 2.54mm thick aluminum plate that is placed over the control boards in the center of the deployer assembly. The control boards are also shielded by the motors of the deployers and the aluminum casing of the deployers on four sides. This Shielding can be seen in Figure 7.1.

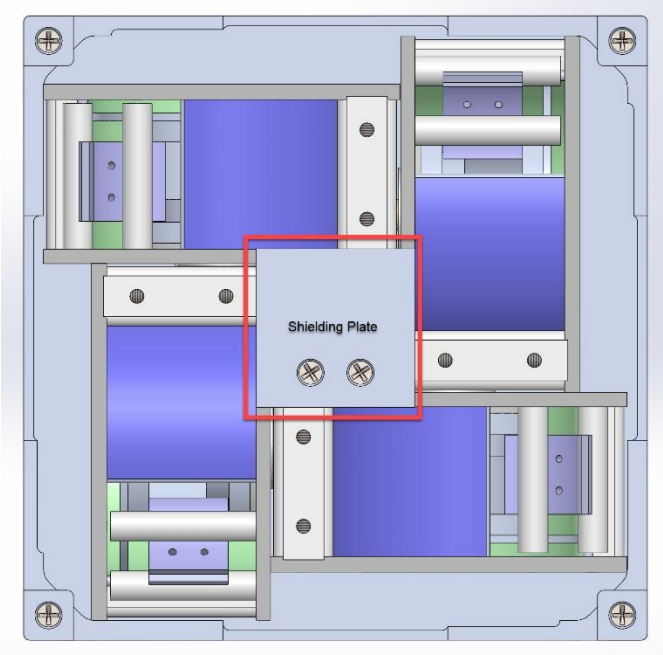

Figure 7.1: Shielding on Drag Sail Deployment Sub-Assembly

7.3 Electrostatic Discharge Risk Analysis

Motivation

CalPoly raised concerns in the beginning of the Spring 2020 semester about the possibility of high static charge build-up for ADE due to the geosynchronous transfer orbit passing both through and beyond the Van Allen Belts. Enough static charge build-up could potentially result in an electrostatic discharge event, which in a worst-case scenario could result in high voltage arcing from the sail to the spacecraft chassis, almost certainly causing damage to the spacecraft and its avionics and likely ending the mission. This concern resulted in the decision to conduct analysis on both the GTO environment as well as risk of arc flashes.

Analysis

One of the most useful research papers was titled Charged Particle Effects on Solar Sails – An Overview. This paper was published by authors from JPL and MSFC in 2014. One particular excerpt was particularly useful:

> *"Problems arise, however, if the sail material backing is non-conductive or electrically decoupled from the front surface. In that case, the shadowed back surface can reach potentials of -30 to -40 V relative to the space plasma in the solar wind. These are on the order of arcing onset potentials (reported by some to be as low as 50 V). The real issue is the geosynchronous environment (or its extension down to low altitudes in the auroral zones) where an isolated surface in the dark can reach 1000's of volts. The issue here is simple; make sure the sail material is conductive front to back and end to end if the sail is to be in*

geosynchronous orbit or in the auroral zone and be very careful with electrically isolated objects in the shadow of the sail."

The second useful article was *Introduction to Spacecraft Charging*, an excerpt from a textbook. In this article, the concepts of surface charging and deep dielectric (bulk) charging were explained. Their traits and differences are described below.

Surface Charing - Build-up of a voltage difference across various materials on the spacecraft. This occurs commonly in GSO due to plasmasphere storms from interactions with solar wind. When these storms occur, high levels of surface charging (or even bulk charging) can occur. These do not typically result in high damage or long distance arcs, as less charge can be built up from surface charging before ESD (electrostatic discharge) occurs.

Deep Dielectric (Bulk) Charging - High energy particles "burrow" into insulators, eventually building up enough charge over time to lead to serious high-energy and long-distance arcing (this is our main concern). This type of charging occurs more commonly in the Val Allen Belts due to the occasional high energy particles (particles above 100 keV, usually MeV electrons, are typically responsible for bulk charging).

An additional literature source that proved to be useful was the textbook *Extreme Events in Geospace*. Chapter 16 discusses exclusively deep dielectric charging and spacecraft anomalies. The following are important quotes summarizing the take-aways.

1. The role of electrons penetrated deep inside dielectrics has been known for years. The electrons penetrated inside provide high internal electric fields which may be responsible for spacecraft anomalies in orbits exposed to MeV electron fluxes in the outer radiation belts.
2. Deep dielectric charging is not directly related to spacecraft anomalies. In a hazardous environment, deep dielectric charging occurs and builds up the internal electric fields. A spontaneous discharge may, or may not, occur even when the electric field reaches sufficiently high values. A triggering impetus may bring forth the occurrence of a discharge. Such triggering events include collisions with micrometeorites, cosmic rays, or exceptionally high energy particles.
3. It has been found that occurrence of these anomalies is higher during the declining/minimum phase of a solar cycle.

These major points all highlight that bulk charging and electrostatic discharge are very real and possible risks for our mission. ADE will be launching near a solar minimum, and we will be passing through the outer radiation belts multiple times with large areas of insulating material exposed.

This textbook section additionally reduced this information into spacecraft design guidelines. These design guidelines were partially derived from the CRRES mission, or the Combined Release and Radiation Effects Satellite. The two most important guidelines are listed below.

Spacecraft Design Guidelines

1. Significant probability of hazard exists when >2 MeV daily electron fluence outside the spacecraft exceeds 3.8×10^9 electrons/cm^2.

2. An extremely significant probability of hazard exists when >2 MeV daily electron fluence exceeds $3.8x10^{10}$ electrons/cm^2.

These two guidelines assume 4.3 mm of aluminum shielding for any insulators, as this is an average CubeSat chassis structure material and thickness. Since this is not the case for the drag sail, much lower energy electrons should be considered in the analysis, although how much lower is debatable.
With all of this literature researched, the next step was to utilize the tool SPENVIS, SPace ENVironment Information System, to evaluate ADE's radiation environment based on its orbital parameters. This tool had been used by Sandeep previously, and he recommended it based on its accuracy. SPENVIS cannot do direct spacecraft analysis, but characterizes the radiation environment for a given orbit.

When running this analysis, >1 MeV energy particles were chosen as a starting threshold. This value was chosen by arbitrarily halving the >2 MeV design guidelines due to the lack of shielding for our drag sail. This resulted in the following plot, where the radiation flux varies over time in an expected fashion for a GTO orbit.

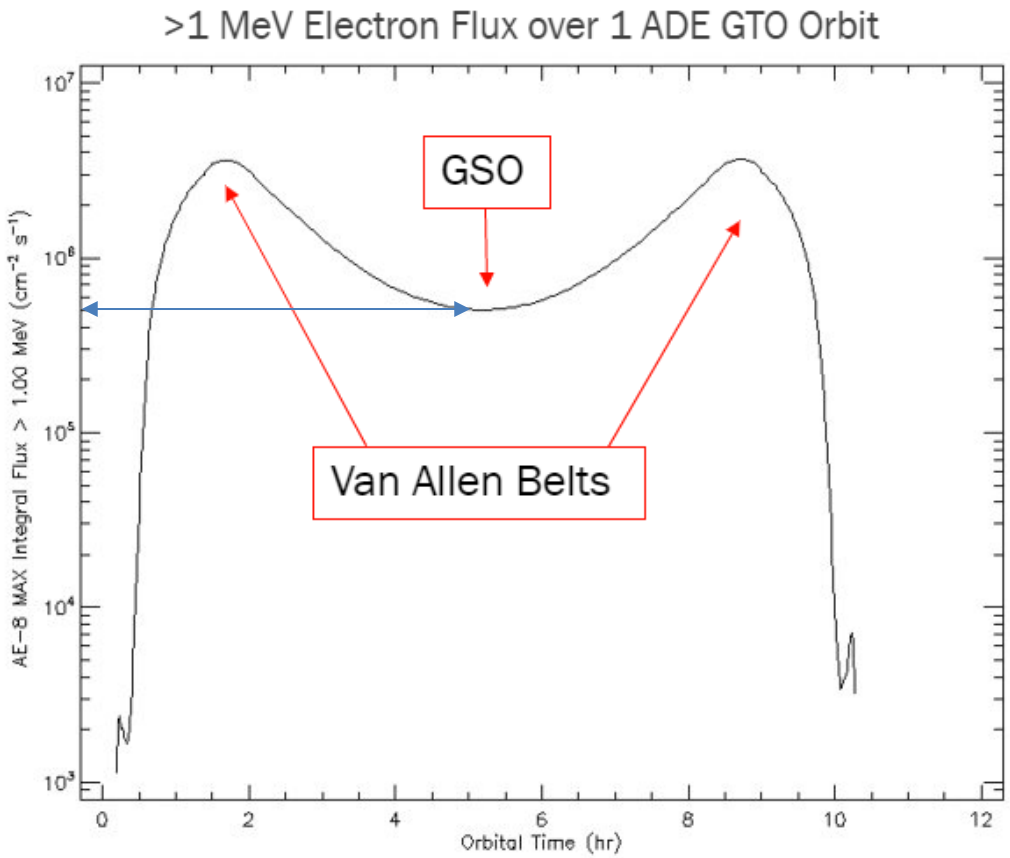

Using this plot, a low-end estimate for daily electron flux can be calculated. At the trough of the plot (GSO) the electron flux per second can be seen as $5x10^5$ >1 MeV /cm^2 /s. When averaged over a day, this results in a daily electron flux of $4.32x10^{10}$ >1 MeV /cm^2 /day. This exceeds the "extremely significant probability of hazard" value from the spacecraft design guidelines.

Based on the arbitrary choice of >1 MeV as the cutoff value and the initially discouraging results, a sensitivity sweep was conducted to evaluate how the results varied for different minimum electron energy thresholds. A range of energies from 500 keV to 2.5 MeV was evaluated for both solar maximum and solar minimum scenarios. The table of results is listed below.

>X MeV Considered	Daily Electron Flux (electrons/cm^2)	
	Solar Maximum	Solar Minimum
>0.5	2.59 e11	2.34 e11
>1.0	3.46 e10	3.25 e10
>1.5	1.29 e10	1.16 e10
>2.0	4.32 e9	4.22 e9
>2.5	1.29 e9	1.18 e9

This table is based on the same low-end averaging used for the plot shown on the previous page. It can be seen that the solar maximum/minimum makes only a minor difference, and that even up to the >2 MeV threshold we are still in the "Significant probability of hazard" range. Additionally, the daily flux increases significantly with lower energy levels, and so a drag sail made of insulating material with no shielding should be considered a high-risk design.

Conclusions and Recommendations

Based on all of the literature and analysis discussed above, there are three major take-aways.

1. Electrostatic discharge and arcing from the sail to the spacecraft chassis is a very real risk and has been documented as a somewhat common failure mode for spacecraft traveling through the radiation belts and geosynchronous orbits.
2. The cause of electrostatic discharge is deep dielectric charging, or bulk charging. This occurs when high energy electrons burrow into insulators and over time build up a large voltage difference. This instability can possibly result in an arcing event, and combined with a triggering event will almost certainly result in an arcing event.
3. The radiation environment we expect to see in ADE's GTO orbit is likely to exceed recommended levels for spacecraft with insulating materials based on analysis from SPENVIS.

Based on these conclusions, the recommendation is to move to a conductive sail material if possible.

Next Steps

1. The first step is to continue researching conductive coatings for CP-1 such as aluminum. If this does not satisfy the requirements for conductive material, alternative drag sail materials may need to be investigated such as aluminized mylar.
2. Additionally, the selection of a conductive sail material will certainly lead to solar radiation pressure effects. Because of this, the effects of SRP on ADE's passive aerodynamic stability and orbit propagation should be evaluated using the 6-DOF code and GMAT.

8 Mission Phases

8.1 Launch & Initial Acquisition

ADE shall be deployed via a standard P-POD. The batteries will begin charging in safe mode and the flight processor will then turn on. The spacecraft shall remain in safe mode until the batteries are charged. There will be no transmissions made until at least 45 minutes have elapsed since launch. ADE shall then deploy the dipole antenna 45 minutes after P-POD deployment. The beacon will then be turned on 46 minutes after P-POD deployment. This signifies the earliest signal acquisition at this point, transmitting spacecraft telemetry every 30 seconds to ground stations.

8.2 Checkout

During the checkout phase all of the spacecraft components will be checked and verified to ensure proper functionality. An evaluation on the health and status of the spacecraft will be conducted that will last 2-3 days during the initial checkout period. Multiple tracking pass stations will be used as checkpoints to assess power, thermal, and other electrical component statuses onboard the spacecraft. The spacecraft clock will be set and updated by ground command followed by the uplink of an updated orbit ephemeris file consisting of perigee time predictions.
Following the verification of spacecraft components, the IMU will be turned on and calibrated. During the IMU checkout gyro and accelerometer data will be collected for 20 minutes centered on predicted perigee passage, per updated orbit ephemeris file. The data will then be stored and downlinked at the next available tracking pass followed by an evaluation to ensure the IMU is functioning properly.

8.3 Deployment

The drag device will be deployed autonomously 7 days after turning on following P-POD deployment and battery charging. The timing may be updated by ground command to occur at another specific time. After the deployment of the booms and drag sail device the spacecraft will be set to experiment mode in order to proceed into the science phase.

8.4 Science Phase

This phase begins once the spacecraft is set to experiment mode. During the science phase of the mission IMU data, camera photos, and radiation data will be collected. The data collected by the radiation sensor will be taken continuously while the IMU data will only be taken for 20-minute intervals at every perigee pass. In order to ensure drag sail deployment, the camera facing the drag sail device will take a photo of its position post-deployment. Photos of the Earth will be taken at every apogee pass until an acceptable quality image is obtained. Data downlink will occur at every viable overflight of Arizona State, Cal Poly, Georgia Tech, and Purdue University ground stations.

8.4.1 Periapsis Timing Analysis

The primary purpose of this mission is to gather scientific data about the drag exerted on the spacecraft as it passes through Earth's atmosphere. This data is collected by the IMU. However, power and data limitations restrict the spacecraft to activating the IMU only when the spacecraft passes through the atmosphere, which occurs around its periapsis. Therefore, being able to predict the time of each periapsis is crucial to mission success. Orbital element updates from JSPOC are limited, so the CubeSat may make several passes through the atmosphere without periapsis time correction from the ground. Prediction of periapsis timing is baselined as a ground-in-the-loop process, with an onboard periapsis timetable updated via ground command. The primary source of error in this method derives from uncertainty in the satellite's coefficient of drag. Additional error is added by the variable atmospheric density in the lower thermosphere, the region in which the satellite's periapsis lies, where rarefied flow is present. As this error builds up over multiple passes through the atmosphere without update from a ground station, the time range for which the IMU must be collecting data would have to increase to account for this error. This would ensure that the full drag pass is encapsulated within the data gathered. In order to avoid the issue of an increasing data collection period, a Periapsis Time Estimator (PTE) will be implemented onboard the ADE CubeSat.

A Periapsis Time Estimator is a software used for autonomously predicting the times of future periapsis passes based upon acceleration data collected during previous periapsis passes. Onboard ADE, this software will be used to update the stored periapsis timetable, which in turn communicates to the flight system when the IMU should begin gathering data. Although periapsis time estimators have been developed in the past, their use has been limited. Any high-profile Earth-based mission in the past has had near-constant communication with a ground station, eliminating the need for autonomous software such as a PTE. Hence the main use of PTEs in the past has been for missions involving Mars aerobraking. These missions include Mars Odyssey, Mars Reconnaissance Orbiter (MRO), and Mars Atmosphere and Volatile Evolution Mission (MAVEN).

The first documented use of a PTE was for Mars Odyssey. It was developed primarily by Lockheed Martin and tested prior to the mission using atmospheric data gathered from Mars Global Surveyor (MGS). This first iteration was based around a periapsis timetable, a list of the predicted times of all future periapsides, which could be updated via ground command. The PTE used a centroiding scheme to calculate the "time-center" of an acceleration curve gathered during a drag pass. The spacecraft's orbit period was assumed to be the period between two consecutive time-centers. These orbit period calculations were then used to provide updates to the periapsis timetable during periods where ground stations were unable to adjust it directly. This method of PTE suffered high inaccuracy in large-period orbits (greater than six hours) but below that value matched navigation reconstructs well. Lockheed Martin's PTE was improved and used again on both MRO and MAVEN. Acceleration data was used to estimate the change in velocity from each drag pass, thus improving the accuracy of the following periapsis time estimation. However, any further details are not documented.

The PTE algorithm has been fully developed, and the PTE flight software implementation is currently in development. The algorithm integrates the magnitude of the acceleration data gathered by the IMU around periapsis to calculate the velocity change during a drag pass and

applies that as an impulsive maneuver in the anti-velocity direction. PTE also calculates the centroid of the acceleration profile and assumes that to be the time of periapsis. Under the assumption of two-body mechanics, PTE then calculates the next orbit period, taking the previous orbit period as the difference between the previous time centroid and the current time centroid. The next predicted time of periapsis is therefore calculated as one orbit period after the current time centroid.

To test the PTE algorithm, a propagator was created in MATLAB to generate simulated acceleration data over the entire mission deorbit timeline. The propagator is based on work by Miele, Zhao, and Lee and includes perturbations due to oblateness and the J2 effect [25]. The propagator adds noise and bias onto the accelerates derived from the ODEs to simulate a data set gathered from the IMU on board.

To filter out noise and temperature-induced bias, PTE is equipped with a noise filter and bias correction algorithm. The noise filter is a simple window filter, and the bias correction uses a temperature data fit to compensate for the bias ramp-up.

Before the software is allowed full functionality and given the ability to actively edit the periapsis timetable in flight, it is planned for it to be run in a "safe mode". In this early-mission mode the PTE will run in the background, estimating the times of future periapsides and reporting but not utilizing its results. If the results are deemed reliable, either by communication with ground stations or autonomously onboard ADE, the PTE will then be put into full effect, writing over the periapsis timetable.

8.5 End of Mission

ADE is expected to deorbit within 34 to 269 days after deployment of the drag device. The average estimated deorbit time is 75 days. It will disintegrate upon re-entry into the Earth's atmosphere signaling the completion of the mission.

9 Mission Operations

9.1 Command Dictionary

This section contains the current development of the command dictionary. The most up to date version of the command dictionary can be found on the OneDrive. Below in table 9.1 is the current command dictionary. A legacy version of the command dictionary can be found on the OneDrive. It is important to note that the legacy version of the command dictionary is not reflective of the current architecture of ADE and should not be used during the mission.

Table 9.1: Command Dictionary

Command	Command Parameters	Function	Description	Resend Safe	Scriptable	Component	Notes
			System Commands				
			Turn the power line for the IMU and Cameras off (PIB Sensors)				Discussed with Cole Fehring
			Turn the power line for the IMU and Cameras on (PIB Sensors)				Discussed with Cole Fehring
			Reboots the Spacecraft				
			Alter the sail deployment timer				
			Modify register to change number of sail deployment motor steps to be executed				
			Modify register to change direction of sail deployment motor				
			Modify register to execute sail deployment motors				
			Initiates sail deployment sequence: IMU data acquisition, camera image acquisition sequence, sail deploys				
			Payload Commands				
			Take pictures using all cameras				
			Attitude Determination Commands				
			Starts the IMU data aquision for a specified desired amount of time and frequency				
			Electrical Power Subsystem Commands				
			Data Handling Commands				
			filemgr Commands				
			Filemanager listing of thumbnail data				
			Filemanager listing of image data				
			Filemanager listing of IMU data				
			Downlink file from filemanager				
			Beacon Commands				
			Reset the step motor count beacon parameter				
			Watchdog Commands				
			Datalogger Commands				

9.2 Telemetry Beacon Definition

Apart from the data downlinks, ADE shall also transmit a telemetry beacon with a 4% duty cycle. This telemetry beacon shall contain the values of all the parameters that are considered system-critical and would need to be tracked more often. It shall also contain the last measured values of the IMU and radiation sensors.

The purpose of the Telemetry beacon is to provide a system status check for the CubeSat and allow any potential issues that might affect performance to be addressed. Unlike regular data downlinks, which would consist of sequential data being downlinked over a longer period, the telemetry beacon transmits a single packet (264 bytes) once every 5.5 seconds. The transmitted telemetry packet contains the following parameters:

Parameter	**Bytes**
Flight Systems board voltage	1
Flight Systems board current	1
Flight Systems board temperature	1
Telecom board voltage	1
Telecom board current	1
Telecom board temperature	1
Battery 1 voltage	1
Battery 1 current	1
Battery 1 Temperature	1
Battery 2 voltage	1
Battery 2 current	1
Battery 2 temperature	1
Battery 3 voltage	1
Battery 3 current	1
Battery 3 temperature	1
Solar Panel 1 Voltage	1
Solar Panel 2 Voltage	1
Solar Panel 3 Voltage	1
Solar Panel 4 Voltage	1
Solar Panel 1 Temperature (Inside)	1
Solar Panel 2 Temperature (Inside)	1
Solar Panel 3 Temperature (Inside)	1
Solar Panel 4 Temperature (Inside)	1
Solar Panel 1 Temperature (Outside)	1
Solar Panel 2 Temperature (Outside)	1
Solar Panel 3 Temperature (Outside)	1
Solar Panel 4 Temperature (Outside)	1
Top Panel (-Z) Temperature (Outside)	1
Uplink RX counter	2
Time since last soft reboot	4
Time since last hard reboot	4
Reset processes identifiers	4

Spacecraft mode	1
Antenna deployed	1
Sail deployment armed	1
Sail deployed	1
Motor count 1	1
Motor count 2	1
Motor count 3	1
Motor count 4	1
Real Time Clock	4
User Time	4
System Time	4
PTE Mode (passive or active)	1
Previous periapsis time value (prediction from PTE)	4
Previous periapsis time value (centroid from IMU)	4
PTE time value	4
Previous PTE error	4
No. Of full pics taken	2
No. Of thumbnails taken	2
Camera A On/Off	1
Camera B On/Off	1
Camera A temperature	1
Camera B temperature	1
IMU X Acceleration	4
IMU Y Acceleration	4
IMU Z Acceleration	4
IMU Angular Velocity X	4
IMU Angular Velocity Y	4
IMU Angular Velocity Z	4
IMU Magnetometer X	4
IMU Magnetometer Y	4
IMU Magnetometer Z	4
IMU Temperature X	1
IMU Temperature Y	1
IMU Temperature Z	1
IMU On/Off	1
IMU Health Register	4
Radiation Sensor data 1	8
Radiation Sensor data 2	8
Radiation Sensor data 3	8
Radiation Sensor data 4	8
Radiation Sensor data 5	8
Radiation Sensor data 6	8
Radiation Sensor data 7	8
Radiation Sensor data 8	8

The values of temperatures, voltages and currents indicate the health of the various components, while the IMU Health register indicates its status. The uplink counter helps to keep track of the number of times a command has been uploaded to the spacecraft, which can help to keep track of the number of data sets downlinked. The IMU and radiation sensor parameters hold the last recorded values from those sensors.

In a single packet, the maximum permitted information field size is 227 bytes. The final readings from the IMU will take 38 bytes. All the parameters can be recorded in the ranges of 'unsigned integer' (1-4 bytes) or 'float' (6 decimals, 4 bytes) data types, each parameter takes up 4 bytes of data. The total information field size for the telemetry beacon is, which is below the single packet limit. Since, at 9600 bps, a single packet transmits in 0.22s. At 4% duty cycle, the beacon transmits once every 5.5s.

The beacon will use Libproc libraries developed by Cal Poly to encode the message using the AX.25 protocol and transmit the message through the CubeSat antenna using "Satcomm" communication Software.

9.3 Tracking Overflight Schedules

Analysis in STK and FreeFlyer was performed to find the first time of contact for the same setup as Deorbit Duration setup, the only difference is that the Epoch with time 12 PM were excluded so the analysis was performed for 8 Epoch spanning over 16 weeks as explained in Ch 3.

The objective of the analysis was to find the minimum, average and maximum time required to establish an uplink connection with the ground stations. In addition, the minimum, average and maximum total contact duration for the four ground stations for initial time of 12 AM 1 Jun 2020 till Deorbit (i.e. reach altitude of 60 km) were found to know what how much total contact time we can expect. The two main constraints were the slant height needed to be below the uplink limit, so the slant height range was set to 22,000 km and the minimum contact duration needs to be more than 5 minutes.

The below table shows the minimum and maximum time that we must wait from epoch from the two-software used for CubeSat to make contact with any one of the four ground station. The last two columns show the minimum contact duration for first time of contact found the multiple test

Table 9.2: First time of contact from Epoch

Ground Station	Min Start Time from Epoch STK	Min Start Time from Epoch FF	Max Start Time from Epoch STK	Max Start Time from Epoch FF	Min Contact Duration: STK	Min Contact Duration: FF
Purdue	41.25 min	63.1 min	21.61 hr	30.22 hr	12.23 min	5.81 min
Georgia Tech	31.29 min	47.45 min	21.52 hr	30.26 hr	9.851 min	5.18 min
Arizona State University	30.59 min	46.85 min	21.53 hr	30.30 hr	5.159 min	5.23 min
CalPoly	33.29 min	50.63 min	21	30.25 hr	9.637 min	5.97 min

From the data we can safely say that the CubeSat will make at least one contact of our 5 minutes within 31 hours of its placement in orbit and the contact can be as early as first 31 minutes of its placement in its orbit. The two software ran the cases with the same initial condition and same setup. The discrepancy in the duration from the two software is due to the underlying setup of software and tolerance decided by the coders.

In STK the "Access" analysis tool was used and in FreeFlyer the function Spacecraft.ConactTimes() was used to obtain the required data.

At the beginning of the mission, the net uplink contact time is substantial (around nine furs) and gradually tapers off as the spacecraft deorbits. This trend is expected, given the high downlink slant range and the fact that the orbit processes over time. Although there are intermittent gaps in contact, the uplink schedule is consistent across the entire mission.

For the next objective of finding the total contact duration for Epoch of 12 AM 1 Jun 2020

till deorbit over multiple RAAN values as discussed above, the below results were found.

Table 9.3: Total Duration till deorbit for 12 AM 1 Jun 2020 over multiple RAAN value, in minutes

	Purdue STK	Purdue FF	G Tech STK	G Tech FF	Cal-Poly STK	Cal-Poly FF	AZ State STK	AZ State FF
Minimum	10,280.7	9,143.8	10,641.7	9,687.5	10,559.1	9,942.8	10,604.8	10,211
Average	20,731.1	17,688	21,298.7	18,531	20,950.0	18,276	21,096.0	18,511
Maximum	33,766.8	30,746.8	34,521.9	32,026	34,310.3	31,849	34,270.0	32,577

By the time the spacecraft has deorbited, well over 9,000 minutes of uplink time can be achieved and we can say that the downlink time will also be close to the uplink duration, indicating a high possibility for downlinking enough IMU data and images during the mission.

9.3.1 Tracking Station Overflights with Only Purdue and CalPoly

Another analysis using GMAT is performed with epoch 1 Jan 2020 with various RAAN value. The objective is to find the individual duration of contact and study the feasibility of obtaining contact with ADE throughout deorbit. As discussed in Chapter 3, value of RAAN will affect the orbit timeline. This analysis looks into the effect of RAAN on the duration of contact. The analysis is done with the help of a customized MATLAB code that divide the entire deorbit into three phases. Each phase contains one thirds of the total amount of contacts. Table 9.4 is an example of the result. We consider 0 degree RAAN as nominal in this study because it give us a deorbit duration of around 80 days which is average from study in chapter 3. The table shows the minimum, maximum and mean of duration of contact. The MATLAB program disregard the contact that are smaller than 60 seconds, but from the results, less than 5% of the contacts are under that threshold. As for this case below, the minimum duration is 5 minutes and the average contact duration range from 45 minutes to almost 300 minutes or 5 hours. Thus, we can conclude that there will be enough contact for ADE to maintain contact for command transition and data downlink.

Table 9.4: Individual Duration till deorbit for 12 AM 1 Jan 2020 over 0 RAAN value, in minutes

Ground Station	Phase	Total Number of Contact Duration: GMAT	Min Duration GMAT	Max Duration GMAT	Mean Contact Duration: GMAT
Purdue	1	57	17.95	547.90	290.32
	2	57	6.23	254.24	141.29
	3	58	9.41	104.63	49.80
CalPoly	1	59	7.27	549.16	292.03
	2	59	8.85	263.74	133.73
	3	59	5.08	101.39	45.40

As for the effect of RAAN on contact windows, the conclusion did change. Within the range between 30 and 90 degrees, we see a dip in minimum contact time, as low as only one minutes, however, this should not be a problem as the number of contact are higher, providing more chance to contact ADE. An example is shown in table 9.5. At 90 degree the results has the

most uncertainty, the standard deviation is the highest among all other cases, yet it still has an average duration of 35.66 minutes even at the minimum duration of contact and the number of contact is much larger and provide us more windows of smaller durations.

Table 9.5: Individual Duration till deorbit for 12 AM 1 Jan 2020 over 90 RAAN value, in minutes

Ground Station	Phase	Total Number of Contact Duration: GMAT	Min Duration GMAT	Max Duration GMAT	Mean Contact Duration: GMAT
Purdue	1	249	20.16	529.20	215.77
	2	249	2.05	165.46	56.38
	3	251	1.71	84.13	39.60
CalPoly	1	285	9.19	538.94	202.51
	2	283	1.01	148.82	51.40
	3	284	1.30	85.38	35.66

The MATLAB code for this analysis can be found in Appendix B.

10 Spacecraft Power Modes

The ADE CubeSat will be utilizing up to five different power modes during its mission. These modes include Safe, Normal, IMU, Data Downlink and IMU & Data Downlink. Throughout the mission, ADE will change modes depending on where in the orbit and what operation is needed from the spacecraft is. Power consumption from the burn wires for deploying the antenna and the motors for deploying the drag sail are considered power events, not power modes.

10.1 Safe Mode

Table 10.1: Safe Mode Power Properties

Safe Mode	Amps	Voltage	Watts	Duty Cycle	Average Power (W)
Avionics	0.075	3.670	0.276	1.000	0.276
Receiver	0.035	3.300	0.114	1.000	0.114
Transmitter (Beacon)	1.372	3.300	4.528	0.040	0.181
ICs, Pull-up Resistors	0.014	3.300	0.047	1.000	0.047
Total			4.965		0.619

Safe mode is the power mode with the least amount of power draw. While in Safe Mode, the spacecraft will still transmit a beacon and can receive commands. This mode occurs when the spacecraft is low on batteries and needs to recharge. This is the mode the system will enter into after a system reboot or fault. This mode will only occur during the mission if a problem arises.

10.2 Normal Mode

Table 10.2: Normal Mode Power Properties

Normal Mode	Amps	Voltage	Watts	Duty Cycle	Average Power (W)
Avionics	0.075	3.670	0.276	1.000	0.276
Receiver	0.035	3.300	0.114	1.000	0.114
Transmitter (Beacon)	1.372	3.300	4.528	0.040	0.181
ICs, Pull-up Resistors	0.014	3.300	0.047	1.000	0.047
Radiation Sensor	0.000	3.300	0.000	1.000	0.000
Cameras	0.005	3.300	0.016	0.050	0.001
Total			4.981		0.619

Normal mode will be the most utilized mode during the mission. Normal mode occurs whenever the spacecraft is far from the Earth's surface. In Normal Mode, the spacecraft will transmit a beacon and can receive commands. The Normal Mode also includes a duty cycle for the camera and radiation sensors. For most of the mission, the spacecraft will be too far from the

atmosphere to collect meaningful IMU data. The spacecraft will also be out of range of ground stations to downlink information collected.

10.3 IMU Mode

Table 10.3: IMU Mode Power Properties

IMU Mode	Amps	Voltage	Watts	Duty Cycle	Average Power (W)
Avionics	0.075	3.670	0.276	1.000	0.276
Receiver	0.035	3.300	0.114	1.000	0.114
Transmitter (Beacon)	1.372	3.300	4.528	0.040	0.181
ICs, Pull-up Resistors	0.014	3.300	0.047	1.000	0.047
Radiation Sensor	0.000	3.300	0.000	1.000	0.000
Cameras	0.005	3.300	0.016	0.050	0.001
IMU	0.197	3.300	0.650	1.000	0.650
Total			5.631		1.270

IMU mode is the mode for data collection from the IMU science unit. The IMU will be collecting acceleration and rotation data for the ADE CubeSat. The IMU has a largest power draw of any single component, so it is important the IMU mode only occur when traveling through earth's atmosphere. This ensures that only data that will contribute to determining aerodynamic stability is collected and the spacecraft stays power positive.

10.4 Data Downlink Mode

Table 10.4: Data Downlink Mode Power Properties

Data Downlink Mode	Amps	Voltage	Watts	Duty Cycle	Average Power (W)
Avionics	0.075	3.670	0.276	1.000	0.276
Receiver	0.035	3.300	0.114	1.000	0.114
Transmitter	1.372	3.300	4.528	1.000	4.528
ICs, Pull-up Resistors	0.014	3.300	0.047	1.000	0.047
Radiation Sensor	0.000	3.300	0.000	1.000	0.000
Cameras	0.005	3.300	0.016	0.050	0.001
Total			4.981		4.966

Data Downlink Mode will be used to transmit data to the ground systems. Whenever the spacecraft is in range of a ground station and data transmission is needed, the spacecraft will be in Data Downlink Mode. During this phase of the mission, the spacecraft is using a significant amount of power. The amount of time the spacecraft needs to be in data downlink mode is directly related to how much data the IMU has collected. Early in the mission less IMU data will be

collected per day because the orbit is larger. As the spacecraft begins deorbiting, the time spent in data downlink mode will increase.

10.5 IMU & Data Downlink Mode

Table 10.5: IMU & Data Downlink Mode Power Properties

IMU & Data Downlink Mode	Amps	Voltage	Watts	Duty Cycle	Average Power (W)
Avionics	0.075	3.670	0.276	1.000	0.276
Receiver	0.035	3.300	0.114	1.000	0.114
Transmitter	1.372	3.300	4.528	1.000	4.528
ICs, Pull-up Resistors	0.014	3.300	0.047	1.000	0.047
Radiation Sensor	0.000	3.300	0.000	1.000	0.000
Cameras	0.005	3.300	0.016	0.050	0.001
IMU	0.197	3.300	0.650	1.000	0.650
Total			5.631		5.616

IMU and Data Downlink Mode will be used when the spacecraft is both close enough to the atmosphere to collect meaningful IMU data, and within range of a useable ground station. In this mode, ADE will be using the maximum average power. As the mission goes on, the need for both IMU data collection and Data Downlink at the same time will likely wane.

11 Ground Systems

The Purdue University Space Flight Projects Laboratory Mission Operations Center will be controlling the tracking station antenna at the Kurtz Purdue Technology Center. The MOC will house all the data gathering and storage hardware and the Kurz Purdue Technology center houses the antenna, amplifier, and radio. These two work in conjunction with other tracking stations across the US to provide uplink and downlink capabilities for the ADE satellite.

11.1 Mission Operations Center

The MOC will handle all uplink and downlink with the CubeSat. This includes the display of information such as space craft status checks from beacon data and the spacecraft orbit at any time. The MOC will have the ability to write and send commands from the command dictionary to the data system to be uplinked during the next possible contact with the CubeSat. This capability will be available both manually and autonomously so that no oversight will be needed to send and receive data.

The Joint Space Operations Center will provide two-line element (TLE) data sets to be used by the mission operations software to produce accurate overflight predictions and periapsis time estimations. These data will be downloaded by the MOC and passed into the ground data system for processing and modeling.

11.2 Ground Data System

The ground data system consists of several layers which control the flow of data between the spacecraft and the ground station, which can be seen in Figure 11.1. The system can operate in two modes, the first of which is an autonomous collection of data from the spacecraft. This allows the spacecraft to offload data as often as possible to maximize the possible data downlink. The second method is one in which communication is initiated manually to send commands or to request specific data downlink. This method can be used for selecting which large photos to downlink and diagnosing any errors that might arise during operation.

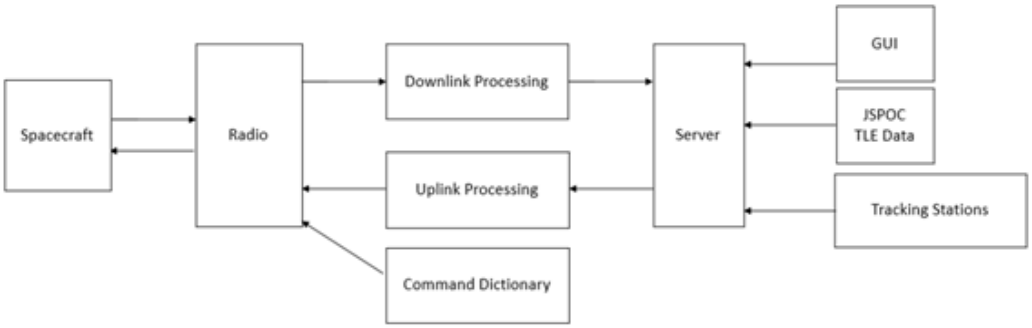

Figure 11.1: Ground Data System Block Diagram

Autonomous operation uses a software developed at Cal Poly to track the satellite and queue data for uplink and downlink. This software will be running in conjunction with in house software to update the overflight and periapsis predictions with modeling from STK including drag and complex orbit perturbations. Most of the mission lifetime will be spent operating in this mode, with little outside intervention. All downlink of beacons, IMU data, and photo thumbnails will be handled in this mode. If unplanned commands are needed or if operators need to interact directly with the spacecraft, the manual method can be used.

To interact directly with the spacecraft, commands from the command dictionary can be sent through the standard software at any time. The commands are added to the queue to be uploaded as soon as possible. This method will be used during nominal operation to request higher resolution versions of several downlinked thumbnails. If the standard software cannot be used, the station can switch to using an alternative tracking software, GPredict, and communications can be processed completely through GNU Radio for uplink and downlink.

11.3 Tracking Stations

The ADE Mission Ground System includes four tracking stations. These stations are located at Purdue University, California Polytechnic State University, Georgia Institute of Technology, and Arizona State University. The locations of these stations are found below in Table 11.1. For the ADE Mission, the tracking stations will be networked and operations will be automated, allowing overflight passes to be routinely supported with minimal operator setup.

Table 11.1: Tracking Station Locations

Tracking Stations	Latitude	Longitude
Arizona State University	33.425	-111.928
California Polytechnic State University	35.305	-120.662
Georgia Institute of Technology	33.776	-84.396
Purdue University	40.424	-86.929

The tracking stations use the TLE data and orbit prediction to align the antennas and to track the ADE spacecraft during passes. The downlinked data will be collected by all of the individual tracking stations and the data will be shared with all other tracking stations in order to be processed and analyzed.

11.3.1 Tracking Station Hardware

Purdue's tracking station will include a 420-440 MHz Quad Yagi Antenna, ASBIG RAS rotor, LNA-70 pre-amplifier, and Ettus N210 Software Defined Radio [24]. The quad Yagi antenna

will be positioned using the rotor. The antenna will receive downlinked telemetry data and will also uplink commands to the ADE spacecraft. The Yagi antennas have a total length of approximately 3.8 m. The antenna can operate at either a right hand or left hand circular polarization. It also has a boom length of 5.5λ, which corresponds to an uplink and downlink frequency of 437.5 MHz. The rotor will be an ASBIG RAS rotator unit. This allows pointing of the antenna to reduce pointing errors, allowing uplink throughout the entire orbit and downlink during a section of the orbit near periapsis.

Figure 11.2: Quad Yagi Antenna at Kurz Purdue Technology Center

The low-power signals will be amplified using a low-noise amplifier coupled with an LNA-70 pre-amp. The LNA-70 is a 70 cm ultra-low noise preamplifier with a 21-dB gain. The tracking software that will be used is Cal Poly's inhouse software, which will be installed at Purdue's Ground station. The tracking software will control the tracking of the ADE spacecraft as well as the pointing of the antenna using, the rotor data.

The software defined radio will be used with GNU Radio. GNU Radio will receive a signal from the antenna. Once a signal has been received, GNU Radio will demodulate and decode the signal. It will then record the raw data and character files. GNU Radio will also modulate and encode a signal to send to the antenna.

Figure 11.3: Ettus N210 Software Defined Radio

12 Systems Analysis

12.1 Systems Overview

ADE consists of multiple systems working together to provide flight qualification for, and to demonstrate the feasibility of, a deployable drag device. In order to meet this objective, requirements, resource allocations, and risk assessments must be constructed and refined to ensure the highest probability of mission success.

12.2 Technical Resource Budgets

Last revision: Spring 2020 – Eduardo L. Toso

Of specific interest to Spinnaker1 are analyses of the Mass Budget, the Power Budget, the Telecommunications Link Budget, the Thermal Model, and the Data Return Analysis. Those will ensure that Spinnaker1 has the necessary resources to complete its mission, and that there is a margin of safety on which the ground operations team can rely on, in case the mission runs across any anomalies.

12.2.1 Mass Budget

The Mass Budget for Spinnaker1 is designed to ensure that the mass of the components does not exceed the given limit. While Spinnaker1 is a 1U CubeSat, the typical standard mass of 1.33 kg is not a hard limit. The updated mass constraint is 2 kg. To meet these constraints, each subsystem has been allocated a specific mass to work with for component design. The current allocations, best estimates, maximum expected values, and contingency/margin values are displayed in Table 12.1.

Table 12.1: Mass Budget for Spinnaker1

Subsystem	Subsystem Allocation (kg)	Component	Current Best Estimate (kg)	Max Expected Value (kg)	Total Subsystem MEV (kg)	Contingency	Margin
Structures/ Mechanisms	0.550	CubeSat Chassis	0.195	0.205	0.732	5%	
		Radiation Shielding	0.502	0.527		5%	
C&DH	0.150	Main Board	0.055	0.058	0.127	5%	
		-Z Board	0.052	0.054		5%	
		Wiring/Harnessing	0.010	0.015		50%	
Power	0.350	Battery (x3)	0.150	0.158	0.325	5%	
		Solar panels	0.160	0.168		5%	
Payload	0.900	Drag sail assembly	0.736	0.773	0.809	5%	
		Payload Interface Board	0.031	0.031		0%	
		Radiation sensor (x8)	0.004	0.004		5%	
		Camera (x3)	0.001	0.001		5%	
Telecom	0.030	Radio Board	0.023	0.024	0.024	5%	
IMU	0.020	IMU	0.011	0.012	0.012	5%	
Total	2.000		1.929	2.028	2.028		-1%

The calculations were completed using the following definitions of contingency and margin:

$$Contingency = \frac{MEV-CBE}{CBE} \text{ (Equation 12.1)}$$

$$Margin = \frac{MPV-MEV}{MEV} \text{ (Equation 12.2)}$$

where, MEV is the Maximum Expected Value, CBE is the Current Best Estimate, and MPV is the Maximum Possible Value. In this case, MPV is the launch mass constraint for the 1U CubeSat, 2 kg. Contingencies are assigned based upon the maturity of the subsystem. The Margin is given in the context of the entire flight system.

12.2.2 Power Budget

Stable and effective performance of the electrical power system (EPS) is crucial to mission success. To model this performance, a Day-In-The-Life (DITL) simulation was created to simulate the minute-by-minute status of the spacecraft. This simulation attempts to recreate the conditions the spacecraft will encounter and the operations it will undergo throughout the mission.

Power generation was estimated using a Monte-Carlo simulation of the spacecraft's solar panel arrangement. The power generation model used a random orientation generator in a 3-2-1 generation sequence to produce the sun pointing vector and relate it to each solar panel. The transparency of the drag sail (0.83) was taken into consideration but was found to have insignificant effect on power generation. Through the Monte-Carlo analysis of our power generation, we validated CalPoly's expected on-orbit power production of 1.5 W from our nominal per-panel production P_0 = 1.9 W.

The Tenergy batteries used have some losses associated with them, and this is included in the DITL simulation. Solar panel degradation is assumed to be minimal during the lifetime of the spacecraft.

The EPS is operated in various power states throughout the mission. These states are defined by the components that are being used/powered on during this time. These states, their power draws, and their descriptions are shown below in Table 12.2.

Table 12.2: EPS Power States and their Properties

Power State	Power Draw (W)	Description
Normal Mode	0.6195	**Normal Operations**. Includes: Avionics, Receiver, Transmitter (Beacon), ICs and Pull-Up Resistors, Radiation Sensors, and Cameras.
Safe Mode	0.6187	**Safe Mode triggered by low power or other concern.** Includes: Avionics, Receiver, Transmitter (Beacon), ICs and Pull-Up Resistors.
IMU Mode	1.2696	**IMU Data Gathering Mode.** Includes: Avionics, Receiver, Transmitter (Beacon), ICs and Pull-Up Resistors, Radiation Sensors, Cameras, and the IMU.
Transmit Mode	4.9660	**Data Transmit Mode.** Includes: Avionics, Receiver, Transmitter, ICs and Pull-Up Resistors, Radiation Sensors, and Cameras.
IMU + Transmit Mode	5.6161	**IMU & Data Transmit Mode.** Includes: Avionics, Receiver, Transmitter, ICs and Pull-Up Resistors, Radiation Sensors, Cameras, and IMU.

Normal and Safe modes are relatively low draws, and the spacecraft can generate more power than those modes consume under most circumstances, the most notable exception being when the spacecraft is in Earth's umbra. IMU mode is more costly, but again the spacecraft can generate more power than this mode consumes when in sunlight. Transmission is by far the biggest draw, and the two modes that use it are of greatest concern when it comes to power consumption.

The IMU is assumed to be active when within a certain time frame around perigee (20 minutes per orbit). Transmission is assumed to occur whenever possible as this data is crucial to mission success and contact times are somewhat limited. The contact stations used are: Cal Poly, Purdue, Arizona State, and Georgia Tech.

The power state of the spacecraft over time is modeled and produced into various power profiles. Three different cases based on deorbit time were simulated: Average, Maximum, and Minimum deorbit time. The properties that influence these cases are outlined in Section 3: Mission Design. A representative power profile of the Average deorbit time case is shown below in Figure 12.1.

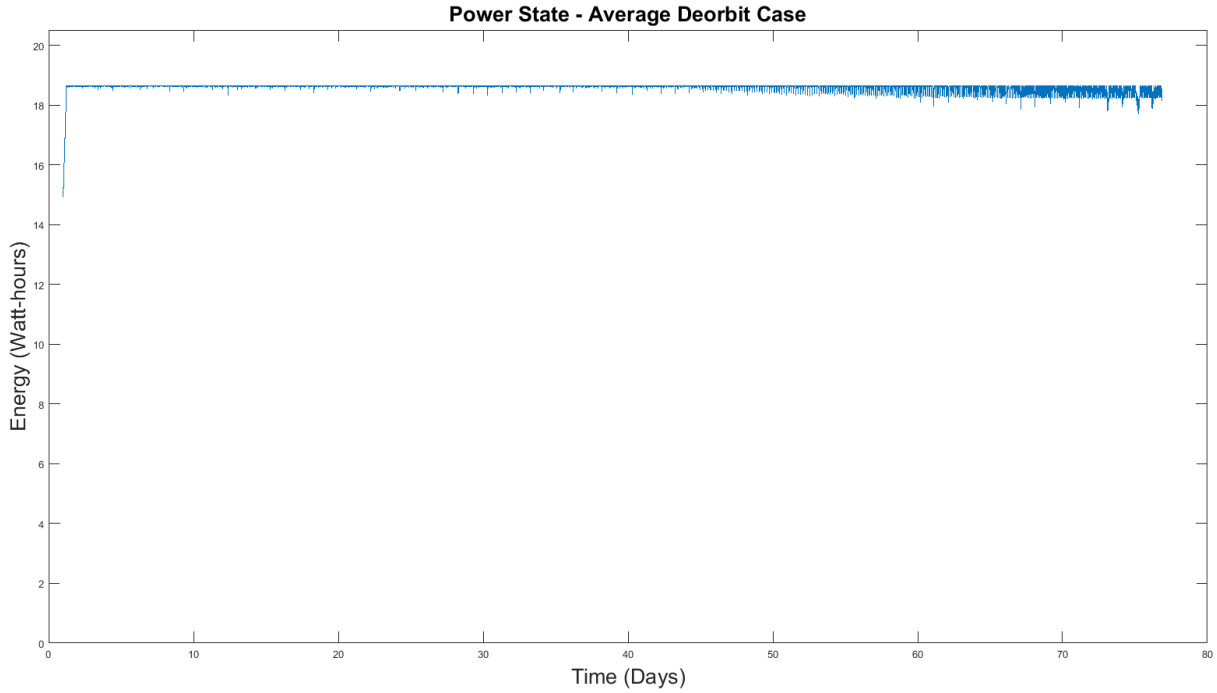

Figure 12.1: Example Power Profile

Several factors influence the behavior of our power state over time. For the majority of the mission, the spacecraft remains power positive. Towards the end of the spacecraft lifetime however, the spacecraft dips lower in power state. This decrease is driven by a few factors that are mainly influenced by the decreasing apogee of the orbit:

- IMU data gathering opportunities increase due to shorter orbit period
- Spacecraft spends more time in Earth's umbra
- Transmission opportunities become more concentrated due to lower flyover altitudes

These factors lead to 1) more data being gathered and transmitted in shorter periods and 2) less power being generated. An example printout of this behavior is shown below in Figure 12.2.

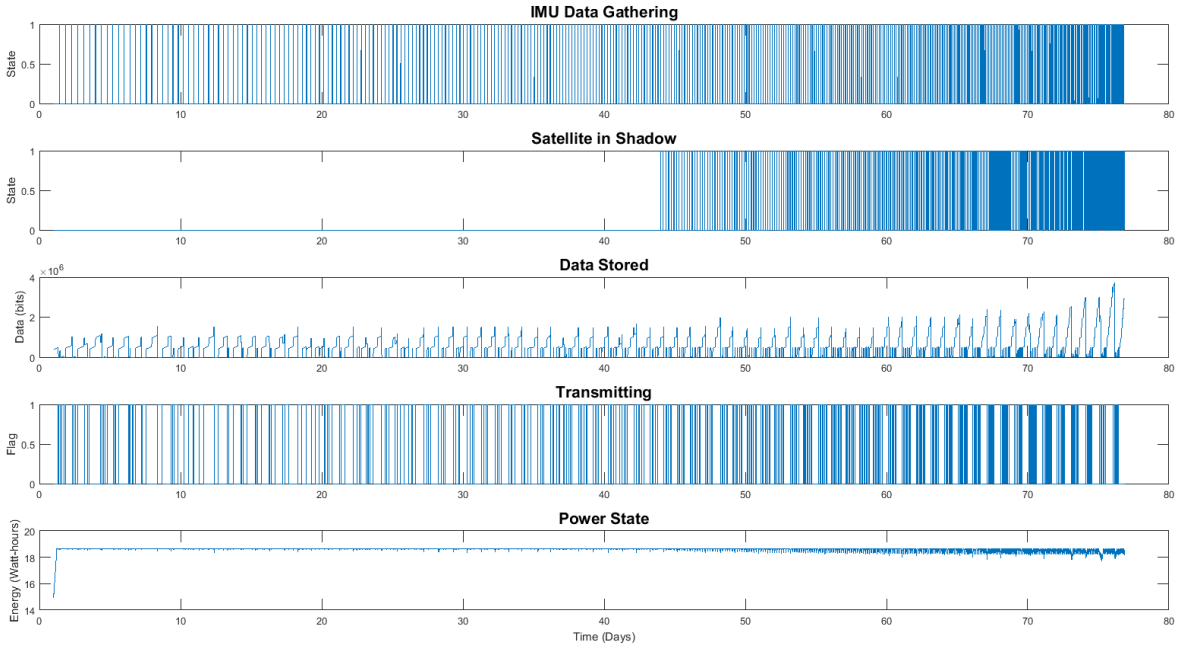

Figure 12.2: Overall EPS Performance - Average Case

Once the spacecraft begins spending significant time in umbra (around day 45 of the mission), power generation opportunities decrease, and data gathering/transmission opportunities increase. Implementation of the safe mode will ensure the longevity of the mission. With the data volumes being worked with, the spacecraft should maintain nominal EPS performance for the duration of the mission.

Future work may determine that descoping some of the EPS components (batteries or solar panels) may be beneficial to the mission. In considering this, failures of these components have been modeled to assess the effect of their loss on the EPS performance. Figure 12.3 below shows this effect on the power profile.

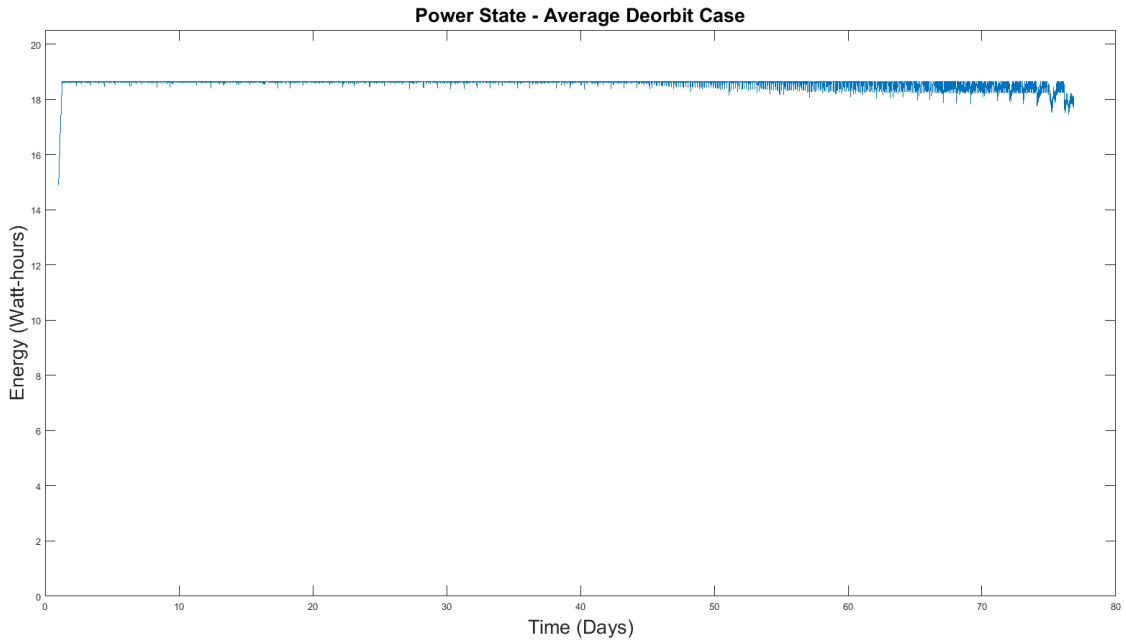

Figure 12.3: Power Profile for One Panel Failure - Average Case

The spacecraft remains power positive towards the end of the mission. This shows that, even if the spacecraft loses one of its solar panels, it will still be able to complete its mission. The same cannot be said if two solar panels are lost. In that case, the spacecraft will eventually lose all power, as shown in Figure 12.4.

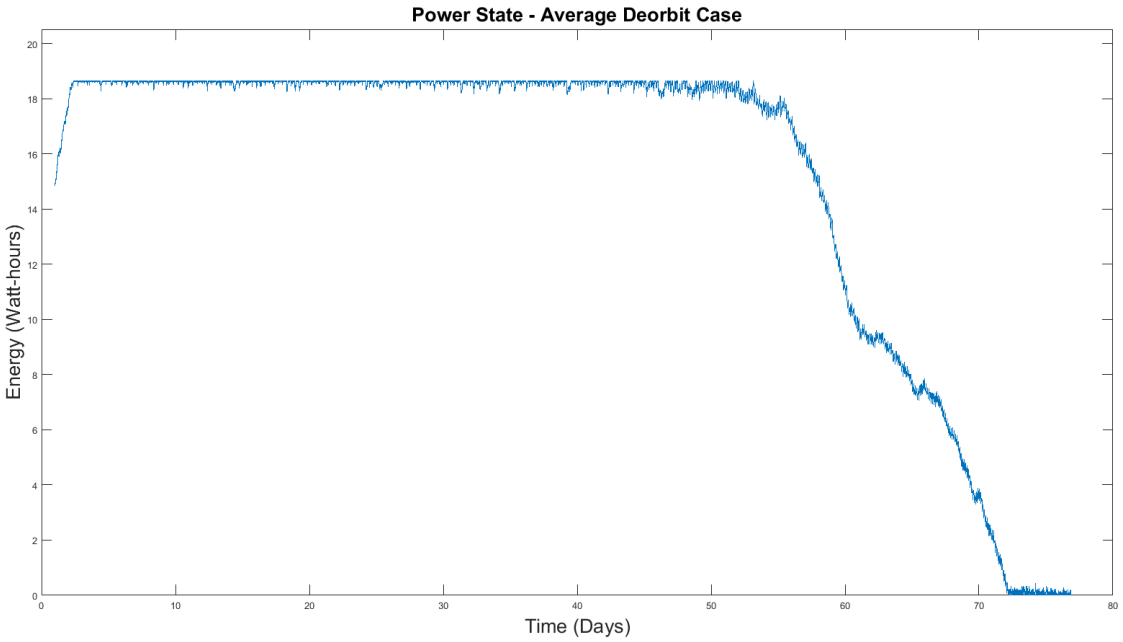

Figure 12.4: Power Profile for Two Panel Failure - Average Case

The spacecraft does seem to be able to operate on one battery under normal conditions (as shown by Figure 12.5). However, reducing the number of batteries from two to one is not recommended due to the desire for redundancy.

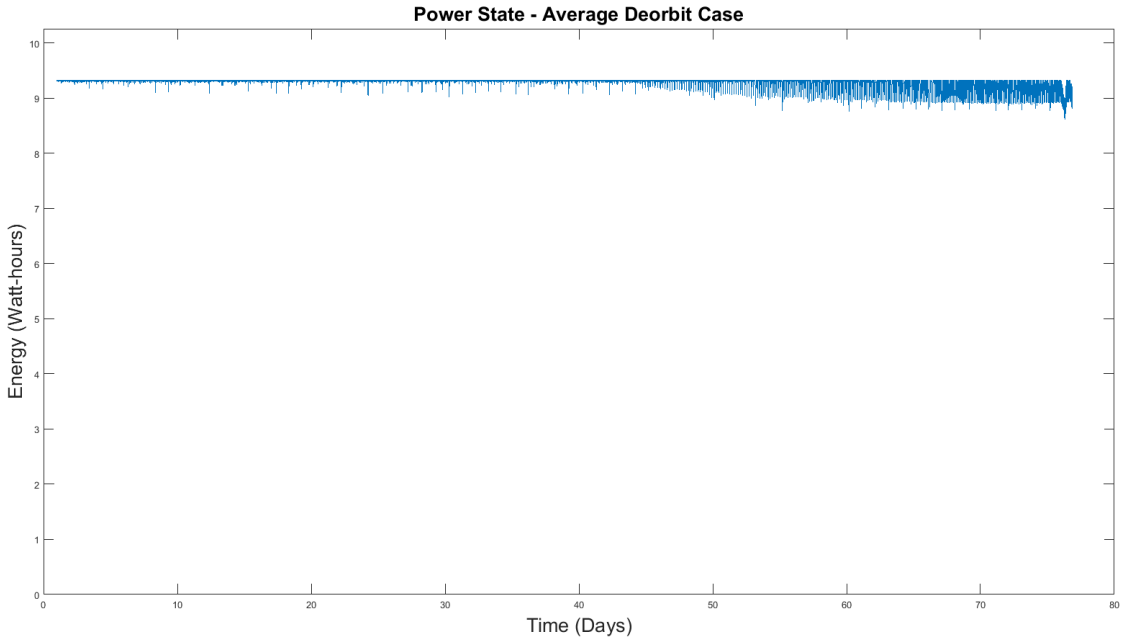

Figure 12.5: Power Profile with one battery - Average Case

12.2.3 Telecommunications Link Budget

To effectively manage communication with the satellite, and successfully plan a data return strategy, the Telecommunications Link Budget for Spinnaker1 needed to be computed. The Link Budget is used to compute the slant range at which a particular ground station can downlink data from the spacecraft, taking into account various limitations in communications, such as: transmitting power limitations, antenna gains, system noise temperature interferences, pointing and polarization losses, modulation losses and path losses.

There are 4 universities whose ground stations are being used for downlinking data from Spinnaker1 - Purdue University, California Polytechnic State University, Georgia Institute of Technology and Arizona State University.

The Telecommunications Link Budget is computed using the *'AMSAT-IARU Link Model Rev2.5.5'* spreadsheet developed by Jan A. King et al.

For Spinnaker1, the fixed parameters for the transmitter system on the CubeSat are tabulated.

Table 12.3: Spacecraft Communication System Parameters

Parameter	Value
Transmitter Power	1 W
Antenna Type	Omnidirectional Dipole
Beam Width	156.2°
Antenna Gain	2.2 dBi
Polarization	Right-Hand Circular Polarization
Modulation Method	Non-Coherent FSK
Operating Frequency	437.5 Mhz
Data Downlink Rate	9600 bps
Data Uplink Rate	1100 bps

For an accurate representation of how the communication strategy with the spacecraft would have to be structured, link budgets have been computed considering the parameters of each of the four ground stations involved in the project.

Additionally, there are parameters in the link budget for which a particular value is hard to define, such as System Noise Temperature (due to difficulty in estimating effects of man-made and solar noise components in UHF) and pointing losses (due to changing attitude of spacecraft). For these factors, the link budget takes conservative estimates – the System Noise value is in the range of 1700-2000 Kelvin, as opposed to the 500 Kelvin range as posited by the Jan King spreadsheet. For pointing losses, models indicate that the loss due to pointing errors remains below 6 dB for a pointing error of up to 75°, as shown in Figure 12.6.

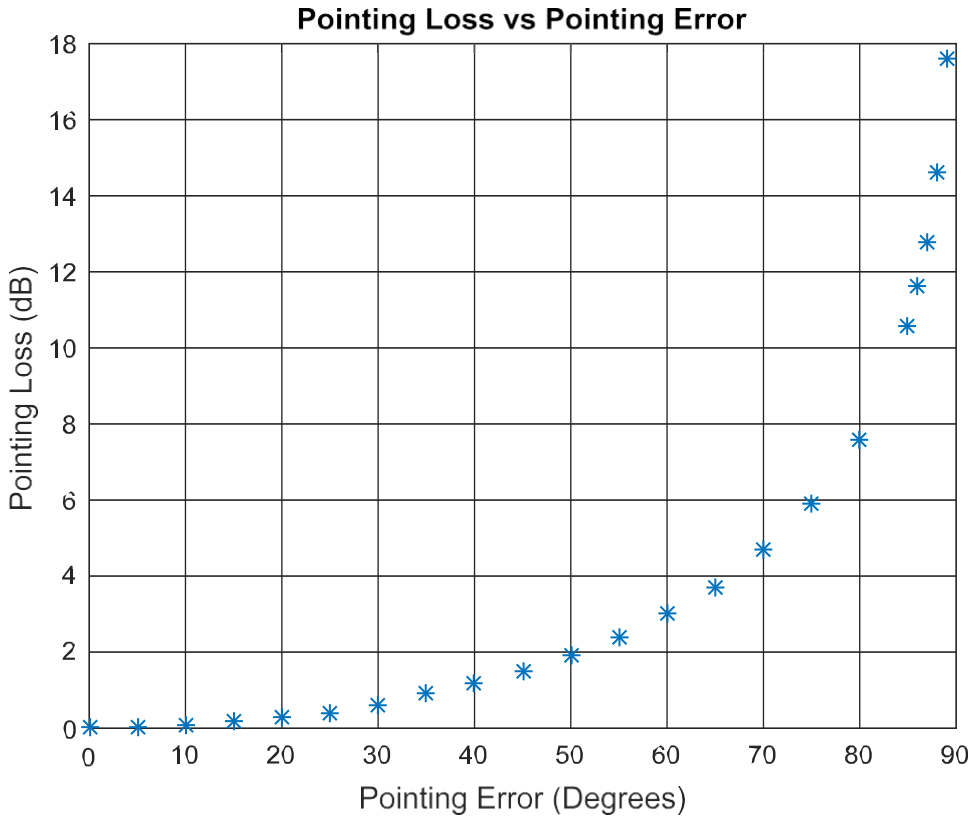

Figure 12.6: Pointing Loss (dB) vs Pointing Error (Degrees)

Purdue Ground Station

The parameters for the Purdue Ground Station are:

Table 12.4: Purdue Ground Station Parameters

Parameter	Value
Downlink Slant Range	24675 km
Antenna Type	Quad-Yagi
Beam Width	10.5°
Antenna Gain	24 dBi
LNA Gain	21 dB
Polarization	Right-Hand Circular Polarization
Modulation Method	Non-Coherent FSK
Operating Frequency	437.5 Mhz
Data Downlink Rate	9600 bps
Data Uplink Rate	1100 bps

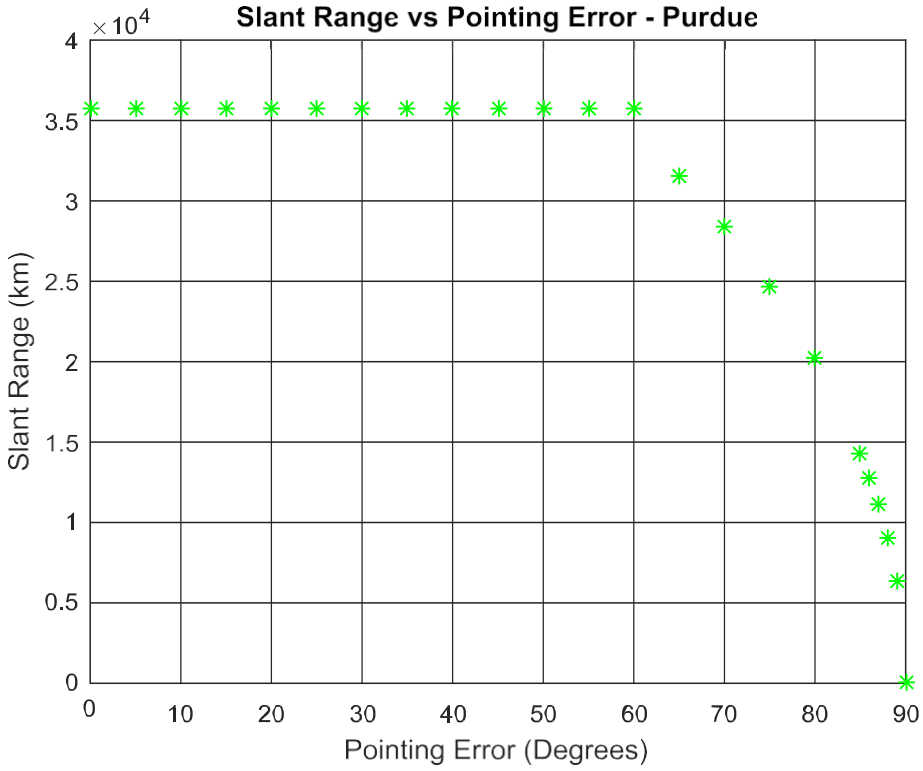

Figure 12.7: Slant Range vs Pointing Error – Purdue

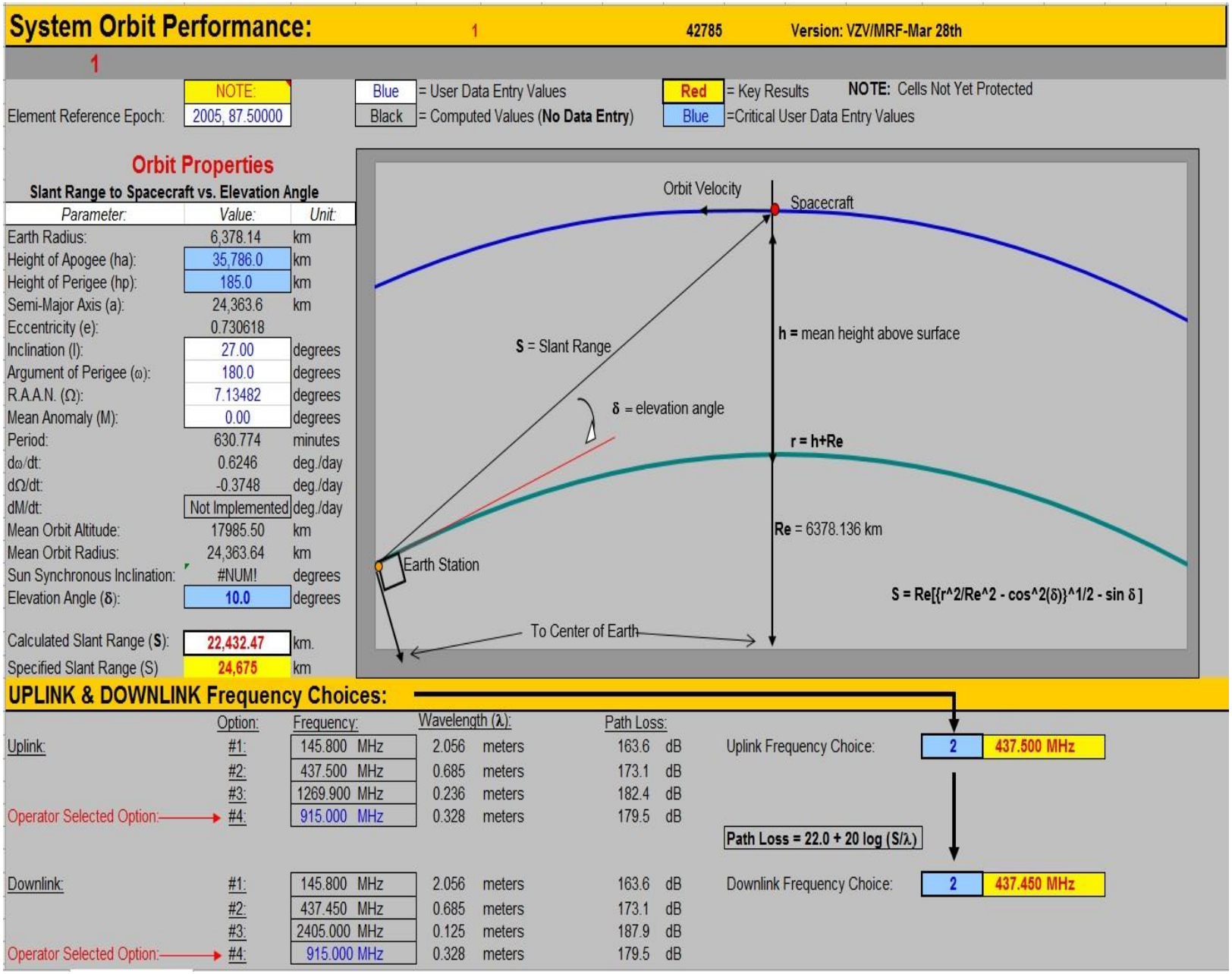

Figure 12.8: Slant Range for Purdue Ground Station

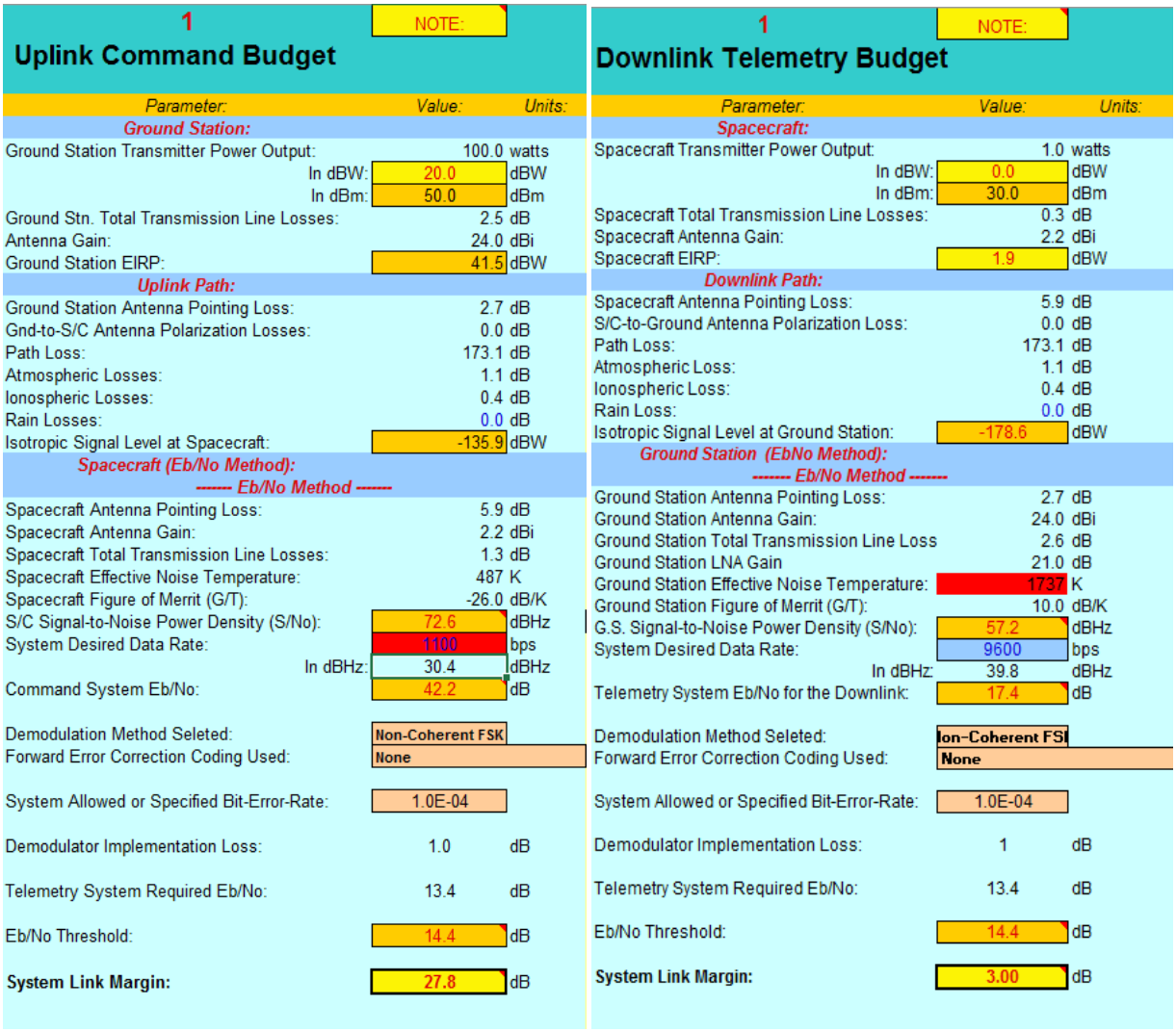

1

NOTE:

Uplink Command Budget

Parameter:	Value:	Units:
Ground Station:		
Ground Station Transmitter Power Output:	100.0	watts
In dBW:	20.0	dBW
In dBm:	50.0	dBm
Ground Stn. Total Transmission Line Losses:	2.5	dB
Antenna Gain:	24.0	dBi
Ground Station EIRP:	41.5	dBW
Uplink Path:		
Ground Station Antenna Pointing Loss:	2.7	dB
Gnd-to-S/C Antenna Polarization Losses:	0.0	dB
Path Loss:	173.1	dB
Atmospheric Losses:	1.1	dB
Ionospheric Losses:	0.4	dB
Rain Losses:	0.0	dB
Isotropic Signal Level at Spacecraft:	-135.9	dBW
Spacecraft (Eb/No Method):		
------- Eb/No Method -------		
Spacecraft Antenna Pointing Loss:	5.9	dB
Spacecraft Antenna Gain:	2.2	dBi
Spacecraft Total Transmission Line Losses:	1.3	dB
Spacecraft Effective Noise Temperature:	487	K
Spacecraft Figure of Merit (G/T):	-26.0	dB/K
S/C Signal-to-Noise Power Density (S/No):	72.6	dBHz
System Desired Data Rate:	1100	bps
In dBHz:	30.4	dBHz
Command System Eb/No:	42.2	dB
Demodulation Method Seleted:	Non-Coherent FSK	
Forward Error Correction Coding Used:	None	
System Allowed or Specified Bit-Error-Rate:	1.0E-04	
Demodulator Implementation Loss:	1.0	dB
Telemetry System Required Eb/No:	13.4	dB
Eb/No Threshold:	14.4	dB
System Link Margin:	27.8	dB

1

NOTE:

Downlink Telemetry Budget

Parameter:	Value:	Units:
Spacecraft:		
Spacecraft Transmitter Power Output:	1.0	watts
In dBW:	0.0	dBW
In dBm:	30.0	dBm
Spacecraft Total Transmission Line Losses:	0.3	dB
Spacecraft Antenna Gain:	2.2	dBi
Spacecraft EIRP:	1.9	dBW
Downlink Path:		
Spacecraft Antenna Pointing Loss:	5.9	dB
S/C-to-Ground Antenna Polarization Loss:	0.0	dB
Path Loss:	173.1	dB
Atmospheric Loss:	1.1	dB
Ionospheric Loss:	0.4	dB
Rain Loss:	0.0	dB
Isotropic Signal Level at Ground Station:	-178.6	dBW
Ground Station (EbNo Method):		
------- Eb/No Method -------		
Ground Station Antenna Pointing Loss:	2.7	dB
Ground Station Antenna Gain:	24.0	dBi
Ground Station Total Transmission Line Loss	2.6	dB
Ground Station LNA Gain	21.0	dB
Ground Station Effective Noise Temperature:	1737	K
Ground Station Figure of Merit (G/T):	10.0	dB/K
G.S. Signal-to-Noise Power Density (S/No):	57.2	dBHz
System Desired Data Rate:	9600	bps
In dBHz:	39.8	dBHz
Telemetry System Eb/No for the Downlink:	17.4	dB
Demodulation Method Seleted:	Non-Coherent FSK	
Forward Error Correction Coding Used:	None	
System Allowed or Specified Bit-Error-Rate:	1.0E-04	
Demodulator Implementation Loss:	1	dB
Telemetry System Required Eb/No:	13.4	dB
Eb/No Threshold:	14.4	dB
System Link Margin:	3.00	dB

Figure 12.9: Uplink and Downlink budgets for Purdue Ground Station at Slant Range

Georgia Tech Ground Station

The parameters for the Georgia Tech ground station are as follows:

Table 12.5: Georgia Tech Ground Station Parameters

Parameter	Value
Downlink Slant Range	26475 km
Antenna Type	Dual-Yagi
Beam Width	21° x 10.5°
Antenna Gain	22 dBi
LNA Gain	24 dB
Polarization	Right-Hand Circular Polarization
Modulation Method	Non-Coherent FSK
Operating Frequency	437.5 Mhz
Data Downlink Rate	9600 bps
Data Uplink Rate	1100 bps

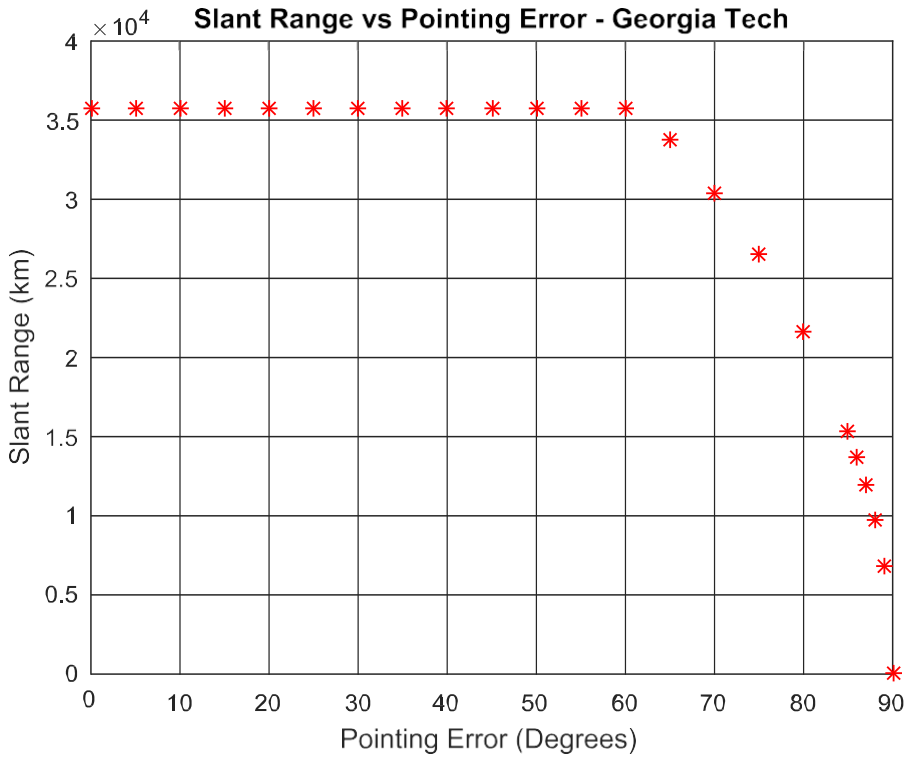

Figure 12.10: Slant Range vs Pointing Error - Georgia Tech

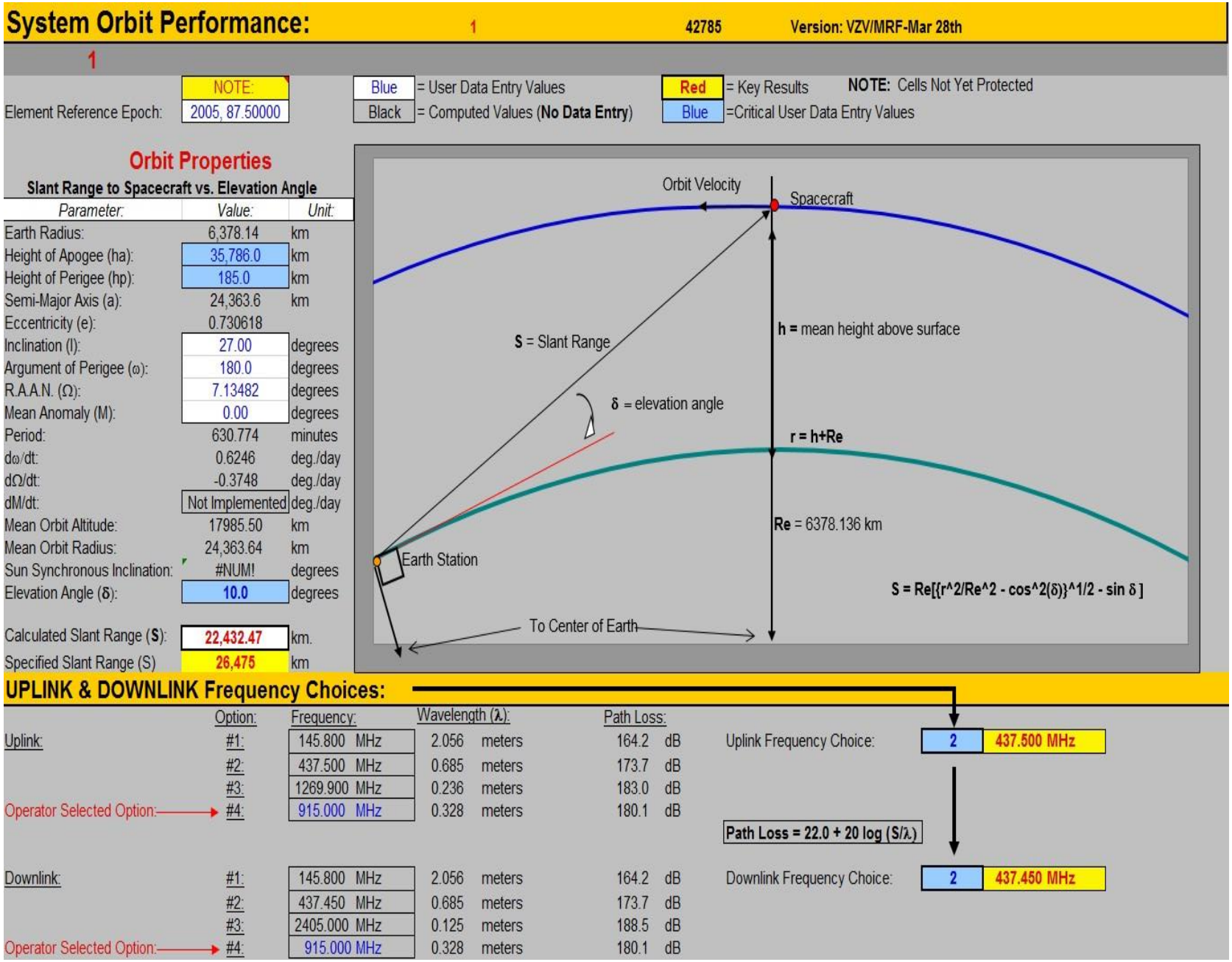

Figure 12.11: Slant Range for Georgia Tech Ground Station

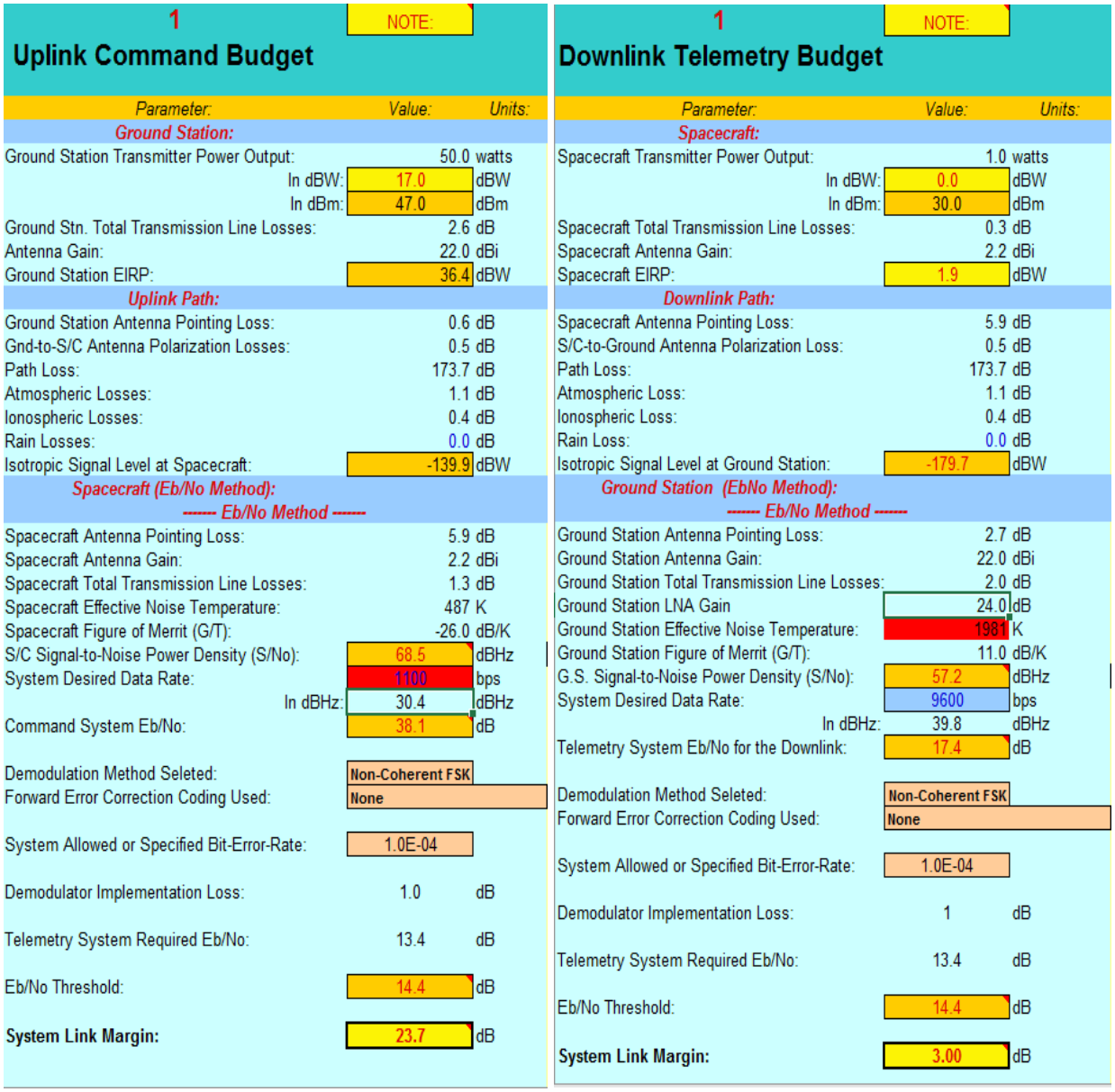

1	NOTE:

Uplink Command Budget

Parameter:	Value:	Units:
Ground Station:		
Ground Station Transmitter Power Output:	50.0	watts
In dBW:	17.0	dBW
In dBm:	47.0	dBm
Ground Stn. Total Transmission Line Losses:	2.6	dB
Antenna Gain:	22.0	dBi
Ground Station EIRP:	36.4	dBW
Uplink Path:		
Ground Station Antenna Pointing Loss:	0.6	dB
Gnd-to-S/C Antenna Polarization Losses:	0.5	dB
Path Loss:	173.7	dB
Atmospheric Losses:	1.1	dB
Ionospheric Losses:	0.4	dB
Rain Losses:	0.0	dB
Isotropic Signal Level at Spacecraft:	-139.9	dBW
Spacecraft (Eb/No Method):		
------- Eb/No Method -------		
Spacecraft Antenna Pointing Loss:	5.9	dB
Spacecraft Antenna Gain:	2.2	dBi
Spacecraft Total Transmission Line Losses:	1.3	dB
Spacecraft Effective Noise Temperature:	487	K
Spacecraft Figure of Merit (G/T):	-26.0	dB/K
S/C Signal-to-Noise Power Density (S/No):	68.5	dBHz
System Desired Data Rate:	1100	bps
In dBHz:	30.4	dBHz
Command System Eb/No:	38.1	dB
Demodulation Method Seleted:	Non-Coherent FSK	
Forward Error Correction Coding Used:	None	
System Allowed or Specified Bit-Error-Rate:	1.0E-04	
Demodulator Implementation Loss:	1.0	dB
Telemetry System Required Eb/No:	13.4	dB
Eb/No Threshold:	14.4	dB
System Link Margin:	23.7	dB

1	NOTE:

Downlink Telemetry Budget

Parameter:	Value:	Units:
Spacecraft:		
Spacecraft Transmitter Power Output:	1.0	watts
In dBW:	0.0	dBW
In dBm:	30.0	dBm
Spacecraft Total Transmission Line Losses:	0.3	dB
Spacecraft Antenna Gain:	2.2	dBi
Spacecraft EIRP:	1.9	dBW
Downlink Path:		
Spacecraft Antenna Pointing Loss:	5.9	dB
S/C-to-Ground Antenna Polarization Loss:	0.5	dB
Path Loss:	173.7	dB
Atmospheric Loss:	1.1	dB
Ionospheric Loss:	0.4	dB
Rain Loss:	0.0	dB
Isotropic Signal Level at Ground Station:	-179.7	dBW
Ground Station (EbNo Method):		
------- Eb/No Method -------		
Ground Station Antenna Pointing Loss:	2.7	dB
Ground Station Antenna Gain:	22.0	dBi
Ground Station Total Transmission Line Losses:	2.0	dB
Ground Station LNA Gain	24.0	dB
Ground Station Effective Noise Temperature:	1981	K
Ground Station Figure of Merit (G/T):	11.0	dB/K
G.S. Signal-to-Noise Power Density (S/No):	57.2	dBHz
System Desired Data Rate:	9600	bps
In dBHz:	39.8	dBHz
Telemetry System Eb/No for the Downlink:	17.4	dB
Demodulation Method Seleted:	Non-Coherent FSK	
Forward Error Correction Coding Used:	None	
System Allowed or Specified Bit-Error-Rate:	1.0E-04	
Demodulator Implementation Loss:	1	dB
Telemetry System Required Eb/No:	13.4	dB
Eb/No Threshold:	14.4	dB
System Link Margin:	3.00	dB

Figure 12.12: Uplink and Downlink Budgets for Georgia Tech Ground Station at Slant Range

Arizona State Ground Station

The parameters for the Arizona State Ground Station are as follows

Table 12.6: ASU Ground Station Parameters

Parameter	Value
Downlink Slant Range	34750 km
Antenna Type	Yagi
Beam Width	21°
Antenna Gain	15.5 dBi
LNA Gain	30 dB
Polarization	Right-Hand Circular Polarization
Modulation Method	Non-Coherent FSK
Operating Frequency	437.5 Mhz
Data Downlink Rate	9600 bps
Data Uplink Rate	1100 bps

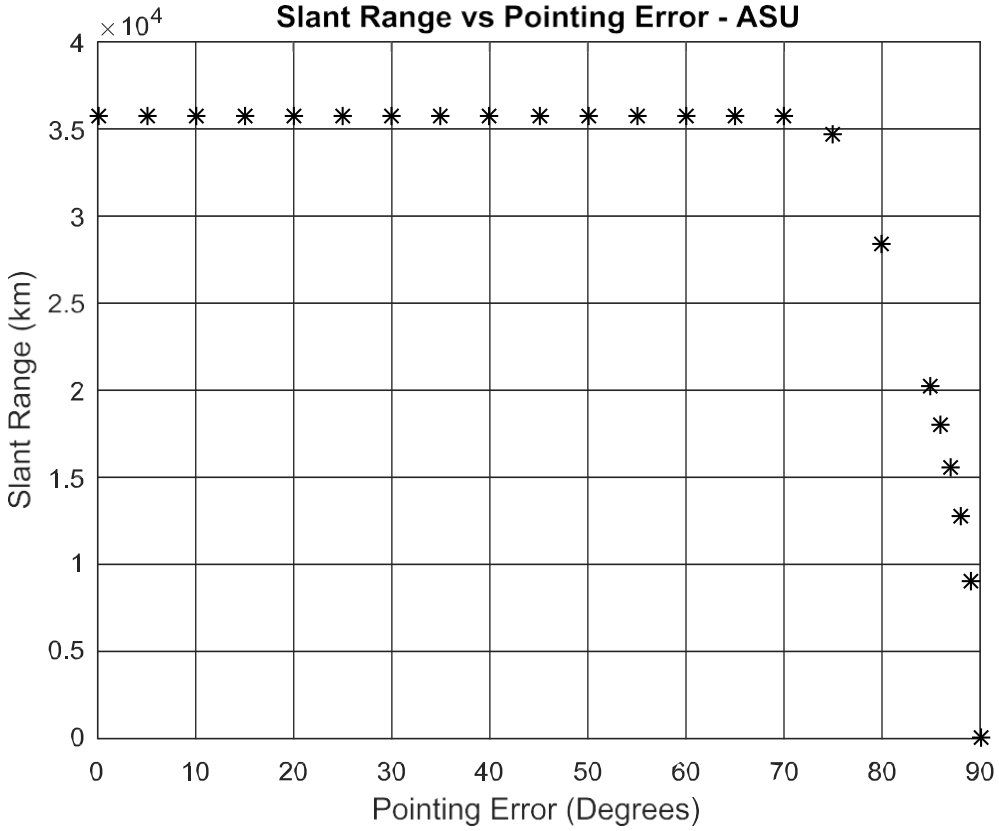

Figure 12.13: Slant Range vs Pointing Error – ASU

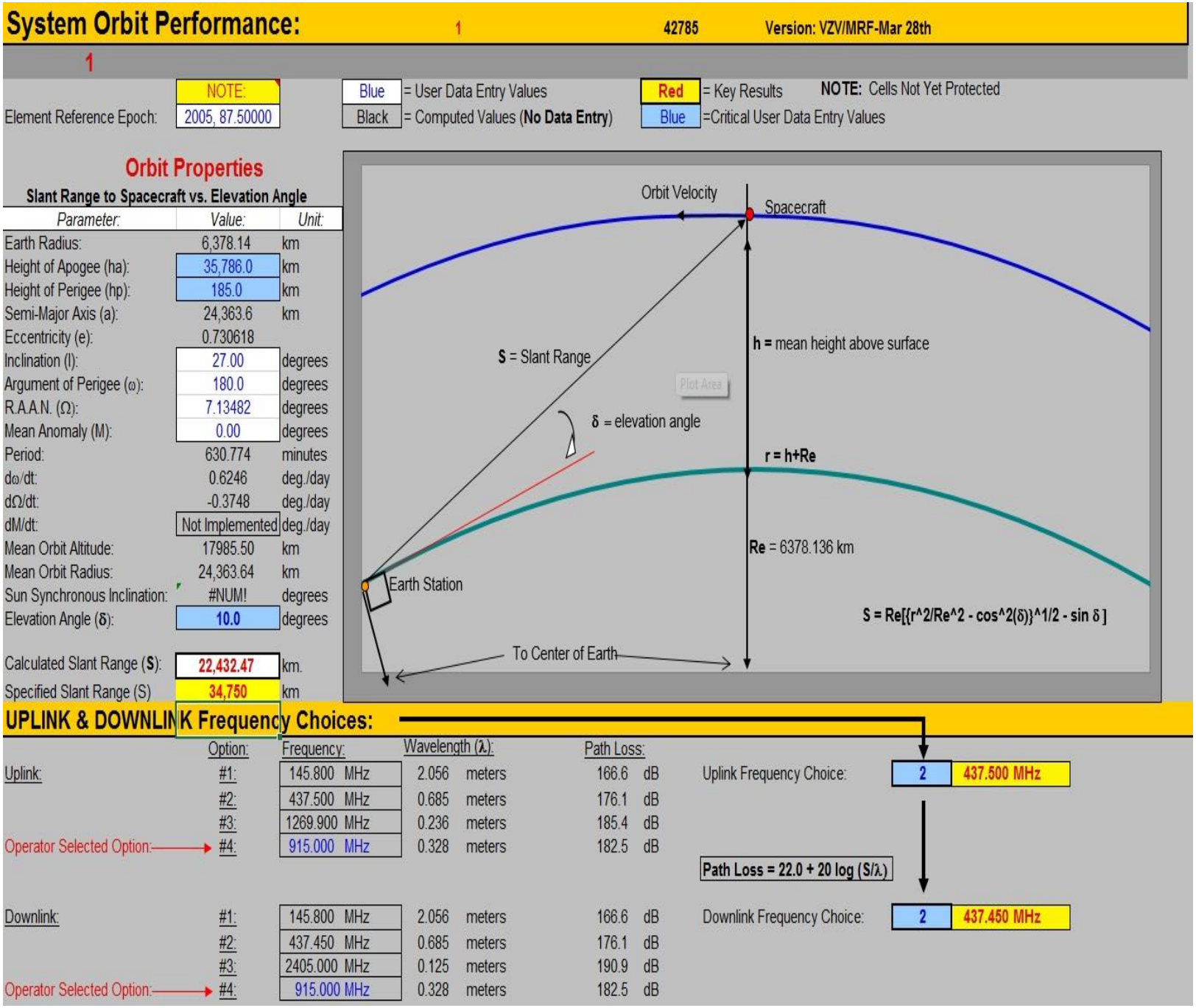

Figure 12.14: Slant Range for ASU Ground Station

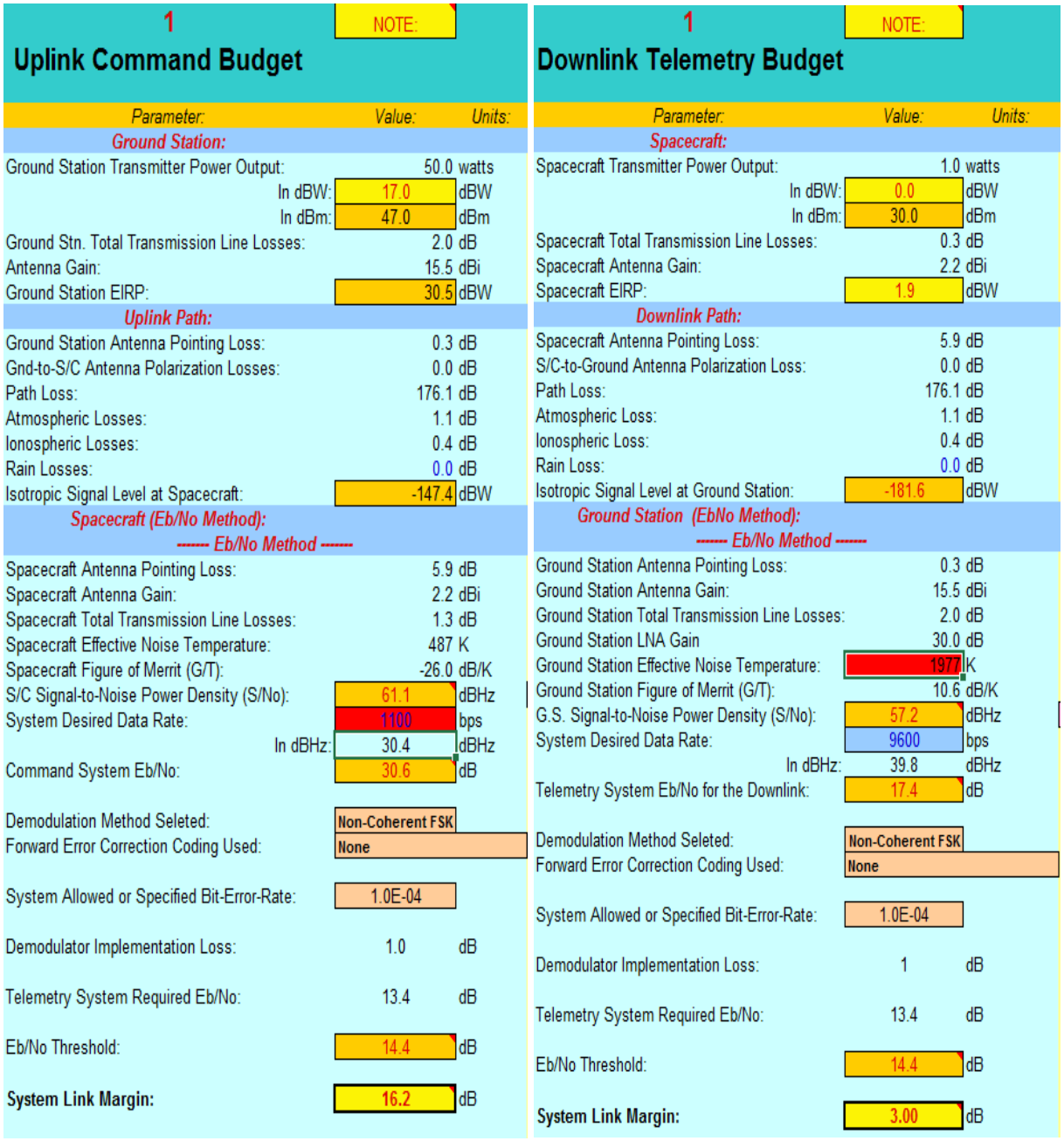

1	NOTE:

Uplink Command Budget

Parameter:	Value:	Units:
Ground Station:		
Ground Station Transmitter Power Output:	50.0	watts
In dBW:	17.0	dBW
In dBm:	47.0	dBm
Ground Stn. Total Transmission Line Losses:	2.0	dB
Antenna Gain:	15.5	dBi
Ground Station EIRP:	30.5	dBW
Uplink Path:		
Ground Station Antenna Pointing Loss:	0.3	dB
Gnd-to-S/C Antenna Polarization Losses:	0.0	dB
Path Loss:	176.1	dB
Atmospheric Losses:	1.1	dB
Ionospheric Losses:	0.4	dB
Rain Losses:	0.0	dB
Isotropic Signal Level at Spacecraft:	-147.4	dBW
Spacecraft (Eb/No Method):		
------- Eb/No Method -------		
Spacecraft Antenna Pointing Loss:	5.9	dB
Spacecraft Antenna Gain:	2.2	dBi
Spacecraft Total Transmission Line Losses:	1.3	dB
Spacecraft Effective Noise Temperature:	487	K
Spacecraft Figure of Merrit (G/T):	-26.0	dB/K
S/C Signal-to-Noise Power Density (S/No):	61.1	dBHz
System Desired Data Rate:	1100	bps
In dBHz:	30.4	dBHz
Command System Eb/No:	30.6	dB
Demodulation Method Seleted:	Non-Coherent FSK	
Forward Error Correction Coding Used:	None	
System Allowed or Specified Bit-Error-Rate:	1.0E-04	
Demodulator Implementation Loss:	1.0	dB
Telemetry System Required Eb/No:	13.4	dB
Eb/No Threshold:	14.4	dB
System Link Margin:	16.2	dB

1	NOTE:

Downlink Telemetry Budget

Parameter:	Value:	Units:
Spacecraft:		
Spacecraft Transmitter Power Output:	1.0	watts
In dBW:	0.0	dBW
In dBm:	30.0	dBm
Spacecraft Total Transmission Line Losses:	0.3	dB
Spacecraft Antenna Gain:	2.2	dBi
Spacecraft EIRP:	1.9	dBW
Downlink Path:		
Spacecraft Antenna Pointing Loss:	5.9	dB
S/C-to-Ground Antenna Polarization Loss:	0.0	dB
Path Loss:	176.1	dB
Atmospheric Loss:	1.1	dB
Ionospheric Loss:	0.4	dB
Rain Loss:	0.0	dB
Isotropic Signal Level at Ground Station:	-181.6	dBW
Ground Station (EbNo Method):		
------- Eb/No Method -------		
Ground Station Antenna Pointing Loss:	0.3	dB
Ground Station Antenna Gain:	15.5	dBi
Ground Station Total Transmission Line Losses:	2.0	dB
Ground Station LNA Gain	30.0	dB
Ground Station Effective Noise Temperature:	1977	K
Ground Station Figure of Merrit (G/T):	10.6	dB/K
G.S. Signal-to-Noise Power Density (S/No):	57.2	dBHz
System Desired Data Rate:	9600	bps
In dBHz:	39.8	dBHz
Telemetry System Eb/No for the Downlink:	17.4	dB
Demodulation Method Seleted:	Non-Coherent FSK	
Forward Error Correction Coding Used:	None	
System Allowed or Specified Bit-Error-Rate:	1.0E-04	
Demodulator Implementation Loss:	1	dB
Telemetry System Required Eb/No:	13.4	dB
Eb/No Threshold:	14.4	dB
System Link Margin:	3.00	dB

Figure 12.15: Uplink and Downlink Budgets for ASU Ground Station at Slant Range

CalPoly Ground Station

The parameters for the CalPoly Ground Station are as follows.

Table 12.7: CalPoly Ground Station Parameters

Parameter	Value
Downlink Slant Range	12350 km
Antenna Type	Quad-Yagi
Beam Width	10.5°
Antenna Gain	24 dBi
LNA Gain	15 dB
Polarization	Right-Hand Circular Polarization
Modulation Method	Non-Coherent FSK
Operating Frequency	437.5 Mhz
Data Downlink Rate	9600 bps
Data Uplink Rate	1100 bps

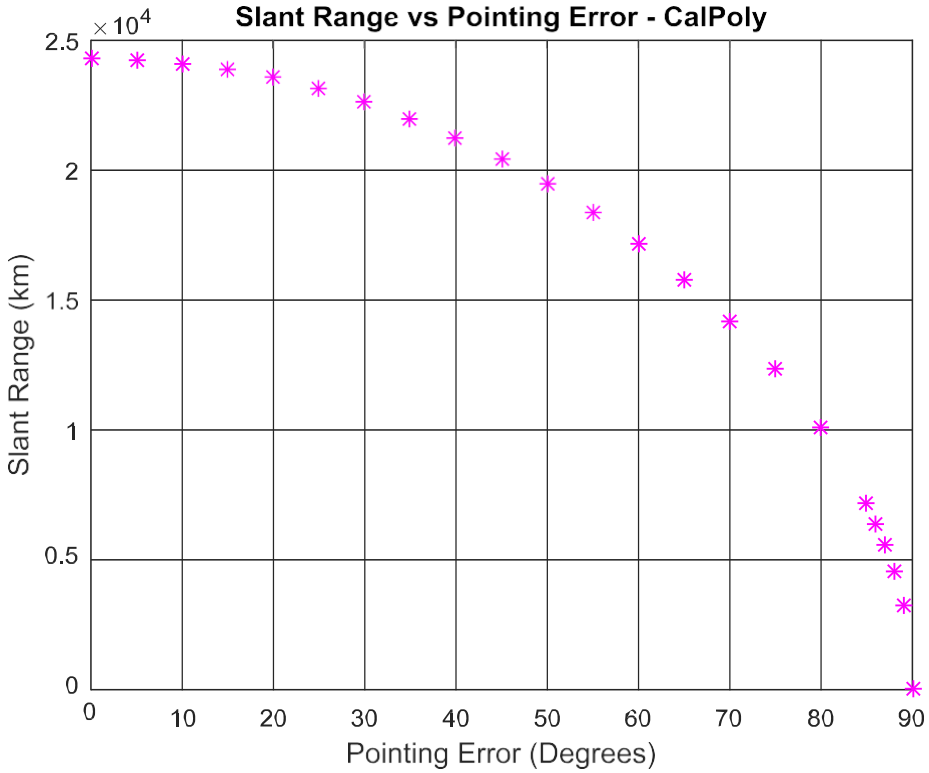

Figure 12.16: Slant Range vs Pointing Error – Calpoly

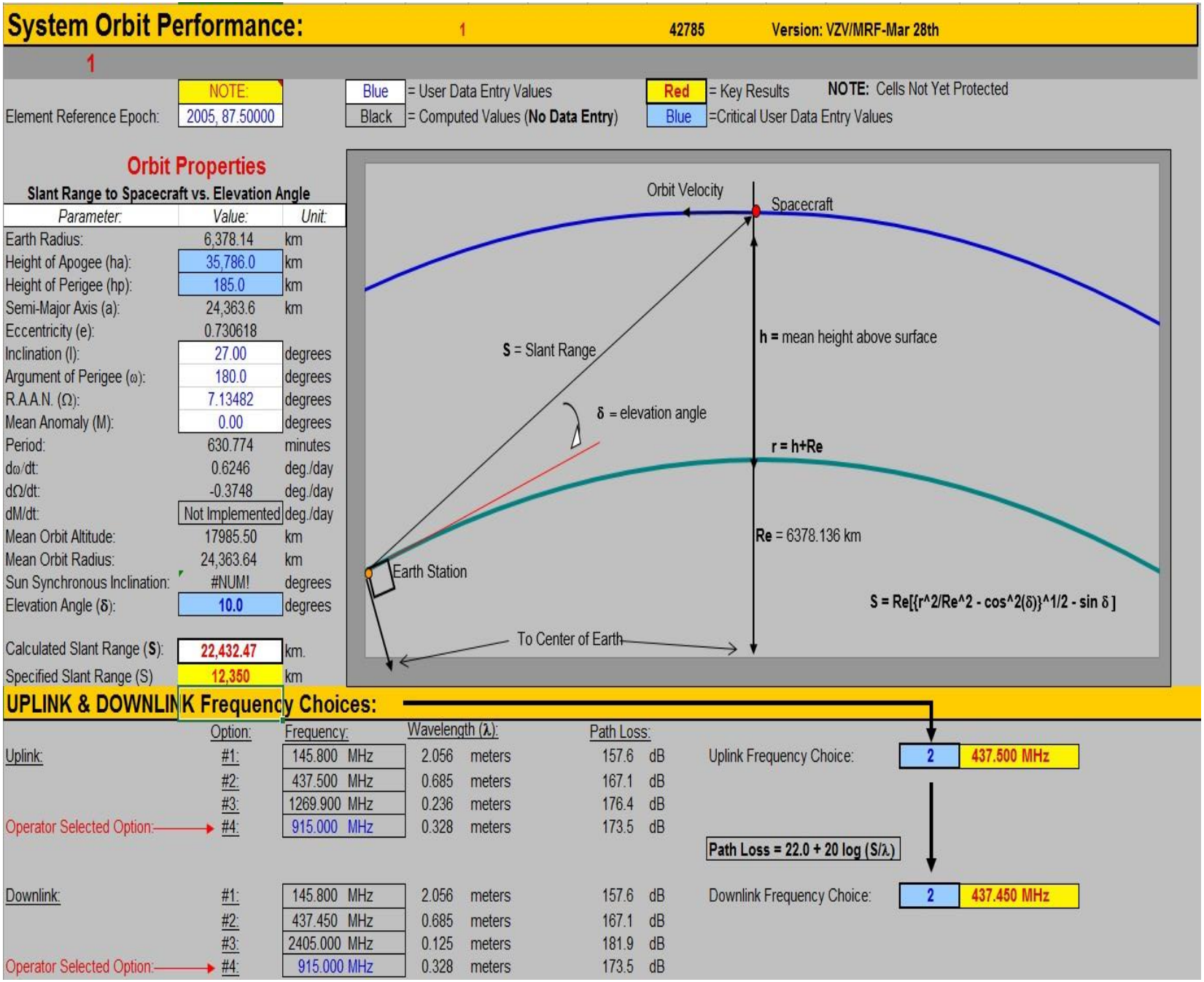

Figure 12.17: Slant Range for CalPoly Ground Station

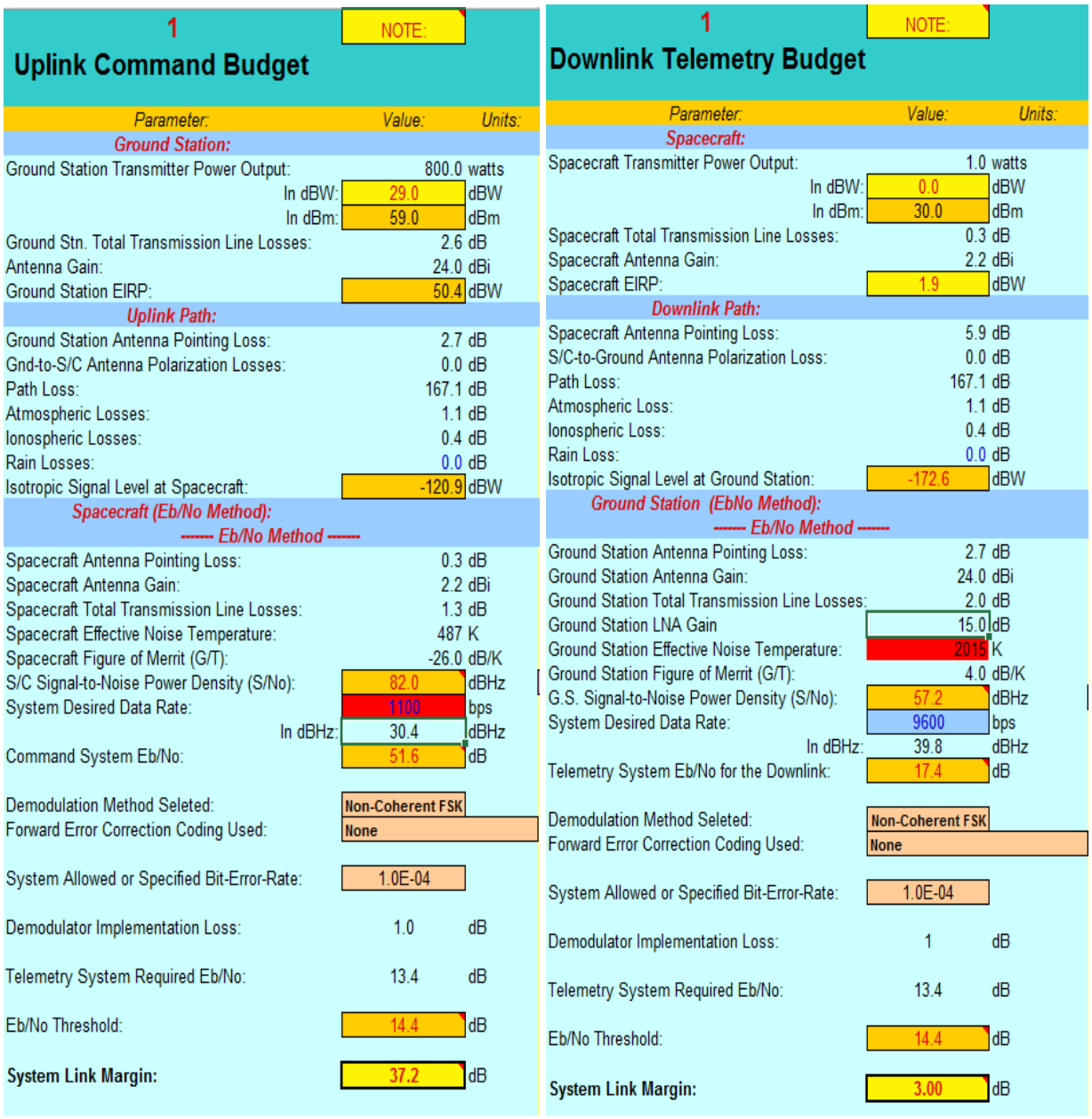

1

NOTE:

Uplink Command Budget

Parameter:	Value:	Units:
Ground Station:		
Ground Station Transmitter Power Output:	800.0	watts
In dBW:	29.0	dBW
In dBm:	59.0	dBm
Ground Stn. Total Transmission Line Losses:	2.6	dB
Antenna Gain:	24.0	dBi
Ground Station EIRP:	50.4	dBW
Uplink Path:		
Ground Station Antenna Pointing Loss:	2.7	dB
Gnd-to-S/C Antenna Polarization Losses:	0.0	dB
Path Loss:	167.1	dB
Atmospheric Losses:	1.1	dB
Ionospheric Losses:	0.4	dB
Rain Losses:	0.0	dB
Isotropic Signal Level at Spacecraft:	-120.9	dBW
Spacecraft (Eb/No Method):		
------- Eb/No Method -------		
Spacecraft Antenna Pointing Loss:	0.3	dB
Spacecraft Antenna Gain:	2.2	dBi
Spacecraft Total Transmission Line Losses:	1.3	dB
Spacecraft Effective Noise Temperature:	487	K
Spacecraft Figure of Merit (G/T):	-26.0	dB/K
S/C Signal-to-Noise Power Density (S/No):	82.0	dBHz
System Desired Data Rate:	1100	bps
In dBHz:	30.4	dBHz
Command System Eb/No:	51.6	dB
Demodulation Method Seleted:	Non-Coherent FSK	
Forward Error Correction Coding Used:	None	
System Allowed or Specified Bit-Error-Rate:	1.0E-04	
Demodulator Implementation Loss:	1.0	dB
Telemetry System Required Eb/No:	13.4	dB
Eb/No Threshold:	14.4	dB
System Link Margin:	37.2	dB

1

NOTE:

Downlink Telemetry Budget

Parameter:	Value:	Units:
Spacecraft:		
Spacecraft Transmitter Power Output:	1.0	watts
In dBW:	0.0	dBW
In dBm:	30.0	dBm
Spacecraft Total Transmission Line Losses:	0.3	dB
Spacecraft Antenna Gain:	2.2	dBi
Spacecraft EIRP:	1.9	dBW
Downlink Path:		
Spacecraft Antenna Pointing Loss:	5.9	dB
S/C-to-Ground Antenna Polarization Loss:	0.0	dB
Path Loss:	167.1	dB
Atmospheric Loss:	1.1	dB
Ionospheric Loss:	0.4	dB
Rain Loss:	0.0	dB
Isotropic Signal Level at Ground Station:	-172.6	dBW
Ground Station (EbNo Method):		
------- Eb/No Method -------		
Ground Station Antenna Pointing Loss:	2.7	dB
Ground Station Antenna Gain:	24.0	dBi
Ground Station Total Transmission Line Losses:	2.0	dB
Ground Station LNA Gain	15.0	dB
Ground Station Effective Noise Temperature:	2015	K
Ground Station Figure of Merit (G/T):	4.0	dB/K
G.S. Signal-to-Noise Power Density (S/No):	57.2	dBHz
System Desired Data Rate:	9600	bps
In dBHz:	39.8	dBHz
Telemetry System Eb/No for the Downlink:	17.4	dB
Demodulation Method Seleted:	Non-Coherent FSK	
Forward Error Correction Coding Used:	None	
System Allowed or Specified Bit-Error-Rate:	1.0E-04	
Demodulator Implementation Loss:	1	dB
Telemetry System Required Eb/No:	13.4	dB
Eb/No Threshold:	14.4	dB
System Link Margin:	3.00	dB

Figure 12.18: Uplink and Downlink Budgets for CalPoly Ground Station at Slant Range

Summary

Taking conservative estimates for System Noise Temperature and Pointing Losses, the slant ranges for the 4 tracking stations are as follows:

Table 12.8: Summary of Slant Ranges for Ground Stations

Parameter	Value
Purdue Slant Range	24675 km
Georgia Tech Slant Range	26475 km
ASU Slant Range	34750 km
CalPoly Slant Range	12350 km

The reason for the abnormally low projected slant range for CalPoly and abnormally high projected slant range for ASU is because of the gain of their LNA – the Low Noise Amplifier, used as a pre-amplifier, at their ground stations. While CalPoly has a relatively low gain LNA (15 dB), ASU has a high gain (30 dB), compared to Purdue (21 dB) and Georgia Tech (24 dB).

These slant ranges are critical for estimating tracking station overflight data, which in turn is essential to computing a viable data downlink/return strategy.

12.2.4 Thermal Model

Four main techniques were conducted to predict the thermal behavior of the spacecraft. The first analysis consisted of a single-node, thermal-equilibrium calculation with MATLAB. The spacecraft temperature was approximated for both worst hot & cold cases and then compared to the results obtained in the Spring of 2017. For the cold case, the spacecraft was assumed to be completely enveloped in the umbra of the earth, in safe mode (thus generating the least amount of electric heat) and encountering no aerothermal heating. The hot case assumed full solar irradiance, maximum aerothermal heating, and that the spacecraft was in transmit mode, generating the most internal electric heat. The maximum aerothermal heating was calculated using an aerothermal flux GUI in MATLAB and resulted in a value of 90ºC – which agreed with the previous estimate. The results for the hoy and cold cases single node analysis are provided in the table below, along with the values from Spring 2017.

Table 12.9: Single Node Analysis – Worst Case Temperature Predictions

	Hot Case (185 km) [°C]	Cold Case (35,786 km)
Spring 2017 Estimate	57.52	-139.12
Fall 2017 Estimate	131.38	-135.76

These values are extremes on both ends of the temperature spectrum and, based on the values presented in Table 5.9: Spinnaker1 Component Temperature Limits, would result in many components failing. The caveat to this analysis method is that it assumes thermal equilibrium whereas the actual spacecraft temperature will likely be highly transient in nature. For instance, consider the hot case scenario where the spacecraft is exposed to the maximum aerothermal heating. This analysis assumes that the spacecraft is exposed to this heating until equilibrium is reached, though the spacecraft will only be exposed to aerothermal heating for at most, 20 minutes. In contrast, the spacecraft may be in complete shadow for a few hours. For that reason, a more accurate hot case temperature should be much closer to the Spring 2017's estimate of 60 °C.

Moving forward, Thermal Desktop was used in an attempt to obtain the transient thermal data for the spacecraft. Thermal Desktop is a highly robust thermal analysis program that allows the user to input orbit parameters in conjunction with a 3D CAD model. The table below shows the additional constants that were required for the Thermal Desktop model.

Table 12.10: Thermal Analysis Variable Definition & Values

Variable	Value	Description
α	0.7	Spacecraft Frame Absorptivity
ϵ	0.9	Spacecraft Frame Emissivity
$\mathbf{A}_{\text{Frontal}}$	0.0141 m^2	Spacecraft Frontal Area
I_s	1444 W	Incident Solar Radiation Flux
$I_{s,Al}$	433.2 W	Incident Earth Albedo Flux
T_{space}	4K	Average Temperature of Local Space
T_{Earth}	290K	Average Temperature of Earth's Surface
Q_{Int}	0.6187 W – 5.6161 W	Upper & Lower Internal Heat Production
σ	5.67E-8	Stefan-Boltzmann Constant

The figure below shows an image of the thermal desktop 3D model with the top face removed. The spacecraft body was approximated as a thin-shelled cube with the appropriate panel thicknesses and material properties (thermal & optical) applied. Additionally, the on-board electronics (UHF Antenna, Flight Board, IMU and Batteries) were implemented in the model. The red arrows indicate contact connections, which enable heat conduction between the components. The actual CAD model was not imported into Thermal Desktop as it was far too intricate and complex for the team's skill level and may have led to erroneous results. To account for this, ANSYS Icepak and SolidWorks were used to estimate the temperature of the internal components, these components were also added into the Thermal Desktop model for redundancy. The respective power generation history for each component was applied for the hot and cold cases in Thermal Desktop, but the temperature profiles over the course of the orbit were unavailable due to limited software permissions at the time.

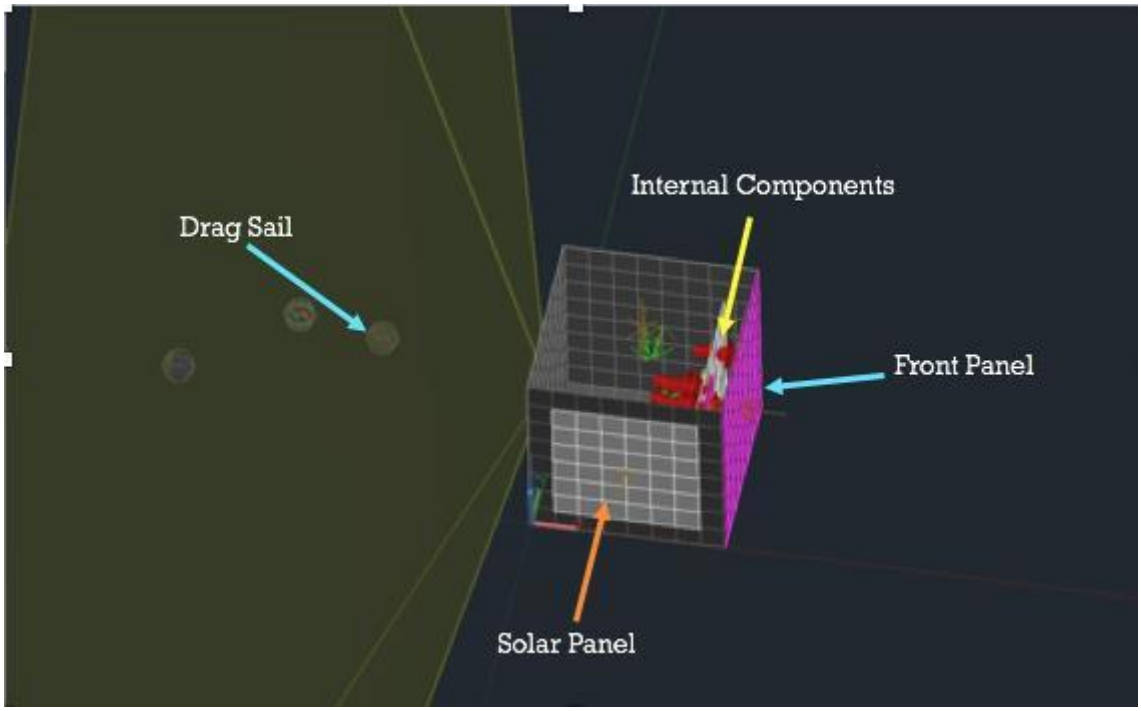

Figure 12.19: Thermal Desktop Model Schematic

The solar panels were approximated with thin-shelled rectangles and a material stack with the appropriate thermal and optical properties of each solar cell layer. The thermal properties of each layer are shown in the table below.

Photovoltaic layer properties.

Layer	Thickness t, (m)	Thermal conductivity k, (W/m·K)	Density ρ, (kg/m^3)	Specific heat Capacity c, (J/kg·°C)
1. Glass	0.003 [11]	1.8 [4]	3000 [5]	500 [5]
2. ARC	100×10^{-9} [13]	32 [14]	2400 [14]	691 [14]
3. PV Cells	225×10^{-6} [11]	148 [12]	2330 [5]	677 [5]
4. EVA	500×10^{-6} [9,12]	0.35 [12]	960 [17]	2090 [17]
5. Rear contact	10×10^{-6} [15]	237 [16]	2700 [16]	900 [16]
6. Tedlar	0.0001 [12]	0.2 [12]	1200 [5]	1250 [5]

Table 12.11: Photocell Layer Material Properties

Figure 12.20 shows the Spinnaker1 orbit input into Thermal Desktop. Under the assumption that the drag sail trims the spacecraft into maximum drag attitude, the front face of the spacecraft is always aligned with the red arrows in the image. Furthermore, the shadow of the earth is projected in the magenta cylinder. This helps to visualize how long the spacecraft will be enveloped in the umbra.

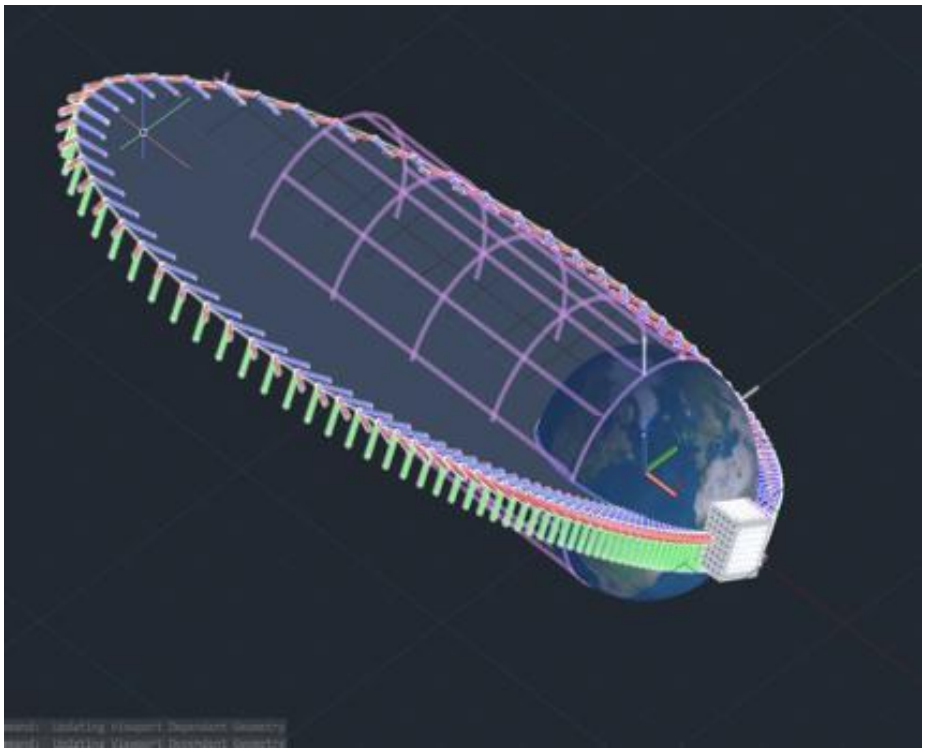

Figure 12.20: Thermal Desktop Orbit

Figure 12.21 below shows an alternate depiction of the Thermal Desktop orbit with the drag sail deployed. As one can see, the spacecraft is oriented such that the front face receives the most drag and thus the most aerothermal heating. This would present the worst case-scenario for heating as most of the flight hardware lies behind the front panel.

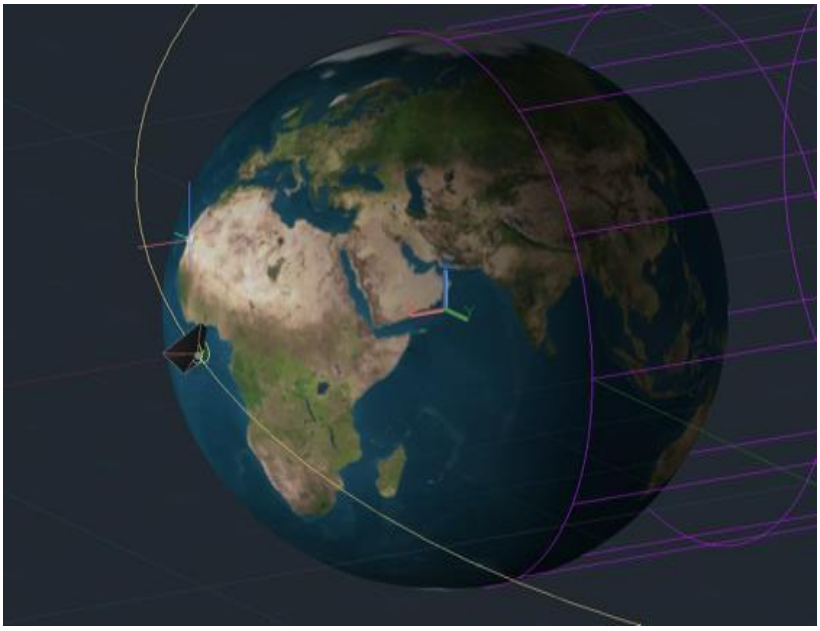

Figure 12.21: Thermal Desktop Orbit with Drag Sail Deployed

Next, the aerothermal flux data for the orbit was inputted into Thermal Desktop based on the output of the MATLAB Aerothermal Flux GUI. Figure 12.22 shows a plot of the aerothermal flux on the front face (the other faces were negligible). A graduate student working on another CubeSat project ran their thermal heating code using Spinnaker1 parameters and predicted about 100W/m² of heat flux at an altitude of 170 km. This agrees with the plot below, which also shows that, above an altitude of 200 km, aerothermal heating does not contribute significantly to heating the spacecraft.

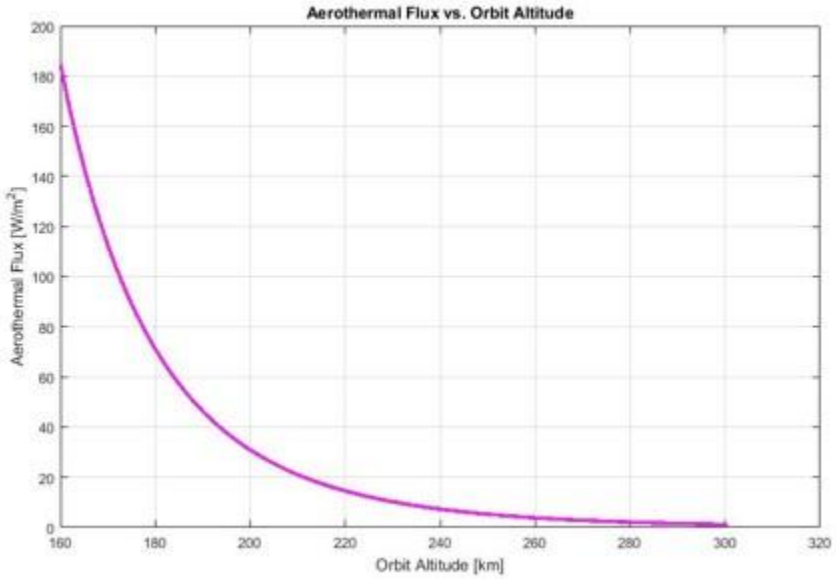

Figure 12.22: Aerothermal Flux vs Orbit Altitude

With the 3D model & orbital parameters in Thermal Desktop, a transient thermal analysis was run, generating a history of absorbed flux values for each face. These values were later inputted into ANSYS and SolidWorks to predict the component temperatures. This was done because of the numerous technical difficulties with Thermal Desktop that prevented transient temperature data from being generated.

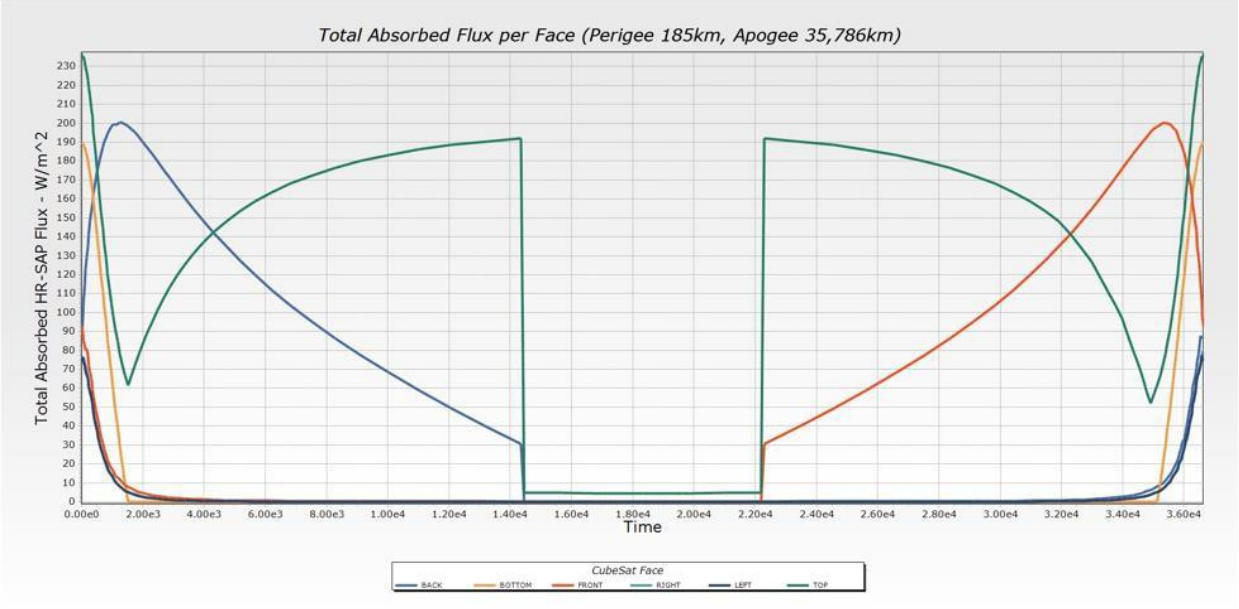

Figure 12.23: Total Absorbed Flux per Face during Orbit

From Figure 12.23 above, one can see that the maximum absorbed fluxes occur at the left and right ends of the plot. These locations correspond to the beginning and end of one orbit, at an altitude of 185 km. At this altitude, the spacecraft will be receiving the most heat (considering the contributions of the Sun, the Earth's albedo, and the aerothermal heating). In contrast, one can see a massive and instantaneous decline in total absorbed flux on all faces for approximately 2 hours in the middle of the plot. This drop is due to the spacecraft moving into the umbra of the Earth. At this location, the spacecraft will not be receiving any solar radiation. Note that this plot does not account for the internal heat generation, as it was included in the ANSYS and SolidWorks internal models. These flux values were merely used as boundary conditions in the other software.

Because worst case scenarios are the only ones of interest, the maximum and minimum absorbed fluxes from Figure 12.23 were inputted into both ANSYS and SolidWorks. Icepak is not conducive to complex geometries. Due to the limited number of mesh refinement options, it was very difficult to create a quality mesh for the actual CAD model. For this reason, the heat loads were applied to a highly-simplified model with similar dimensions. What Icepak does provide is the ability to define separate geometries in different ways. All the electronic components were defined as sources, while the bulk payload body was defined as a block. The "source" definition provided the option to assign the internal heat productions to the respective components. Average power values for each component were taken from Table 10.1 and Table 10.4 for the cold and hot cases respectively. Figure 12.24 and Figure 12.25 below show the cold & hot case temperature contour.

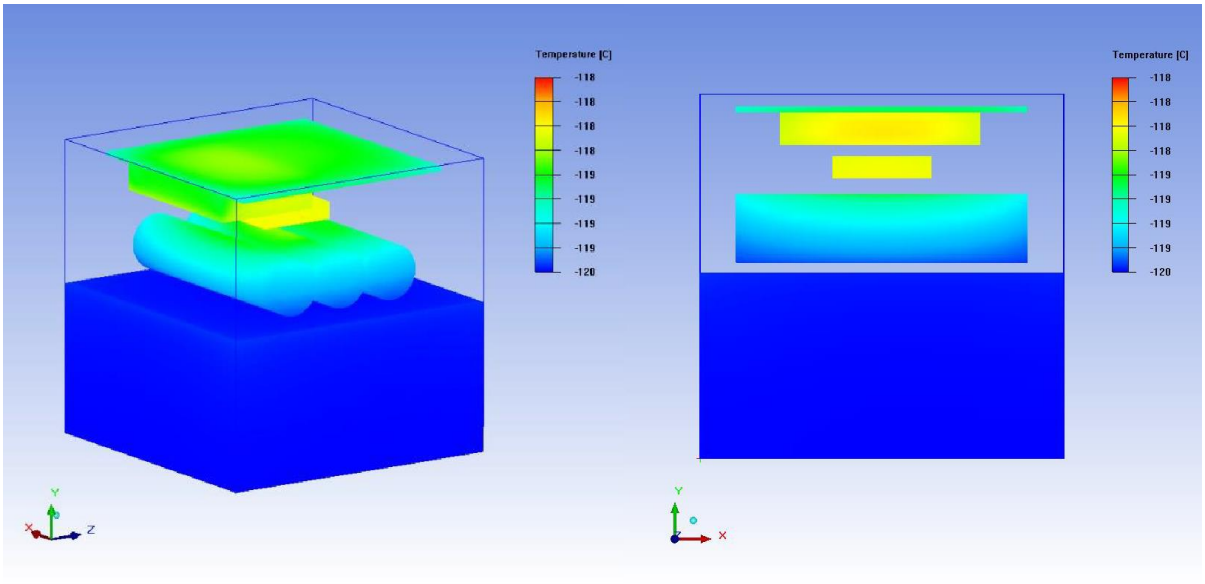

Figure 12.24: Cold Case Temperature Map – ANSYS Icepak Initial Analysis

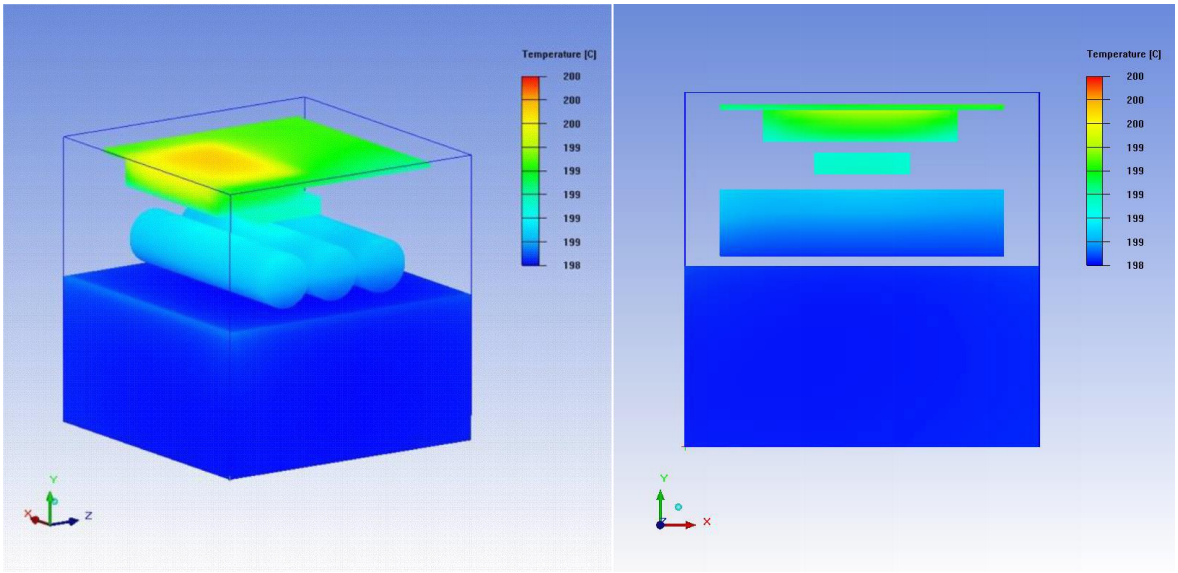

Figure 12.25: Hot Case Temperature Map – ANSYS Icepak Initial Analysis

The minimum and maximum temperatures for each component for the hot and cold case are summarized in the table below. The temperature range across the spacecraft is very minimal. For the cold case, the results were about 10 degrees warmer than the single node analysis. The hot case result, however, was about 70 degrees hotter than the single node analysis at 185 km (the case in Thermal Desktop), and about 30 degrees cooler than the single node case at 165 km. The results of the Ansys analysis are summarized in Table 12.12.

Table 12.12: Initial Component Temperature Estimates for ANSYS Icepak

Component	Cold Case Min [°C]	Cold Case Max [°C]	Hot Case Min [°C]	Hot Case Max [°C]
Flight Computer	-119.0	-118.0	209.3	210.5
UHF Board	-118.7	-118.0	209.3	210.5
IMU	-118.2	-118.2	209.4	209.4
Batteries	-119.5	-118.5	209.0	209.3
Payload	-119.6	-119.5	209.0	209.1
Global	-119.6	-117.8	209.0	210.5

Table 12.13 below shows the temperature predictions from Spring 2017. The temperature predictions are clearly very different. The exact cause is still unknown, but the team is hopeful that transient temperature results will produce more reasonable results eventually.

Table 12.13: Previous Semester Component Temperature Estimates

Component	Cold Case [°C]	Hot Case [°C]
Flight Computer	19.3	34.1
UHF Board	19.3	34.1
IMU	20.6	41.1
Batteries	26.5	47.0
Payload	8.4	38.1
Global	-22.2	42.3

If a more reliable model is produced in the future, and the values are still out of the operating ranges of the components, there are not too many options left available. If only one case is the issue, one adjustment that could be made is changing the properties of the aluminum surface. The absorptivity and emissivity of the aluminum could be altered by changing the level of polishing or adding a coating of some sort (weight permitting). A lot of work was done this semester to explore other ways of producing transient temperature results, but none of them yielded enough success to be worth documenting. SolidWorks Simulation and Icepak were eventually used to run transient solutions, but both yielded unrealistic results. Icepak showed an increase in 100 degrees Kelvin over the course of 6 hours, which corresponds to about 5.5 degrees over 20 minutes. This may seem more plausible given the 15 to 30-degree temperature swings predicted in Spring 2017

Ideally, Thermal Desktop will be used to obtain transient heat flux and temperature values. Two more analyses will then be run with a software such as ANSYS Icepak or Workbench. One to corroborate the transient temperature values given by Thermal Desktop using the heat fluxes as boundary conditions, and the other to predict the temperature of the internal components, using the face temperatures as boundary conditions, and including the heat produced by the components themselves. The steady state and transient thermal tiles in ANSYS Workbench may be used to help refine the results in the future. If the boundary conditions can be applied accurately, ANSYS

Workbench provides much more mesh refinement options. A fine and quality mesh could very well make all the difference in getting reasonable transient temperature results.

12.2.5 Data Return Analysis

Data production and transmission were simulated as part of the Day in the Life (DITL) simulation begun by the Electrical Power System (EPS) team. The main issues facing the Spinnaker1 spacecraft included a low downlink rate together with high losses from poor orientations, the need to retransmit data, and extra data fillers in the encoding packaging. Because of these hurdles, the Data Return Analysis focused on identifying cadences for each subsystem which would achieve FMSC and maximize data return during the Science Phase of the mission. The downlink process for the subsystems is summarized in Figure 12.26**,** which identifies the cadences, data draw rates, and compression strategies for the Spinnaker1 mission.

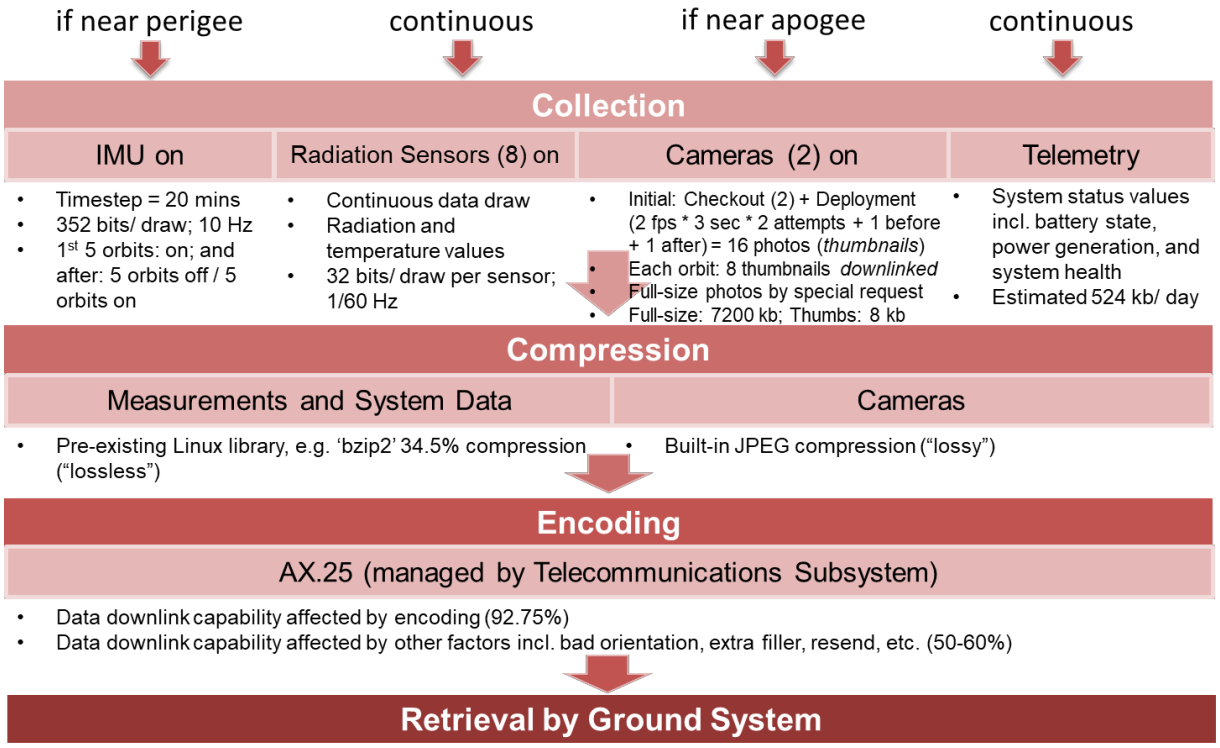

Figure 12.26. Data Return Analysis Summary, Considering 'Short' Slant Range Case.

Analysis of the data transmission using the DITL ran through the 'Average' orbit case created in STK and used both conservatively short and optimistically long estimated slant ranges, which greatly affect the contact times with the ground stations. The simulation also accounts for Normal, IMU, and Transmit modes, but conditions are integrated for the transition into Safe Mode. Safe Mode is especially important as the long slant range estimates would enable very long downlink durations, draining the batteries. Spinnaker1 has a downlink rate of 9600 bps, which defines the transmission capabilities during each of these contacts with the ground. The Data

115

Return Analysis included measurements from the IMU, full-size photos and thumbnails, and continuously recorded flight system status data—telemetry—as well as radiation sensor data. The result is a graph given in Figure 12.27 reflecting the total data produced over the course of the mission compared to the total data downlink.

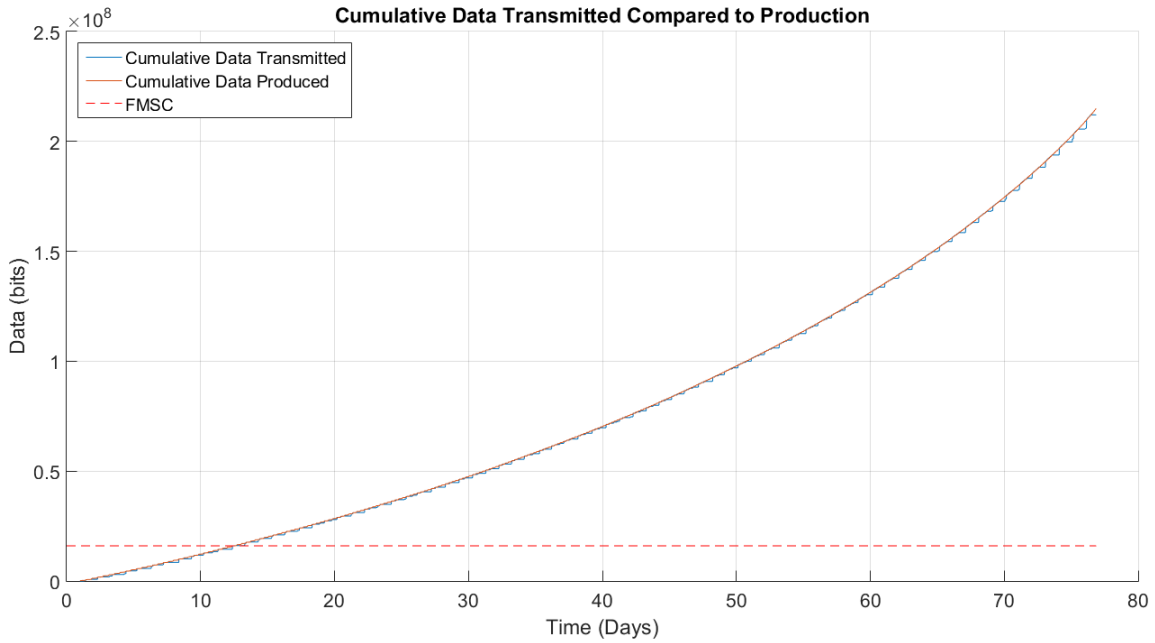

Figure 12.27. Comparison of Cumulative Data Produced to Cumulative Transmission

The most important design decisions in closing the downlink budget included the incorporation of compression and identification of subsystem cadences. Compression tools are easily implemented in a Linux system and are a standard practice for spacecraft. Spinnaker1 will utilize the 'bzip2' compression tool, which gives an average compression ratio of 34.5%. The actual compression ratio will of course vary with each data package, depending on the variability of actual data within the package, but this average provides useful insight for pre-mission analysis.

Multiple cadence options were considered. Those could change the amount of IMU and radiation data drawn, or the number of full-size photos and thumbnails. However, CalPoly's slant range calculations were later determined to be too conservative. This meant that the contact durations were longer than what was initially expected, and that obtaining enough downlink was no longer a problem. Where the more conservative slant ranges had limited Spinnaker1 to downlinking only eight thumbnails and zero full-size photos once every two weeks, the new estimates allow at least one full-size photo every orbit, without approaching the transmission limit. However, full-size photos will only be taken when requested, in an effort to maintain a more conservative return strategy. Radiation measurements, being a very small percentage of the total data production, will be collected continuously throughout the mission. A summary of subsystem data production is given in Figure 12.28.

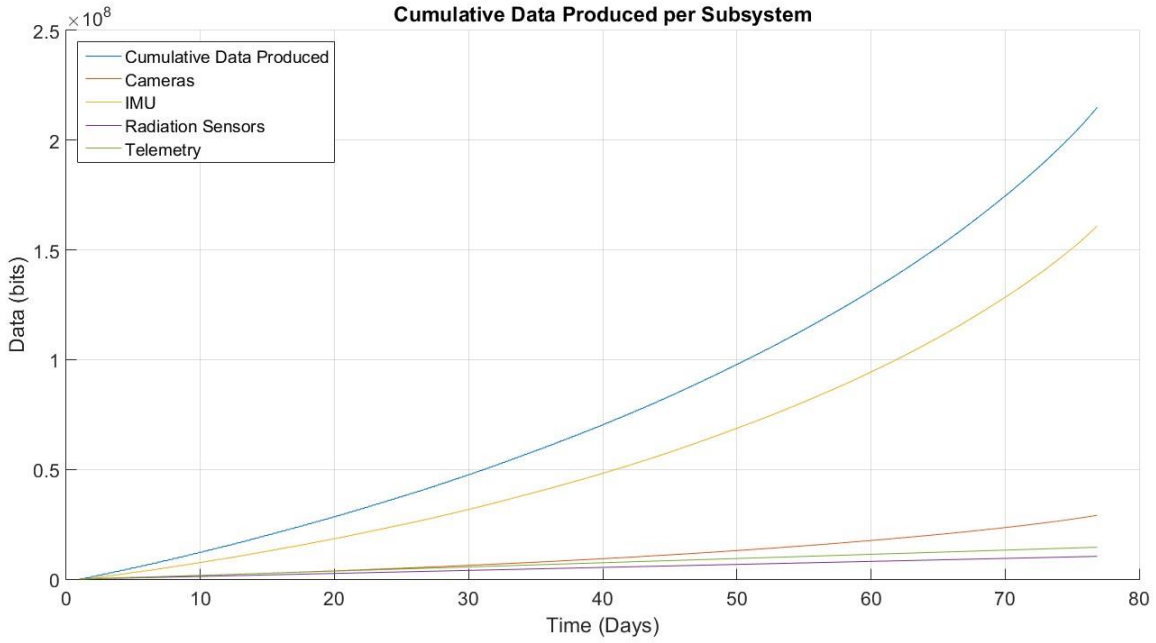

Figure 12.28. Data Production by Spinnaker1 Subsystems over time.

The total production must lie within the system's storage capabilities of 32 GB, or 2.56 x 10^{11} bits. Whether the data downlinked is immediately deleted, as represented in Figure 12.29, or kept onboard, the storage capacity is more than sufficient. The final consideration is the timeframe in which the FMSC will be met. As outlined in Section 5.6.3, the FMSC data totals 28.39 Mb, or 12.39 Mb after processing/compression, taking the JPEG compression factor to be around 70%. The timeframe to complete the FMSC data return is primarily dependent on the time for the spacecraft to complete 5 orbits (3.14 days), though shorter slant ranges may have restricted FMSC return.

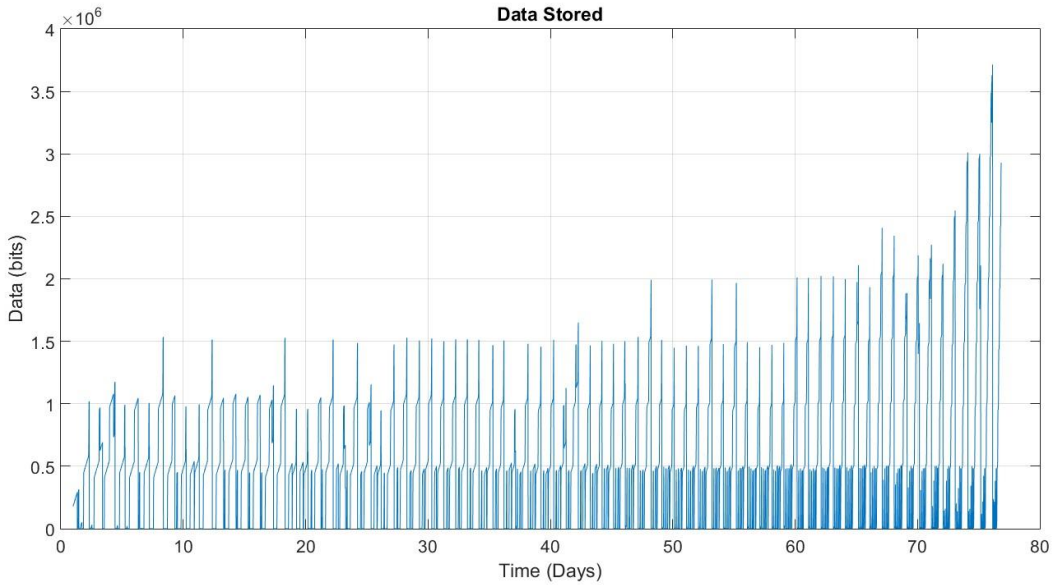

Figure 12.29: Data Storage over Time, when data is removed immediately after transmission.

12.2.6 Next steps

The next step to be taken regarding the Technical Resource Budgets is trying to refine the thermal analysis, either by trying to run the analysis on a different software than the ones previously used, or, by using the same software with different techniques. An accurate thermal analysis is fundamental to determine if the instruments onboard Spinnaker1 will keep functioning when exposed to the temperature range that the spacecraft is expected to operate at.

Moreover, members of the Technical Resources team should remain attentive to design changes made by the other teams involved on this project, since those can directly affect the Technical Resource Budgets.

12.3 Risk Assessment

Every mission has its own set of risks associated with it. These risks vary based on the likelihood of occurrence, and how detrimental they will be to the overall mission. In order to visualize the severity of this mission's risks, a risk matrix was constructed based on NASA's grading scale. The definitions for how likely a risk is to occur are as follows:

1. Very Low (<1%)
2. Low (between 1% - 10%)
3. Moderate (between 10% - 50%)
4. High (between 50% - 80%)
5. Very Likely (>80%)

Using knowledge of older missions and a current understanding of the equipment on board, the Systems team was able to match each risk to a specific likelihood. The consequences of each

risk were determined based on whether or not the mission could still be successful. The criteria for each rank are as follows:

1. Minimal Impact – Minor delay in obtaining non-critical data
2. Minor Impact – Loss of non-critical data, delay in critical events
3. Moderate Impact – Loss of science objective, failure to meet full mission success criteria
4. Major Impact – Loss of instrument or critical mission data set, failure to meet minimum mission success criteria
5. Mission Catastrophic – Loss of mission, mission cancellation, failure to achieve any mission objectives

The risks were put in a list and then given likelihood and consequence ratings based on the information above.

Table 12.14: List of Risks Associated with ADE

ID	Risk	C	L
1	Periapsis timing file error	2	4
2	Large orbit determination uncertainty	2	4
3	IMU failure before 5 perigee passes	3	2
4	Poor IMU data quality	2	3
5	Permanent loss of uplink prior to spacecraft checkout	4	1
6	Poor communications due to unfavorable attitude	2	4
7	Data corruption within data set	2	5
8	Data file headers corrupted by radiation	3	2
9	Initial boot up failure	5	2
10	Sail deployment degrades telecom	2	3
11	Data loss due to poor ground system performance	2	2
12	Primary electronics failure due to radiation damage	4	2
13	Cannot charge batteries	3	2
14	Spacecraft not power positive	2	2
15	Failed antenna deployment	4	2
16	Premature sail deployment	1	2
17	Sail deployment door mechanism failure	4	2
18	Drag sail component malfunction impedes full deployment	4	3
19	Failure to initiate deployment sequence	4	2
20	Spacecraft gets stuck in P-POD	5	1
21	Drag sail degradation	2	2
22	Drag sail not visible from camera	3	3
23	Earth not captured in an image	3	2
24	All radiation sensors fail	3	2

Once each risk was given a consequence and likelihood score, they were entered into a risk matrix in order to visualize which risks needed to be dealt with first. The risk matrix breaks down risks into three categories: minor, moderate, and severe.

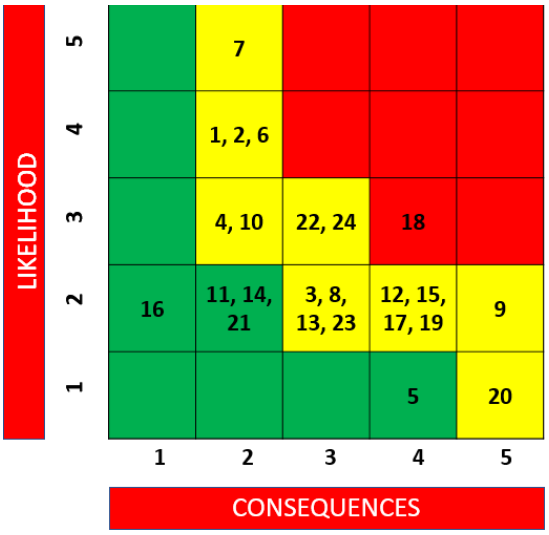

Figure 12.30: Risk Matrix

It's clear to see that most of the risks associated with ADE fall into the moderate category, with only one being identified as severe. The risk identified as severe deals with if a part of the drag sail assembly malfunctions and stops the drag sail from deploying altogether. If this were to happen, the mission would not be able to be counted as successful since the whole mission depends on the sail deploying. This needs to be tested on the ground to ensure that all mechanisms are acting according to plan.

12.3.1 Contingency Plans

Once the risks are tabulated, plans must be made to mitigate the risks that can occur once the mission has already started. The table below includes all of the significant mission risks. Following the table are detailed contingency plans for each specific risk scenario.

Table 12.15: Contingency Plans

Risk Scenario	Subsystem
Loss of Downlink	Comms
Loss of Uplink	Comms
Initial Bootup Failure	System Level
Payload Not Power Positive	EPS
Drag Sails Fail to Deploy	Payload
All Radiation Sensors Fail	C&DH
Data Corruption Within Set	C&DH
Data File Headers Corrupted by Radiation	C&DH
Primary Electronics Failure Due to Radiation Damage	C&DH

Drag Sails Fail to Deploy

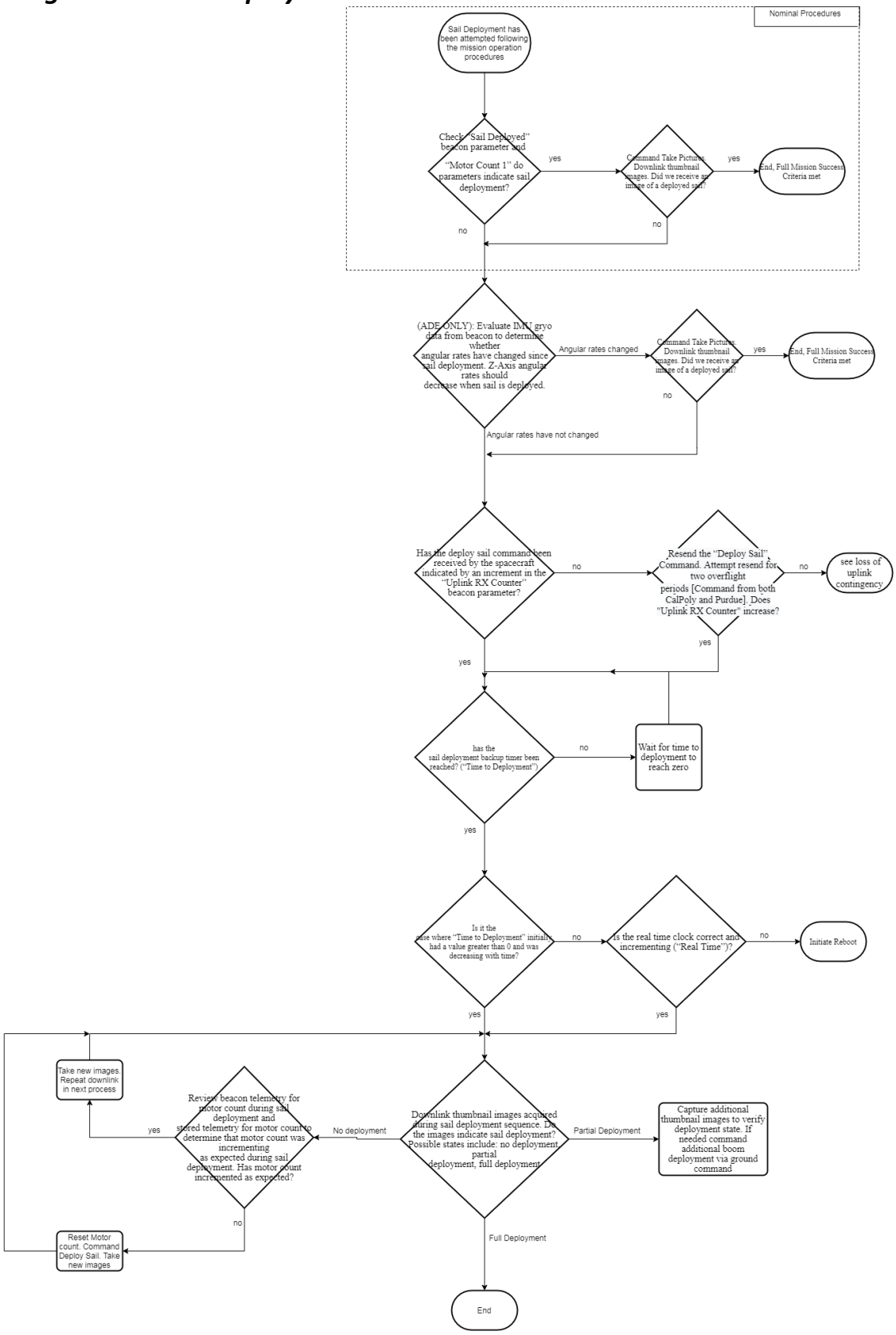

Loss of Downlink

Need to generate contingency plan

Loss of Uplink

Need to generate contingency plan

Initial Bootup Failure

Need to generate contingency plan

Payload Not Power Positive

Need to generate contingency plan

13. Test Plans

In order to verify and validate design decisions, many tests have been designed on the component, subsystem, and system level. This chapter discusses these tests in detail, discussing the inputs, hardware, preparation, and success criteria for every test. Further, a full set of procedures and desired outputs is included to describe every step for each test.

13.1 Long Range Telecom Testing

ADE will use the ground stations from four universities -Purdue University, California Polytechnic State University, Georgia Institute of Technology and Arizona State University- to downlink data. The long-range telecommunication test is defined to evaluate the performance of Purdue's Ground Station. This is accomplished by using attenuators to simulate the orbital conditions and evaluate the range over which an acceptable data-loss is achieved.

The satellite radio used to perform the test does not correspond to the radio that will be on board during the mission. The communication will be performed using SatNet, the tracking Station Network Software designed by PolySat.

Objectives & Success Criteria

Objectives

- Use SatNet to achieve a two-way communication between the CubeSat radio and the Purdue Ground Station.
- Obtain the maximum communication range under different conditions with the use of attenuators.
- Evaluate the effect of noise temperature on the maximum range by testing at different times of the day.
- Evaluate the effect of pointing losses on the maximum range by testing at different orientations.

Success Criteria

The test shall stablish a telecommunication range of 24675 km with a maximum data loss of 40% (60% of the packets sent shall be received). This target range corresponds to 173.13 dB of attenuation.

Test Procedure

Test Conditions

The test will be performed under the following conditions.

Test Orientation: To test the effect of pointing losses, the test will be performed in four orientations of the CubeSat antenna relative to the line of sight with the ground station antenna.

0 degrees
45 degrees
90 degrees
Tumbling

Attenuation: To quantify line losses, the attenuation will change according to Table 13.1.

Time of day to test: To test the effect of the Sun interference with the signal, the test will be performed at three different times.

Noon
6pm
Midnight
Distance to test: 150 m from the ground station
Altitude to test: 5.25 m from the ground station

Table 13.1: Attenuation setups and corresponding slant ranges

Attenuation Set-up (dB)	Total Attenuation (dB)	Slant Range (km)
(30) x1	30	0.00
(30) x2	60	0.05
(30) x3	90	1.72
(30) x4	120	54.43
(30) x4 + (5)	125	96.79
(30) x4 + (10)	130	172.12
Perigee	**130.63**	**185.00**
(30) x4 + (15)	135	306.09
(30) x4 + (20)	140	544.31
(30) x4 + (25)	145	967.93
(30) x5	150	1721.24
(30) x5 + (5)	155	3060.85
(30) x5 + (10)	160	5443.05
(30) x5 + (15)	165	9679.27
(30) x5 + (20)	170	17212.45
(30) x5 + (25)	170.5	18232.35
Current Range	**173.13**	**24675.00**
Apogee	**176.36**	**35786.00**
(30) x5 + (30)	180	54430.54

Initial Procedure

This initial procedure consists on the initial assembly of components and has already been done. This will not need to be done during the test.

1. Ensure that an ESD mat (blue mat) is available for the system board.
2. Ground yourself with an ESD strap.
    a. Wrap the strap band on your wrist.
    b. Attach the opposite end to a metal component.
3. Connect the SMA/u.fl antenna to the UHF board.
    a. The connector on the UHF side is shown in the purple circle in Figure 1.
    b. Connect the female u.fl connector on the end of the SMA/u.fl adaptor cable to the connector on the UHF board.
    c. Note: an antenna must be attached to the UHF board before external power is sent into the system. DO NOT proceed to steps 4 and 5 without attaching an antenna to the UHF board.
4. Attach the UHF board to the system board in the slot shown in the green circle in Figure 1. Use any two screw holes separated by the diagonal of the UHF board.
    a. Connect the system board to an external power supply at 4.2 V.
    b. Connect the connector highlighted in the blue circle from Fig. 13.1 to the Power

supply.

c. Connect the connector highlighted in the orange circle from Fig 13.1 to Ground.

Attenuator setup: this process is unnecessary once the configuration file local.cfg from Cal Poly is loaded.

1. Open a Linux command terminal on the control computer
2. At the terminal
    - Input: `sudo rotctld -m 901 -t 4533 - vvvv -4 /dev/Rotator -C az_resolution=2 el_resolution2`
    - Output: the system will ask for the password.
    - Input: `space_lab`
3. Open a new command terminal
4. Input: `sudo rigctld -m 334 -r /dev/Icom -s 9600`
    - Output: the system will ask for the password.
    - Input: `space_lab`
5. Open a new command terminal
6. Input: `sudo chmod 777 /dev/ttyS6`
    - Output: the system will ask for the password.
    - Input: `space_lab`
7. Input: `sudo picocom /dev/ttyS6 -b 9600 -f h`
    - Output: the system will ask for the password.
    - Input: `space_lab`

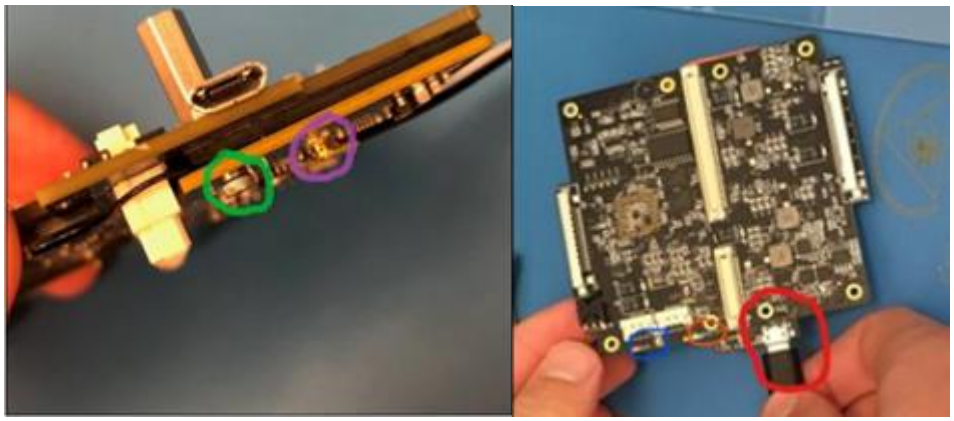

Figure 13.1: UHF and system board connections

Test-Day Procedure

Hardware Check

1. Booting control computer into Ubuntu operating system
    - Check that the antenna line is connected on the back of the radio control cabinet as represented in Fig. 13.2.
    - Turn on power switch of the rotor controller (on the back of the controller).
    - Turn on switch 3 of Radio Control Cabinet power strip to power TNC.
    - Open Amcrest Surveillance Pro in the control computer and select Live View to enable antenna camera.

Figure 13.2: Antenna line connection

2. Attenuator Setup. Connecting attenuators between UHF board and antenna, to confirm functionality retained after attenuator addition.
    - Screw in the female end of the attenuator combination to the male end of the SMA antenna.
    - Screw in the male end of the attenuator combination to the female end of the SMA/u-fl cable.
3. Remoting into Raspberry Pi.
    - Turn on power switch on CubeSat System.
    - Boot up laptop.
        i. Open terminal in Linux.
    - Connect to 192.168.1.2
        i. Connect the system board to the developer laptop.
            1. Connect with a micro USB to USB cable the connection highlighted in the red circle from Fig. 13.1 to the USB connection of the lap
        ii. Input: type in terminal `ssh root@192.168.1.2`
        iii. Output: the system will ask for credentials.
        iv. Input Username: `pi`
        v. Input Password: `space_lab`
    - Output: Desktop of Raspberry Pi will appear.
4. SSH into Flight Computer
    - From Raspberry Pi desktop open terminal.
        i. Input: `cd documents`
        ii. Input: `cd  picocom-3.1`
        iii. Input: `sudo chmod/dev/ttyUSB0`
        iv. Input: `sudo ./picocom./dev/ttyUSB0 -b 115200 -f n -p n`
    - Output: The system will ask for credentials:
        i. Input Username: `root`
        ii. Input Password: `calpoly`
        iii. Input: `cd ~/usr/sbin`

- Start Satcomm:
    i. Input: `./satcomm&`
- Open a different command window.
    i. Input: `cd desktop`
    ii. Input: `cd attenuate`
    iii. Input: `select variable attenuation (0-30 dB)`

Uplink

1. To load configuration file, open ground station terminal
    - Input: `cd satnet`
    - Input: `cd satnet-groundstation`
    - Input: `sudo ./ run_pi.sh local.cfg`
    - Output: the system will ask for pasword
    - Input password: `space_lab`
2. Communicate with the satellite
    - Input: `ping 192.168.200.1`
    - To stop the process, input Ctrl+C
    - Output: at ground station terminal, the data loss information (nº of pings sent and nº of pings received) will appear.

Downlink

1. At the terminal that is SSH into the flight computer type
    - Input: `ping 192.168.200.2`
    - To stop the process, input Ctrl+C
    - Output: at Flight Computer terminal, the data loss information (nº of pings sent and nº of pings received) will appear.

During Long-Range Telecommunications test

The following steps will need to be performed for each of the test configurations that will be tested:

1. Apply the hardware check for the desired attenuation/Test hour/Test orientation combination.
2. Begin transmission from PTC to satellite (Uplink procedure).
3. Record data loss values (number of packets received, and number of packets sent).
4. Record Attenuation and convert to equivalent range using Table 13.2
5. Begin transmission of signal from PTC (Downlink procedure).
6. Record data loss values (number of packets received, and number of packets sent).
7. To perform a test with different attenuation, turn power system off and reboot every component (Ground Computer, Flight Computer, Control Cabinet).
8. To test a different attenuation, repeat from step 1.

Test Materials, Facilities and Equipment

The test will be performed at Purdue Ground Station, which is located at the Purdue Technological Center.

Ground Station Equipment

The equipment used in the Ground Station to track the satellite is listed in Table 13.2 and represented in Fig. 13.3.

Table 13.2: Ground station components

Ground Station Components

Component	Model
Quad Yagi Antenna	M2 Antenna Systems Model nº 436CP42UG
Antenna Controller	AlfaSpid ROT2 Prog Controller
Rotor Controller	AlfaSpid Bigras
Low Noise Amplifier (LNA)	MHP-70 by SSB electronics
Radio Control Cabinet	icom IC-821H
Terminal Node Controller (TNC)	Kantronics TPC 9612+
Ground Station Computer	

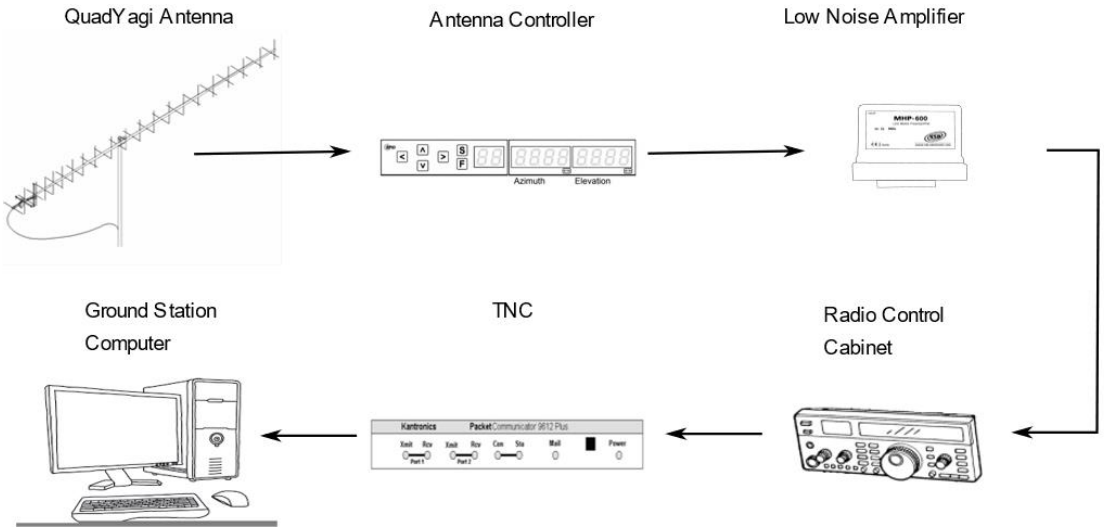

Figure 13.3: Ground station components

CubeSat radio components

To perform the test emulating the flight conditions, it is required to setup the Flight Computer (Intrepid board) with the antenna and the attenuators following the procedure. The equipment used is listed in Table 13.3 and represented in Fig. 13.4.

Table 13.3: Satellite radio components

Satellite Radio Components	
Component	**Model**
UHF Board	EXSCM transceiver
Attenuators	mini-circuits VAT -30+30 db attenuators
Antenna	NA-772 144/430 MHz Dual band antenna by Quanzhou truest communication co
Flight Systems Board	Intrepid byTibak
Raspberry Pi	Raspberry Pi 3
Power Supply	Dr Meter DC Power Supply PS-305DM
Laptop	

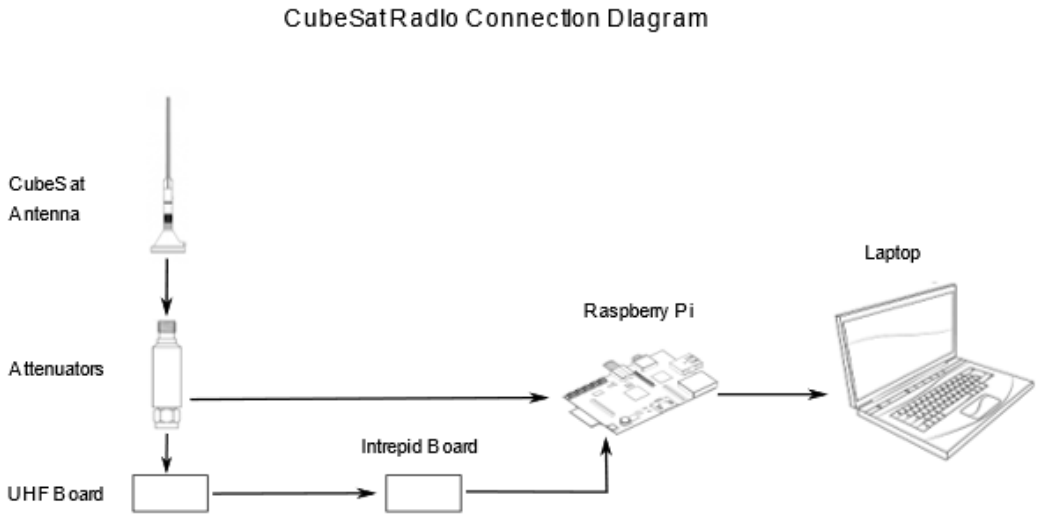

Figure 13.4: Satellite radio components

Expected Results

When the ping command is stopped, a message appears at the terminal of the device, providing information about the number of packets sent and received and the data loss. The expected result is to obtain a data loss less than 40% when communicating with an attenuation of 173.13 dB. After this point, a small increase in attenuation (the minimum available is 1 dB) will represent a larger increase in range, and therefore data loss is expected to increase exponentially.

Possible Anomalies

A possible anomaly is that the signal is not being picked up by the Ground Station Antenna. If this occurs, check that the TNC is set to a frequency of 437 MHz and that port 2 of the TNC is the one in use.

13.2 Beacon Testing

ADE will send a beacon to transmit telemetry data with the objective of providing a system check for the CubeSat. This beacon will include values measured from the IMU and radiation sensors, the voltage and temperature of several subsystems and the state of the cameras. The beacon will send a single packet at a duty cycle of 4%, which corresponds to a packet every 5.5 seconds. The maximum size of information that can be transmitted by the beacon using the Ax.25 protocol is 227 bytes.

Objectives & Success Criteria

To define the test objectives and test success criteria, it is important to make a clear distinction between the current development of the beacon code, and the final beacon code that will be used during flight. Therefore, we will define two different tests with different objectives and criteria.

Test 1. Beacon transmission using Satcomm

The current development of the code has consisted in creating a code that is compatible with the Libproc libraries developed by Cal Poly and that uses Satcomm to send a beacon. Moreover, the beacon content has been modified to transmit a counting number to keep track of the number of packets sent and received. The code has proven to successfully send a beacon over the CubeSat radio, but the message has not been successfully decoded.

The objectives for this test 1 are:

- Send a beacon over the CubeSat radio and decode the message at the ground station.
- Successfully define the package sending interval.
- Set message to be an increasing counter.

The success criteria is:

- Obtaining the decoded message at the TNC terminal with the specified time interval.

If this test is successfully completed, the beacon can be used to perform the downlink part of the telecommunications test.

Test 2. Telemetry beacon test

After test 1 is performed and the drivers for the IMU are developed, allowing to extract the IMU data, the beacon code will be modified, and a final beacon test will be performed.

The objectives for test 2 are:

- Correctly obtain the parameters required listed in Tables 1-5, using the Libproc libraries.
- Transmit and decode telemetry data containing the parameters listed in Section 9.2.
- Perform the transmission at a 4% duty cycle.

Test Procedure

Pre-test: Buildroot

To be able to modify and compile the beacon code, it is required to have buildroot installed. The process to achieve this is described in the public_documentation repository at Github, but will be summarized to avoid confusion.

1. Download a virtual machine (VMware workstation works correctly and can be found at: https://www.vmware.com/products/workstation-pro/workstation-pro-evaluation.html).
2. Download **Ubuntu 14** and run it with the virtual machine. It is important to use version 14 to avoid incompatibility errors when installing buildroot.
3. Open the terminal at Ubuntu and run:
   Input: `sudo apt-get install git bison g++ flex gettext texinfo lib32z1 lib32ncurses5 lib32bz2-1.0`
4. Clone the repository with:
   Input: `git clone https://github.com/PolySat/buildroot.git`
5. Configure the build machine with authentication credentials running:
   Input: `echo "--no-check-certificate --user=purdue --password=UPJDHsbC" > ~/.polysat_fsw.auth`
6. Change into buildroot directory:
   Input: `cd buildroot`
7. Build the Flight Software Image. Expect the process to take 6 hours
   Input: `Make`
8. Output: the buildroot process installs a set of libraries and compilers that are required to develop

code using Libproc.

Pre-test: Set-up alias for cross-compiler

To correctly compile the code using a makefile, it is useful to create an alias for the cross compiler.

1. Open the barsh file by typing at the Ubuntu terminal:
   Input: `nano ~/.bashrc`
2. Set up the alias by adding the following at the end of the file (change username by your username in Ubuntu):
   ```
   export ARM_TOOLCHAIN_PATH=/home/username/buildroot/output/host/usr
   alias arm-gcc=$ARM_TOOLCHAIN_PATH/bin/arm-unknown-linux-uclibcgnueabi-gcc
   ```
3. Close the file:
   - Input: `Ctrl+x`
   - Output: prompt message asking yes or no
4. Choose yes to save
5. Copy the folder BeaconCode from the SharedDrive in the Home directory in Ubuntu
6. Open Make.Rules.Arm

Change username by your username in the ARM_TOOLCHAIN_PATH definition. For example, if your Ubuntu username is Purdue, set:

```
ARM_TOOLCHAIN_PATH=/home/Purdue/buildroot/output/host/usr
alias arm-gcc=$ARM_TOOLCHAIN_PATH/bin/arm-unknown-linux-uclibcgnueabi-gcc
```

Test-day procedure

1. Compile the beacon in ubuntu
   a. Change directory to the folder where the beacon files are stored:
      Input: `cd Beacon`
   b. Compile using arm:
      Input: `make TARGET=arm`
2. SSH into flight computer
   a. Connect flight computer (Intrepid Board) to Ubuntu using USB cable from Micro-USB connection in intrepid board to USB connection in Laptop.
   b. SSH typing in terminal:
      Input: `ssh root@10.162.6.1`
3. Open a new terminal (use one for the flight computer and one for Ubuntu).
4. Copy executable and config file in flight computer:
   a. Copy the typing the following in the Ubuntu terminal:
      Input: `scp beacon root@10.162.6.1:/data/beacon`
      Input: `scp beacon.cmd.cfg root@10.162.6.1:/data/beacon.cmd.cfg`
5. Execute satcomm in flight computer typing the following in the Flight Computer terminal
   a. Input:`cd usr/sbin`
   b. `./satcomm&`
6. Go back to the data folder where the executable is:
   a. Input: `cd ../..`
   b. Input: `cd data`
   c. Input: `./beacon`
   d. Output: A message will appear on the terminal requesting the time interval between beacons.

7. Introduce the time interval in seconds (5.5 seconds to achieve a 4% duty cycle).
    a. Input: `5.5`

At the terminal connected to the TNC, the decoded message will appear if the decoding process works correctly.

Test Materials, Facilities and Equipment

The test will use the same materials from the Long-Range Telecommunications test described in section 13.1.1. The only difference is that in this case the laptop used to SSH into the Flight Computer is required to have buildroot installed, following the process described in Pre-Test: Buildroot.

Expected Results

The output of the test is a message that will be decoded by the TNC and printed at the Ground Station computer terminal. The message will be a number, starting at 1 and adding 1 in every reception. Since a data loss is expected due to the attenuation, some of the numbers will not be received and it will be possible to keep track in real time of the messages that have been lost. Although the communication mechanism is different from the ping described in section 13.1.1 the data loss will depend on the radio and antenna used, and therefore the same behavior is expected.

Possible anomalies

1. Failure to compile the code

If the code does not compile at Ubuntu, check that the path described for the compiler is correct.

2. Failure to execute the code

If the code cannot be executed, check that the configuration file (beacon.cmd.cfg) has been copied in the same folder where the executable is located.

3. Failure to pick up signal

Check that Satcomm has been started. It should be printing configuration messages on the terminal, starting with the word Satcomm. If the process did not start correctly, repeat step 4 of the Hardware Check.

13.3 Sail Folding and Stow Testing

The steps for folding a quarter dragsail with the folding machine are

1. Setup
    (a) Power Up
    (b) Wifi Connect
2. Stage 1 – Long Fold
    (a) Loading
    (b) Folding
    (c) Unloading
3. Stage 2 – Short Fold
    (a) Loading
    (b) Folding
    (c) Unloading

Setup

Power Up

Plug in Alcatel pump (no switch) and switch on Welch pump, switch on air compressor (Fig. 13.5) and set to 2 psi. Plug in valve array (gray cord). Set power supply to 5V and enable output (Fig. 13.6).

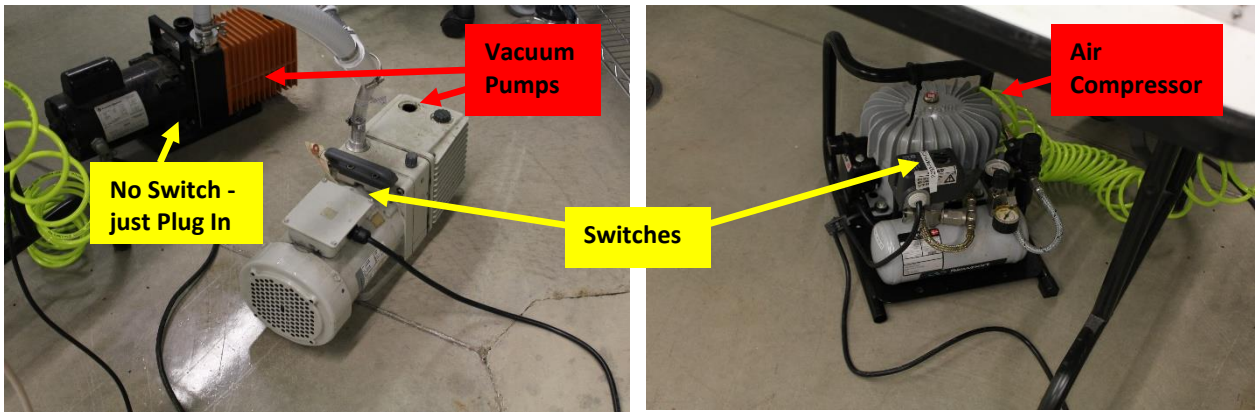

Figure 13.5: Vacuum pumps and Air Compressor

Figure 13.6: Power Supply and Pressure Sensor Controller

Wifi Connect

1. Using any Windows based computer with wifi
2. Change wifi adapter to static IP address in the 192.168.1.xxx range by
3. Open "Network and Sharing Center" in control panel and click on "Change adapter settings" (Fig. 13.7) right click on wireless network and select "Properties".
4. Click on "Internet Protocol Version 4 (TCP/IPv4) then click properties button (Fig. 13.8).

Select "Use the following IP address:" then enter 192.168.1.xxx where xxx is any number 1 – 255 different from the address of the Pi you are wanting to connect to (Fig. 13.9) click OK.

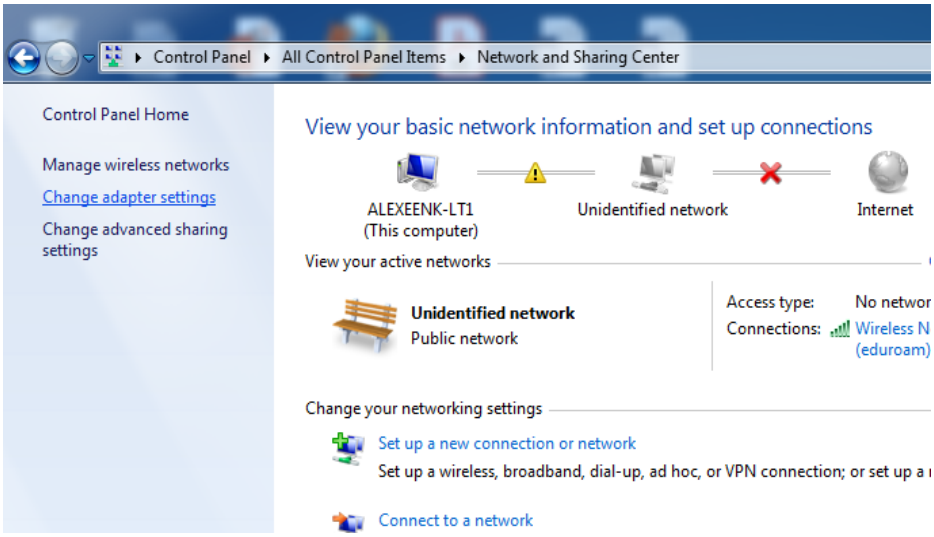

Figure 13.7: Network and Sharing Center

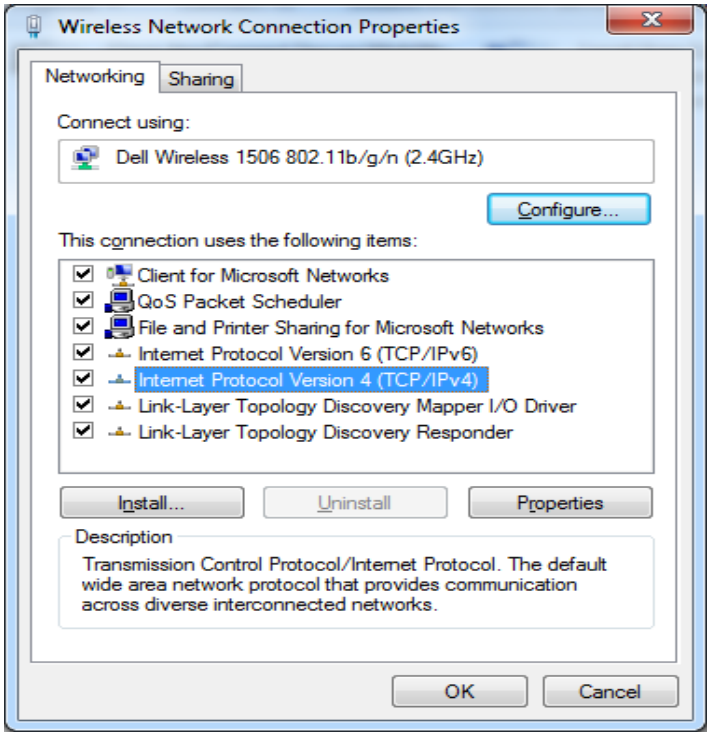

Figure 13.8: Wireless Network Connection Properties

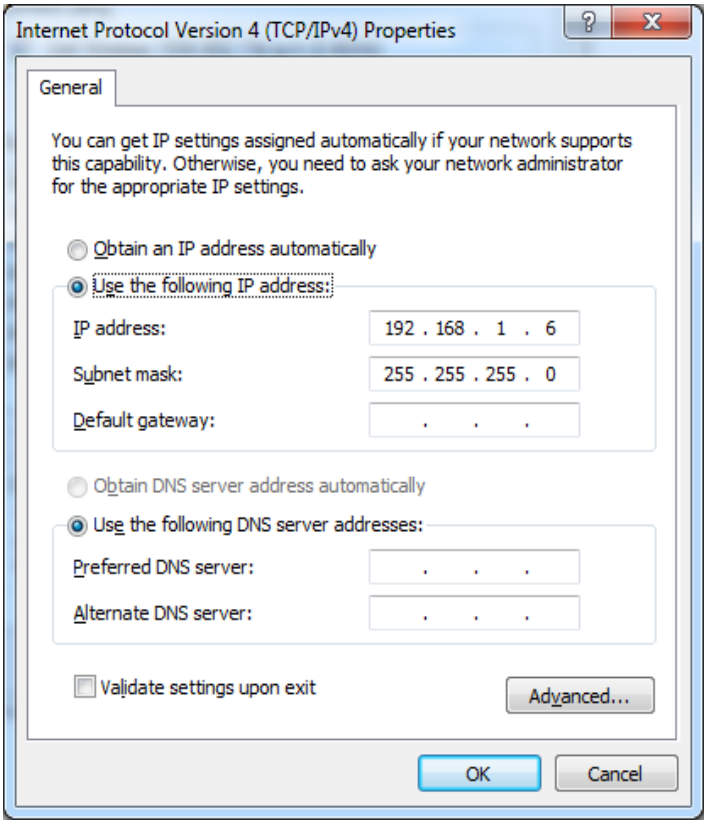

Figure 13.9: Internet Protocol Version 4 Properties

Connect to Raspberry Pi

1. Connect to ad-hoc network of choice (see Fig. 13.10 and Table 13.4).

Table 13.4: Wifi connection details for test devices

Device	Network	IP Address	Username	Password
Sail Folder	RPiAdHocNetwork	192.168.1.8	Pi	vac-lab
Boom Deployer	RPiAdHocNetwork2	192.168.1.9	Pi	vac-lab
Cubesat Radio	RPiAdHocNetwork	192.168.1.2	Pi	space-lab

2. Open Remote Desktop Connection and enter IP address of choice (see Fig. 13.10 and Table 13.4).
3. Connection warning will appear; click “Yes” then Remote Desktop Window will appear – enter username and password (see Fig. 13.11 and Table 13.4).

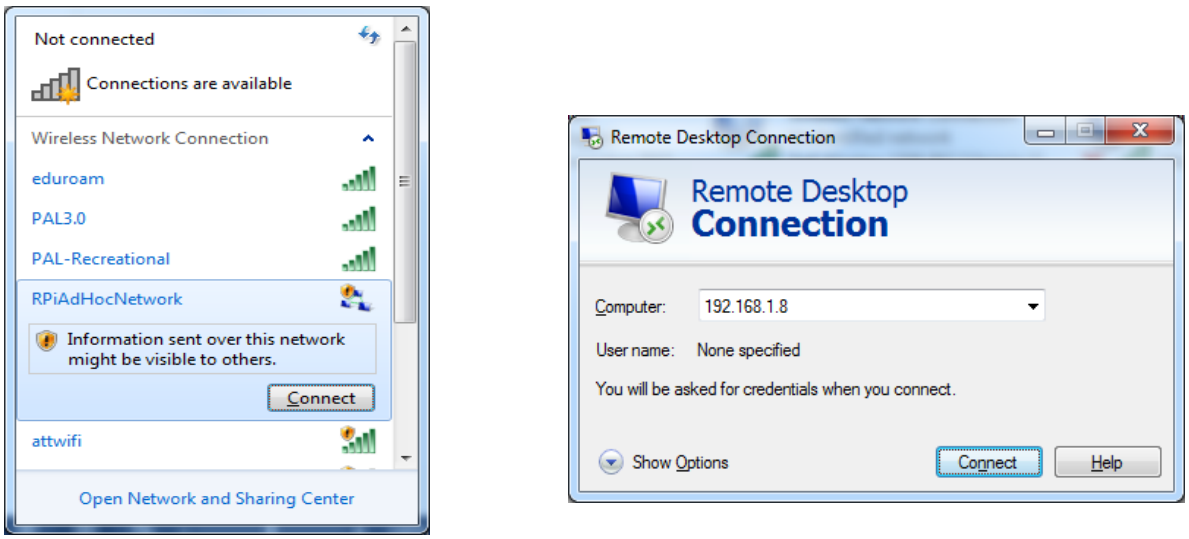

Figure 13.10: Available networks (left) and Remote Desktop Connection box (right)

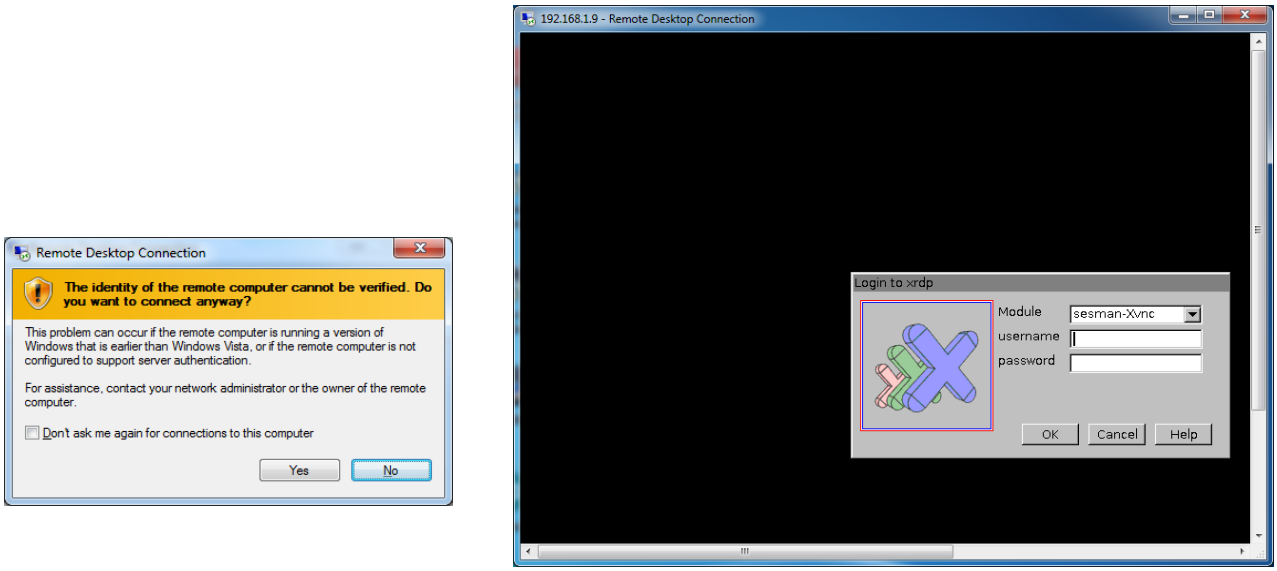

Figure 13.11: Connection warning (left) and Remote Desktop Window (right)

Stage 1 – Long Fold

Loading

1. In Remote Desktop, open a terminal and type “cd Desktop/sail_folder”, then press enter
2. Type “sudo ./fold_long” and press enter
3. A menu should appear, press “l” then enter to set loading configuration
   (a) The sail is spread out over the loading table with the hypotenuse hanging between the folding arms (Fig. 13.12).
4. Gently push the sail edge against folding arm A until the sail seals the vacuum holes

(Fig. 13.13).

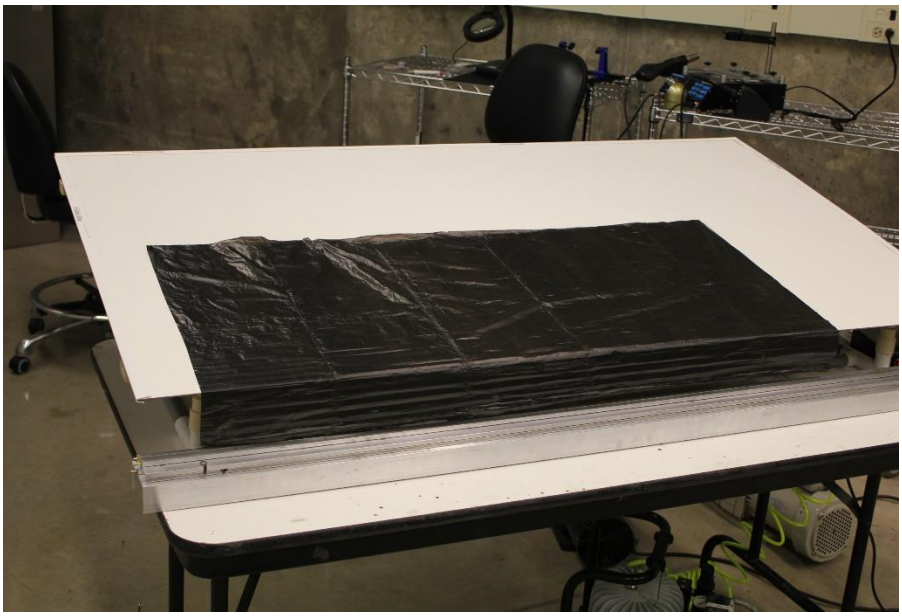

Figure 13.12: Sail on loading table

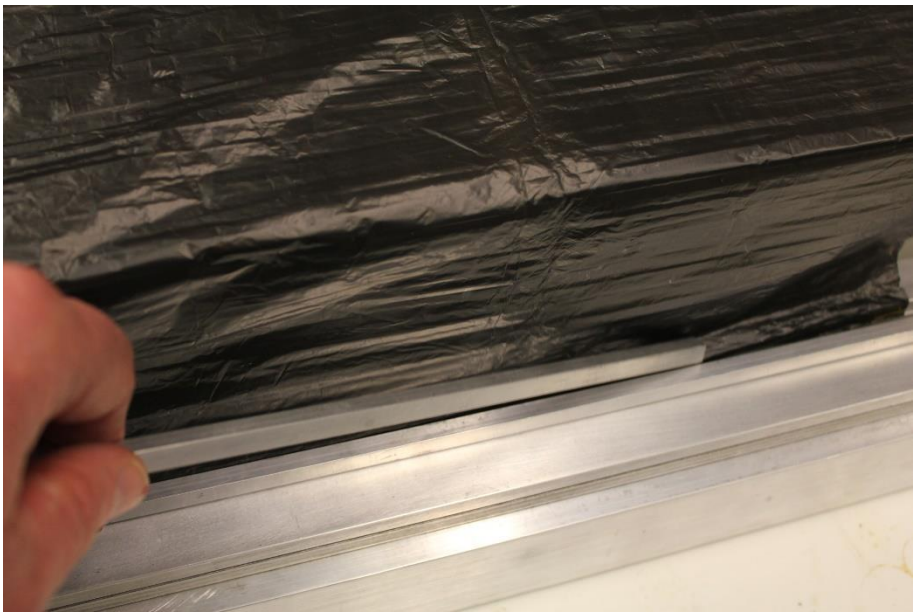

Figure 13.13: Vacuum attachment of sail to folding arm

Folding

Press “f” then “Enter” on the control laptop, then enter number of steps (102 for typical sail) then “Enter again. Wait for folding to cease, there should be ½” of sail left to fold. Remove tension line then fold 2 more steps to finish.

Unloading

Press “u” then “Enter”, this should route compressed air underneath and on top of the folded sail to allow easy extraction from the end of the machine.

Stage 2 – Short Fold – (Pending completion of machine)

Loading

Kill fold_long program with “CTRL + C” and start fold_short with “sudo ./fold_short”, select load (“l”) and press “Enter”. Pull sail from end of stage 1 machine and press against stage 2 folding arm C.

Folding

Press “f” then “Enter” on the control laptop, then enter number of steps (28 for typical sail). Wait for folding to cease.

Unloading

Folded sail can be pushed out from feed side through exit side. Back fold the stack halfway through where the apex is to finish.

Stowing

Attach apex grommet to mounted spring on deployer, push sail into storage compartment. Attach corner springs.

Finished.

13.4 Sail-Boom Attachment Testing

The total testing procedure involves three individual tests.

A. Sail attachment point testing
B. Boom attachment point testing
C. Combined robustness and stow test

Sail attachment point testing

Objective:

To identify the most feasible sail attachment point option with maximum possible robustness and minimum possible size.

Success criteria:

1. The attachment point can sustain expected loads on the drag sail without damaging the sail.
2. The attachment point does not hinder with the sail-folding or stowing method.

Procedure:

1. Calculate approximate total force experienced by sail at the attachment point.
2. Take two separate CP1 sections of equal area.
3. Attach grommet to one drag sail, about 0.5” diagonally inward from the corner.
4. Fold the corner of the other drag sail segment around the D-ring, stick it to the rest of the drag using glue, and then reinforce using Kapton tape.
5. Apply an incremental force of about 0.1 N using slotted weights or a tension type load frame

(or any other feasible/available method).

6. Record the load at which structural damage (tearing of the CP1) occurs.
7. Compare the maximum load taken by each option and determine the most durable/reliable one.

Sample Results:

Table 13.5: Sail Attachment Point Testing Sample Results

Attachment Point Option	Fits inside payload casing?	Maximum mass (m) supported before damage [kg]	Maximum force (F) applied before damage [Newton] {F = m x g}
E.g.: Grommet	E.g.: Yes	E.g.: 0.5	E.g.: 4.905

Additional Remarks:

Some testing was done for the grommets/eyelets. All of them had rough jagged edges once compressed using the setting tool. It is suspected that this is because the CP1 is too thin for their design, as a result of which they are compressed more than they should be in their intended application (like leather or fabric). So far, the best results were achieved with the Nickel grommets (We R Memory Keepers brand).

Figure 13.14: Grommet on CP1 Sample

Additional grommets may be required, that are designed for paper or thin material so that they have smooth edges after compression.

Boom attachment point testing

Objective:

To identify the most feasible boom attachment point option with maximum possible robustness and minimum possible size.

Success criteria:

1. The attachment point can sustain expected loads on the boom without bending or breaking the boom.
2. The attachment point does not hinder with the stowing method.

Procedure:

1. Take all possible combinations of boom materials, connectors and attachment options.
    a. Options for booms: Metallic TRAC, in-house carbon fiber TRAC and NASA SHEARLESS.
    b. Options for connectors: Springs (with split rings) and fabric loop.
2. Apply an incremental force of about 1 N using slotted weights or a tension type load frame (or any other feasible/available method).
3. Record the load at which structural damage (both bending and breaking) occurs.
4. Compare the maximum load taken by each combination and determine the most durable/reliable one.

Sample Results:

Table 13.6: Boom Attachment Point Testing Sample Results

Attachment Point Option	**Fits inside payload casing?**	**Maximum mass (M) supported before bending [kg]**	**Maximum mass (m) supported before breaking [kg]**	**Force (F) applied before minimum damage [Newton] {F=min (M, m) x g}**
E.g.: Metal boom (direct hole) + spring	E.g.: Yes	E.g.: 0.5	E.g.: 0.7	E.g.: 4.905

Combined robustness and stow test

Objective:

To ensure that the complete sail-boom attachment assembly is small and sufficiently robust.

Success criteria:

1. Attachment assembly fits inside stowage space.
2. Attachment assembly can take the expected loads without any damage to the itself or the sail and boom materials.

Procedure:

A. Part A: Stow test
    1. Fix the sail attachment point onto the drag sail.
    2. Fold the sail according to the pre-decided procedure.

3. Roll boom around the motor hub, as decided.
4. Attach the sail to the boom using the connector.
5. Stow the sail in the payload casing.

B. Part B: Robustness test - Deploy the sail-boom assembly and carefully check for any visible structural damage to the sails, booms and attachment points.

Sample Results:

Table 13.7: Robustness and Stow Test Sample Results

Attachment Point Option	Fits inside payload casing?	Damaged during deployment?
E.g.: Grommet, spring, metal TRAC boom (direct hole).	E.g.: Yes	E.g.: No

Additional Remarks:

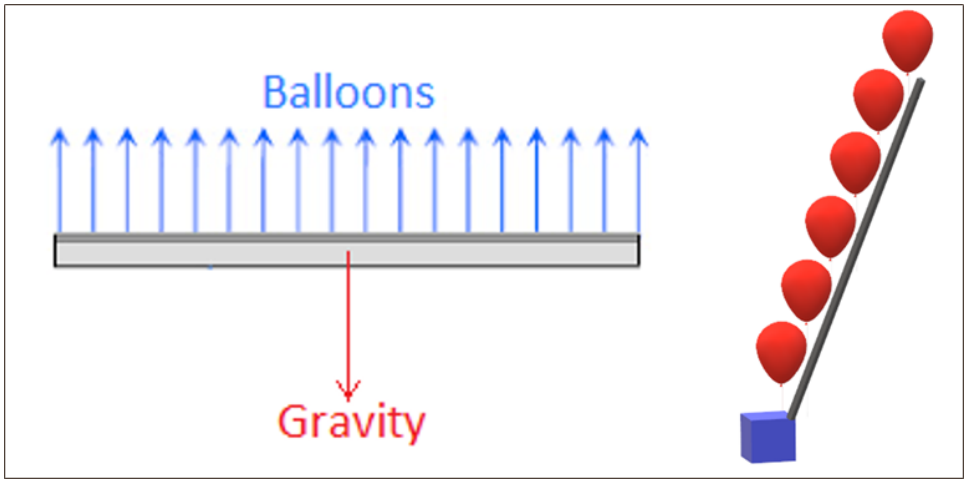

Figure 13.15: Gravity Offload Technique

To simulate the microgravity environment that the CubeSat will operate in, a simple technique for gravity offload may be used. During boom deployment, several stops may be incorporated to attach strings or balloons (filled with hydrogen or helium) at regular intervals, that will cumulatively exert a uniform upward force to counteract the downward gravitational force. The length of the intervals would depend on the number of strings/balloons used and the weight of the boom. The total upward force (i.e. the product of the number of strings/balloons and the upward force exerted by each string/balloon) must be equal (or almost equal) to the weight of the boom, which will vary with the type of boom used.

Materials Required for testing

The following materials are required for sail-boom deployment testing. Remarks regarding their current status have been added next to each item.

1. Booms (metal & CF) - acquire from Anthony Cofer and Ariel Black.
2. CP1 - available (residual segments from previous semester).
3. Grommets/Eyelets - samples of 3 types purchased.
4. Grommet setting tool - purchased
5. Kapton tape - available.
6. D-ring - commercial sizes are too big. In-house manufacturing needed.
7. Super glue - purchased.
8. Ribbon/shoe lace/fabric loop - can be acquired easily.
9. Spring - samples of 3 sizes purchased.
10. Split rings - samples of 3 sizes purchased.
11. Slotted weights/force meter/load frame - need to borrow or request usage permission.
12. Payload casing - acquire from Anthony Cofer.

Purchases Made:

The following were purchased in Spring 2019 for testing purposes. Links have been included for the ease of reordering.

- Eyelets:
  - We R Memory Keepers Eyelet and Washer - Nickel - 60 Pieces [worked best]
  - Fiskars Crafts 197700 Tag Maker 3/16in Silver Eyelets, 50 Pack 3/16" [blunt/short]
- Eyelet setting tool + eyelets:
  - Katzco Eyelet Grommet Pliers Setting, Steel Hole Punch Eyelet Setter Kit [Pliers work fine; grommets did not work too well]
- Split rings:
  - Stainless Steel Split Rings 50 pack – Sizes 00, 0 and 1 [larger size may be required]
- Springs: [not tested yet]
  - Steel extension springs with Loop Ends, 0.5" Long, 0.125" OD, 0.014" Wire Diameter
  - Steel extension springs with Loop Ends, 0.625" Long, 0.125" OD, 0.014" Wire Diameter
  - Steel extension springs with Loop Ends, 0.75" Long, 0.125" OD, 0.016" Wire Diameter

Additional Remarks:

A larger size of split rings may be required, as the ones currently available (sizes 00, 0 and 1) have been found to be too small for proper attachment to the sail (grommet).

Potential Testing Locations

Table 13.8: Potential Testing Locations

Department	Lab	Person-in-charge	Approval status	Test
Material Science & Engineering	Schuhmann Lab (ARMS 2172)	Jeffrey Youngblood	May use 1 kN load frame with permission from PIC.	AP Load
	Mech. Testing Lab (ARMS 2191)	David Johnson	Has a load frame, but lab supports 3 courses in Spring 2019; may be available for use in Fall.	AP Load
Aeronautical & Astronautical Engineering	CubeSat Lab (ARMS 3089)	James Doyle	Access can be granted by Prof. Spencer.	Prototyping, Load
	Aero Labs ASL (ARMS 3106)	Waterloo Tsutsui	Access to lab & equipment granted.	AP Load
	AAE Build Lab (ARMS 2098)	Phil Baldwin	Access to lab & equipment granted; willing to help with additional resources and advice.	AP Load

Note: Final stow/deployment testing shall be done in the clean room (ARMS B191).

13.5 Sail Deployment Testing

Setup

- Connect deployer to driver board and driver board to Raspberry Pi as shown in Fig. 13.16. Pinouts are found in main.c file in Desktop/deployer/manual folder of Pi
- Connect Pi to power adapter and driver board to 5V supply

Deploy

- Connect to Raspberry Pi with laptop as described in section 13.3
    - Type “cd Desktop/deployer/manual” then enter
    - Type “sudo ./open” then enter – booms should deploy as seen in Fig 13.7
- **Retract**
    - Type “sudo ./close” then enter – booms should retract back into device

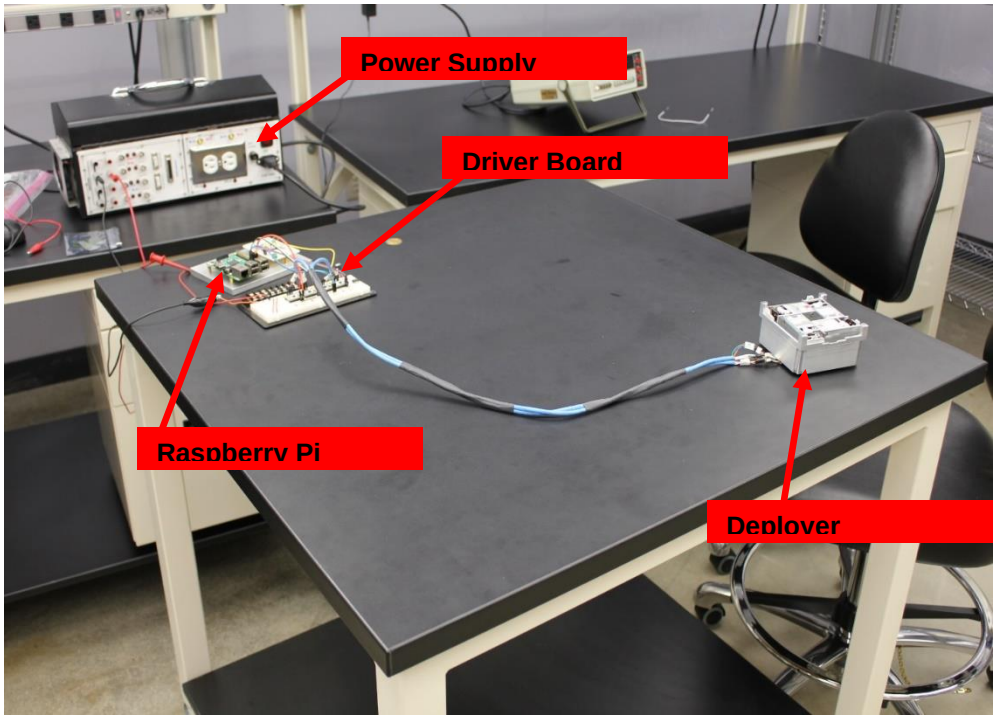

Figure 13.16: Deployer Testing Setup

Figure 13.17: Fully deployed sail

13.6 Radiation Testing

The general radiation test should be performed initially with the motor driver board. This section will outline the radiation test and describe the facilities that were identified for performing the radiation test. All assumptions are based on the AE9/AP9 radiation environment model.

Objectives

To test the motor driver board for radiation effects and simulate the conditions it will experience through the Van Allen radiation belts

Identify the maximum radiation dosage the board can handle

Test functionality of the board after performing radiation tests.

Success Criteria

Initial Radiation Test will be successful if the following criteria are met:

Board shall be able to withstand a dosage of at least 6 krads without Single Event Upset (SEU)

Motor

Test Facilities

Facilities are in the basement of the Materials Science and Electrical Engineering building, by the nuclear reactor

3 facilities identified:

Chamber within the basement of EE building

Ideal for small radiation dosage for initial testing

Steel Chamber

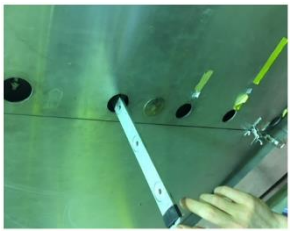

Figure 13.18: Steel chamber

Ideal for overnight radiation testing

Nuclear Reactor

Nuclear Reactor

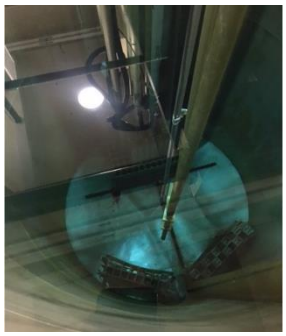

Inside of Nuclear Reactor

Nuclear Reactor Controls

Figure 13.19: Nuclear reactor

Ideal for testing the motor driver board and simulating space conditions

General Procedure

The overall procedure for this test is relatively simple. It should be apparent, given the

objectives, that the board shall be allowed to accumulate 6 k-rads of radiation dosage for simulating ideal radiation conditions. The following table outlines the times at which we should test the board with the motor to make sure it works. When testing this board with the motor, we must make sure that the code is uploaded successfully and drives the motors as expected.

Table 13.9: Radiation dosage accumulation

Radiation Dosage Accumulation (rads)
0
500
1000
1500
2000
2500
3000
3500
4000
4500
5000
5500
6000

After 6,000 rads, the board should have accumulated enough radiation dosage to simulate the mission for one month. Therefore, if it survives all the testing with the motor, the board should survive the space conditions. The table above highlights the specific radiation dosage at which we should test the board with the motor to see if it functions as expected. This will also help with identifying the maximum radiation capacity of the board and whether or not the chip can handle the 6 k-rads radiation dosage, as given by the AE9/AP9 radiation environment. In order to test the board, we need to make sure that the code that was written is successfully uploaded to the ATTiny 1616 chip. After Uploading the code, run the code to make sure that it rotates the motor as programmed in the code. If the motor is rotated for the same number of degrees that it is programmed to rotate, then we know that the test was successful, and can be repeated again with more dosage. Continue the same sequence until the board has reached the predicted radiation dosage of 6 k-rads. If testing the board with the motor is still successful, continue adding radiation dosage in increments of 500 rads, until the code is no longer being uploaded to the board. This will give us the maximum radiation dosage that the chip is able to withstand. As previously mentioned, this procedure for performing the test is relatively simple; the entire test can likely be performed in less than one day, provided we have access to the nuclear reactor and its operating controls.

13.7 Vibration Testing

Objective

The objective of the vibration test is to subject the CubeSat to the vibrational loads of the Atlas V launch environment. This is needed in order to ensure that the CubeSat's structure and electronics will survive the launch environment.

Success Criteria

The vibration test will succeed if the CubeSat's structure and electronics remain intact. Success for the structure and the electronics is determined by the following:

Structure

1. The sail deployment mechanism will need to be able to deploy the sail.
2. The joints of the CubeSat structure remain intact
    a. All screws, nuts, etc. should remain in their respective place
3. No portion of the CubeSat's structure should be greatly deformed
    a. The walls of the CubeSat should stay in place to contain all the electronics and deployment mechanism.

Electronics

1. All sensors need to remain functional before and after the test
    a. To test this, we will take readings before and after the test and compare the data. The data should be similar between the two readings
2. All soldered joints remain soldered together.

Equipment

1. Full assembled CubeSat
    a. Should be as similar to the launch ready CubeSat as possible.
2. Electrodynamic shaker
    a. Look in facilities
3. Testing fixture
    a. This will be manufactured based around the CubeSat's final design.
        i. Manufacturer is currently undetermined until the CubeSat is finished
    b. Currently this is undesigned due to the CubeSat being unfinished.
4. Baseplate
    a. This will be manufactured based around the CubeSat's final design.
    b. Currently this is undesigned due to the CubeSat being unfinished.

Facilities

The test will be performed at Ray W. Herrick laboratory with the assistance of Dr. Jeff Rhoads. Dr.Rhoads is in charge of the electrodynamic shaker at the lab and will run the test for us. The following procedure will be completed by a lab tech that works for Dr.Rhoads due to laboratory rules. However, when checking the CubeSat that will be up the member of the ADE team present at the experiment. More will be covered in the procedure.

Procedure:

Before we continue it is important to understand the types of vibration testing, sine-sweep and random vibration tests. A sine sweep uses a gradually increasing or decreasing frequency which tests a lot of the structural integrity of the system. The random vibration test has the shaker introduce various frequencies between 20 to 2000 Hz to test the integrity of soldered joint, electrical joints, fasteners and sensors. Finally, below is the vibration profile for the Aft Bulkhead Carrier (ABC) of the Atlas V which is used to determine the vibrational loads for the sine sweep.

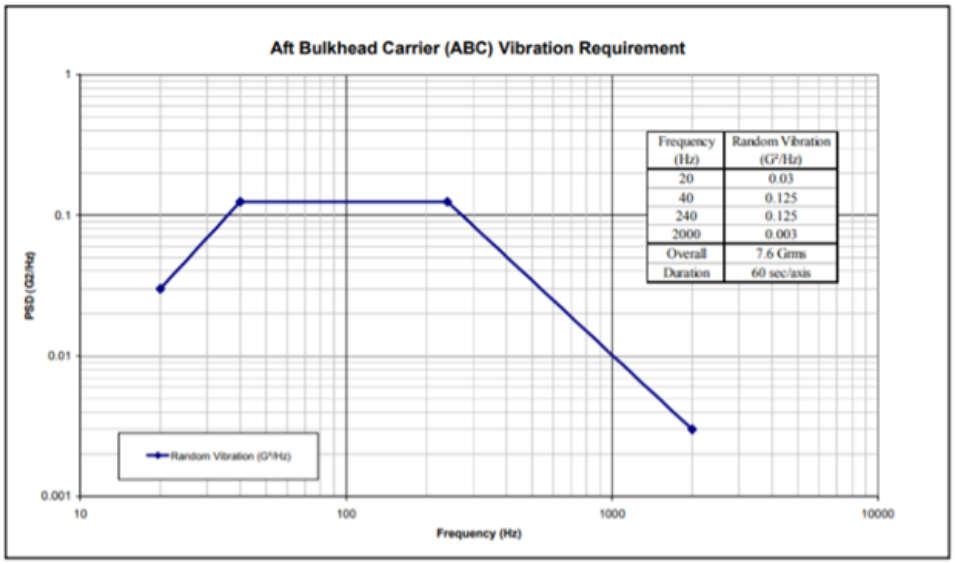

Figure 13.20: ABC vibration requirement from ULA Atlas V ABC User's Guide [1]

1. Attach the baseplate to the shaker head ensuring torque specifications are met
2. Attach the experimental fixture to the baseplate using the necessary bolts and hardware
3. Perform preliminary checks for the shaker
4. Power the shaker and allow to warm up
5. Apply the Aft Bulkhead Carrier to the electrodynamic shaker's interface it will use the curve to perform the following tests
    a. It will use the entire curve above.
6. Perform a Sine-sweep
    a. Option on the shaker. The same for random vibration test.
7. Perform a random vibration test
8. Perform a Sine-sweep
    a. This second Sine-sweep is to ensure that the CubeSat can still handle the vibrational load after the random vibration test
9. Detach the CubeSat from the shaker and check that the CubeSat meets all the success criteria above
    a. If the CubeSat doesn't meet any of the success criteria, for either the structural or electronic requirements, adjust the CubeSat so that it meets the success criteria and it will succeed the following vibration test. Reattach the CubeSat to the shaker. Repeat steps 6-9.
    b. If the CubeSat meets all the success criteria move on the Step 10
10. Allow shaker to cool down

11. Power off the shaker
12. Detach experimental fixture and baseplate from the shaker head.

Additional Remarks:

Two things I wish to mention about the vibration test that is not part of the procedure. The first is that after vibration testing is complete the CubeSat should undergo a process called a "Bake out". This will let the CubeSat outgas and will generally be the last thing you do. Secondly, it may be necessary to do a separate vibration test for the Sail deployment mechanism. This will be mostly the same process except the testing fixture would be different. The tests will be the same, but the success criteria may change to include more specifics for the Sail deployment mechanism.

13.8 Data Flow Testing

The IMU Data Flow Test Procedure demonstrates the steps followed to obtain the data of the UM7 IMU. For the test, the IMU will interface with a Raspberry Pi0 and a Raspberry Pi, while in the mission the IMU will be directly interfacing with the Flight Computer. Two different codes are being tested. The "cali_pass_test.c" was developed on previous semesters to obtain the data from the IMU and using the Raspberry Pi0 copy that data into a .csv file. This code will be referred to as the IMU C code. On the other hand, the UM7 code has been developed to interface with the Flight Software, read the IMU data and translate it to a format compatible with the Flight Computer. This code will be referred to as the IMU interface.

Objectives & Success Criteria

Objectives

- Extract accelerometer, gyroscope, magnetometer, temperature and time data from the IMU using drivers developed by Cal Poly.
- Obtain IMU values from the code developed in C to serve as trueset
- Obtain and compare values of IMU with C code with the code developed to interface with flight software and use the config files which are being developed by Cal Poly as input.

Success Criteria

- Replicate with the IMU interface Code the results obtained with the IMU C code.
- Obtain the required values in real time without any observable lag.

Test Materials, Facilities and Equipment

Test Materials

The following Components will be used to perform the test:

1. Inertial Measurement Unit: UM7 IMU
2. L298 H-Bridge
3. Raspberry Pi 3
4. Raspberry Pi Zero
5. Power Boost TPS71030
6. 1.2-5V Battery
7. Motor

8. Power Plug Computer Input
9. Power adaptor to Micro USB
10. Ethernet cable
11. Laptop with Buildroot installed

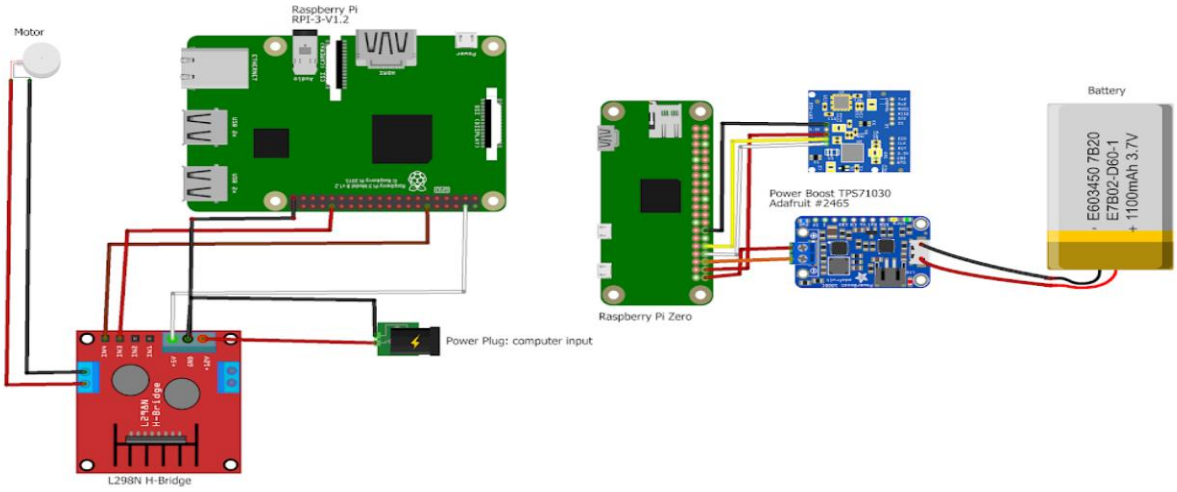

Figure 13.21: IMU and Raspberry Pi schematics

Facilities

Previous IMU tests have been performed in the vacuum chamber to replicate the conditions of space. Since the objective of the test is to check that the IMU interface code is consistent with the results of the IMU C code, the test can be performed at any facility that has access to electricity (power plug).

Equipment

The test will be performed with the IMU mounted on a turning table (Figure X). This device is composed by a disk mounted on a base. The disk is attached by a rotating structure powered by a motor.

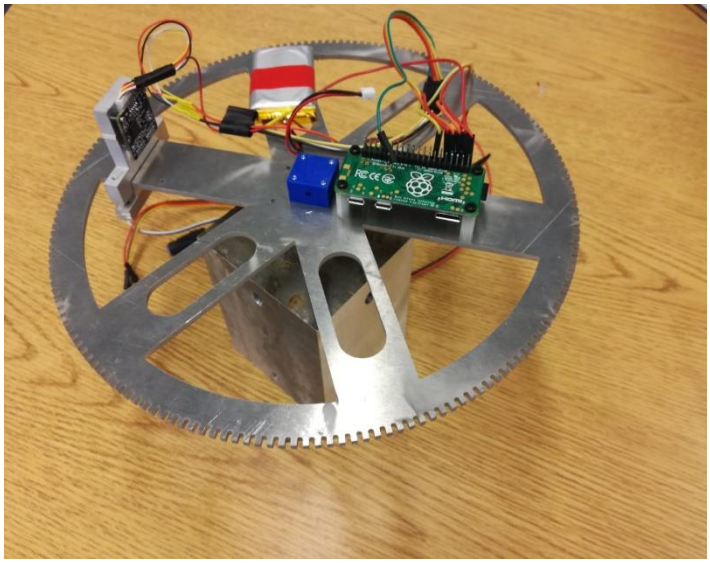

Figure 13.22: IMU on turntable

Test Procedure

The test procedure is divided in three sections: the networking guide, the IMU test and the IMU interface-Cal Poly test. The networking guide explains how to set-up the system to network with the Raspberry Pi. The IMU test guide consists the procedure required to operate the turning table and transferring the IMU results from the pi0 through FileZilla. The IMU interface test contains the procedure to set up buildroot and run the C code to read the IMU data using Libproc.

Networking Guide

1. Power on the Pi0 with the Battery.
    a. Connect the Battery to the Power Boost connector as shown in Fig. 13.23.
    b. Pi0 will be operational when the "ADE_Network" wifi signal can be found on any device.
2. Remote into the Raspberry Pi.
    a. Download and install VNC Viewer on your computer.
    b. Open VNC Viewer.
    c. Power on the Raspberry Pi
        i. Connect the power cable to a regular plug and the male microUSB to the female microUSB port on the Raspberry Pi
    d. Connect ethernet cable from computer to Raspberry Pi ethernet port.
    e. In VNC Viewer, under the "Enter a VNC Server address or search", enter: 169.254.245.239
        i. Note: if this address does not work you will need to find the IP address. To do so:
            1. Connect a monitor, keyboard and mouse to the Raspberry Pi.
            2. The Raspberry Pi desktop will appear at the monitor.
            3. Open the terminal by clicking the "terminal" button on the top left corner.

4. Input: `sudo hostname -I`
5. Output: The first 4 numbers that appear will be the IP address.

ii. When the correct IP address is inputted, the Raspberry Pi desktop will appear on VNC Viewer and you will have remoted into the Raspberry Pi.

3. From the Rasspberry Pi desktop(on the VNC Viewer), SSH into the Raspberry Pi0
   a. Connect the Raspberry Pi to the wifi network "ADE_Network".
      i. Go to the wifi symbol (📶) and click on the ADE_Network.
      ii. Select Connect.
      iii. Input the password: ade_test
   b. Right click the wifi symbol and select "Wireless and Wired Network Settings".
   c. Set the Configure options to SSID and then select ADE_Network in the drop-down menu that pops to the right.
   d. Check "Disable IPv6"
   e. Set the IPv4 address to 192.168.42.137
   f. Set the router to 192.168.42.1
   g. Close the "Wireless and Wired Network Settings" window.
   h. Open the terminal
   i. Input: `ssh pi@192.168.42.1`
   j. The password will be requested
   k. Input password: `raspberry`

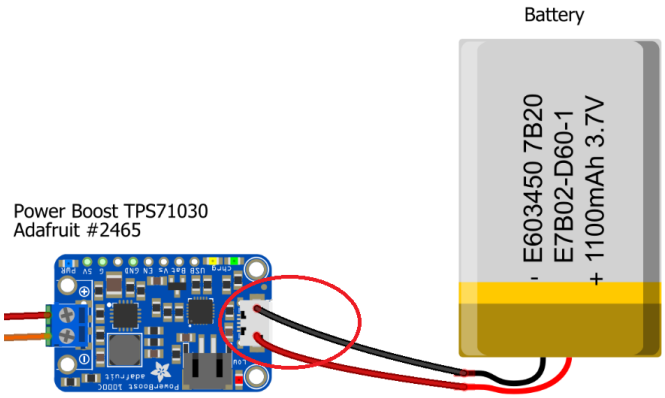

Figure 13.23: Raspberry Pi schematic

IMU Test Procedure

IMU C code (reads registers of UM7 and saves it into file, used as trueset)

1. Make sure that the connections between the test components are consistent with the Wiring Diagram attached in Fig. 13.21.
2. Apply Networking guide steps 1-3 to remote into the base pi using ethernet.
3. Start the turntable:
   a. On the Raspberry Pi desktop, search PWM_Drive.py file
   b. Open the file
   c. Click Run

    d. Output: the system will ask for a duty cycle.
    e. Open "speed_loop_up.txt". This document contains the duty cycle to motor rpm equivalence.
    f. Input the duty cycle corresponding to the desired rpm.
4. Run the test
    a. On the Raspberry Pi terminal input: `cd ADE_IMU/Testing`
    b. If changes are made to the cali_pass_test.c file, create a new executable
        i. Input: `gcc -lwiringPi filename.c -o filename.o`
        ii. Output: the executable file "filename.o" will be created
    c. Run the executable (change "executable filename" for the filename of the executable, which if nothing is modified is cali_pass_test.o)
        i. Input: `./filename.o`
        ii. Output: csv files are created with the IMU readings.
5. Stop the test
    a. Stop turntable
        i. Input: `Ctrl+C`
    b. Stop executable
        i. Input: `Ctrl+C`
6. To transfer the files, the Raspberry Pi needs to be connected to the Laptop by wifi on the ADE_Network, instead of by ethernet.
    a. On your laptop go to: Control Panel → Network and Internet → Network Connections
    b. Right Click on WiFi and go to properties
    c. Click "Internet Protocol Version 4 (TCP/IPv4) and select Properties
    d. Select "Use the following IP address" and enter the following:
        i. IP Adress: 192.168.42.137
        ii. Subnet mask: 255.255.255.0
        iii. Default gateway: 192.168.42.1
    e. In VNC Viewer, under the "Enter a VNC Server address or search", enter: 192.168.42.137
    f. Note: after finishing the test change IPv4 settings back to "Obtain an IP address automatically" to connect to normal networks again.
7. Transfer files through FileZilla
    a. At the laptop, open FileZilla. At the initial window, enter
        i. Host: `sftp://192.168.42.1`
        ii. Username: `pi`
        iii. Password: `raspberry`
        iv. Port: `22`
    b. Two windows will appear in FIleZilla with the directories from the raspberry pi0 and the laptop directories.
    c. Drag the desired .cvs files from the Pi0 directory to the desired directory on your laptop,

IMU Interface-Cal Poly code (read data from Config files being developed by Cal Poly and saves them in the required structures and print the values in the terminal)

1. Make sure that the connections between the test components are consistent with the Wiring

Diagram attached in Fig. 13.21.

2. Apply Networking guide steps 1-3 to remote into the base pi using ethernet.
3. Download Buildroot on developer computer
    a. Download a virtual machine (VMware workstation works correctly and can be found at : https://www.vmware.com/products/workstation-pro/workstation-pro-evaluation.html) or use a Linux Computer.
    b. Download **Ubuntu 14** and run it with the virtual machine. It is important to use version 14 to avoid incompatibility errors when installing buildroot.
    c. Open the terminal at Ubunutu and run: Input: `sudo apt-get install git bison g++ flex gettext texinfo lib32z1 lib32ncurses5 lib32bz2-1.0`
    d. Clone the repository with: Input: `git clone_ https://github.com/PolySat/buildroot.git`
    e. Configure the build machine with authentication credentials running: Input: `echo "--no-check-certificate --user=purdue --password=UPJDHsbC" > ~/.polysat_fsw.auth`
    f. Change into buildroot directory: `Input: cd buildroot`
    g. Build the Flight Software Image. Expect the process to take 6 hours; Input: `Make`
    h. Output: the buildroot process installs a set of libraries and compilers that are required to develop code using Libproc.

(Refer to PolySat/public_documentation/Building FSW.md in Github inside the PolySat repository provided by Cal Poly)

4. Install Libraries and header files to Raspberry Pi
    a. Create a “Libraries” folder in Raspberry Pi to copy all the required headers, libraries and the code itself. (This can be done by accessing the Raspberry Pi remotely using VNC or connecting a monitor, mouse and keyboard to it).
    b. The folder should contain these header files

NOTE: In the code written to interface with the flight software, remove the path of the files when running the code in Raspberry Pi as all the files will be in the same folder. For instance, change polysat_pkt/status-structs.h to status-structs.h.

These header files can be found inside the folder output in buildroot created in Step 3. The original UM7.c consist of the files with their paths. For instance, for status-structs.h, there can be multiple files with the same name at different location in buildroot, but go to polysat_pkt folder and copy the one in the folder and past it in the folder created in raspberry pi.

a. polysat_pkt/status-structs.h
b. polysat_pkt/shared-structs.h
c. polysat_pkt/payload_cmd.h
d. polysat_drivers/drivers/accelerometer.h
e. polysat_drivers/drivers/gyroscope.h

f. polysat_drivers/drivers/magnetometer.h
g. polysat_drivers/drivers/temp.h
h. polysat_drivers/driverdb.h
i. polysat/polysat.h
j. polysat_pkt/filemgr_cmd.h
k. polysat_pkt/datalogger_cmd.h
l. limits.h
m. string.h
n. sys/types.h
o. sys/stat.h
p. sys/time.h
q. time.h
r. unistd.h
s. stdio.h
t. fcntl.h
u. stdlib.h
v. signal.h
w. errno.h
x. ctype.h
y. um7-telemetry.h

5. In the folder, copy UM7.c, um7-util.c, and um7.cmd.cfg (Located on the shared drive under ADE/IMU Flight Software/2.Code/UM7
6. Follow step 3 in Procedure A to run the turntable
7. Compile UM7.c, run UM7.c and then UM7-util.c at Raspberry Pi terminal
    a. Input: cd Libraries
    b. Input: `gcc -lwiringPi UM7.c -o UM7.o`
    c. Output: the executable file "UM7.o" will be created
    d. Input: `gcc -lwiringPi UM7-util.c -o UM7-util.o`
    e. Output: the executable file "UM7.o" will be created
    f. Input: `./UM7.o`
    g. Input: `./UM7-util.o`
8. The readings of the IMU will appear in the terminal
9. To stop running the code, enter:
    a. Input: `Ctrl+C`

Expected Results and Anomalies

Expected Results

When the IMU is kept on a flat table then

a. Accelerometer should be 0,0,-1
b. Gyroscope 0,0,0
c. Magnetometer 0,0,0
d. Temperature: Room temperature
e. Time should be continuously changing

Anomalies

The axis of the motor is known to be tilted by 1° to 0.5°, so there will be out of plane components of the 9 degree of freedom.

13.9 PTE Tests

The goal of the PTE tests is to demonstrate a variety of functions. Each test outlined below is designed to add a layer of complexity to the preceding test. Note that "PTE algorithm" refers to the core PTE itself, or the code that takes acceleration as input and outputs periapsis time estimations. "PTE FSW" refers to the PTE algorithm along with the temperature correction process, noise filter, and libproc functions that control event scheduling and other flight software-specific tasks. Procedures for connecting to Raspberry Pi and IMU have been detailed in preceding tests, so they will not be gone into detail for sake of not repeating.

Requirements

Raspberry Pi
UM7 IMU
Computer
Ethernet port and cable

Pre-test

1. Install buildroot onto computer running Ubuntu 14 on virtual machine. VMWare is what has been used so far.
2. Remote into Raspberry Pi.
    1. Open VNC Viewer on desired laptop.
    2. Power on the Raspberry Pi and connect with ethernet cable.
    3. VNC server address: 196.254.245.239
3. Install required libraries onto Raspberry Pi, including libproc, libsat, and libpolydrivers. At the time of writing, libpolydrivers is not yet available.
4. Edit .bashrc file to define ARM_TOOLCHAIN_PATH as pointing towards the file where PolySat libraries were installed by buildroot.

Test 1

Objectives

The objective of Test 1 is to test the temperature correction, noise filter, and PTE algorithm as a unit. It will ensure that data can properly flow across all three parts.

Procedure

1. Copy test data file of three passes of acceleration data into same folder at PTE.c. on either Raspberry Pi or computer with appropriate libraries installed.
2. Compile PTE.c using gcc cross-compiler.
    a. gcc -Wall -Werror -I$ARM_TOOLCHAIN_PATH/include -L$ARM_TOOLCHAIN_PATH/lib PTE.c -lproc -o PTE
3. Run PTE.
    a. ./PTE

Success Criteria

1. 0 compile-time errors or warnings
2. 0 runtime errors (for example, segmentation faults)
3. *Expected results*: same time to periapsis estimation from comparison to MATLAB results for first 3 passes using same data

Test 2

Objectives

The objective of Test 2 is to test the PTE FSW end-to-end, simulating the on-orbit environment. Test 2 will demonstrate PTE's ability to initiate by command and its ability to reschedule itself.

Procedure

1. Copy PTE.c and test data file of three passes of acceleration data into same folder at PTE.c on either Raspberry Pi with appropriate libraries installed.
2. Compile PTE.c on Raspberry Pi using gcc cross-compiler.
    a. gcc -Wall -Werror -I$ARM_TOOLCHAIN_PATH/include -L$ARM_TOOLCHAIN_PATH/lib PTE.c -lproc -o PTE
3. Execute PTE initialization command ("PTE_init") in terminal.
    a. ./PTE_init

Success Criteria

1. 0 compile-time errors or warnings
2. 0 runtime errors
3. Measured time in between runs is within 5% of designated scheduled time
4. *Expected results:* same time to periapsis estimation from comparison to MATLAB results for first 3 passes using same data
5.

Test 3

Objectives

The objective of Test 3 is to demonstrate PTE's abilities to read data from the IMU and to write to the Periapsis Time Table (PTT). Test 3 also includes the objectives of Test 2, as it adds a level of complexity.

Procedure

1. Connect IMU to Raspberry Pi.
2. Copy PTE.c onto Raspberry Pi.
3. Compile PTE.c on Raspberry Pi using gcc cross compiler.
    a. gcc -Wall -Werror -I$ARM_TOOLCHAIN_PATH/include -L$ARM_TOOLCHAIN_PATH/lib PTE.c -lproc -o PTE
4. Execute PTE initialization command ("PTE_init") in terminal.
    a. ./PTE_init

Success Criteria

1. 0 compile-time errors or warnings
2. 0 runtime errors

3. Measured time in between runs is within 5% of designated scheduled time
4. *Expected results:* read IMU data displayed on terminal should match expectations of static IMU.
    a. Approximately 0 g in axes perpendicular to gravity vector.
    b. Approximately 1 g in axis parallel to gravity vector.
5. *Expected results:* value written to PTT should be either:
    a. Value hardcoded within PTE or
    b. Sample IMU data set to ensure data read is flowing through PTE.

Common Errors

The most common errors encountered during the processes of compiling software relate to being unable to find the libraries or headers. Possible fixes include:

- ensuring that ARM_TOOLCHAIN_PATH points to the correct filepath
- using ldd PTE to diagnose which libraries are being accessed
- using ldconfig to manually add the library path to the working folder
- ensuring that the required libraries have been installed

14 References

[1] Lee, S., et al. (2014, February 20). CubeSat Design Specification Rev. 13. Retrieved November 30, 2017, from https://static1.squarespace.com/static/5418c831e4b0fa4ecac1bacd/t/56e9b62337013b6c063a655a/1458157095454/cds_rev13_final2.pdf

[2] Dr. David Spencer. Purdue University (May 2017). Application for STEM CubeSat Launch Opportunity.

[3] PolySat, Cal Poly (February 2017). Initial Proposal.

[4] United Launch Alliance (April 2016). ULA STEM CubeSat Program 2016 Request for Applications. Retrieved November 30, 2017, from http://www.ulalaunch.com/uploads/docs/CubeSats/ULA_Cubesat_RFP_2016_FINAL.pdf

[5] Ridenoure, R. W., Spencer, D. A., Stetson, D. A., Betts, B., Munakata, R., Wong, S. D., Diaz, A., Plante, B., Foley, J. D., and Bellardo, J. M. "Status of the Dual CubeSat LightSail Program," AIAA SPACE 2015 Conference and Exposition. American Institute of Aeronautics and Astronautics, 2015. doi:doi:10.2514/6.2015-4424

[6] Alhorn, D. C., Casas, J. P., Agasid, E. F., Adams, C. L., Laue, G., Kitts, C., and O'Brien, S., "NanoSail-D: The Small Satellite That Could!", 25th Annual AIAA/USU Conference on Small Satellites

[7] Shmuel, B., Hiemstra, J., Tarantini, V., Singarayar, F., Bonin, G., & Zee, R. E. (2012). The Canadian Advanced Nanospace eXperiment 7 (CanX-7) Demonstration Mission: De-Orbiting Nano- and Microspacecraft. *26th Annual AIAA/USU Conference on Small Satellites*, *7*, 1–10. Retrieved from utias-sfl.net

[8] Kelso, D. S. (2017, January 6). Orbital Coordinate Systems, Part I. Retrieved April 20, 2017, from http://www.celestrak.com/columns/v02n01/

[9] Conventional Celestial Reference System. (2012, February 23). Retrieved April 16, 2017, http://www.navipedia.net/index.php/Conventional_Celestial_Reference_ System

[10] Coordinate Systems. (2016, October 22). Retrieved April 20, 2017, from http://www.dirsig.org/docs/new/coordinates.html#_the_earth_centered_earth_fixed_ecef_coordinate_system

[11] United Launch Alliance. (May 2014). Aft Bulkhead Carrier Auxiliary Payload User's Guide. Retrieved from http://www.ulalaunch.com/uploads/docs/Launch_Vehicles/ABC_Users_Guide_2014.pdf.

[12] Oh, H.-U., Jeon, S.-H., and Kwon, S.-C., “Structural Design and Analysis of 1U Standardized STEP Cube Lab for On-Orbit Verification of Fundamental Space Technologies,” *International Journal of Materials, Mechanics and Manufacturing*, vol. 2, Aug. 2014.

[13] Asif Israr, "Vibration and Modal Analysis of Low Earth Orbit Satellite," Shock and Vibration, vol. 2014, Article ID 740102, 8 pages, 2014. doi:10.1155/2014/740102

[14] NASA JSC, "Structural Design Requirements and Factors of Safety for Spaceflight Hardware" Rev.A 10/21/2011, accessed 11/26/2017, https://ntrs.nasa.gov/archive/nasa/casi.ntrs.nasa.gov/20110023499.pdf

[15] Plastics International, 'FR-4 Glass/Epoxy Phenolic', Accessed 11/26/2017, https://www.plasticsintl.com/datasheets/Phenolic_G10_FR4.pdf

[16] ASM Aerospace Specification Metals Inc. 'Aluminium 6061-T6; 6061-T651', Accessed 11/26/2017, http://asm.matweb.com/search/SpecificMaterial.asp?bassnum=ma6061t6

[17] Tyvak Nano-Satellites Systems LLC. (2012). Intrepid Pico-Class CubeSat System Board R5 [PDF]. Rev. D.

[18] CH Robotics. (2014, October 27). UM7 Datasheet [PDF]. Rev. 1.3.

[19] Long, A. C., & Spencer, D. A. (AIAA 2016-5676). Stability of a Deployable Drag Device for Small Satellite Deorbit. *AIAA/AAS Astrodynamic Specialist Conference, SPACE Conference and Exositions.* Long Beach, California.

[20] Dalla Vedova, F., et al. (2011). The Solar Sail Materials (SSM) Project - Status of Activities. Advances in Space Research, 48, 1922-1926.

[21] *UM7 Datasheet*. (2017, November 26). Retrieved from RedShift Labs: https://www.redshiftlabs.com.au/sensors/um7-lt-orientation-sensor

[22] CH Robotics. (2016). *UM7 Datasheet* (Rev. 1.6). Retrieved from http://www.chrobotics.com/docs/UM7%20Datasheet_v1-6_10.1.2016.pdf

[23] OmniVision. (n.d.). OV3642 3 Megapixel Product Brief. Retrieved November 30, 2017, from http://www.comedia.com.cn/OV%20SENSOR%20PB/300W/OV3642_PB_(1.1)_web.pdf

[24] Ettus Research (2017). *Ettus URSP N210*. Retrieved from https://goo.gl/images/NA3REc

[25] Miele, A., Zhao, Z. G., and Lee, W. Y. (1989). "Optimal trajectories for the aeroassisted flight experiment, part 1, equations of motions in an earth-fixed system." Retrieved from https://ntrs.nasa.gov/archive/nasa/casi.ntrs.nasa.gov/19900012464.pdf

[26] Fernandez, Juan & Rose, Geoff & R. Stohlman, Olive & J. Younger, Casey & D. Dean, Gregory & E. Warren, Jerry & Ho Kang, Jin & G. Bryant, Robert & W. Wilkie, Keats. (2018). An Advanced Composites-Based Solar Sail System for Interplanetary Small Satellite Missions. 10.2514/6.2018-1437.

[27] Garner, C. and Leipold, M., "Developments and Activities in Solar Sail Propulsion," AIAA00-0126. Presented at 36th AIAA Joint Propulsion Conference, 2000.

[28] Leipold M: Solar Sail Mission Design, Dissertation, Technical University of Munich, 2000, DLR FB 2000-22.

[29] The Planetary Society, "LightSail 1 Solar Sail Design and Qualifications (2008)", Accessed 01/24/2019, http://www.planetary.org/explore/projects/lightsail-solar-sailing/Aerospace-Mechanisms-Symposium_Chris-Biddy.pdf

[30] AIAA, "COMPARISON OF MSIS AND JACCHIA ATMOSPHERIC DENSITY MODELS FOR ORBIT DETERMINATION AND PROPAGATION (2003)", Accessed 04/25/2019, https://drum.lib.umd.edu/bitstream/handle/1903/3031/2003-akins-healy-coffey-picone.pdf;jsessionid=FEFAC5E42B216EA5BD99A012523103C8?sequence=2

[31] JPL, "Radiation Test Results for Common CubeSat Microcontrollers and Microprocessors (2015)", Accessed 04/25/2019, https://ieeexplore.ieee.org/stamp/stamp.jsp?tp=&arnumber=7336730

Appendix A – Requirements

This section is current as of May 1st 2020. For the most up-to-date requirements, see the ADE OneDrive.

Mission Design

SPINNAKER 1 Mission Statement												
The Aerodynamic Deorbit Experiment (SPINNAKER 1) 1U CubeSat will provide flight qualification and characterize the performance of a deployable drag device to accelerate the deorbit of small satellites.												
Requirement Number		Description	Source	Verification Method	Mapped?	Verification Document	Last Updated	Current As Of	Status			
MMSC		Minimum Mission Success Criteria							Pending	In Process	Complete	
MMSC-1		SPINNAKER 1 shall be a 1U CubeSat launched as a secondary payload and deployed via a P-POD into a geosynchronous transfer orbit	MS	Inspection			9/21/2017	2/18/2020	x			
MMSC-2		SPINNAKER 1 shall deploy a drag sail providing increased drag area to accelerate the deorbit timeline	MS	Test			10/26/2017	2/18/2020	x			
MMSC-3		The passive aerodynamic stability provided by the drag sail shall be assessed	MS	Analysis			2/5/2019	2/18/2020	x			
FMSC		Full Mission Success Criteria	Source	Verification Method	Mapped?	Verification Document	Last Updated	Current As Of	Pending	In Process	Complete	
FMSC-1		SPINNAKER 1 shall downlink IMU data for at least 5 perigee passes	IPPS	Test			10/26/2017	2/20/2020	x			
FMSC-2		A radiation sensor shall characterize the radiation environment in GTO for 3 orbits	IPPS	Test			2/5/2019	2/20/2020	x			
FMSC-3		SPINNAKER 1 shall take and return one image of the deployed sail	IPPS	Test	Y		12/15/2017	2/20/2020	x			
MD		Mission Design	Source	Verification Method	Mapped?	Verification Details	Last Updated		Pending	In Process	Complete	
MD-1		SPINNAKER 1 shall be a 1U CubeSat	MMSC-1	Constraint			-	2/20/2020				
	MD-1.1	SPINNAKER 1 shall be a secondary payload via an Atlas V	MD-1	Constraint			-	2/20/2020				
	MD-1.2	SPINNAKER 1 shall be deployed via a 3U P-POD	MD-1	Constraint			-	2/20/2020				
	MD-1.3	SPINNAKER 1 shall be launched into a geosynchronous transfer orbit with a nominal perigee altitude of 185 km and apogee altitude of 35,756 km	MD-1	Constraint			-	2/20/2020				
	MD-1.4	SPINNAKER 1 shall be launched into a 27.0° inclination orbit	MD-1	Constraint			-	2/20/2020				
MD-2		SPINNAKER 1 shall incorporate all of the ULA "Do-No-Harm" requirements	ULA	Test	Y		9/27/2017	2/20/2020	x			
	MD-2.1	SPINNAKER 1 shall be powered off and remain motionless while integrated into the P-POD	MD-2	Test	Y		1/27/2018	2/20/2020	x			
	MD-2.2	Drag Sail shall remained undeployed while in the P-POD	MD-2	Test	Y		1/27/2018	2/20/2020	x			
MD-3		SPINNAKER 1 must be able to recover from faults via ground-in-the-loop intervention	SPINNAKER 1APP	Test	Y		9/28/2017	2/20/2020	x			
MD-4		SPINNAKER 1 shall meet certification criteria of the FCC, NOAA, IARU, and shall have a completed ODAR	MMSC-1	Inspection			11/9/2017	2/20/2020	x			
MD-5		SPINNAKER 1 shall be protected from inadvertently sent critical commands	MMSC-1	Test	Y		11/9/2017	2/20/2020	x			
MD-6		Following deployment, SPINNAKER 1 will power on and begin battery charging in safe mode	SPINNAKER 1APP	Test	Y		1/27/2018	2/20/2020	x			
MD-7		SPINNAKER 1 shall deploy RF antennas 45 minutes after P-POD deployment	CDS13	Test	Y		9/21/2017	2/20/2020	x			
MD-8		SPINNAKER 1 shall begin transmissions no sooner than 45 minutes after P-POD deployment	SPINNAKER 1APP	Test	Y		9/21/2017	2/20/2020	x			
MD-9		SPINNAKER 1 shall establish two-way communications with Earth and perform a flight system functional checkout	FMSC-1				-	2/20/2020	x			
MD-10		SPINNAKER 1 shall send out beacon providing telemetry data every 30 seconds	MD-9	Test	Y		9/21/2017	2/20/2020	x			
MD-11		SPINNAKER 1 shall perform a full system checkout following deployment from the P-POD in order to verify functionality of all engineering subsystems	MD-9	Test	Y		9/21/2017	2/20/2020	x			
MD-12		SPINNAKER 1 shall collect and store IMU 3-axis accelerometer and gyro data for 20 minutes per orbit (centered at time of perigee) for later downlink	FMSC-1	Test	Y		11/1/2017	2/20/2020	x			
MD-13		SPINNAKER 1 shall deploy a thin-membrane drag sail through either ground command or backup timer	MMSC-2	Test	Y		9/28/2017	2/20/2020	x			
MD-14		The orbital decay rate shall be assessed based upon two-line elements	MMSC-2	Inspection	Y		2/5/2019	2/20/2020	x			
MD-15		The IMU data shall provide the performance and stability of the drag sail	MMSC-3				-	2/20/2020				
MD-16		SPINNAKER 1 shall take photos of the drag sail to confirm deployment	FMSC-3	Test	Y		2/6/2019	2/20/2020	x			
	MD-16.1	SPINNAKER 1 shall take a 5 thumbnail photo sequence of drag sail deployment	FMSC-3				-	2/20/2020	x			
MD-17		SPINNAKER 1 shall take photos of the Earth from near apogee	FMSC-4	Test	Y		9/28/2017	2/20/2020	x			

Flight System

Requirement Number			Flight Systems	Source	Verification Method	Mapped?	Verification Document	Owner	Last Updated	Current as of	Status		
FS											Pending	InProcess	Complet
FS-1			The flight system shall be designed as a 1U CubeSat, for deployment by a P-POD	MD-1, MD-	Constraint								
FS-2			The flight system shall be designed to withstand the Atlas V/Centaur launch environment.	MD-1.1	Constraint								
FS-3			The flight system shall be capable of operating in orbits ranging from GTO to LEO.	MD-1.1, MD-1.3	Constraint								
FS-4			The flight system shall use UHF telecommunications for both uplink and downlink.	MD-9	Constraint								
FS-5			The flight system shall accommodate the payloads, providing structural mounting, electrical power, thermal control, commanding and data management for each payload element.	MD-1	Inspection			FSE	1/27/2018	2/18/2020	x		
FS-6			The flight system shall be designed based on the CalPoly CubeSat Design Specification Rev 13	CDS13	Inspection				11/2/2017	2/18/2020	x		
THM			**Thermal**	**Source**	**Verification Method**	**Mapped?**	**Verification Document**	**Owner**	**Last Updated**	**Current as of**			
THM-1			All flight system components shall have established operational temperature limits.	FS-3	Inspection		F17 MP - 5.5		12/7/2017				x
THM-2			All flight system components shall have established survivable temperature limits.	FS-3	Inspection		F17 MP - 5.5		12/7/2017				x
THM-3			The thermal control subsystem shall monitor the temperatures of the flight systems board, UHF board, payload interface board, IMU, batteries, and the inner and outer faces of each panel.	FS-5	Testing	Y		Thermal Group	12/7/2017	2/18/2020		x	
THM-5			The thermal model of the flight system shall include nodes modeling all components.	FS-3	Analysis				12/7/2017	2/18/2020		x	
THM-6			Thermal vacuum bakeout shall be performed to insure proper outgassing of components in accordance with ULA test specifications.	FS-6	Testing	Y			12/7/2017	2/18/2020	x		
A			**Attitude**	**Source**	**Verification Method**	**Mapped?**	**Verification Document**	**Owner**	**Last Updated**	**Current as of**			
A-1			IMU shall be capable of recording 20+ minutes of data per orbit	MD-12	Testing	Y			11/1/2017	2/18/2020	x		
A-2			IMU shall be capable of recording angular rate change via accelerometer and gyro data	MD-12	Testing	Y			11/1/2017	2/18/2020	x		
	A-2.1		Any accumulated orientation error (drift) outside of +/- 5 deg during data collection for each perigee pass is characterized and corrected for in a static environment.	A-2	Testing	Y			10/10/2017	2/18/2020	x		
	A-2.2		Any accumulated orientation error (drift) outside of +/- 5 deg during data collection for each perigee pass is characterized and corrected for in a dynamic environment.	A-2	Testing	Y			4/14/2018	2/18/2020			
	A-2.3		The bias of the IMU shall be in the range of 0.06 deg/s for the gyro in a static environment.	A-2	Testing	Y		IMU Group	10/10/2017	2/18/2020	x		
	A-2.4		The bias of the IMU shall be in the range of 0.06 deg/s for the gyro in a dynamic environment.	A-2	Testing	Y			4/14/2018	2/18/2020			
A-3			IMU shall have a maximum data production rate defined as 200 bytes/s	SPINNAKER	Testing	Y			10/10/2017	2/18/2020	x		
A-4			Attitude, acceleration rates, magnetometer data, temperature and timestep shall be acquired at 10 Hz for 20 min centered on each perigee following drag sail deployment	MD-12	Testing	Y			11/1/2017	2/18/2020	x		
A-5			IMU checkout shall occur after flight system turns on.	MD-9	Testing	Y			11/1/2017	2/18/2020	x		
A-6			IMU data shall be collected to verify the drag sail deployment	MD-16	Testing	Y			10/12/2017	2/18/2020	x		
A-7			The IMU shall not exceed the defined operating temperature range at any point during the mission	FS-5	Testing	Y				2/18/2020			
STR			**Structure**	**Source**	**Verification Method**	**Mapped?**	**Verification Document**	**Owner**	**Last Updated**	**Current as of**			
STR-1			The mass of SPINNAKER 1 shall not exceed 2.0 kg. Special permission has been granted to surpass the	FS-1	Testing	Y			1/24/2017	2/18/2020	x		
STR-2			SPINNAKER 1 shall be designed to withstand the launch vehicle shock and vibroacoustic environment.	FS-2	Testing	Y			12/7/2017	2/18/2020		x	
	STR-2.1		SPINNAKER 1 shall be capable of withstanding an acceleration load factor that corresponds to worst-case launch load environments	STR-2	Testing	Y			1/24/2017	2/18/2020		x	
STR-3			The remove-before-flight pin shall not exceed 6.5 mm	FS-1	Inspection				12/7/2017	2/18/2020	x		
STR-4			Pyrotechnic devices/mechanisms shall not be used on SPINNAKER 1	FS-1	Inspection		F17 MP		12/7/2017	2/18/2020			x
STR-5			All Parts shall remain attached to SPINNAKER 1 during launch, ejection, and operation. No additional space debris shall be created	FS-1	Inspection		F17 MP		12/7/2017	2/18/2020			x
	STR-5.1		Retaining devices that rely solely on friction as a means of retention (such as, but not limited to: crimps, worm gears, lead screws, and motor detent torques) shall not be used on SPINNAKER 1	STR-5	Inspection		F17 MP		12/7/2017	2/18/2020			x
STR-6			The SPINNAKER 1 structure shall accommodate the mounting, placement, and structural support needs of all components of engineering subsystems	FS-5	Inspection				12/7/2017	2/18/2020		x	
STR-7			SPINNAKER 1 shall interface with a 3U P-POD and provide for an uninhibited deployment of the	FS-1	Inspection				12/7/2017	2/18/2020		x	
	STR-7.1		The entire CubeSat must fit within a 1U cubesat space inside the P-POD.	STR-7	Inspection				12/7/2017	2/18/2020		x	
		STR-7.1.1	A single Cubesat shall be 103.5±0.1 mm wide	STR-7.1	Inspection				12/7/2017	2/18/2020		x	
		STR-7.1.2	A single Cubesat shall be 113.5±0.1 mm tall	STR-7.1	Inspection				12/7/2017	2/18/2020		x	
	STR 7.2		At least 75% of the rail shall be in contact with the P-POD rails	STR-7	Inspection				12/7/2017	2/18/2020		x	
	STR-7.3		Exterior Cubesat components shall not contact the interior surface of the P-POD , other than the designated Cubesat rails.	STR-7	Inspection			Structures Group	12/7/2017	2/18/2020		x	
STR-8			Aluminum 7075 or 6061 shall be used for both the main Cubesat structure and the rails	FS-1	Inspection		F17 MP		12/7/2017	2/18/2020			x
STR-9			The cubesat side panels shall incorporate a copper shell for radiation shielding purposes	FS-3	Inspection				12/7/2017	2/18/2020		x	
STR-10			The –Z face of the CubeSat will be inserted first into the P-POD.	FS-1	Inspection				9/28/2017	2/18/2020	x		
STR-11			No components shall exceed 6.5 mm normal to the surface.	FS-1	Inspection				12/7/2017	2/18/2020		x	
STR-12			Deployables shall be constrained by the CubeSat, not the P-POD.	FS-1	Inspection		F17 MP		12/7/2017	2/18/2020			x
STR-13			Rails shall have a minimum width of 8.5mm.	FS-1	Inspection				12/7/2017	2/18/2020		x	
STR-14			Rails will have a surface roughness less than 1.6 µm.	FS-1	Inspection				9/28/2017	2/18/2020	x		
STR-15			The edges of the rails will be rounded to a radius of at least 1 mm	FS-1	Inspection				12/7/2017	2/18/2020		x	
STR-16			The ends of the rails on the +/- Z face shall have a minimum surface area of 6.5 mm x 6.5 mm contact area for neighboring CubeSat rails	FS-1	Inspection				12/7/2017	2/18/2020		x	
STR-17			At least 75% of the rail will be in contact with the P-POD rails. 25% of the rails may be recessed and no part of the rails will exceed the specification.	FS-1	Inspection				12/7/2017	2/18/2020		x	
STR-18			The CubeSat center of gravity shall be located within 20 mm from its geometric center in the X, Y and Z directions	FS-1	Testing	Y			12/7/2017	2/18/2020		x	
STR-19			The CubeSat rails and standoff, which contact the P-POD rails and adjacent CubeSat standoffs, shall be hard anodized aluminum to prevent any cold welding within the PPOD.	FS-1	Inspection				9/28/2017	2/18/2020	x		
STR-20			The compressed separation springs shall be at or below the level of the standoff. The separation spring will be centered on the end of the standoff on the CubeSat's –Z face	FS-1	Inspection				9/28/2017	2/18/2020	x		
STR-21			SPINNAKER 1 shall incorporate a structural safety factor of 1.4 according to NASA standard (NASA-STD-	MD-2	Analysis				12/7/2017	2/18/2020		x	
EPS			**EPS**	**Source**	**Verification Method**	**Mapped?**	**Verification Document**	**Owner**	**Last Updated**	**Current as of**			
EPS-1			The EPS shall provide power for the duration of the mission	FS-5	Testing	Y			11/1/2017	2/18/2020	x		
	EPS-1.1		The EPS shall produce power by means of solar arrays	EPS-1	Testing	Y			10/11/2017	2/18/2020	x		
		EPS-1.1.1	The solar arrays shall provide a minimum of 1.9W while exposed to direct sunlight	EPS-1.1	Testing	Y			1/27/2017	2/18/2020	x		
		EPS-1.1.2	The solar arrays shall have a minimum efficiency of 28%	EPS-1.1	Testing	Y			12/6/2017	2/18/2020	x		
EPS-2			The EPS shall provide electrical power storage for the duration of the mission	FS-5	Testing	Y			10/11/2017	2/18/2020	x		
	EPS-2.1		The batteries shall never fall below a charge capacity of 20% to maintain voltage levels	EPS-2	Testing	Y			1/27/2017	2/18/2020	x		
	EPS-2.2		The batteries shall incorporate circuit protection for charging/discharging to prevent unbalanced cell conditions and faults	EPS-2	Testing	Y			9/7/2017	2/18/2020	x		
EPS-3			The EPS shall provide power distribution and management for the duration of the mission	FS-5	Testing	Y			10/11/2017	2/18/2020	x		
	EPS-3.1		The EPS shall provide continuous power to the timing circuitry	EPS-3	Testing	Y			1/27/2017	2/18/2020	x		
	EPS-3.2		The EPS shall open circuit flight hardware before receiving deployment signal	EPS-3	Testing	Y		Hilker	1/27/2017	2/18/2020	x		
	EPS-3.3		The EPS shall open circuit to the batteries when fully charged to float the solar cells	EPS-3	Testing	Y			1/27/2017	2/18/2020	x		
	EPS-3.4		The EPS shall utilize an operating bus voltage of 4.2V	EPS-3	Testing	Y			4/10/2017	2/18/2020	x		
	EPS-3.5		The EPS shall provide regulated power at 3.3V and 5.0 V	EPS-3	Testing	Y			4/10/2017	2/18/2020	x		
	EPS-3.6		The EPS shall electrically disconnect the power system from the powered functions (including real time clocks) while the deployment switch is in the actuated state	EPS-3	Testing	Y			9/7/2017	2/18/2020	x		
EPS-4			Current and voltage measurements shall be provided for solar panels,batteries,and power buses	FS-5	Testing	Y			10/11/2017	2/18/2020	x		
	EPS-4.1		The EPS shall update the current and voltage measurements at a minimum rate of 0.2 Hz	EPS-4	Testing	Y			1/27/2017	2/18/2020	x		
	EPS-4.2		The EPS shall monitor individual solar panels	EPS-4	Testing	Y			1/27/2017	2/18/2020	x		
EPS-5			The EPS shall be capable of fully charging the batteries in 3 GTO periods during nominal operations	FS-5	Analysis				2/1/2018	2/18/2020			

COM			Telecom	Source	Verification Method	Mapped?	Verification Document	Owner	Last Updated	Current as of			
COM-1			The COM Subsystem shall receive uplink commands from the Purdue/GT/Cal Poly ground stations.	FS-4	Constraint								
COM-2			The COM subsystem shall utilize UHF for uplink and downlink communications	FS-4	Constraint								
	COM-2.1		The COM subsystem shall be capable of receiving uplinked commands at a data rate of 1100 bps.	COM-2	Testing	Y			3/10/2017	2/18/2020	x		
	COM-2.2		The COM Subsystem shall be capable of downlinking stored telemetry at a data rate of 9600 bps.	COM-2	Testing	Y			3/24/2017	2/18/2020	x		
	COM-2.3		The Com subsystem shall employ a Beacon as well as a continuous transmission mode.	COM-2	Testing	Y		Mathur	10/5/2017	2/18/2020	x		
COM-3			The COM Subsystem shall maintain a link margin of at least 3 dB for uplink/downlink communications with the exception of the case when antenna null is aligned toward Earth.	FS-4	Testing	Y			3/24/2017	2/18/2020	x		
C&DH			**Command & Data Handling**	**Source**	**Verification Method**	**Mapped?**	**Verification Document**	**Owner**	**Last Updated**	**Current as of**			
C&DH-1			The C&DH subsystem shall process all sensor and payload data	FS-5	Testing	Y			9/7/2017	2/18/2020	x		
	C&DH-1.1		The C&DH subsystem shall process IMU data at 10 Hz for 20 minutes per orbit	C&DH-1	Testing	Y			9/7/2017		x		
	C&DH-1.2		The C&DH subsystem shall process 1 full-size photo and 8 thumbnails per orbit when the cameras are turned on.	C&DH-1	Testing	Y		C&DH Group	9/7/2017	2/18/2020	x		
	C&DH-1.3		The C&DH subsystem shall process radiation data at 0.0167 Hz.	C&DH-1	Testing	Y			9/7/2017		x		
	C&DH-1.4		The C&DH subsystem shall process telemetry consisting of system status check data at 0.52 Mb per day.	C&DH-1	Testing	Y			9/28/2017	2/18/2020	x		
C&DH-2			The C&DH subsystem shall provide command and data interfaces for each subsytem	FS-5	Constraint								
	C&DH-2.1		The C&DH subsystem shall use the UART communication protocol	C&DH-2	Constraint								
	C&DH-2.2		The C&DH subsystem shall use the SPI communication protocol	C&DH-2	Constraint								
C&DH-3			The C&DH subsystem shall have a system watchdog to monitor active processes.	FS-5	Inspection				10/11/2017	2/18/2020	x		
	C&DH-3.1		The C&DH subsystem shall have a backup watch dog.	C&DH-3	Inspection				9/7/2017	2/18/2020	x		
C&DH-4			The C&DH subsystem shall be capable of storing all data produced during the lifetime of the mission	FS-5	Testing	Y			10/11/2017	2/18/2020	x		
	C&DH-4.1		The C&DH subsystem shall be capable of storing at least 1.06 Mb of IMU data per orbit.	C&DH-4	Testing	Y			10/11/2017	2/18/2020	x		
	C&DH-4.2		The C&DH subsystem shall be capable of storing at least 7.26 Mb of image data per orbit.	C&DH-4	Testing	Y			10/11/2017	2/18/2020	x		
	C&DH-4.3		The C&DH subsystem shall be capable of storing at least 0.0768 Mb of radiation data per orbit.	C&DH-4	Testing	Y			10/11/2017	2/18/2020	x		
	C&DH-4.4		The C&DH subsystem shall be capable of storing 0.52 Mb of telemetry per day.	C&DH-4	Testing	Y			11/1/2017	2/18/2020	x		
C&DH-5			The C&DH subsystem shall be able to function through all defined spacecraft power modes	FS-5	Testing	Y			9/7/2017	2/18/2020	x		
	C&DH-5.1		Following a system reboot, the C&DH shall configure the spacecraft to safe mode	C&DH-5	Testing	Y		C&DH Group	10/11/2017	2/18/2020	x		
C&DH-6			The C&DH subsystem shall be capable of in-flight reprogramming	FS-5	Testing	Y			10/11/2017	2/18/2020	x		
	C&DH-6.1		The C&DH subsystem shall be capable of identifying and correcting flight anomalies	C&DH-6	Testing	Y			11/2/2017	2/18/2020	x		
C&DH-7			The C&DH subsystem shall compress all onboard data prior to transmission	FS-5	Testing	Y			10/11/2017	2/18/2020	x		
C&DH-8			The C&DH subsystem shall encode all data for proper downlink through the transmitter	FS-5	Testing	Y			10/11/2017	2/18/2020	x		
C&DH-9			The spacecraft real time clock shall be checked and updated when the flight system turns on	MD-10	Testing	Y			9/21/2017	2/18/2020	x		
C&DH-10			Critical system commands shall be activated by a two-step command	MD-5	Testing	Y			9/21/2017	2/18/2020	x		
	C&DH-10.1		Commanded drag sail deployment shall be activated by a two-step command	C&DH-10	Testing	Y			11/9/2017	2/18/2020	x		
	C&DH-10.2		Passivation of spacecraft shall be activated by a two-step command	C&DH-10	Testing	Y			11/9/2017	2/18/2020	x		
C&DH-11			The C&DH subsystem shall command all burnwire activations	FS-5	Testing	Y			11/9/2017	2/18/2020	x		
C&DH-12			The system board shall provide power and data connections to the UHF board	FS-5	Testing	Y			4/16/2018	2/18/2020	x		

Payload

Requirement Number			Payload	Source	Verification Method	Verification Document	Owner	Last Updated	Current as of	Status		
										Pending	InProcess	Complete
			Drag Sail Mechanism	**Source**	**Verification Method**	**Verification Document**	**Owner**	**Last Updated**	**Current as of**			
DS-1			SPINNAKER 1 shall have a deployable dragsail	MD-13	Inspection		Black	1/27/2018	2/18/2020	x		
	DS-1.1		The sail shall be shaped like a square pyramid	DS-1	Inspection		Black	9/7/2017		x		
		DS-1.1.1	There shall be four triangularly shaped sails	DS-1.1	Inspection		Black	9/7/2017	2/18/2020	x		
	DS-1.2		The sail shall have rigid booms that support the thin sail material CP-1.	DS-1	Inspection		Black	9/14/2017	2/18/2020	x		
		DS-1.2.1	There shall be four booms	DS-1.2	Inspection		Black	9/14/2017	2/18/2020	x		
		DS-1.2.2	The booms shall be 0.8 m long	DS-1.2	Inspection		Black	9/7/2017	2/18/2020	x		
		DS-1.2.3	The booms shall have an angle of 70° from the central sail subsystem axis	DS-1.2	Inspection		Black	9/7/2017	2/18/2020	x		
DS-2			The sail shall have a thickness of 5 microns to withstand expected atomic oxygen erosion	DS-1	Inspection		Black	11/1/2017	2/18/2020	x		
DS-3			The sail shall have a mechanism to prevent the propagation of tears	DS-1	Testing	Y	Black	11/1/2017	2/18/2020	x		
	DS-3.1		The sail shall have tape that inhibits tears to grow beyond 260 mm (the diagonal of each square)	DS-3	Testing	Y	Black	9/21/2017	2/18/2020	x		
DS-4			The booms shall be deployed by hub-mounted motor controller initiation	MD-13	Testing	Y	Black	2/5/2019	2/18/2020	x		
DS-5			The dragsail shall withstand thermal limits of 263°C from the CP-1 thermal constraints	DS-1	Testing	Y	Black	11/1/2017	2/18/2020	x		
DS-6			The dragsail shall be designed to provide SPINNAKER 1 with passive aerodynamic stability	MD-13, MD-15	Analysis		Tamrazian	2/5/2019	2/18/2020		x	
			Cameras	**Source**	**Verification Method**	**Verification Document**	**Owner**	**Last Updated**	**Current as of**	**Pending**	**InProcess**	**Complete**
C-1			SPINNAKER 1 shall have two OV3642 3 MP cameras	MD-16,OR-4	Inspection		Bruno	2/5/2019	2/18/2020	x		
	C-1.1		One camera shall be located on the side panel with a view of the deployed drag sail	MD-16	Inspection		Bruno	9/7/2017	2/18/2020	x		
	C-1.2		The second camera shall be located on the -Z panel with an unobstructed field of view	OR-4	Inspection		Bruno	9/7/2017	2/18/2020	x		
C-2			Each camera shall have a power consumption of no more than 3W	EPS-1	Testing	Y	Bruno	12/15/2017	2/18/2020	x		
			Radiation Detector	**Source**	**Verification Method**	**Verification Document**	**Owner**	**Last Updated**	**Current as of**			
RD-1			SPINNAKER 1 shall have 8 radiation dectectors, 4 located within the radiation shielding and another 4 outside the structure and exposed to space.	FMSC-2	Testing	Y	Bruno	2/1/2018	2/18/2020	x		
	RD-1.1		The radiation detectors located within the radiation shielding shall monitor the radiation environment within SPINNAKER1	RD-1	Testing	Y	Bruno	2/1/2018		x		
	RD-1.2		The radiation detectors located on the outside of the spacecraft shall characterize the outside radiation environment	RD-1	Testing	Y	Bruno	2/1/2018	2/18/2020	x		
RD-2			Each sensor shall perform a reading once per minute continuously for the mission.	FMSC-2	Testing	Y	Bruno	11/1/2017	2/18/2020	x		
RD-3			The radiation detectors shall each have a power draw of 4 microWatts	FMSC-2	Testing	Y	Bruno	11/1/2017	2/18/2020	x		

Mission Operations

Requirement Number			Mission Operations	Source	Verification Method	Mapped?	Verification Document	Owner	Last Updated	Current as of	Status		
											Pending	In Process	Complete
GDS			**Ground Data System**										
GDS-1			GDS shall receive two-line elements (TLEs) from the 18th Space Control Squadron at a frequency of 1-5 days.	MD-14	Testing	Y	Tracking Testing V&V closeout	Hurt	12/7/2017	2/18/2020			x
	GDS-1.1		GDS shall decode TLE data into orbital elements within one orbital period.	GDS-1	Testing	Y	Tracking Testing V&V closeout		12/7/2017	2/18/2020			x
GDS-2			GDS shall determine times for SPINNAKER 1 to collect data after receiving from CSPOC	MD-12	Testing	Y			1/27/2018			x	
	GDS-2.1		GDS shall calculate a time interval of 20 minutes centered around SPINNAKER 1 perigee	GDS-2	Testing	Y			1/27/2018			x	
GDS-3			GDS shall determine satellite ground tracks and time/duration of passes	MD-9	Analysis				12/7/2017	2/18/2020		x	
	GDS-3.1		GDS shall determine when spacecraft passes into sight of ground stations for uplink and downlink	GDS-3	Analysis				12/7/2017	2/18/2020			x
	GDS-3.2		GDS shall calculate maximum communication distance over UHF	GDS-3	Testing	Y			12/7/2017	2/18/2020		x	
GDS-4			GDS shall use a protocol for collecting, distributing, and storing data	MD-9	Inspection				12/7/2017	2/18/2020		x	
GDS-5			GDS shall be able to deploy the drag sail using two-step command.	MD-5	Testing	Y			11/9/2017	2/18/2020	x		
GDS-6			GDS shall be able to passivate the spacecraft with a two-step command.	MD-4	Testing	Y			11/9/2017	2/18/2020	x		
TS			**Tracking Stations**	**Source**	**Verification Method**		**Verification Document**	**Owner**	**Last Updated**	**Current as of**			
TS-1			Purdue and affiliated ground stations shall be able to send commands and recieve data from SPINNAKER 1	MD-9	Constraint								
	TS-1.1		Purdue ground station shall receive data from SPINNAKER 1 at 9600 bps	TS-1	Testing	Y		Hurt	12/7/2017	2/18/2020		x	
	TS-1.2		Purdue ground station shall send data to SPINNAKER 1 at 1100 bps	TS-1	Testing	Y			12/7/2017	2/18/2020		x	
TS-2			Purdue ground station shall estimate SPINNAKER 1 position in spherical coordinates centered at tracking	MD-9	Analysis		Tracking		12/7/2017	2/18/2020			x
TS-3			Purdue ground station shall facilitate the evaluation of health and status of SPINNAKER 1	MD-9	Testing	Y			12/7/2017	2/18/2020	x		
TF			**Test Facilities**	**Source**	**Verification Method**		**Verification Document**	**Owner**	**Last Updated**	**Current as of**			
TF-1			SPINNAKER 1 hardware shall be maintained at the Visibly Clean* (VC) level	-	Constraint								
TF-2			Work surfaces shall be maintained at the VC level	-	Constraint								
TF-4			Work surfaces shall provide ESD protection	-	Constraint								
TF-3			SPINNAKER 1 hardware shall be transported in a hard, foam interior case whenever removed from the laboratory environment	-	Constraint								
EGSE			**Electrical Ground Support Equipment**	**Source**	**Verification Method**		**Verification Document**	**Owner**	**Last Updated**	**Current as of**			
EGSE-1			Attenuators for link budget testing shall reduce the signal to accurately reproduce the effects of path loss expected up to apogee	-	By Design			Telecom/ GDS/Tracking	2/1/2018	2/20/2020	x		
EGSE-2			Power supplied for all testing shall be at the same voltage and current levels as if from the flight EPS	-	By Design			EPS Group	2/20/2020	2/20/2020	x		
MGSE			**Mechanical Ground Support Equipment**	**Source**	**Verification Method**		**Verification Document**	**Owner**	**Last Updated**	**Current as of**			
MGSE-1			A winding mechanism shall be developed to re-stow the booms into the pre-deployed configuration	-	By Design			Long	2/1/2018	2/20/2020	x		
	MGSE-1.1		The mechanism shall work for both the stand-alone dragsail assembly as well as the integrated CubeSat	-	By Design				2/1/2018	2/20/2020	x		
	MGSE-1.2		The mechanism shall include a "lock" which inhibts deployment separate from the doors	-	By Design				2/1/2018	2/20/2020	x		

STEM

Requirement Number	STEM Outreach	Source	Verification Method	Mapped?	Verification Document	Owner	Last Updated	Status		
								Pending	InProcess	Complete
OR-1	The design process of the SPINNAKER 1 capsule shall engage local high school students	ULA RFP	Inspection			Spencer	9/28/2017	x		
OR-2	Undergraduate members of the SPINNAKER 1 design team shall act as mentors for STEM students	ULA RFP	Inspection			Spencer	9/28/2017	x		
OR-3	The SPINNAKER 1 team shall maintain a consistent social media presence in order to keep the public informed about the team's progress.	SPINNAKER 1 App	Inspection			Spencer	9/28/2017		x	
OR-4	An image capturing the full disk of Earth shall be acquired and downlinked	IPPS	Test	Y		Spencer	2/5/2019	x		

External Sources

External Sources	
Abbreviation	**Reference**
CDS13	CubeSat Design Specifications Rev. 13. The CubeSat Program, Cal Poly SLO. Feb 2014.
ADEAPP	Application for STEM CubeSat Launch Opportunity. Dr. David Spencer, Purdue University, May 2016
IPPS	Initial Proposal by PolySat. Cal Poly, Feb 2017
ULA	ULA STEM CubeSat Program 2016 - Appendix 1: Do-no-Harm. ULA, April 2016
F17 MP	Fall 2017 Mission Plan. A subsection may be specified for V&V purposes.

Appendix B – MATLAB Code

Attitude Stability Code

```
%%%%%%%%%%%%%%%%%%%%%%%%%%%%%%%%%%%%%%%%%%%%%%%%%%%%%%
% alt_plot:
% Input: altplot figure, total AOA;
% Output: plot of total AOA with altitude for each orbit
%%%%%%%%%%%%%%%%%%%%%%%%%%%%%%%%%%%%%%%%%%%%%%%%%%%%%%
```

read altplot for altitude history

```
fig=openfig('altplot.fig');
axObjs = fig.Children;
dataObjs = axObjs.Children;
Time = dataObjs(1).XData';
Altitude = dataObjs(1).YData';

T=table(Time,Altitude);
writetable(T,'alt_hist.csv');
```

plot <=300km tAOA

```
atm_data=csvread('AtmosAngles.csv',1,0);
atm_time=atm_data(:,1);
atm_taoa=atm_data(:,4);

apogee=find(islocalmax(Altitude));

for i=1:length(apogee)-1

   % pick out start and end point of 300 km in alt plot
   alt_p=Altitude(apogee(i):apogee(i+1));
   time_p=Time(apogee(i):apogee(i+1));

%////////////////////////////////////////////////////////
   %switch case 1 time
%        bar=600;
%        perigee=find(islocalmin(alt_p));
%        alt300=find(abs(time_p-time_p(perigee)) <= bar);
   %switch case 2 altitude
       bar=600;
       alt300=find(alt_p<=bar);
%////////////////////////////////////////////////////////

   Start=alt300(1);
   End=alt300(end);
   t1=time_p(Start);
   t2=time_p(End);

   % pick out start and end point of 300km in aoa data
   aoa_start=find(abs(atm_time-t1)<=10,1);
   aoa_end=find(abs(atm_time-t2)<=10,1);
   perigee=find(alt_p==min(alt_p));
   time_min=time_p(perigee);
```

```
    % plotting
    figure
    plot(atm_time(aoa_start:aoa_end)-
time_min,atm_taoa(aoa_start:aoa_end),'k-')
%     axis([-200,200,0,35])
    yyaxis left
    xlabel('T to perigee (sec)')
    ylabel('Total AOA (deg)')
    title(['Total AOA at orbit #',num2str(i),' (under
 ',num2str(bar),'km)'])
%     title(['Total AOA at orbit #',num2str(i),num2str(bar),' sec from
 perigee'])
    yyaxis right
    plot(time_p(Start:End)-time_min,alt_p(Start:End))
    ylabel('Altitude (km)')
    grid minor
    savefig(['figure',num2str(i),'.fig'])

    %stats

    taoa.mean(i)=mean(atm_taoa(aoa_start:aoa_end));
    taoa.max(i)=max(atm_taoa(aoa_start:aoa_end));
    taoa.min(i)=min(atm_taoa(aoa_start:aoa_end));
    taoa.std(i)=std(atm_taoa(aoa_start:aoa_end));

end


Mean=taoa.mean';
Max=taoa.max';
Min=taoa.min';
StD=taoa.std';

T = table(Mean,Max,Min,StD);

writetable(T,"tAOA_statistics.csv")
save("taoa.mat")
```

Published with MATLAB® R2018b

Tracking Station Overflights Code

Table of Contents


```
%%%%%%%%%%%%%%%%%%%%%%%%%%%%%%%%%%%%%%%%%%%%%%%%%%%%%%%%%%%%%%%%%%%%%%%%%%%%
%%%%%%
% Goundstation statistics
%
% function:
% data into 3 phases, perform basic statistical analysis
%
% definition:
% Phase 1: first 1/3 of cotacts
% Phase 2: second 1/3 of cotacts
% Phase 3: approximately last 1/3 of cotacts (the rest)
%
% to use: change fid -> run program
%
%%%%%%%%%%%%%%%%%%%%%%%%%%%%%%%%%%%%%%%%%%%%%%%%%%%%%%%%%%%%%%%%%%%%%%%%%%%%
%%%%%%
close all
clear
clc
```

data input

```
fid = fopen('ts_contact.txt');
data = textscan(fid, '%s%s%s%s%s%s%s%s%s');
fclose(fid);
size(data);

duration_in=data(:,9);
duration_in=str2double(duration_in{:});

DD_start=data(:,1);
DD_start=str2double(DD_start{:});
MM_start=data(:,2);
MM_start=MM_start{:};

T_start=data(:,4);
T_start=T_start{:};
T_stop=data(:,8);
T_stop=T_stop{:};

YY_start=data(:,3);
YY_start=str2double(YY_start{:});
TT_start=data(:,4);
```

```
TT_start=str2double(TT_start{:});

DD_stop=data(:,1);
DD_stop=str2double(DD_stop{:});
MM_stop=data(:,2);
MM_stop=MM_stop{:};
YY_stop=data(:,3);
YY_stop=str2double(YY_stop{:});
TT_stop=data(:,4);
TT_stop=str2double(TT_stop{:});
```

identify tracking station and start and end point of data

```
n=0;
j=1;

index=find(isnan(duration_in));
for x=2:length(index)
    if index(x) - index(x-1) > 10
        term_pt(j)=index(x);
            i_start(j)=index(x-1)+1;
            i_end(j)=index(x)-1;
            name(j)=MM_start(i_start(j)-2);
        n=n+1;
        j=j+1;
    end
end
```

statistics for each tracking station

```
for j=1:n

    for k=1:3

        %divide data to three phase, find corresponding index
        phase1cut=floor((i_end(j)-i_start(j))/3);
        phase2cut=2*floor((i_end(j)-i_start(j))/3);


 phase=[i_start(j),i_start(j)+phase1cut,i_start(j)+phase2cut,i_end(j)];
        duration=duration_in((phase(k)+1):phase(k+1));

        for i=1:length(duration)

            if duration(i) <= 60
                duration(i)=NaN;
            end
        end

        %stats
```

```
        ts_count(k)=length(duration)-sum(isnan(duration));
        ts_mean(k)=nanmean(duration);
        ts_max(k)=nanmax(duration);
        ts_min(k)=nanmin(duration);
        ts_std(k)=nanstd(duration);
    end

    %write results
        count=ts_count';
        mean=ts_mean';
        max=ts_max';
        min=ts_min';
        std=ts_std';
        results={"Phase 1";"Phase 2";"Phase 3"};

        T=table(results,count,mean,max,min,std);
        out_name=sprintf("tracking station %s stats.csv",name{j});
        writetable(T,out_name)


end
```

Published with MATLAB® R2018b